

**APPLICATION OF THE NOYORI ANNULATION
REACTION TO THE CEPHALOTAXINE
SPIROCYCLE**

Submitted in fulfilment of the requirements
for the degree of

MASTER OF SCIENCE

By


Jean Mary-Anne McKenzie

December 2001

School of Chemical and Physical Sciences
University of Natal
Pietermaritzburg

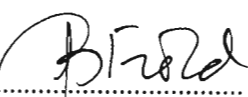
DECLARATION

I hereby certify that this research is a result of my own investigation which has not already been accepted in substance for any degree and is not being submitted in candidature for any other degree.

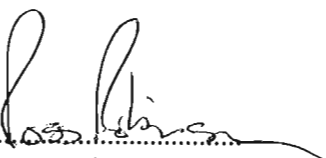
Signed.....

Jean Mary-Anne McKenzie

I hereby certify that this statement is correct.

Signed.....

pp. Doctor D. Gravestock
Supervisor

Signed.....

Doctor R.S. Robinson
Co-Supervisor

School of Chemical and Physical Sciences
University of Natal
Pietermaritzburg

December 2001

CONTENTS

ACKNOWLEDGEMENTS.....	iv
ABBREVIATIONS.....	v
CONFERENCE PROCEEDINGS AND PUBLICATIONS.....	vii
ABSTRACT.....	viii

1. INTRODUCTION

1.1. BRIEF INTRODUCTION TO ALKALOIDS.....	1
1.2. ISOLATION AND CHARACTERISATION OF CEPHALOTAXINE.....	2
1.3. USES OF CEPHALOTAXINE ESTERS.....	3
1.4. SYNTHESSES OF CEPHALOTAXINE.....	5
1.4.1. Total Syntheses of Cephalotaxine.....	6
1.4.2. Formal Syntheses of Cephalotaxine.....	22
1.5. AIMS OF THE INVESTIGATION.....	24

2. DISCUSSION OF SYNTHETIC WORK

2.1. APPLICATION OF THE NOYORI ANNULATION REACTION TO THE CEPHALOTAXINE SPIROCYCLE.....	30
2.1.1. Mechanism of The Noyori Annulation Reaction.....	30
2.1.2. Synthesis of 1,3-Dimethyl-1,4,5,6,7,7a- hexahydro-2 <i>H</i> -inden-2-one (115).....	31
2.1.3. Attempted Reaction of Methyl 2,4-dibromo-3-oxobutanoate (116) and 1-Benzyl-2-methylenepyrrolidine (117).....	35
2.1.4. Reaction of 2,4-Dibromo-3-pentanone (114) and 1-Benzyl-2-methylenepyrrolidine (117).....	42
2.1.5. Synthesis of 1-Benzyl-7,9-dimethyl-8- oxo-1-azaspiro[4.4]nonane-6-carbonitrile (130).....	46

2.2. PROGRESS TOWARDS THE CEPHALOTAXINE	
PENTACYCLIC SKELETON.....	57
2.2.1 Synthesis of 2-(1,3-Benzodioxol-5-yl)-1-ethanol (60).....	58
2.2.2. Synthesis of 2-(6-Iodo-1,3-benzodioxol-5-yl)-1-ethanol (97).....	58
2.2.3. Synthesis of 2-(6-Iodo-1,3-benzodioxol-5-yl)ethyl 4-methylbenzenesulfonate (98) and 2-(6-Iodo-1,3- benzodioxol-5-yl)ethyl 4-nitrobenzenesulfonate (15a).....	59
2.2.4. Synthesis of 1-[2-(6-Iodo-1,3-benzodioxol-5-yl)ethyl]- 2-pyrrolidinone (99).....	62
2.3. CONCLUSIONS AND FUTURE WORK.....	64
3. CONFORMATIONAL ANALYSIS	
3.1. INTRODUCTION.....	69
3.2. X-RAY STRUCTURE OF TOSYLATE (98).....	74
3.3. INTRODUCTION TO MM CALCULATIONS.....	76
3.4. DEVELOPMENT OF FORCE FIELD PARAMETERS AND GEOMETRY OPTIMISATION.....	83
3.5. ¹ H NMR SPECTROSCOPIC STUDIES.....	87
3.6. TORSION ANGLE ANALYSIS.....	89
3.7. π -STACKING AND X-RAY STRUCTURE OF NOSYLATE (15a).....	96
3.8. CONCLUSION.....	99
4. EXPERIMENTAL	
4.1. INSTRUMENTATION AND CHEMICALS.....	101
4.1.1. Solvents, Reagents and Reaction Conditions.....	101
4.1.2. Chromatography.....	101
4.1.3. Spectroscopy and Physical Data.....	101
4.1.4. X-ray Structure Collection.....	102
4.2. PREPARATIONS.....	103
5. REFERENCES.....	116

APPENDICES

APPENDIX A: Crystallographic data for spirocycle (130).....	II
APPENDIX B: Crystallographic data for tosylate (98).....	XI
APPENDIX C: Crystallographic data for nosylate (15a).....	XXIV

ACKNOWLEDGEMENTS

Many thanks must go to my supervisor, Dr David Gravestock, for all his assistance in this project. His enthusiasm and attention were extremely encouraging and much appreciated. Thanks also to my co-supervisor, Dr Ross Robinson, for his help in the laboratory and for having sympathetic ear about anything and everything. Dr Orde Munro must be specially mentioned for the large amount of time he spent assisting me with the conformation analysis work and having been the person to recognise the need for the conformation analysis study. Also, he must be acknowledged for solving all three crystal structures in this thesis.

For technical assistance I would like to thank specifically Martin Watson (NMR); James Ryan (X-ray); Paul Forder (Glass blowing); Raj Somaru, Wilson Zondi, and Craig Grimmer (Warren Laboratory). I also extend my appreciation to the rest of the technical and support staff for general assistance. Dr P.R. Boshoff of the Mass Spectrometry Unit at the Cape Technikon is acknowledged for carrying out the HRMS analysis. And for assistance in proof reading various parts of this thesis thanks go to Prof Drewes.

Finally I would like to thank all my colleagues in the Warren Laboratory for making research enjoyable, and Graeme, my family and friends for their companionship and support.

ABBREVIATIONS

Å	Angstrom
Ar	aryl
aq.	aqueous
Bn	benzyl
Boc	<i>tert</i> -butoxycarbonyl
b.p.	boiling point
Bu	butyl
conc.	concentrated
COSY	correlation spectroscopy
Cp	cyclopentadienyl
d	doublet
dd	doublet of doublets
DEPT	distortionless enhancement over polarisation transfer
DMAP	4-dimethylaminopyridine
DMF	<i>N,N</i> -dimethylformamide
DMSO	dimethylsulfoxide
Et	ethyl
GC	gas chromatography
GHMQC	gradient heteronuclear multiple quantum correlation
GHSQC	gradient heteronuclear single quantum correlation
HPLC	high performance liquid chromatography
$h\nu$	irradiation
Hz	hertz
<i>i</i>	iso
IR	infrared
LDA	lithium diisopropylamide
m	multiplet
Me	methyl
m.p.	melting point
Ms	mesylate (CH_3SO_2^-)

MsCl	CH ₃ SO ₂ Cl
MS	mass spectrometry
<i>n</i>	normal
NMR	nuclear magnetic resonance
NOESY	nuclear Overhauser effect spectroscopy
Ns	nosyl (<i>p</i> -NO ₂ PhSO ₂ -)
4-NsCl	4-nitrobenzenesulfonyl chloride
<i>o</i>	ortho
OAc	CH ₃ CO ₂ -
<i>p</i>	para
Ph	phenyl
ppm	parts per million
Pr	propyl
q	quartet
ROESY	rotating-frame Overhauser effect spectroscopy
RT	room temperature
s	singlet
sat.	saturated
soln.	solution
t	triplet
<i>t</i> or <i>tert</i>	tertiary
TBAF	tetrabutylammonium fluoride
THF	tetrahydrofuran
TLC	thin layer chromatography
TMSCl	chlorotrimethylsilane
tol	tolyl
Ts	tosyl (<i>p</i> -CH ₃ PhSO ₂ -)
<i>p</i> -TsOH	<i>p</i> -toluenesulfonic acid
<i>p</i> -TsCl	<i>p</i> -toluenesulfonyl chloride
UV	ultraviolet
Δ	heat

CONFERENCE PROCEEDINGS

The following poster presentations were made on various aspects of this research project.

(i) D. Gravestock and J.M. McKenzie, *Studies Towards the Synthesis of Cephalotaxine*, 35th Convention of the South African Chemical Institute, Potchefstroom, September 2000.

(ii) D. Gravestock and J.M. McKenzie, *Progress Towards the Synthesis of Cephalotaxine*, 1st Binational Royal Society of Chemistry/South African Chemical Institute International Conference on Organic Chemistry, Cape Town, January, 2001.

(iii) D. Gravestock and J.M. McKenzie, *Novel Approach to the Synthesis of Spiro-Fused Azacycles*, Royal Society of Chemistry Perkin Division 17th International Symposium: Synthesis in Organic Chemistry, Oxford, July 2001.

PUBLICATIONS

The following publications are being submitted as a result of this research project.

(i) Publication to be submitted to Perkin Transactions 2 in January 2002: O.Q. Munro, J.M. McKenzie and D. Gravestock, *Conformational Analysis: Crystallographic and Computational Studies of a Flexible Sulfone Derivative with Hairpin (π -stacked) and Stepped (open-chain) Conformations*.

(ii) Publication to be submitted to Perkin Transactions 1 in 2002: D. Gravestock and J.M. McKenzie, *Expedient Synthesis of 8-Oxo-1-spiro[4.4]nonanes*.

ABSTRACT

Cephalotaxine is a naturally occurring alkaloid which is the structural motif of a number of compounds which have shown promising anti-cancer properties. This fact together with its relatively complex pentacyclic structure, which incorporates an azaspirocycle annular to a benzazepine moiety, has resulted in its popularity as a synthetic target.

The aim of this project was to synthesise the azaspirocycle of cephalotaxine using a Noyori annulation method involving the reaction of an enamine and an α,α' -dibromo ketone in the presence of $\text{Fe}_2(\text{CO})_9$. In the first attempt the reaction of 1-benzyl-2-methylenepyrrolidine (**117**) with methyl 2,4-dibromo-3-oxobutanoate (**116**) proved to be unsuccessful, the electron withdrawing ester functionality of methyl 2,4-dibromo-3-oxobutanoate (**116**) being unable to stabilise the intermediates formed during the reaction and thus resulting in its failure. Reaction of 1-benzyl-2-methylenepyrrolidine (**117**) and 2,4-dibromo-3-pentanone (**114**) resulted in the formation of an azaspirocycle though in an extremely poor yield and the reaction was deemed inefficient for the synthesis of the cephalotaxine spirocycle. Finally, reaction of 2-(1-benzyl-2-pyrrolidinylidene)acetonitrile (**129**) and 2,4-dibromo-3-pentanone (**114**) resulted in the successful synthesis of a novel azaspirocycle. The product, 1-benzyl-7,9-dimethyl-8-oxo-1-azaspiro[4.4]nonane-6-carbonitrile (**130**), contained four stereogenic centres and one of the diastereomers was successfully crystallised out. The X-ray structure in conjunction with NOESY NMR experiments showed the relative stereochemistry to be $5S^*$, $6S^*$, $7S^*$, $9S^*$.

Significant progress was made in the application of this methodology to the construction of the cephalotaxine pentacyclic skeleton with the synthesis of a novel lactam, 1-[2-(6-iodo-1,3-benzodioxol-5-yl)ethyl]-2-pyrrolidinone, being achieved. In the course of this work a novel compound, 2-(6-Iodo-1,3-benzodioxol-5-yl)ethyl 4-methylbenzenesulfonate (**98**), was also synthesised and its X-ray structure revealed it to be conformationally interesting. As a result a conformation analysis study was carried out on this compound as well as 2-(6-Iodo-1,3-benzodioxol-5-yl)ethyl 4-nitrobenzenesulfonate (**15a**). The Noyori annulation reaction was not implemented in the route to the basic pentacyclic structure of cephalotaxine due to time constraints, however synthesis of analogues of cephalotaxine and other alkaloids possessing azaspirocycles should now be possible based on the methodology developed in this project.

Chapter 1

Introduction

1.1. BRIEF INTRODUCTION TO ALKALOIDS

Alkaloids are a unique class of natural products found predominantly in plants though they are also present in animals, insects and marine organisms to a lesser extent. Most of us are familiar with alkaloids such as caffeine, quinine, strychnine, morphine and nicotine. These compounds, as well as many other alkaloids, are well known to be biologically-active and thus alkaloids have become one of the classes of compounds used in the development of pharmacologically-active compounds. Alkaloids always have at least one nitrogen atom present, usually as a primary, secondary, or tertiary amine. The biological activity of many alkaloids stems from this amine functionality which can be transformed into a quaternary system by protonation at pH's found in the body. Defining an alkaloid precisely is no easy task and workers in the field have agreed that the various proposed definitions are guidelines with numerous exceptions.¹ However, to obtain an impression of an alkaloid one suggested "definition" is as follows: "An alkaloid is a cyclic organic compound containing nitrogen in a negative oxidation state which is of limited distribution among living organisms."¹

Though drugs containing alkaloids have been used for about 4000 years,² interest in alkaloids themselves started from 1803 when a semipure alkaloid named narcotine was isolated from opium.² Synthetic organic chemists have also come to see alkaloids as challenging synthetic targets with coniine being the first alkaloid synthesised in 1886.¹ With 40 % of plant families having at least one species containing an alkaloid¹ there is still plenty of opportunity for isolation of unknown alkaloids and subsequent synthesis and investigation of their biological activity. Alkaloids are sure to hold the attention of natural product chemists, pharmacologists, and organic synthetic chemists for many years to come.

Our interest in alkaloids lies with one particular compound, cephalotaxine. This naturally occurring alkaloid is structurally interesting and certain esters of the compound have anti-cancer properties which is why it has excited not only our interest but that of many others. A fuller introduction to this compound will now be given.

1.2. ISOLATION AND CHARACTERISATION OF CEPHALOTAXINE

In 1963 Paudler *et al.* investigated the alkaloids of the trees *Cephalotaxus fortunei* and *Cephalotaxus drupacae*.³ *Cephalotaxus fortunei* is found only in North China and is commonly called the Chinese plum yew while *Cephalotaxus drupacae*, also known as the Japanese plum yew, is found in both China and Japan. In their work Paudler *et al.* reported the isolation of the major alkaloid in these trees.³ The alkaloidal material was first extracted from the powdered leaves and stems of the plants using a standard acid-base extraction of the concentrated alcohol extracts. *Cephalotaxus fortunei* was found to contain 0.39 % alkaloidal material and *Cephalotaxus drupacae* 0.35 %. Of the four alkaloids present in *Cephalotaxus fortunei*, one alkaloid constituted 50 % of the mixture. Similarly, 54 % of the alkaloidal material of *Cephalotaxus drupacae* was a single alkaloid, five alkaloids being present in all. Comparison of the major alkaloid of each tree indicated they were in fact the same, and this crystalline compound was named cephalotaxine (1). Paudler *et al.* obtained a molecular formula, $C_{18}H_{21}NO_4$, and achieved a partial elucidation of the structure of cephalotaxine. The actual structure was later determined by NMR,⁴ and X-ray diffraction of cephalotaxine methiodide.⁵ These characterisations provided the relative configuration for cephalotaxine with an absolute configuration being provided later by Arora *et al.*⁶ who carried out an X-ray crystallographic study of the *p*-bromobenzoate of cephalotaxine and showed that natural (-)-cephalotaxine has a 3*S*, 4*S*, 5*R* configuration (Figure 1.1). The unique and challenging structure of cephalotaxine (1), which contains two spiro-fused five-membered rings annular to a benzazepine moiety with three stereogenic centres, has excited general interest in its laboratory synthesis. A further reason for interest in its synthesis is that it provides access to related esters which have pharmacological activity.

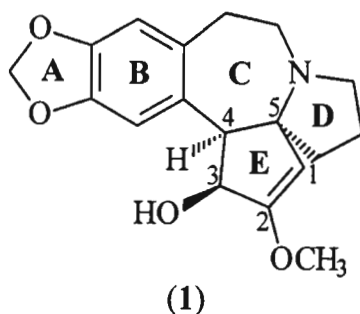


Figure 1.1. (-)-Cephalotaxine.

1.3. USES OF CEPHALOTAXINE ESTERS

Harringtonine (2), isoharringtonine (3), homoharringtonine (4), and deoxyharringtonine (5) (Figure 1.2) are esters of cephalotaxine which were first isolated from *Cephalotaxus harringtonia*,^{4,7,8} and are now known to be present in other plants of the *Cephalotaxus* genus.⁹ Though cephalotaxine itself is pharmacologically inactive these esters show anti-tumor activity with harringtonine (2), isoharringtonine (3), and homoharringtonine (4) having marginal activity against L1210 leukemia in mice with more significant activity being shown against P388 leukemia.¹⁰ Deoxyharringtonine (5) only shows activity against the latter type.

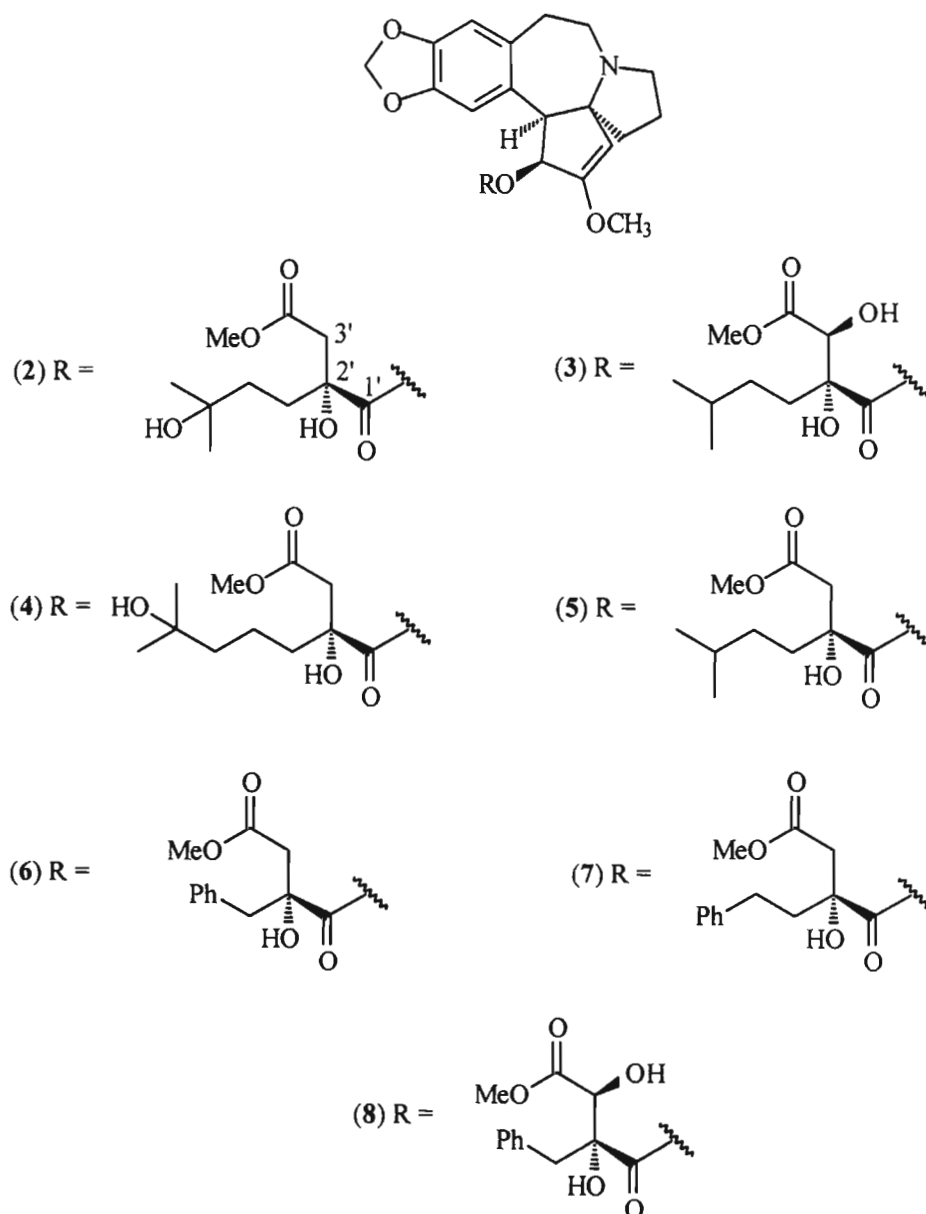


Figure 1.2. Some esters of cephalotaxine which exhibit anti-cancer properties.

More recently other minor ester-type *Cephalotaxus* alkaloids isolated from *Cephalotaxus harringtonia* have shown activity against P388 leukemic cells as well.¹¹ These esters, neoharringtonine (**6**), homoneoharringtonine (**7**), and 3' *S*-hydroxyneoharringtonine (**8**), are also shown in Figure 1.2. Interestingly, all the above-mentioned compounds exhibit the same *R* stereochemistry at the 2' position in the ester side chain and furthermore (**3**) and (**8**) have identical *S* stereochemistry at the secondary alcohol chiral centre 3'.

The anti-tumor activity of the cephalotaxine esters results from the inhibiting effect they have on protein synthesis in eukaryotic cells.¹² They act by blocking peptide bond formation and aminoacyl-tRNA binding.¹³ Though all of the cephalotaxine esters shown in Figure 1.2 have exhibited anti-cancer activity, most interest has been focussed on homoharringtonine (**4**). Investigations into its biological activity have shown it to be active against a number of different types of cancer such as mouse colon carcinoma;¹⁴ breast, lung, ovarian, and cervical tumors to varying degrees;¹⁵ and acute nonlymphoblastic leukemia (a particularly promising study showed a 25 % remission in patients with this disease).¹⁶ The use of homoharringtonine in the treatment of chloroquine-resistant malaria has even been investigated and has proved effective in initial testing.¹⁷ A study on the pharmacology of homoharringtonine concluded that it is rapidly metabolised in the body with the resulting metabolites having very different pharmacokinetics from homoharringtonine itself.¹⁸ It seems to be mainly eliminated from the body by metabolism or tissue sequestration as urinary excretions play only a small part in removal of homoharringtonine from the body. Unfortunately phase II trials of homoharringtonine have not produced encouraging results. In a trial which treated patients with a variety of solid tumors that had been exposed previously to chemotherapy it was concluded that homoharringtonine given by an intermittent schedule was inactive for these cases.¹⁹ Another phase II trial dealing with advanced acute nonlymphocytic leukemia (ANLL) stated that even though homoharringtonine has an anti-leukemic effect it is not useful on its own in treating ANLL, as no patients treated experienced remission.²⁰ Recently, in 1999, a trial using homoharringtonine for the treatment of patients with advanced large bowel cancer concluded that it had no activity against colorectal carcinoma.²¹ This trial was actually terminated prior to completion because of the unacceptable toxicity of homoharringtonine which was experienced. In fact, toxicity of homoharringtonine is noted by almost all workers who carried out human trials. The major side effects are cardiovascular with tachycardia, arrhythmia and ECG changes being experienced by patients.²²

Other side effects noted in a phase I trial treating children with refractory leukemia included nausea, vomiting, mucositis, diarrhoea, and skin rashes, with this study finding that the dose-limiting toxic effect was pain.²³ A phase I trial using adult patients noted the dose-limiting effect was myelosuppression.²⁴ Obviously the toxicity of homoharringtonine is the major obstacle to it becoming widely used as an anti-cancer agent. There is no doubt it has some anti-cancer properties but, as the phase II trials indicate, these are not necessarily as effective as initially hoped. Clearly structure-activity relationship (SAR) studies should be carried out on homoharringtonine and the other cephalotaxine esters so even though they may not become widely used as drugs themselves, other drugs may be developed based on their structures, with these drugs having reduced toxicity and increased activity. So far what is known from SAR studies is that a slight modification of the ester moiety significantly affects the anti-tumor activity of the esters of cephalotaxine.¹⁰ This is obviously not surprising as cephalotaxine itself is inactive as was mentioned earlier. What is also known from SAR studies is that the presence of the nitrogen lone pair is required for the anti-cancer properties to exist.²⁵ Thus it appears that more SAR studies will have to be carried out on the cephalotaxine esters in order to identify the structural features directly responsible for the anti-cancer properties and the groups that cause the toxicity.

1.4. SYNTHESSES OF CEPHALOTAXINE

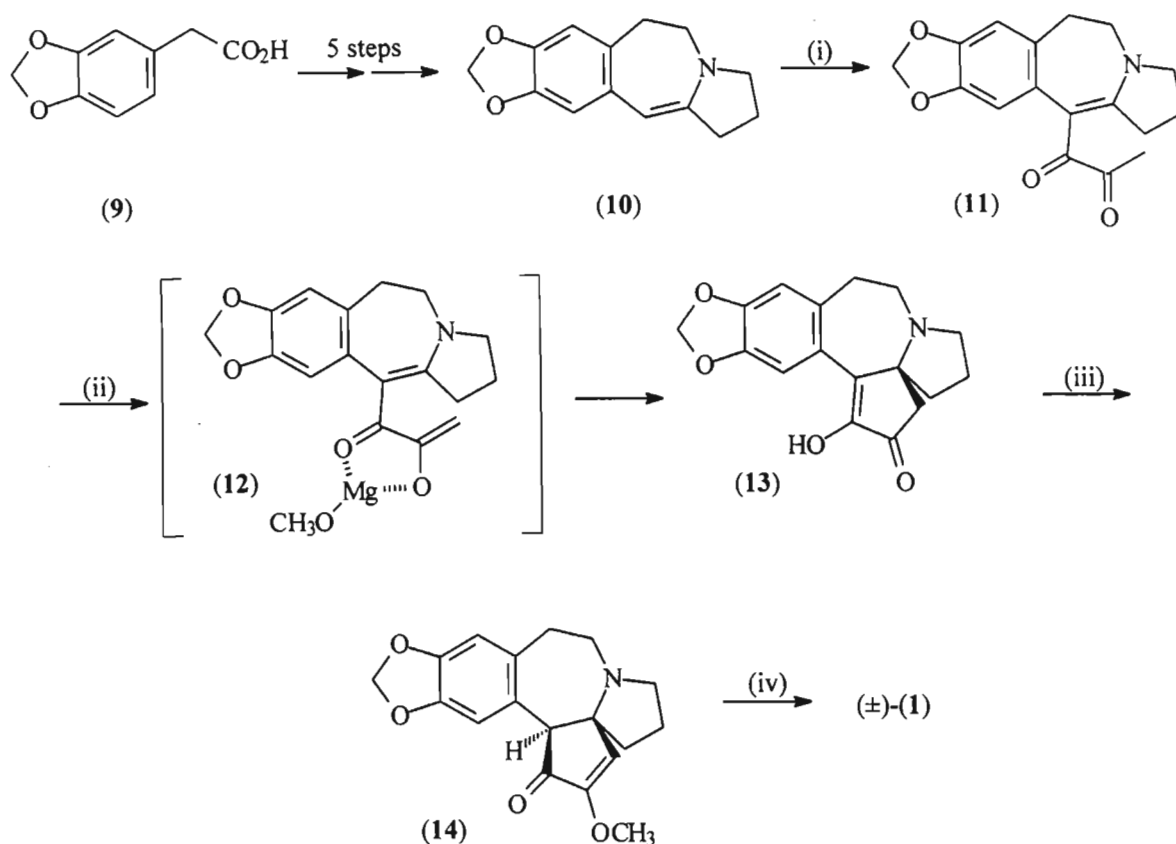
It should now be clear why cephalotaxine has become a well researched synthetic target. Not only is it structurally challenging for the synthetic chemist but there is real value in finding an efficient route to synthesise cephalotaxine as it provides direct access to its biologically active ester derivatives. As the *Cephalotaxus* trees are not widely available²⁶ and the alkaloids are only minor constituents of the trees,³ it is not ecologically or financially viable to obtain cephalotaxine or its ester derivatives from their natural sources. Thus a laboratory synthesis of cephalotaxine is especially appealing to allow reasonable quantities of the cephalotaxine esters to be obtained for further SAR studies. To date seven total syntheses of (\pm)-cephalotaxine have been published²⁷⁻³⁸ along with two papers on the total synthesis of (-)-cephalotaxine,^{39,40} one of which also reported the synthesis of (+)-cephalotaxine.⁴⁰ In addition, five formal syntheses have been reported for (\pm)-cephalotaxine⁴¹⁻⁴⁵ and one for (-)-cephalotaxine.⁴⁶ The first synthesis was published in 1972²⁷ with the most recent appearing in 1999,⁴⁶ indicating that an efficient synthetic route to cephalotaxine is still of current interest. Following is a review of the different syntheses of

cephalotaxine which analyses the approaches of other researchers and will serve as a reference for a comparison with our proposed synthetic route. The work which we carried out revolved around developing a novel method to form the azaspirocycle, thus in the syntheses reviewed here it is mainly the method for constructing the cephalotaxine azaspirocycle that is summarised. The azaspirocycle is the most challenging feature of the cephalotaxine structure, and general routes for the formation of spirocycles are not widely found in the literature. In general a basic outline of the method for each cephalotaxine synthesis is given with detail being shown for the formation of the azaspirocycle. Reference to the A, B, C, D, and E rings of cephalotaxine will often be made and so the reader is referred back to Figure 1.1 which shows these ring labellings. The syntheses have been divided into total and formal syntheses and are discussed in chronological order though parallels are sometimes drawn between the approaches of different workers.

1.4.1. Total Syntheses of Cephalotaxine

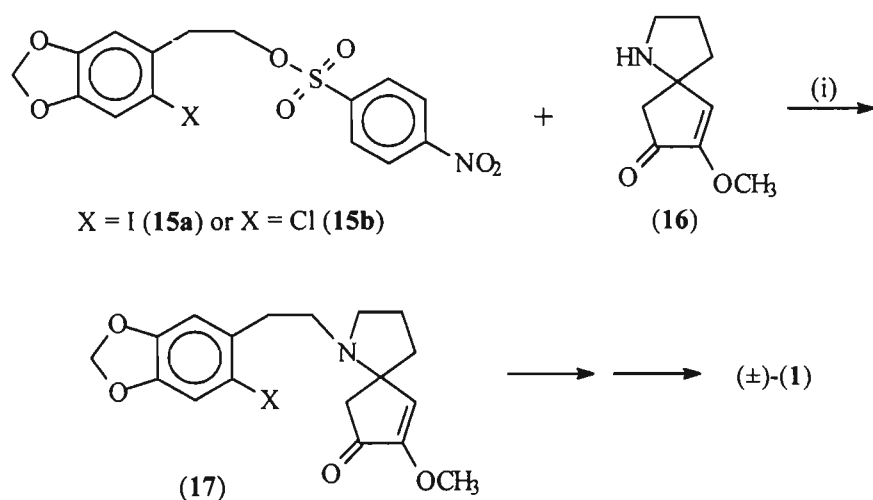
Auerbach and Weinreb were the first workers to publish a total synthesis of (\pm)-cephalotaxine. This synthesis appeared as a communication in October 1972²⁷ and was followed up with a full paper in 1975.²⁸ Their approach (Scheme 1.1) was linear with the synthesis starting with the A and B rings of cephalotaxine intact and then the D, C and E rings were built on sequentially in that order. This means the spirocycle was the last major feature built into the molecule and its formation started once Auerbach and Weinreb had obtained enamine (**10**) in five steps from 3,4-methylenedioxyphenylacetic acid (**9**). The enamine (**10**) was added to a mixture of pyruvic acid and ethyl chloroformate which formed a mixed anhydride that reacted with (**10**) to form the diketone (**11**) in 73 % yield. The cyclisation to form the spirocycle was an intramolecular Michael reaction using magnesium methoxide in methanol. The intermediate (**12**) was probably formed during this reaction by the chelation of the enolate of (**11**) with magnesium methoxide. The compound formed as a result of the Michael addition is known as demethylcephalotaxinone (**13**) and is also a naturally-occurring *Cephalotaxus* alkaloid which was first isolated and identified by Powell and Mikolajczak from *Cephalotaxus harringtonia*.⁴⁷ Demethylcephalotaxinone (**13**) was converted to cephalotaxinone (**14**) by methylation using 2,2-dimethoxypropane and *p*-TsOH. Cephalotaxinone (**14**) is also a naturally-occurring *Cephalotaxus* alkaloid⁴⁸ and was easily reduced to give (\pm)-cephalotaxine (**1**) which was obtained in an overall yield of 8 % from 3,4-methylenedioxyphenylacetic acid (**9**). Even though this was the first synthesis of cephalotaxine published it is one of the more elegant being carried out in

only nine steps. The formation of the spirocycle structural unit was notably achieved in an efficient manner.



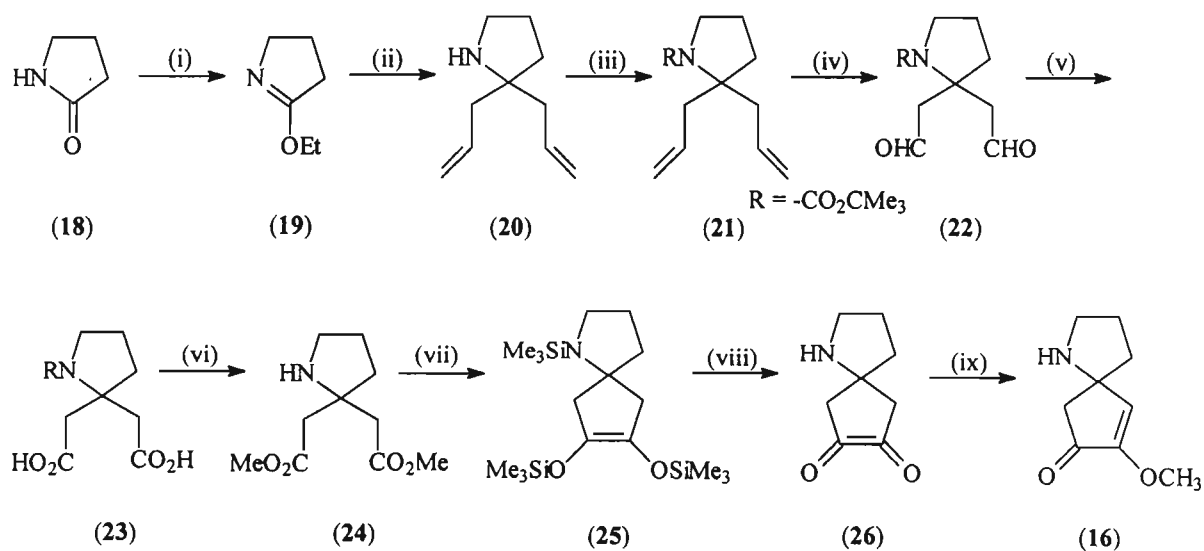
Scheme 1.1. (i) pyruvic acid, ethyl chloroformate, 0 °C, 73 %; (ii) MgOMe, MeOH, 58 %; (iii) 2,2-dimethoxypropane, *p*-TsOH, 45 %; (iv) NaBH₄, 85 %.

Semmelhack *et al.* published their synthesis of (±)-cephalotaxine in November 1972 as a communication,²⁹ following closely on the heels of Auerbach and Weinreb.²⁷ The full paper of their work appeared alongside that of Auerbach and Weinreb²⁸ in 1975.³⁰ In contrast to that of Auerbach and Weinreb their synthesis featured a convergent strategy in which two major portions of the molecule were prepared independently of each other before being brought together in the final stages of the synthesis. The two key intermediates formed were *p*-nitrobenzenesulfonate ester (15), containing the A and B rings of cephalotaxine, and the spirocycle (16) which contains the D and E rings. The two bicycle moieties were joined (Scheme 1.2) to form the four-ring backbone (17) which was finally cyclised and reduced to form (±)-cephalotaxine (1).



Scheme 1.2. (i) Diisopropylethylamine, MeCN, 70 % (X = I) or 88 % (X = Cl).

Scheme 1.3 shows the synthesis of the spirocycle (**16**) which Semmelhack *et al.* achieved in nine steps from pyrrolidinone with a 22-23 % yield.³⁰ The first step in the spirocycle formation was the addition of triethyloxonium fluoroborate to pyrrolidinone (**18**) in order to form the imidate ester (**19**) in 73 % yield.

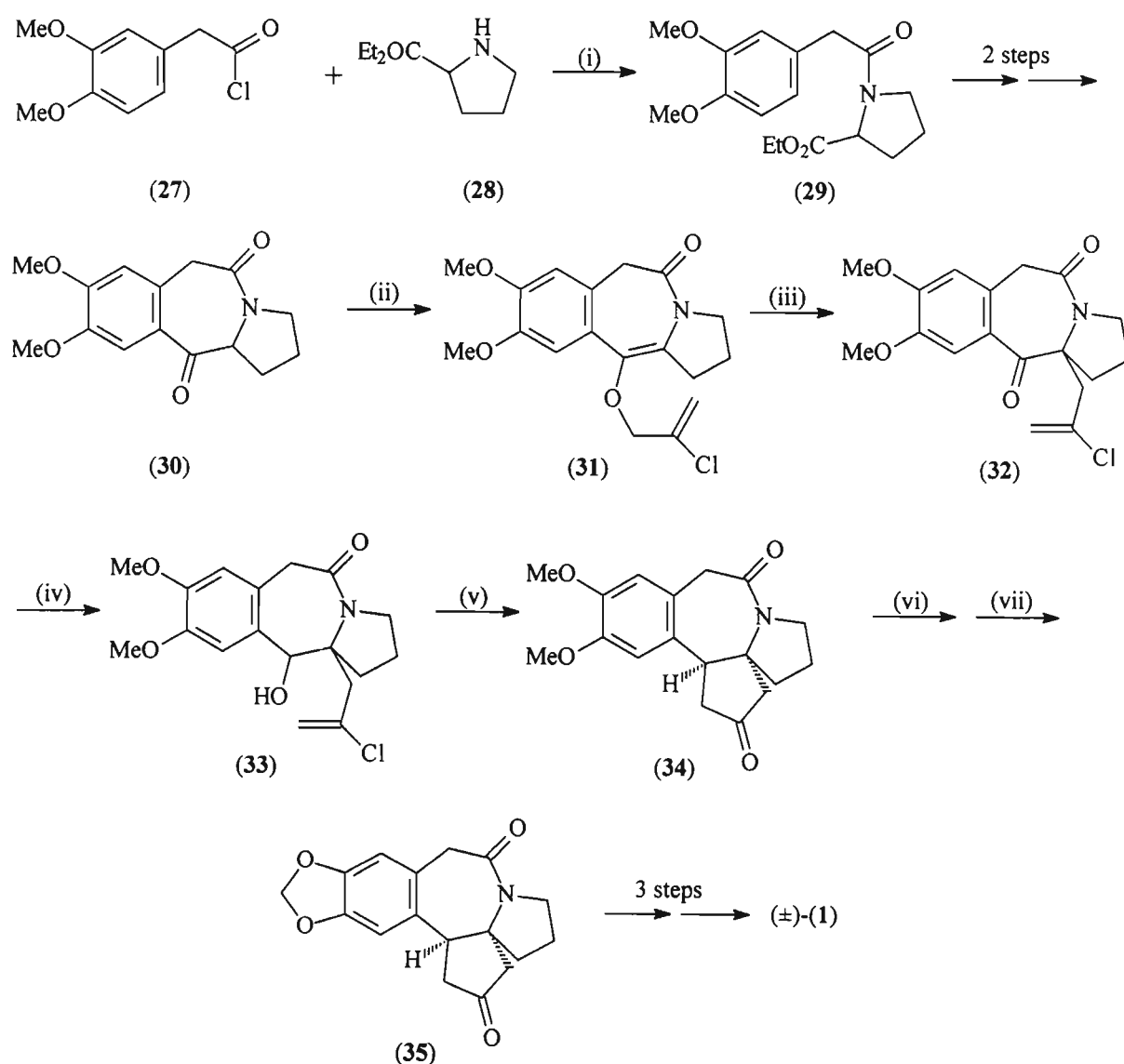


Scheme 1.3. (i) triethyloxonium fluoroborate, 0 °C, 73 %; (ii) Mg, BrCH₂CH=CH₂, 78 %; (iii) *tert*-butoxycarbonyl azide, MgO, Δ, 100 %; (iv) (a) O₃, MeOH, -78 °C, (b) Me₂S; (v) Ag₂O, 13 % KOH; (vi) MeOH, H⁺, triethyl orthoformate; (vii) Na/K alloy, TMSCl; (viii) Br₂, -78 °C; (ix) CH₂N₂, 0 °C.

The diallyl derivative (**20**) was obtained by addition of the Grignard reagent allylmagnesium bromide to imidate ester (**19**). In order to achieve the ring closure of the second five membered ring in the spirocycle the two allyl groups were converted to methyl esters. However, before this could be carried out the amine of the diallyl derivative (**20**) was protected using *tert*-butoxycarbonyl azide. Without distillation or chromatography the protected amine (**21**) was obtained quantitatively in what was considered to be sufficient purity. Conversion of carbamate (**21**) to the required diester (**24**) was carried out in three steps without isolation of the intermediates. Ozonolysis of carbamate (**21**) followed by the addition of Me₂S resulted in the formation of the dialdehyde (**22**) which was oxidised to the diacid (**23**) by addition of Ag₂O in the presence of an aqueous KOH solution. In order to obtain the diester (**24**) a Fisher esterification was used with the conditions of this reaction also resulting in the removal of the *tert*-butoxycarbonyl protecting group. The three-step conversion of the protected diallylpyrrolidine (**21**) to the diester (**24**) was achieved in a 61 % overall yield. The final three steps of the synthesis to form the desired azaspirocycle (**16**) were again carried out without isolation of the intermediates because of the tendency of these compounds to decompose. In an acyloin condensation reaction the diester (**24**) was reacted with a 1:5 sodium-potassium alloy and TMSCl to effect the ring closure of the second five-membered ring. The structure of the silylated spirocycle (**25**) was not assigned with complete confidence as only a crude sample was analysed due to the decomposition of the compound during attempted purification by distillation. The silylated compound was oxidised with a solution of bromine in dichloromethane to give the diketone (**26**) which was finally selectively methylated with diazomethane to give the required azaspirocycle (**16**). The conversion of the diester (**24**) to the azaspirocycle (**16**) was achieved in a 66 % yield. For further reactions involving the azaspirocycle (**16**) the crude product was used because large amounts were lost during purification steps as the compound was found to be fairly unstable. The synthesis of cephalotaxine by Semmelhack *et al.* was fairly lengthy in contrast to that of Auerbach and Weinreb.^{27,28} However, the overall yield achieved by Semmelhack's group was 16 % from 3,4-methylenedioxyphenylacetic acid which was an improvement on that of Auerbach and Weinreb's 8 %.

Hanaoka and co-workers synthesised (±)-cephalotaxine in 12 steps with an overall yield of 6%.³¹ Starting with the condensation of 3,4-dimethoxyphenylacetyl chloride (**27**) and ethyl prolinatate (**28**) the amide (**29**) was formed to join the B and D rings of cephalotaxine (Scheme 1.4). A

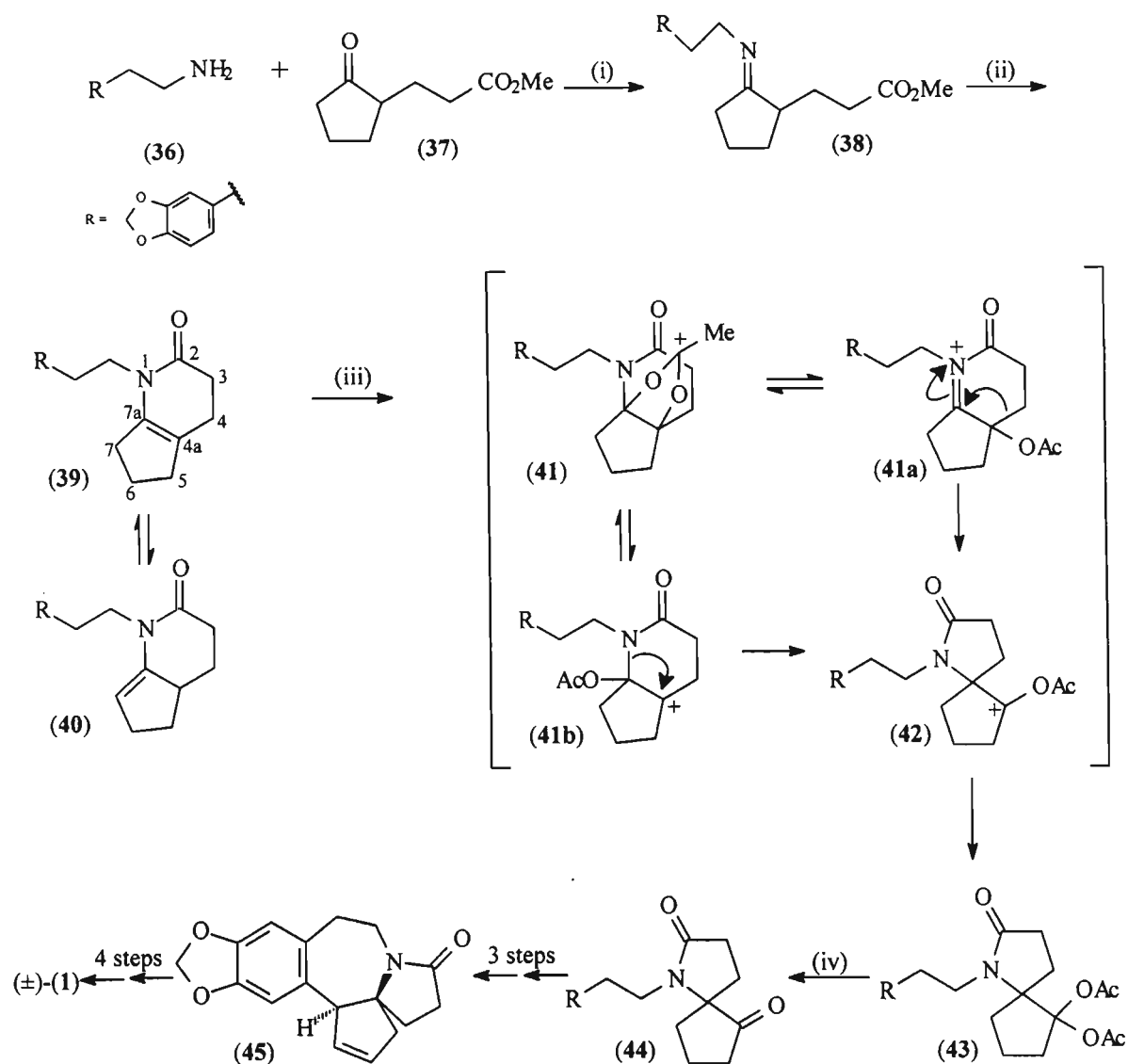
further two steps facilitated the closure of the C ring to form tricycle (30). At this point the spirocycle formation was carried out starting with the addition of 2,3-dichloropropene and NaH in DMF to tricycle (30) giving the allyl vinyl ether (31) in a 91 % yield. Heating of the allyl vinyl ether (31) to 150 °C induced a Claisen rearrangement which formed tricycle (32). A quantitative NaBH₄ reduction of tricycle (32) afforded the alcohol (33) which was cyclised to provide the spirocycle (34).



Scheme 1.4. (i) 89 %; (ii) 2,3-dichloropropene, NaH, 91 %; (iii) 150 °C, 97 %; (iv) NaBH₄, 100 %; (v) 90 % H₂SO₄, Δ, 69 %; (vi) BBr₃, -78 °C, 79 %; (vii) CH₂Br₂, KF, 33 %.

Before the functionalisation of the spirocycle was carried out the A ring was formed in two steps. This was accomplished by demethylation of the dimethoxy unit with boron tribromide to give the diol which was then reacted with CH_2Br_2 to close the A ring giving the 3,4-methylenedioxy derivative (**35**). The final three steps of the synthesis resulted in the correct functionalisation of the E ring to give (\pm)-cephalotaxine (**1**) as required. In this synthesis the spirocycle moiety was created efficiently and with good yields, thus it was unfortunate that the overall yield of (\pm)-cephalotaxine was reduced by low yields for the formation of the A ring. The A ring formation took two steps with the first step having a yield of 79 % and the second step a yield of only 33 % - the lowest yield of all 12 steps in this synthesis! Hanaoka and co-workers did not give a reason why it was necessary to build the A ring during the synthesis rather than have it intact from the beginning as in other syntheses of cephalotaxine. They may have experienced a situation similar to that of Isono and Mori in their synthesis of (-)-cephalotaxine³⁹ (reviewed later) where they found that the presence of the methylenedioxy A ring inhibited the cyclisation of the seven-membered C ring. As a result the A ring formation was carried out in the later stages of the cephalotaxine synthesis after the seven-membered ring had been successfully formed.

In 1988 Kuehne and co-workers published a synthesis of (\pm)-cephalotaxine which they carried out in twelve steps from 3,4-(methylenedioxy)nitrostyrene.³² The spirocycle formation in this synthesis followed a notably different approach from that of the other groups reviewed up to this point. Their spirocycle synthesis started with a cyclopentane ring fused to a δ -lactam. Their intention was that this system could be rearranged to the desired spirocycle as they expected that a γ -lactam would be favoured over a δ -lactam should these two be in a situation where they were in equilibrium, as this is found to be the case for lactones. The overall cephalotaxine synthesis of Kuehne and co-workers (Scheme 1.5) started with the amine (**36**) which had been formed from the corresponding nitrostyrene. This amine (**36**) was reacted with the cyclopentanone derivative (**37**) (previously obtained from the alkylation of the pyrrolidine enamine of cyclopentanone) to form the imine (**38**). Heating under vacuum effected the cyclisation of the imine (**38**) to the desired lactam (**39**) and its unwanted double-bond isomer (**40**). Separation of the two isomers was carried out and it was found that under mild conditions the purified compounds isomerised to a 6:4 mixture of (**39**) and (**40**) respectively. Thus to improve yields of lactam (**39**) the unwanted lactam (**40**) was isomerised after its initial separation from (**39**).

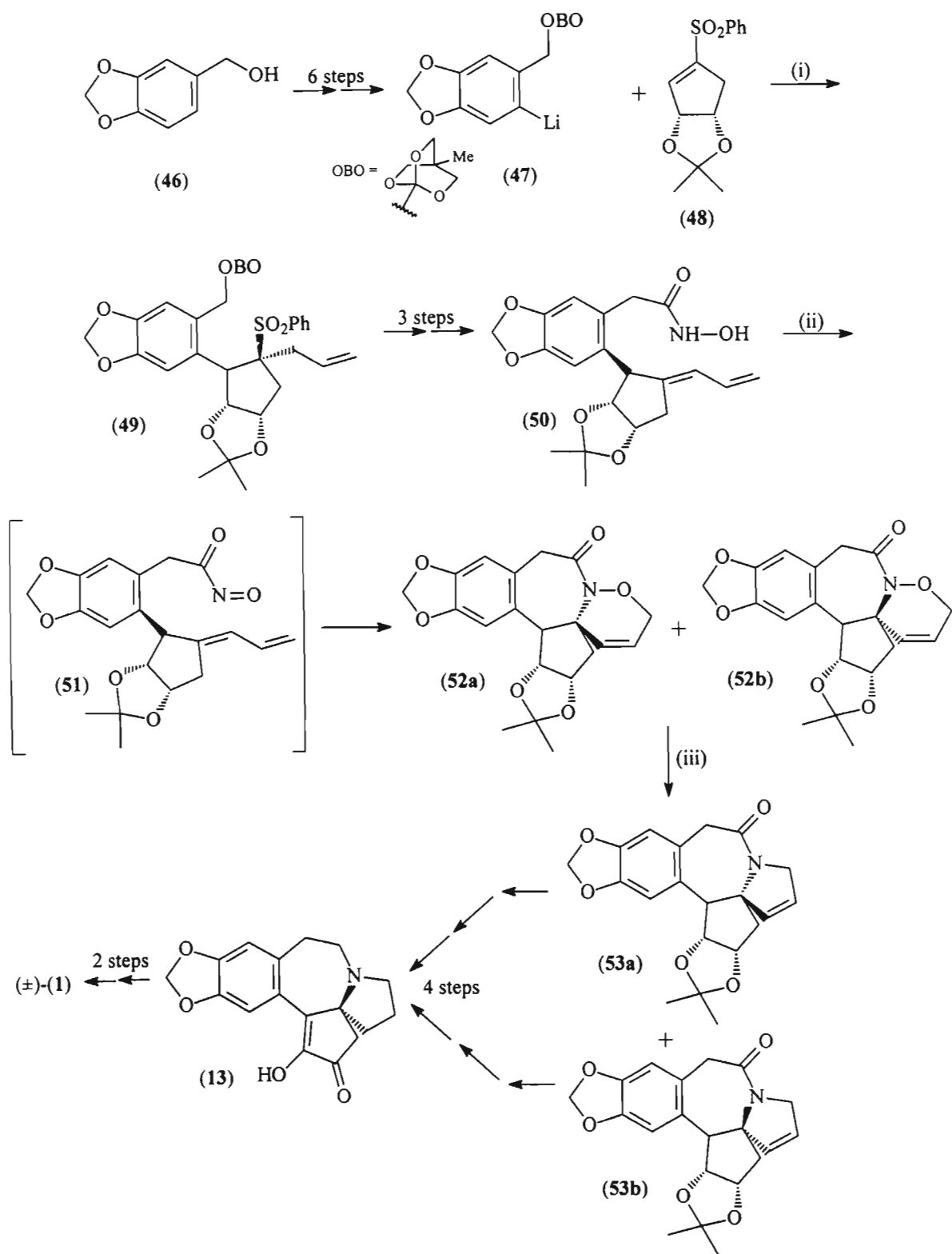


Scheme 1.5. (i) *p*-TsOH; (ii) Δ , vacuum, 96 % from (36); (iii) $\text{Pb}(\text{OAc})_4$, Δ ; (iv) NaOMe, MeOH, 78-94 % from (39).

To carry out the rearrangement to form the spirocycle the lactam (39) was reacted with $\text{Pb}(\text{OAc})_4$ and the desired spirocycle (44) was obtained along with the diacetate (43). This mixture was converted entirely to (44) on stirring with NaOMe in MeOH resulting in a 89 % yield from (39). It was thought that the spirocycle formation might follow a pathway in which a bridging acetal carbocation (41) was formed initially from (39) with this resulting in the generation of either the iminium ion (41a) or the carbocation (41b). A rearrangement of the C-C bond in the iminium ion intermediate (41a) would effect the contraction of the δ -lactam to the γ -lactam (42) while a N-C bond shift in (41b) would give the same product (42). Evidence for the existence of both

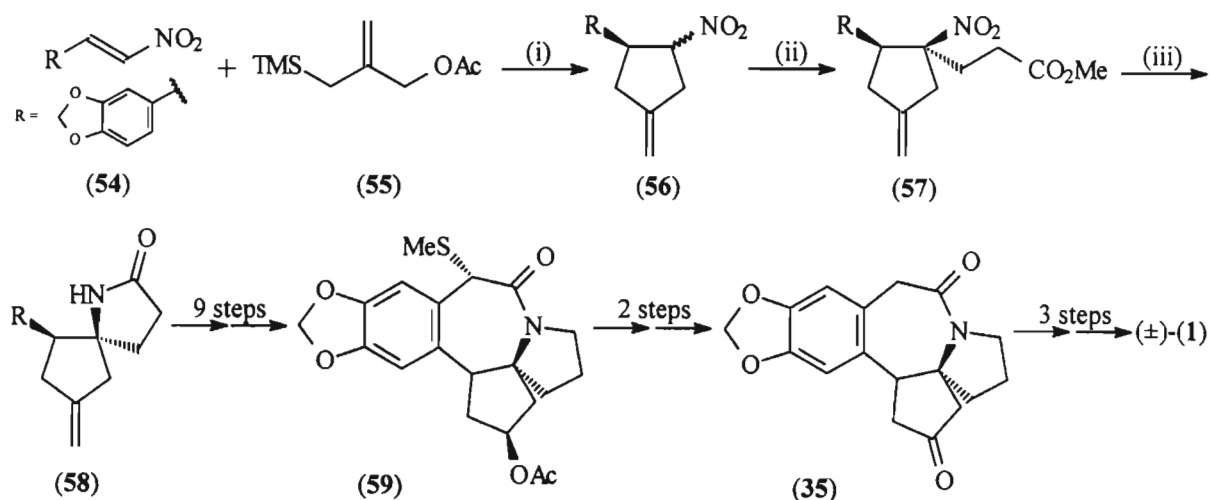
pathways was obtained when a deuterium analogue of (39) (substituted at C-7) was used in the reaction with Pb(OAc)₄. The authors also felt that radical equivalents of the intermediates (41), (41a), (41b), and (42) were feasible as oxidations with Pb(OAc)₄ at elevated temperatures are recognised as homolytic processes. The remainder of the synthesis of Kuehne and co-workers resulted in the closing of the seven-membered C ring to give pentacycle (45) and the correct functionalisation of the E ring to afford (±)-cephalotaxine in a 33 % overall yield from 3,4-(methylenedioxy)nitrostyrene without double-bond isomerisation of the unwanted lactam (40) or a 53 % yield with the double-bond isomerisation carried out. In comparison with the yields of other syntheses of (±)-cephalotaxine the yield of Kuehne and co-workers is excellent.

Burkholder and Fuchs published a communication of their (±)-cephalotaxine synthesis in 1988³³ followed by the corresponding full paper in 1990.³⁴ Their synthesis was comparatively lengthy, requiring 18 steps to achieve the target molecule. It began with the A and B rings of cephalotaxine intact in the form of piperonal alcohol (46) (Scheme 1.6). In six steps this was converted to the lithiated compound (47) which underwent a conjugate addition to vinyl sulfone (48). The α-sulfone anion intermediate that was formed was trapped with allyl bromide to give allyl sulfone (49) which now also contained the cephalotaxine E ring. A further three steps provided the correct functionalisation for the molecule to undergo an intramolecular Diels-Alder reaction which resulted in the formation of the seven-membered ring and provided the basis of the spirocycle. Thus the hydroxamic acid (50) was reacted with tetra-*n*-butyl ammonium periodate at -78 °C giving the acyl nitroso intermediate (51) which was allowed to warm to room temperature over seven hours affording two Diels-Alder products (52a) and (52b). Because the diene could attack from either face of the phenyl ring it resulted in two lactam isomers (52a) and (52b) being formed. With the seven-membered ring formed the spirocycle was obtained in three further steps without isolation of the intermediates or separation of isomers. The reductive cleavage of the N-O bond of both lactam isomers (52a) and (52b) afforded the corresponding allylic alcohols which could be separated but were rather carried through the next two steps where they were reacted with MsCl to give the corresponding mesylates and subsequently reacted with NaH to effect the ring closure to afford spirocycles (53a) and (53b). At this point (53a) and (53b) were separated and treated individually, both isomers ultimately leading to demethylcephalotaxinone (13), which was converted in a further two steps to the desired (±)-cephalotaxine (1) by a modification of the Auerbach and Weinreb procedure.^{27,28}



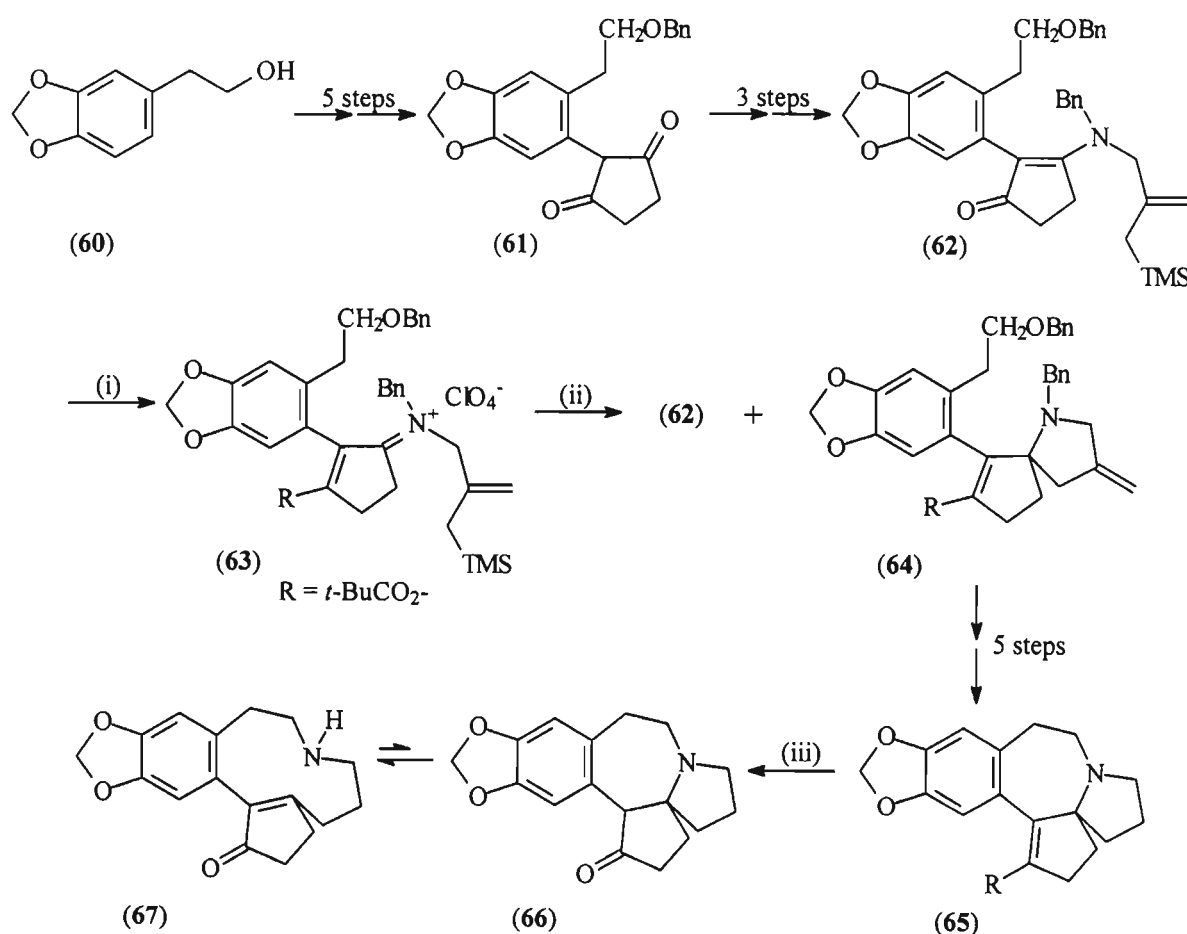
Scheme 1.6. (i) (a) $-78\text{ }^{\circ}\text{C}$, (b) $\text{CH}_2=\text{CHCH}_2\text{Br}$, 77 %; (ii) tetra-*n*-butyl ammonium periodate, $-78\text{ }^{\circ}\text{C}$ to RT, 71 %; (iii) (a) 6 % Na(Hg), EtOH, (b) MsCl, Et_3N , $0\text{ }^{\circ}\text{C}$; (c) NaH, 23 % (53a), 45 % (53b).

Ikeda and co-workers achieved the synthesis of (\pm)-cephalotaxine in 17 steps from 3,4-(methylenedioxy)nitrostyrene, the overall yield being 21 %.^{35,36} Scheme 1.7 shows how the spirocycle formation was achieved in only three steps from the start of the synthesis which began with the [3+2] cycloaddition of 3,4-(methylenedioxy)nitrostyrene (**54**) and 2-(trimethylsilylmethyl)-2-propenyl acetate (**55**) to form the methylenecyclopentane (**56**). This was then alkylated with methyl acrylate in a Michael addition reaction to give the ester (**57**). Reduction of nitroester (**57**) with zinc in boiling ethanolic HCl resulted in a cyclisation reaction to form the spirocycle moiety in the form of the lactam (**58**). At this point four of the five rings of cephalotaxine were present with only the seven-membered C ring remaining to be formed. It was the formation of the C ring which required more effort but was finally achieved in a further nine steps by mean of a sulfur-assisted aromatic cyclisation giving pentacycle (**59**). Desulfurisation of (**59**) followed by conversion of the acetyl group into a ketone gave the ketolactam (**35**). This compound was an intermediate in the synthesis of Hanaoka and co-workers³¹ and so following their procedure, Ikeda and co-workers achieved the conversion of the ketolactam (**35**) to (\pm)-cephalotaxine (**1**).



Scheme 1.7. (i) (*i*-PrO₃)P, Δ , 90 %; (ii) methyl acrylate, Triton B, *t*-BuOH, 100 %; (iii) (a) Zn, EtOH, HCl, Δ , (b) NaOH, Δ , 81 %.

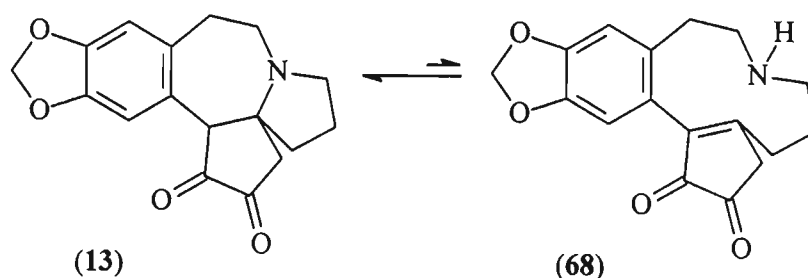
Mariano and co-workers succeeded in making (\pm)-cephalotaxine by two different routes with both leading to the same intermediate which was then converted to (\pm)-cephalotaxine in six steps.^{37,38} Their first route was quite lengthy and formed the spirocycle using a single electron transfer (SET) promoted photocyclisation reaction. However, the spirocycle functionality was later destroyed and reformed in the last six steps of the synthesis having made its original formation unnecessary. This led to the development of the second, shorter route in which the spirocycle formation was left to the end of the synthesis. Even though the second route was shorter and more efficient both routes will be reviewed here as the SET promoted photocyclisation of the first route is an interesting method for the spirocycle formation.



Scheme 1.8. (i) *t*-BuCOCl, AgClO₄, 97 %; (ii) hv, MeCN, 46 % (64), 40 % (62); (iii) NaOMe, MeOH, 79 %.

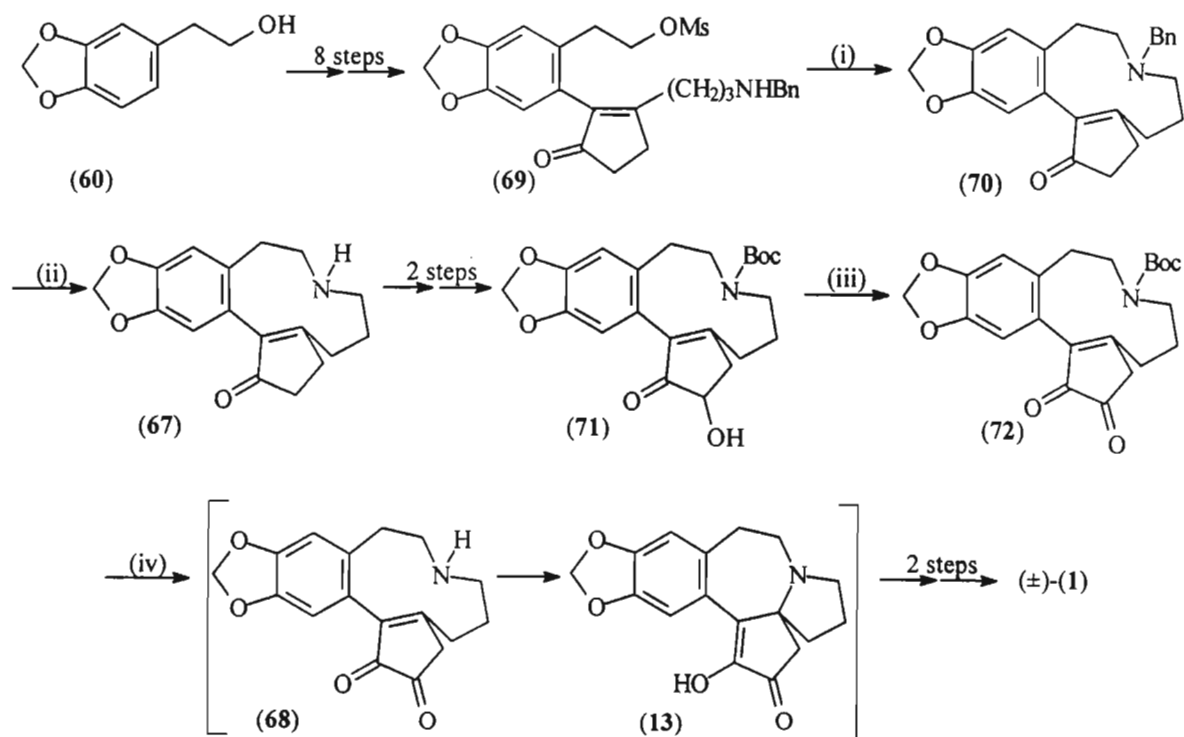
The first route (Scheme 1.8) began with 3,4-methylenedioxyphenyl alcohol (60) which was converted to the diketone (61) in five steps to join the A and B rings to the E ring. The SET

promoted cyclisation to form the spirocycle was based on methodology that Mariano's group had previously developed^{49,50} and required the formation of a silylallyliminium salt. So in three further steps the diketone (**61**) was converted to enaminone (**62**) which underwent *O*-pivaloylation to afford the desired silylallyliminium salt (**63**). The cyclisation was carried out by irradiation of an acetonitrile solution of the salt (**63**) to give the spirocycle (**64**). Only about 50 % of the salt was converted as prolonged irradiation tended to lower the yield of the spirocycle (**64**) as it was able to undergo a second photoreaction in its protonated form. Based on the quantity of the salt converted the spirocycle (**64**) was obtained in a 46 % yield along with the enaminone precursor (**62**) being obtained in a 40 % yield as a result of depivaloylation of the salt (**63**). From mechanistic studies it appeared that the silylallyliminium salt forms a diradical intermediate that can undergo either cyclisation followed by desilylation or desilylation followed by cyclisation, both routes giving the desired spirocycle (**64**). With the spirocycle intact a further five steps enabled the C ring of cephalotaxine to be formed creating the basic pentacyclic structure. Unfortunately the next step destroyed this structure, notably the spirocycle moiety. The original intention was to transform the pentacyclic ester (**65**) to the corresponding ketone and then form the Auerbach and Weinreb intermediate, demethylcephalotaxinone (**13**), which can be easily converted to cephalotaxine.^{27,28} Reduction of pentacyclic ester (**65**) with NaOMe in MeOH gave the desired ketone (**66**). Unfortunately (**66**) was only the minor part of an inseparable 10:1 mixture, the other major part consisting of the ring opened amino enone (**67**). Spectroscopic data confirmed the presence of both products with evidence indicating that (**66**) and (**67**) interconvert rapidly, as neither reaction temperature nor chromatography altered the 10:1 ratio. This situation did not fit in with the intended strategy to form demethylcephalotaxinone but the opportunity to take advantage of this ring opening phenomenon was seen.



Scheme 1.9.

Mariano and co-workers suggested that this rapid equilibrium might also exist with demethylcephalotaxinone, but here the equilibrium would favour the ring closed form. Scheme 1.9 shows this interconversion between demethylcephalotaxinone (**13**) and the ring opened enedione (**68**). Here demethylcephalotaxinone (**13**) exists as the keto tautomer rather than as the enol tautomer we have seen earlier. The strategy based on this hypothesis was to use the ring opened enone (**67**), that was unintentionally formed, and convert it to the enedione (**68**) which would spontaneously cyclise to the desired demethylcephalotaxinone (**13**). This strategy essentially meant that many of the steps leading up to forming enone (**67**) were unnecessary, most especially the spirocycle formation. Thus a significantly shorter route to (**±**)-cephalotaxine taking 16 steps.

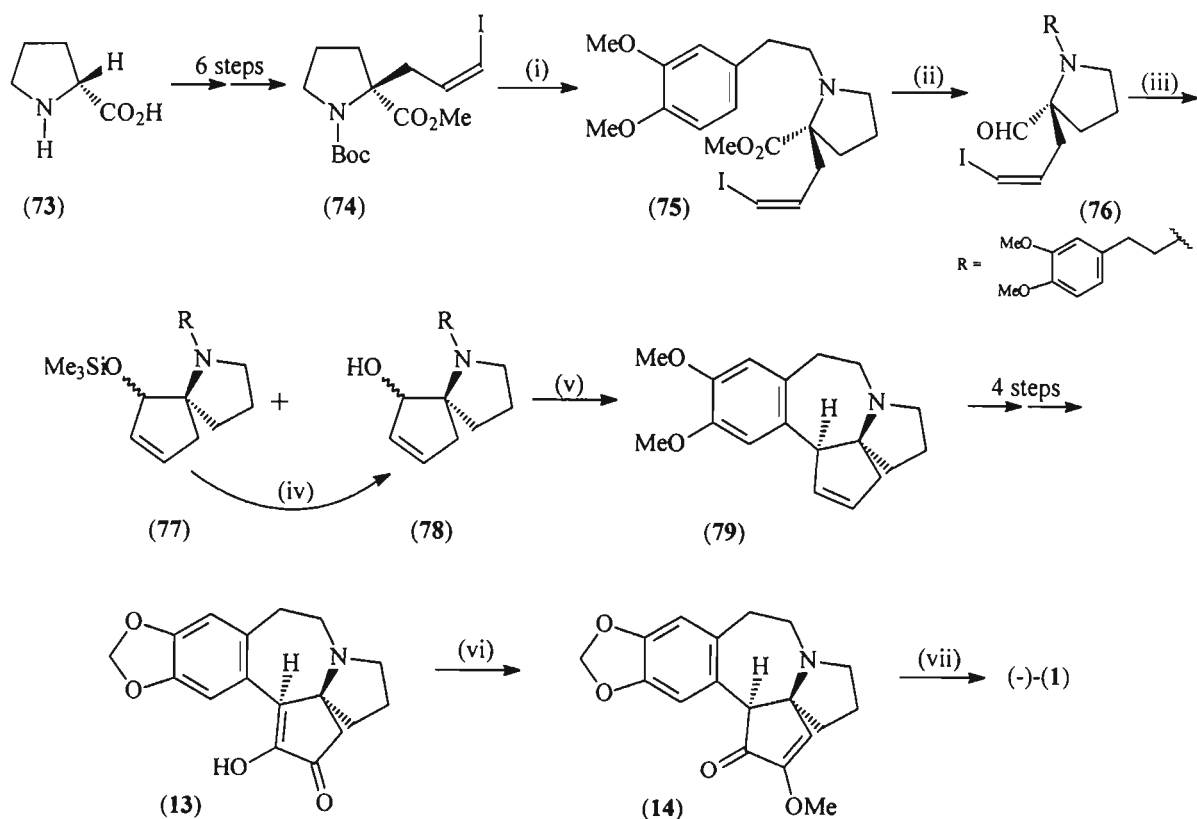


Scheme 1.10. (i) diisopropylethylamine, 64 % (reductive amination and cyclisation steps); (ii) H_2 , Pd/C, 83 %; (iii) DMSO, trifluoroacetic anhydride, -78°C ; (iv) trimethylsilyl trifluoromethanesulfonate, 0°C , 50 % [from (**71**)].

The second route is shown in Scheme 1.10 and again started with the alcohol (**60**) which was converted to the mesylate (**69**) in eight steps. Ring closure of (**69**) carried out by treatment with diisopropylethylamine afforded the macrocycle (**70**) which gave the desired product (**67**) on debenzoylation. With enone (**67**) formed via a shorter route, the rest of the synthesis, which is also shown in Scheme 1.10, could be attempted. The nitrogen atom of the amino enone (**67**) was protected with a Boc group and the alcohol functionality incorporated to give the α -hydroxy ketone (**71**) in two steps. This was oxidised to the diketone (**72**) which only required deprotection of the amine to form the hypothesised ring-opened form of demethylcephalotaxinone (**68**) which would presumably cyclise spontaneously to demethylcephalotaxinone (**13**). This is the result that was obtained, thus proving the theory proposed by Mariano and co-workers correct. Again the modified Auerbach and Weinreb procedure was employed to convert demethylcephalotaxinone (**13**) to (\pm)-cephalotaxine.^{27,28} The shorter of the two routes provided (\pm)-cephalotaxine in 16 steps with a 7 % overall yield from the 3,4-methylenedioxyphenyl alcohol (**60**). It is interesting to note that Mariano's group was dynamic and flexible in carrying out this work. The group started with a specific route in mind which would make use of a SET promoted photocyclisation reaction developed in their laboratory, but when this did not work as planned they capitalised by taking advantage of the results they had obtained and completely abandoned the original route containing the novel methodology to develop a new and quicker route to form their target molecule.

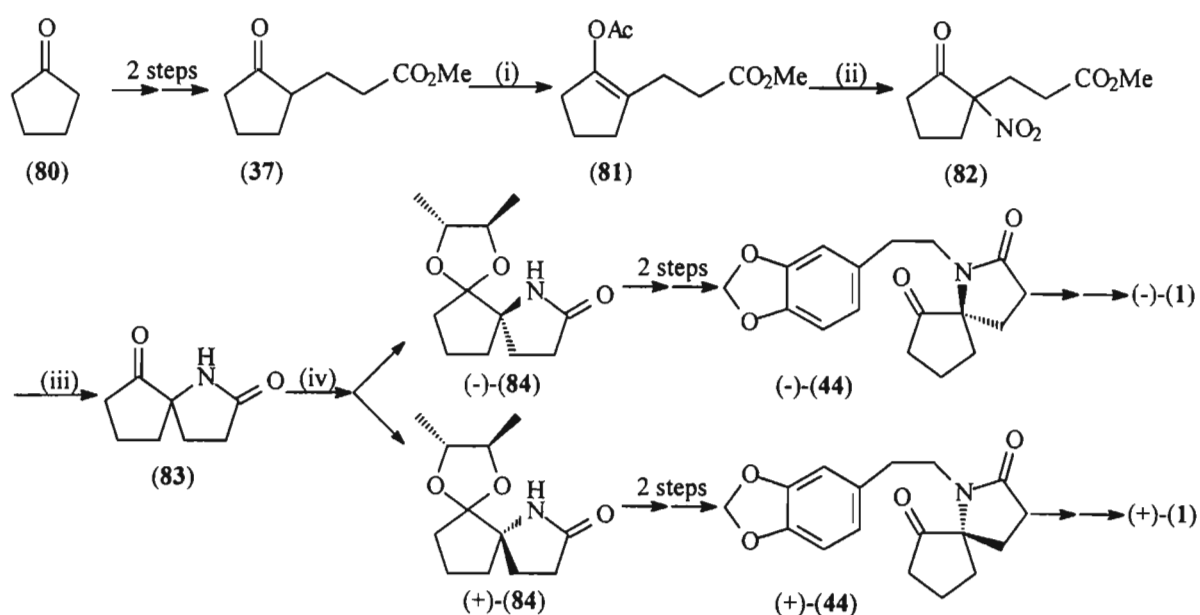
In 1995 Isono and Mori published the first synthesis of enantiomerically pure (-)-cephalotaxine.³⁹ As for the syntheses of many enantiomerically pure compounds their route started with a substance from the chiral pool, in this case *R*-proline (**73**), which was converted into the *N*-protected vinyl iodide (**74**) over six steps (Scheme 1.11). Removal of the Boc protecting group followed by addition of 2-(3,4-dimethoxyphenyl)ethyl alcohol *p*-nitrobenzenesulfonate ester afforded the bicycle (**75**) in an 88 % yield. To set the stage for the spirocycle formation the ester functionality of (**75**) was reduced to give the aldehyde (**76**) with the cyclisation of (**76**) being achieved by reaction with Me₃SiSnBu₃ and CsF giving two products (**77**) and (**78**). The desired product was the alcohol (**78**) which was obtained in an 85 % yield, while the undesired silyl ether (**77**) was only obtained in a 3 % yield and could be easily converted to (**78**) by treatment with TBAF. With the B, D, and E rings intact, cyclisation to form the C ring of cephalotaxine was achieved by reaction of the alcohol (**78**) with polyphosphoric

acid. This reaction had been attempted with the methylenedioxy A ring already intact but was unsuccessful, thus the A ring was formed after the seven-membered C ring in two steps using the same procedure as Hanaoka and co-workers.³¹ This was followed by the conversion of the alkene to a diol which was oxidised to give demethylcephalotaxinone (**13**). Reaction of (**13**) with 2,2-dimethoxymethane in the presence of *p*-TsOH gave the expected product of cephalotaxinone (**14**) though it was found to be racemic which, for the purposes of Isono and Mori, was undesirable. The desired (-)-cephalotaxinone (**14**) was however obtained in a 47 % yield when (**13**) was reacted with methyl orthoformate and *p*-TsOH. Finally the reduction of (**14**) with NaBH₄ afforded the enantiomerically pure product (-)-cephalotaxine (**1**) in an overall yield of 1.8 % in 16 steps from *R*-proline (**73**).⁵¹



Scheme 1.11. (i) (a) CF₃COOH, (b) 2-(3,4-dimethoxyphenyl)ethyl alcohol *p*-nitrobenzenesulfonate ester, *i*-Pr₂NEt, 88 %; (ii) (a) LiAlH₄, (b) Et₃N, SO₃-pyridine, 81 % from (**75**); (iii) Me₃SiSnBu₃, CsF, 3 % (**77**), 85 % (**78**); (iv) TBAF, 86 %; (v) polyphosphoric acid, 66 %; (vi) (MeO)₃CH, *p*-TsOH, 47 %; (vii) NaBH₄, 95 %.

Nagasaka *et al.* also completed a synthesis of naturally occurring (-)-cephalotaxine as well as its enantiomer, (+)-cephalotaxine.⁴⁰ Their synthesis of the two enantiomers was used to demonstrate an application of their methodology for the synthesis and separation of enantiomers of 1-azaspiro[4.4]nonane-2,6-dione (**83**). This spirocycle synthesis (Scheme 1.12) started with the alkylation of cyclopentanone (**80**) which was achieved in two steps by conversion of cyclopentanone (**80**) to the pyrrolidine enamine and then reaction with methyl acrylate to give keto ester (**37**). Reaction of keto ester (**37**) with isopropenyl acetate afforded the enol acetate (**81**) which was converted to the nitro ester (**82**) with a mixture of trifluoroacetic anhydride and NH₄NO₃. Finally, reduction of the nitro ester (**82**) to give the racemic spirocycle (**83**) was achieved with zinc in an acetic acid-ethanol mixture, the overall yield from cyclopentanone being 27%. To facilitate the separation of the enantiomers, the spirocycle (**83**) was reacted with (*R,R*)-2,3-butanediol and a catalytic amount of *p*-TsOH. The resulting diastereomeric acetals (+)-(**84**) and (-)-(**84**) were then easily separated by HPLC using CHCl₃ on a silica gel column. The application of this methodology to the synthesis of cephalotaxine was then demonstrated. From (+)-(**84**) and (-)-(**84**) two further steps allowed for the addition of the cephalotaxine A and B rings to the spirocycle and removal of the acetal to reveal the ketone functionality of (+)-(**44**) and (-)-(**44**). Racemic (**44**) was an intermediate seen earlier in the (±)-cephalotaxine synthesis of Kuehne and co-workers.³²



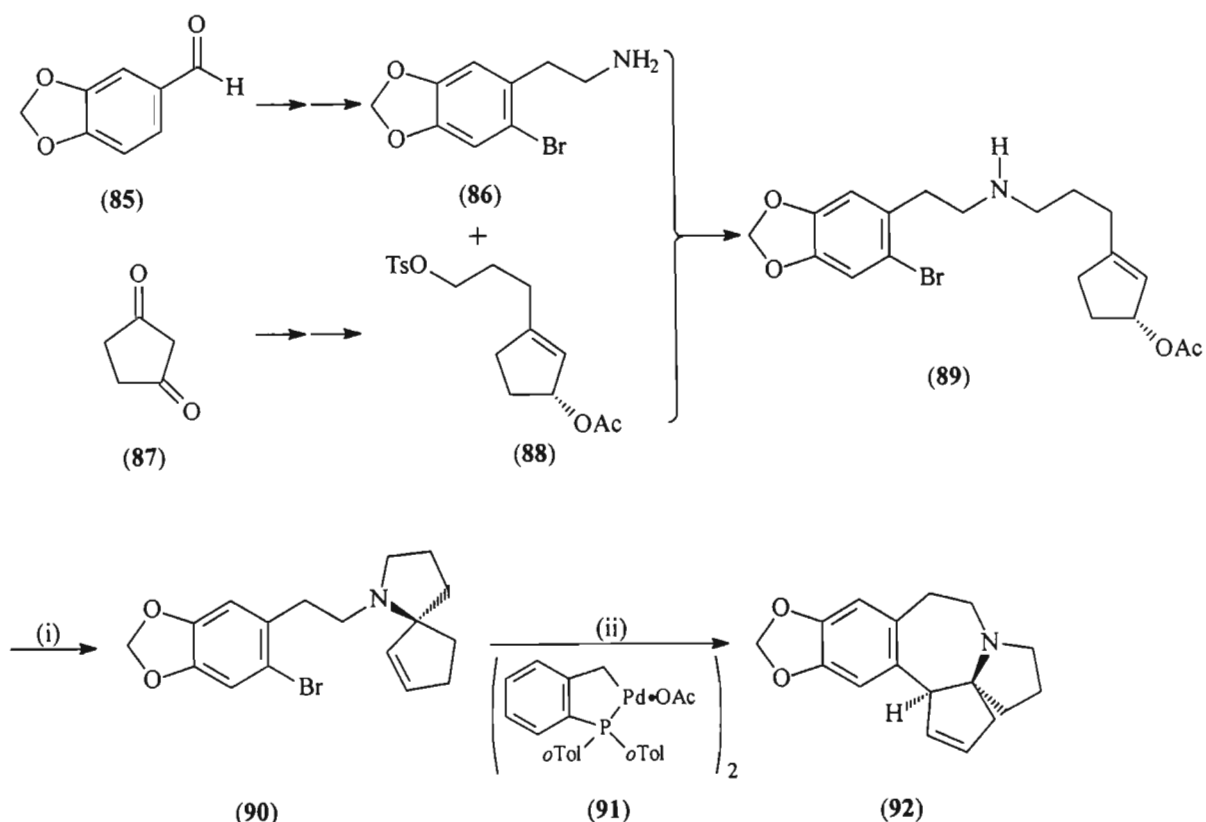
Scheme 1.12. (i) isopropenyl acetate, *p*-TsOH, Δ , 72%; (ii) (CF₃CO)₂O, NH₄NO₃, 68%; (iii) Zn, CH₃CO₂H-EtOH, 80%; (iv) (*R,R*)-(-)-2,3-butanediol, *p*-TsOH, Δ , 100%.

Nagasaka *et al.* did not show the steps past this intermediate but stated that they synthesised (+)-cephalotaxine and (-)-cephalotaxine by making use of the methods reported by Kuehne and co-workers³² and Isono and Mori.³⁹ Nagasaka and co-workers' synthesis of enantiomerically pure (-)-cephalotaxine differs from that of Isono and Mori as it relied on the production of a racemic mixture followed by separation of the enantiomers which were then converted to the enantiomerically pure products. In contrast Isono and Mori used a compound from the chiral pool to initiate their enantiomerically pure route which required no separation of racemic mixtures during the course of its preparation.

1.4.2. Formal Syntheses of Cephalotaxine

By synthesising the enamine intermediate (**10**)^{41,42,43} found in the Auerbach and Weinreb^{27,28} synthesis or a precursor to it⁴⁴ a number of research groups have succeeded in achieving formal syntheses of (±)-cephalotaxine. The synthesis of this enamine (**10**) does not involve the formation of the spirocycle and thus is not of great interest to us, as a result the work of these groups has not been reviewed here. However the 1999 formal synthesis of (-)-cephalotaxine published by Tietze and Schirok⁴⁵ did involve a novel spirocycle synthesis and so will be reviewed here.

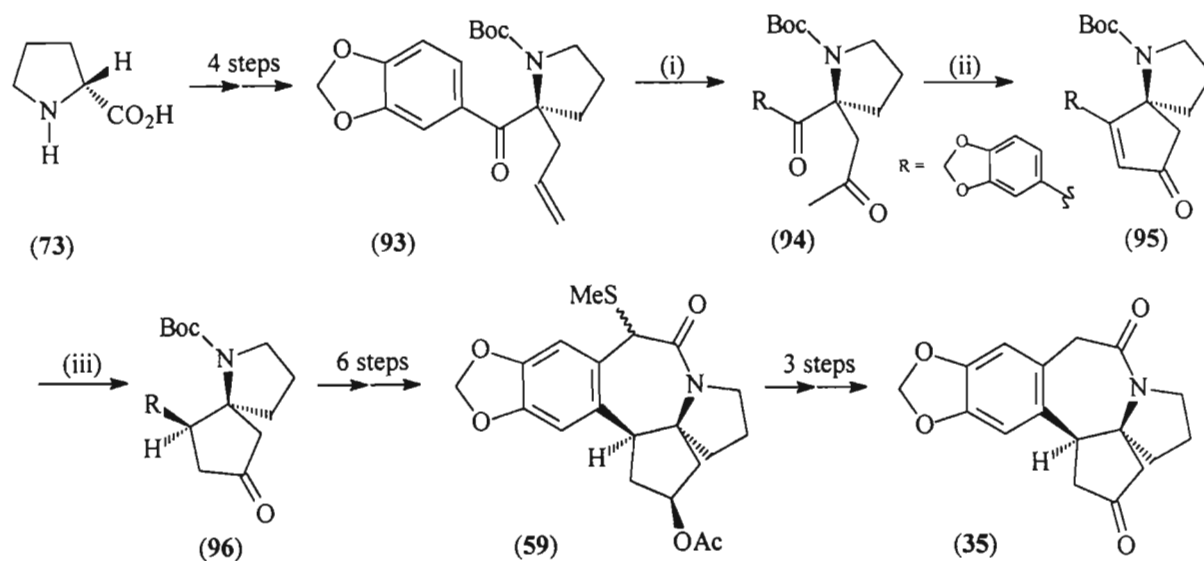
The synthesis of Tietze and Schirok utilized two efficient palladium-catalysed cyclisations the first of which resulted in the formation of the spirocycle and the second formed the seven-membered C ring. The general outline of their work can be seen in Scheme 1.13. Amine (**86**), synthesised from piperonal (**85**), was alkylated with the tosylate (**88**) which had been previously obtained from cyclopentane-1,3-dione (**87**). The resulting secondary amine (**89**) then underwent an allylic amination, this being the first of the Pd-catalysed cyclisation reactions, and gave the spirocycle (**90**) in 88 % yield. Next a palladacycle catalyst (**91**) was used to carry out the second cyclisation to form the pentacycle (**92**). At this point Tietze and Schirok claimed a formal synthesis stating that the pentacycle (**92**) could be converted to (-)-cephalotaxine (**1**) in four steps following the procedure Isono and Mori used in their synthesis of (-)-cephalotaxine (**1**).³⁹



Scheme 1.13. (i) $\text{Pd}(\text{PPh}_3)_4$, tetramethylguanidine, Δ , 88 %; (ii) $n\text{-Bu}_4\text{NOAc}$, Δ , 81 %.

Ikeda and co-workers, in addition to their total synthesis of (\pm)-cephalotaxine,^{35,36} also published a formal synthesis⁴⁶ of (-)-cephalotaxine in 1999. Their formal synthesis was achieved with the formation of the enantiopure ketolactam (**35**) which they had formed during their (\pm)-cephalotaxine route as had Hanaoka and co-workers.³¹ Ikeda and co-workers began their synthesis of (-)-cephalotaxine with *R*-proline (**73**), as had Isono and Mori for their enantiopure synthesis,³⁹ and converted it to the *N*-protected product (**93**) in four steps (Scheme 1.14). Wacker oxidation of (**93**) resulted in the diketone (**94**) which underwent base catalysed aldol condensation with sodium 2-methyl-2-butanolate (formed from NaH and 2-methyl-2-butanol) to form the α,β -unsaturated ketone spirocycle (**95**) in 43 % yield. Though this yield was only moderate it was significantly better than the yields obtained under a number of other conditions that were investigated. Ketone (**96**) was formed as a single isomer by hydrogenation of (**95**), the premise being that the hydrogen attacks from the less hindered *re* face of the double bond leading to the stereochemical assignment for (**96**). A further six steps led to the formation of the enantiopure pentacycle (**59**), seen earlier in the racemic cephalotaxine synthesis of Ikeda and co-

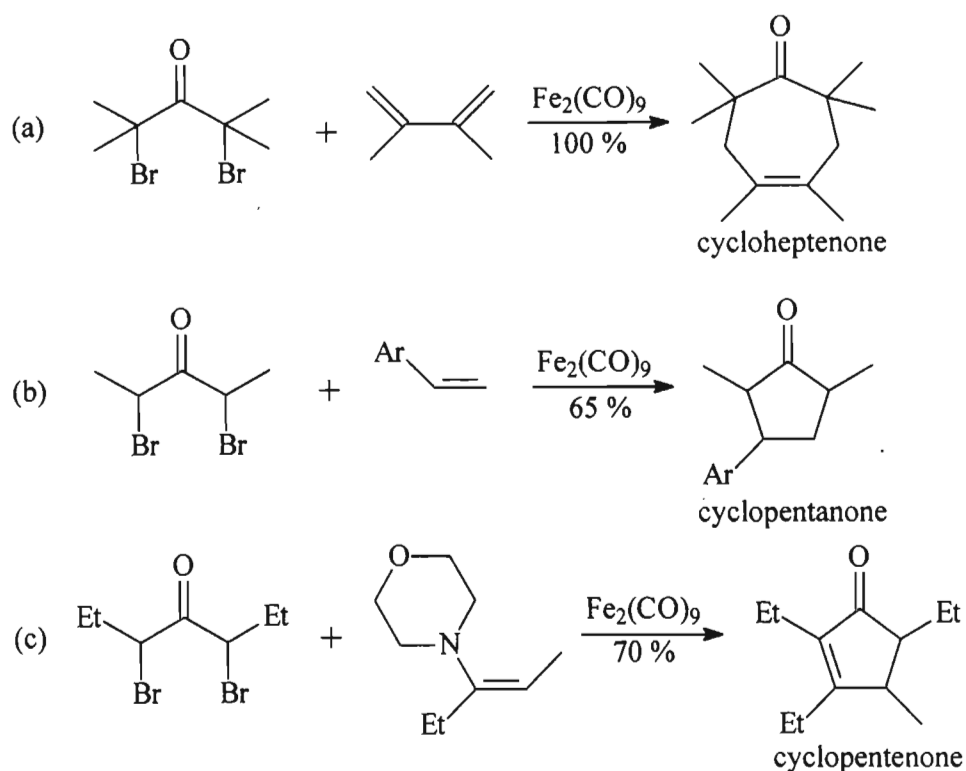
workers^{35,36} (Scheme 1.7). Finally (**59**) was converted into the desired enantiopure ketolactam (**35**) resulting in a formal synthesis of (-)-cephalotaxine. To the best of our knowledge this is the most recently published synthesis of cephalotaxine.



Scheme 1.14. (i) O₂, PdCl₂, CuCl, 67 %; (ii) NaH, 2-methyl-2-butanol, 43 %; (iii) H₂, PtO₂, 84 %.

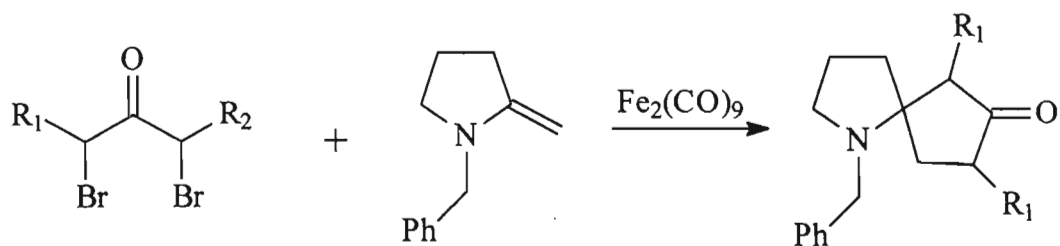
1.5. AIMS OF THE INVESTIGATION

The aim of this project was to apply the Noyori annulation reaction to the synthesis of the cephalotaxine spirocycle. Noyori himself is a well respected chemist with his contributions to organic chemistry being recognised in 2001 with the award of the Nobel Prize for Chemistry. Though it will be dealt with in detail in Chapter 2, a brief introduction to the Noyori annulation reaction will be given here. The reaction is an Fe₂(CO)₉ mediated cycloaddition reaction involving a polybromoketone (di-, tri, or tetra-substituted bromoketone) and a compound containing an electron-rich double bond to yield a cyclocoupled reaction product. Noyori and co-workers showed this reaction could be carried out using 1,3-dienes,⁵² aromatic olefins,⁵³ and enamines.⁵⁴ One example of each of these reactions is shown in Scheme 1.15.



Scheme 1.15. Examples of Noyori annulation reactions between dibromoketones and (a) a 1,3-diene, (b) an aromatic olefin, and (c) an enamine.

One of the useful aspects of the Noyori annulation reaction is its ability to synthesise rings containing an odd number of atoms as in general rings containing an even number of atoms are more easily prepared e.g. six-membered rings by the Diels-Alder reaction.⁵² Applications of the annulation reaction were demonstrated by Noyori and co-workers with the synthesis of troponoid compounds⁵⁵ and tropane alkaloids⁵⁶ which all contain seven-membered rings. Our interest in the Noyori annulation reaction lies particularly with the cyclocoupling reaction involving an enamine as shown in Scheme 1.15 (c). As in this example, all the enamine reactions carried out by Noyori and co-workers used a morpholine derivative with the nitrogen ring always being eliminated in the reaction.⁵⁴ Our intended investigation of the Noyori reaction to form the cephalotaxine spirocycle is shown in Scheme 1.16. The reaction would involve a dibromoketone and an enamine, though here the enamine double bond is directly connected to the azacycle while in the work of Noyori and co-workers it was along the alkyl chain attached to the nitrogen. This is a subtle but important difference as it should result in the formation of the desired azaspirocycle as shown in Scheme 1.16.

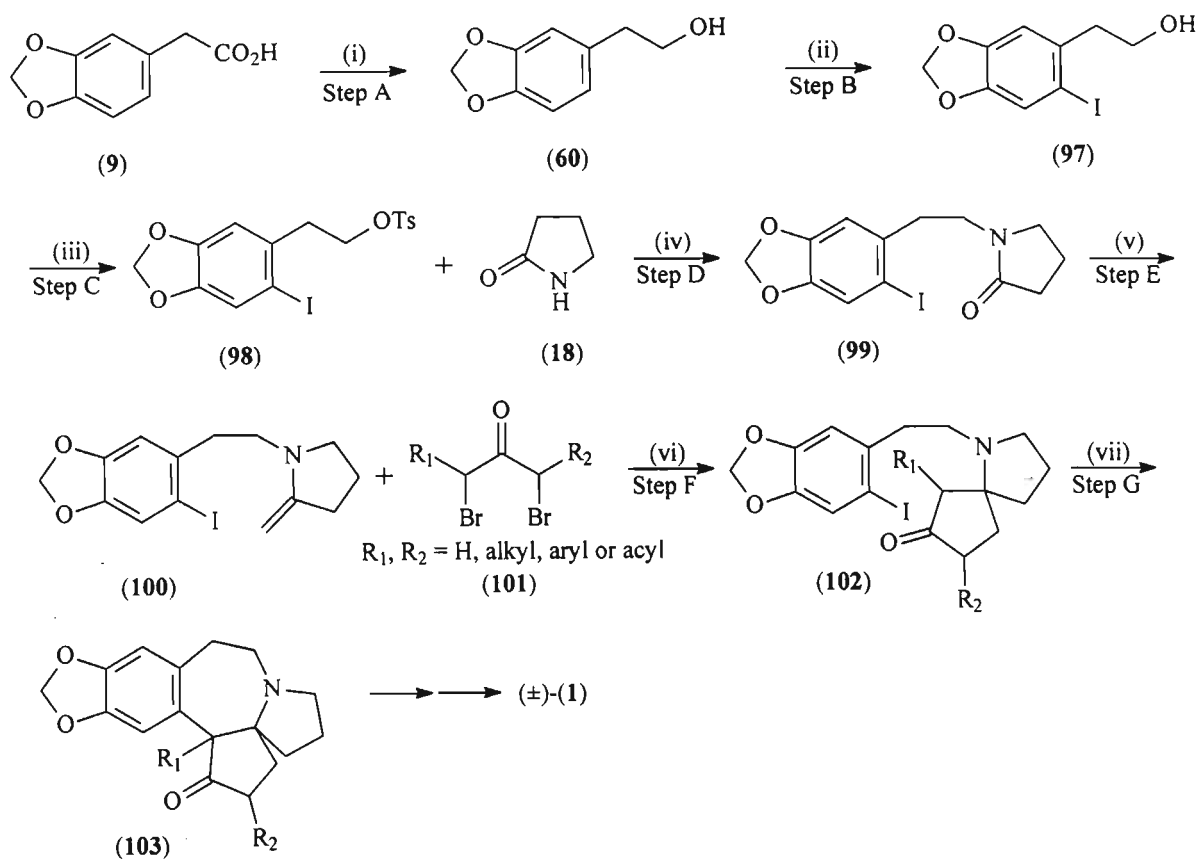


$R_1, R_2 = \text{H, alkyl, acyl or aryl}$

Scheme 1.16. Model study of the Noyori annulation reaction to form the cephalotaxine azaspirocycle.

In Scheme 1.16 the functionalisation of the dibromoketone is not specified as the intention was to investigate the tolerance of the reaction to various functional groups. This would be important when the reaction was applied to the synthetic route to form the cephalotaxine skeleton as will be seen shortly. The enamine chosen for our “test” Noyori reaction in Scheme 1.16 was intended to be a model compound so that the initial investigative reactions into the Noyori coupling reaction were carried out on a cheaper and more simply prepared compound than if the rest of the cephalotaxine skeleton, namely the A ring and B ring, was already intact.

A further aim of the investigation was to pursue a novel route to the basic pentacyclic cephalotaxine structure based on the spirocycle synthesis. The proposed synthetic route to apply the Noyori coupling reaction to the synthesis of the cephalotaxine pentacyclic skeleton is shown in Scheme 1.17. The proposed reagents for each step are shown. Most of the elements of the route not involved with the spirocycle synthesis were based on the (\pm)-cephalotaxine synthesis of Semmelhack *et al.*^{29,30} Each step in the proposed route will now be briefly discussed, with potential problems being identified.



Scheme 1.17. (i) LiAlH_4 ; (ii) I_2 , AgO_2CCF_3 ; (iii) pyridine, *p*-TsCl; (iv) MeCN, *i*-Pr₂NEt; (v) Cp_2TiMe_2 ; (vi) $\text{Fe}_2(\text{CO})_9$, $h\nu$, Δ ; (vii) potassium *t*-butoxide, NH_3 , $h\nu$.

Steps A and B: These first two steps of the synthesis were based on the work of Semmelhack *et al.*^{29,30} 3,4-Methylenedioxyphenylacetic acid (**9**) is a readily available starting material and it was anticipated it should be easily reduced to the corresponding alcohol (**60**) with the commonly used reducing agent, LiAlH_4 . Step B is an electrophilic aromatic substitution reaction to place an iodine atom on the cephalotaxine B ring thus forming iodoalcohol (**97**). The presence of the iodine atom was required to facilitate the ring closure to form the seven-membered C ring in Step G.

Step C: This step converts the iodinated alcohol (**97**) to the tosylate (**98**), thus inserting a good leaving group in preparation for the next step involving the addition of the pyrrolidinone ring. In the work of Semmelhack *et al.* a nosylate rather than tosylate leaving group was used. Our

reason for preferentially intending to synthesise the tosylate (**98**) was simply that at the start of the project there was no 4-nitrobenzenesulfonyl chloride in our laboratories, and this is the reagent required for the nosylate synthesis. As large quantities of *p*-TsCl were available it seemed reasonable to synthesise the tosylate (**98**) as the tosylate moiety itself should act as a good enough leaving group for Step D even though nosylates, in relative terms, are approximately twenty times better leaving groups than tosylates.⁵⁷

Step D: This step was intended to result in the coupling of the pyrrolidinone ring (**18**) (D ring) to the cephalotaxine A and B rings. Again the intention was to use the method of Semmelhack *et al.*,^{29,30} though in their work the coupling was of the already completed spirocycle to the A and B rings. Should the tosylate be an adequate leaving group it was not anticipated that this step should present any problems.

Step E: The enamine (**100**) is formed in this step by the reaction of the corresponding lactam (**99**) with Cp₂TiMe₂. We intended using the method of Petasis and Lu.⁵⁸

Step F: This is the point at which the Noyori annulation reaction was to be implemented. For this step the synthesis of the dibromoketone (**101**) is required. An idea of how successful this Noyori annulation reaction of the dibromoketone (**101**) and the enamine (**100**) would be would have been gained from the earlier model studies outlined in Scheme 1.16. Three chiral centres are being created in this reaction and it was anticipated that a mixture of diastereomers of the spirocycle (**102**) would be formed.

Step G: Should this step where the seven-membered ring is formed be reached, few problems were anticipated in carrying it out. Semmelhack *et al.*^{29,30} investigated a number of methods to achieve this ring closure and showed that the use of a base combined with irradiation of the reaction mixture achieved cyclisation efficiently. As discussed in Steps A and B, the presence of the labile iodine atom should facilitate this ring closure based on the findings of Semmelhack *et al.*^{29, 30} Thus using this method the pentacyclic cephalotaxine skeleton (**103**) would be obtained.

Should the route be carried out as intended it would take only seven steps to achieve the pentacyclic cephalotaxine skeleton (**103**). The functionality of the dibromoketone (**101**) would then become important as it would determine the degree of ease that the five-ring system (**103**) could be correctly functionalised to form cephalotaxine (**1**). In addition, varying R_1 and R_2 will allow the flexibility to synthesise various analogues of cephalotaxine. It was known that realistically, in the MSc time frame, it would not be possible to complete the synthesis of cephalotaxine itself during this particular study. Thus the principal aim of this project was to determine if the Noyori annulation reaction could be used to assemble the azaspirocycle of cephalotaxine. Thereafter, if successful, there was every possibility that the work may be completed by other members of the research group and so the overall synthetic route to cephalotaxine was kept in mind and a broader approach was considered.

In the following chapters the work that has been carried out based on the above aims has been described. It is now relevant to mention that the original intention was that the work for this thesis be based purely in synthetic organic chemistry. However, during the course of the work as a result of the synthesis, *en route*, of a particularly interesting novel compound, the opportunity presented itself to carry out a conformational analysis study. Thus Chapter 2 covers a discussion of the synthetic work carried out in this project while Chapter 3 describes the conformational analysis study.

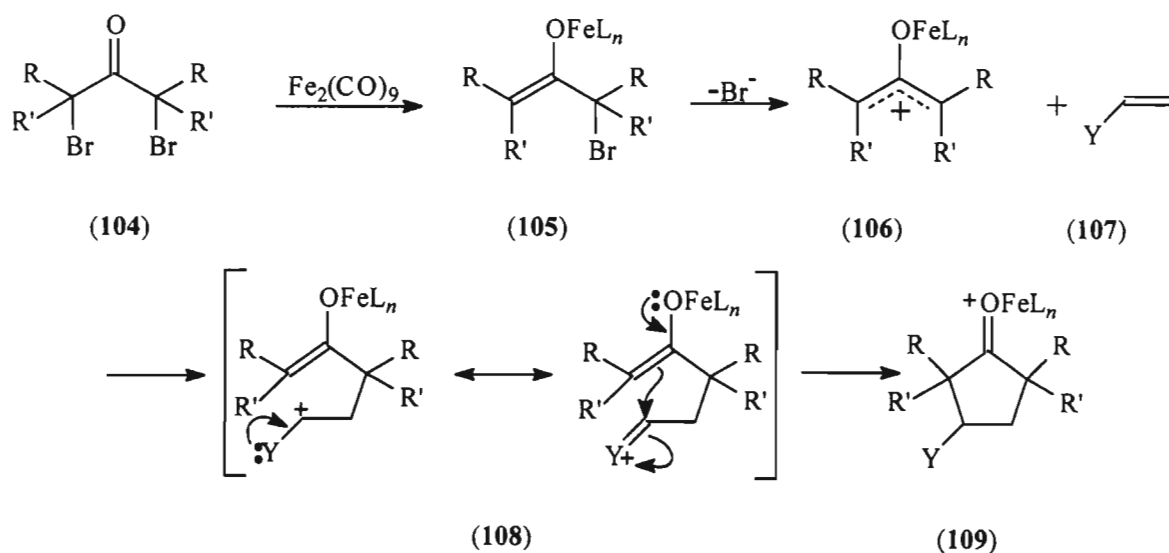
Chapter 2

Discussion of Synthetic Work

2.1 APPLICATION OF THE NOYORI ANNULATION REACTION TO THE CEPHALOTAXINE SPIROCYCLE

2.1.1. Mechanism of The Noyori Annulation Reaction

It is relevant at this point to discuss the mechanism of the Noyori annulation reaction introduced in the previous chapter. The mechanism of the reaction between α,α' -dibromo ketones and $\text{Fe}_2(\text{CO})_9$ was investigated thoroughly by Noyori and co-workers and is shown in Scheme 2.1.⁵⁹ In the first step one of two things occurs. Either the dibromo ketone (**104**) undergoes a two electron reduction to form the enolate (**105**) or an oxidative addition of the carbon-bromine bond of (**104**) onto a zerovalent iron atom takes place which is followed by a rearrangement into the enolate (**105**). In the next step the allylic bromine atom is removed by an $\text{S}_{\text{N}}1$ -type or ferrous ion assisted elimination to give the oxyallyl-Fe(II) intermediate (**106**). In their paper on the mechanism of the reaction between dibromo ketones and $\text{Fe}_2(\text{CO})_9$, Noyori and co-workers showed evidence for the existence of both the iron enolate species (**105**) and the oxyallyl-Fe(II) intermediate (**106**).⁵⁹



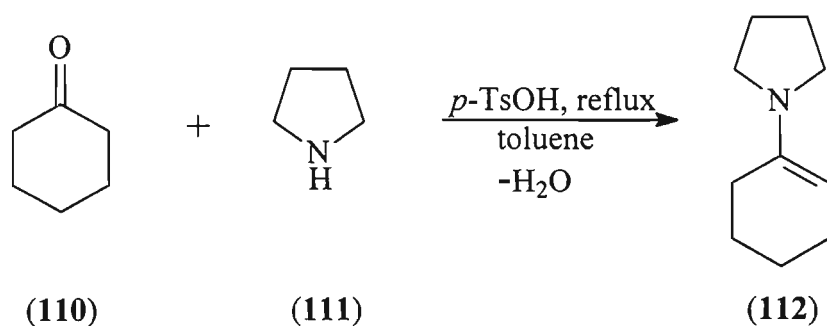
Scheme 2.1.

Also shown in Scheme 2.1 is the reaction of the oxyallyl-Fe(II) intermediate (**106**) with a heteroatom substituted olefin (**107**),⁵⁴ where in our case the heteroatom would be nitrogen. The zwitterionic intermediate (**108**) that forms is stabilised by the presence of the heteroatom due to resonance involving a non-bonding electron pair on the heteroatom. The annulation can then occur to form the cyclised product (**109**).

Noyori and co-workers noted in their mechanistic studies⁵⁹ that alkylated α,α' -dibromo ketones undergo reactions characteristic of the oxyallyl-Fe(II) intermediate (**106**) while α,α' -dibromoacetone does not. They reason that carbocation-stabilising substituents are required at the cationic termini of the α,α' -dibromo ketone in order to stabilise the reactive enolate (**105**) and the oxyallyl-Fe(II) intermediate (**106**). As α,α' -dibromoacetone does not contain any such substituents it is unable to stabilise the intermediates. Thus in order for the Noyori annulation reaction to take place the reactivity and stability of the enolate (**105**) and oxyallyl (**106**) intermediates needs to be controlled using the electronic effects of the dibromo ketone substituents. With the Noyori annulation reaction and its mechanism now having been introduced, the stage is set to discuss the work carried out using this reaction.

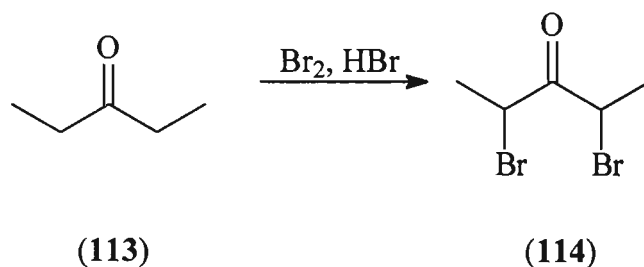
2.1.2. Synthesis of 1,3-Dimethyl-1,4,5,6,7,7a-hexahydro-2H-inden-2-one (**115**)

The conditions under the which the Noyori annulation are carried out were not standard practice in our laboratories at the start of this project and so in order to ensure that the correct conditions were used in our proposed spirocycle syntheses a “test” reaction was carried out. This reaction involved the coupling of a cyclic enamine, similar to those used by Noyori and co-workers,⁵⁴ and a simple α,α' -dibromo ketone to give a known Noyori annulation product, 1,3-dimethyl-1,4,5,6,7,7a-hexahydro-2H-inden-2-one (**115**).⁵⁴ Both reactants, the enamine, 1-(1-cyclohexen-1-yl)pyrrolidine (**112**), and the α,α' -dibromo ketone, 2,4-dibromo-3-pentanone (**114**), had to be synthesised first. Synthesis of the enamine (**112**) was carried out by refluxing a toluene solution of cyclohexanone (**110**) and pyrrolidine (**111**) in the presence of a catalytic amount of *p*-toluenesulfonic acid (Scheme 2.2).⁶⁰ Water was continuously removed from the reaction using a Dean and Stark apparatus. The resulting liquid was purified using a Kugelrohr distillation apparatus to remove the lower boiling impurities, giving enamine (**112**) in a 56 % yield. These types of enamines are better used without purification as this results in lowering of the yield as the mediocre 56 % seen here illustrates. However, for our purposes a pure product was required.



Scheme 2.2.

The synthesis of the dibromo ketone, 2,4-dibromo-3-pentanone (**114**), was achieved by a bromination of the corresponding ketone, 3-pentanone (**113**), using molecular bromine and hydrobromic acid (Scheme 2.3). The method followed was that of De Kimpe *et al.*⁶¹ who had reported an explosion when carrying out this reaction on a molar scale, thus extreme caution was exercised during the experiment. The product was purified by vacuum distillation and was kept in the freezer under N₂. Before use in any reactions the dibromo ketone (**114**) was passed through a basic alumina column. As with a number of organobromine compounds, this substance was a strong lachrymator and extremely unpleasant to work with.



Scheme 2.3.

In the GC-MS analysis, the GC trace of the dibromo ketone (**114**) showed two peaks, which according to their mass spectra, both corresponded to the correct mass for the compound. Similarly, in the ¹H and ¹³C NMR spectra two sets of signals were observed. This is as a result of there being two diastereomers, (*R*^{*}, *R*^{*}) and (*R*^{*}, *S*^{*}), with stereogenic centres being present at both carbons α to the carbonyl group. Thus one set of signals is attributable to the (*R*^{*}, *R*^{*})-diastereomer and the other set of signals to the (*R*^{*}, *S*^{*})-diastereomer. This is clearly seen in the ¹H NMR spectrum shown in Figure 2.1. The doublet at 1.80 and the quartet at 4.98 ppm are due to the CH₃ and CH, respectively, for one diastereomer while the doublet at 1.88 and quartet at

4.77 ppm are due to the other diastereomer. From the ^1H NMR spectrum shown it appears that the reaction to form the dibromo ketone (**114**) is diastereoselective, with one diastereomer being present in significant excess. This is however not the case as according to the literature the reaction produces a 1:1 diastereomeric mixture.⁶² In our case the ratio of diastereomers was presumably altered during the distillation process. The yield for this reaction was low, being only 36 %, compared with other literature values of 70 to 80 %.^{61,62}

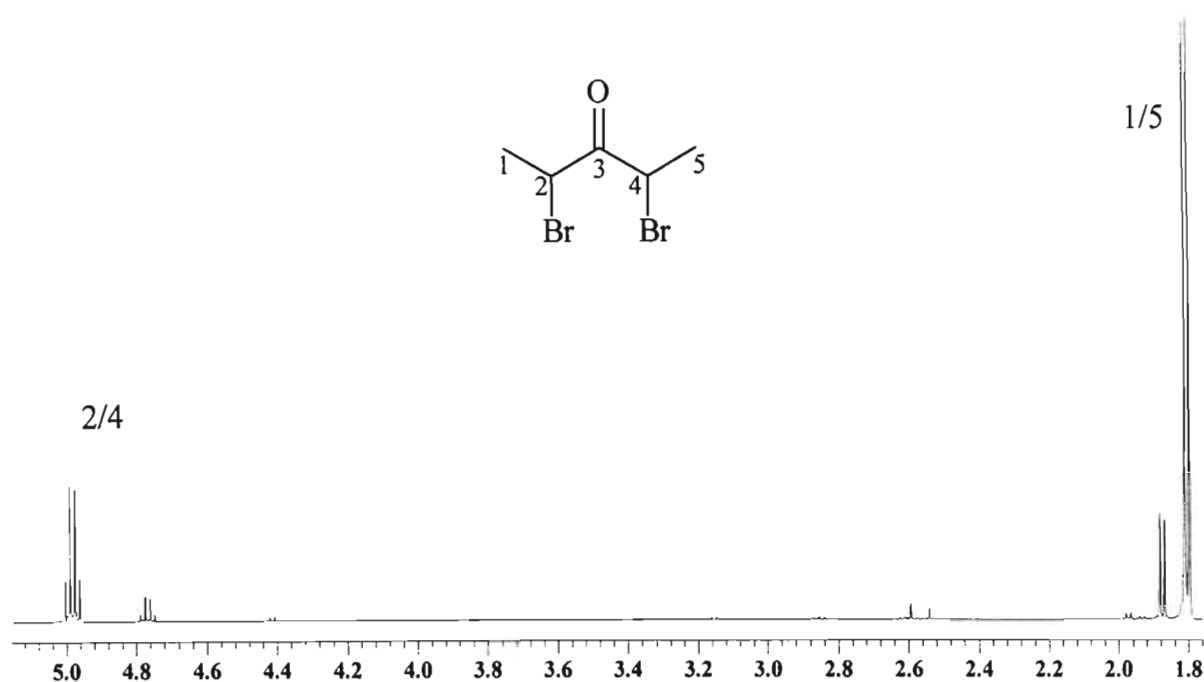
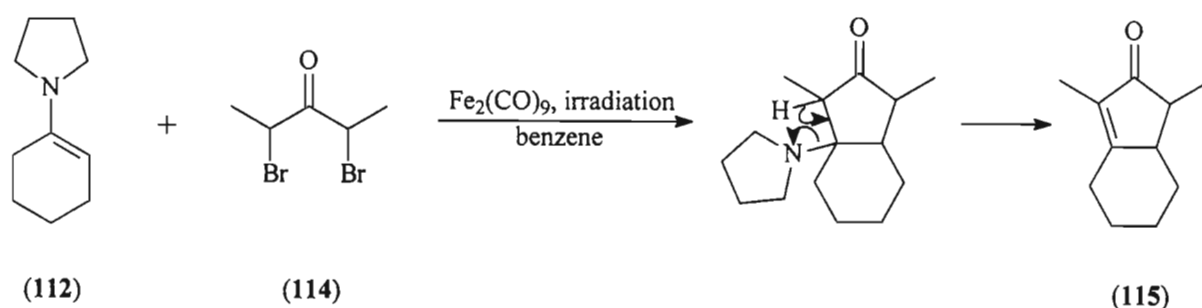


Figure 2.1. ^1H NMR spectrum of 2,4-dibromo-3-pentanone (**114**).

With both the required enamine (**112**) and dibromo ketone (**114**) in hand the “test” Noyori annulation reaction could be carried out (Scheme 2.4). The required quantity of $\text{Fe}_2(\text{CO})_9$ was measured out into a flame-dried flask in a N_2 atmosphere glove-box. The two flasks containing the enamine (**112**) and dibromo ketone (**114**) were evacuated and then filled with nitrogen before adding an equal quantity of anhydrous benzene to both flasks. The two benzene solutions were then transferred *via* a cannula into the flask containing the $\text{Fe}_2(\text{CO})_9$. The reaction mixture was heated to 60 °C for 10 minutes with irradiation using a 400 W high pressure Hg lamp. To block wavelengths of less than 350 nm, a 10 % aqueous CuSO_4 solution was used as a filter, being placed between the Hg lamp and the reaction flask. Though Noyori and co-workers⁵⁴ did not

elaborate on the need for the CuSO_4 solution, it is suspected that this prevents the occurrence of unwanted side reactions that would be caused by the low wavelength radiation. After the 10 minutes of heating the reaction mixture was left to stir overnight at room temperature with continued irradiation. After dilution with ethyl acetate, washing with aq. NaHCO_3 and brine solutions, and evacuation, the remaining liquid was purified by radial chromatography to afford the desired cyclopentenone (**115**) as a mixture of two diastereomers in a 35 % yield. The two diastereomers were separated by preparative TLC and the NMR data compared favourably with those reported by Noyori and co-workers⁵⁴ who had synthesised the cyclopentenone (**115**) from the morpholine enamine of cyclohexanone and the same dibromo ketone (**114**). In Noyori's reaction the morpholine moiety was eliminated from the enamine during the reaction to give the product (**115**). Similarly, from Scheme 2.4, it can be seen that the pyrrolidine moiety of the enamine (**112**) was eliminated in the reaction which we carried out which is why the same product was obtained in both cases. The elimination in these reactions takes place after the annulation has occurred. From the annulation reaction the resulting β -substituted cyclopentanone intermediate contains a labile hydrogen atom in the position α to the carbonyl. The loss of the labile hydrogen atom results in facile elimination of the β -substituent, in our case pyrrolidine, to give the cyclopentenone (**115**).

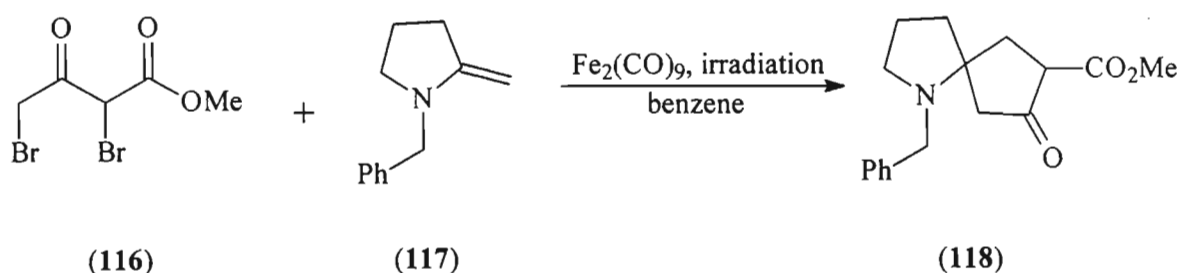


Scheme 2.4.

Though the 35 % overall yield of the reaction was low it had been successful meaning that the intended spirocycle syntheses could be attempted.

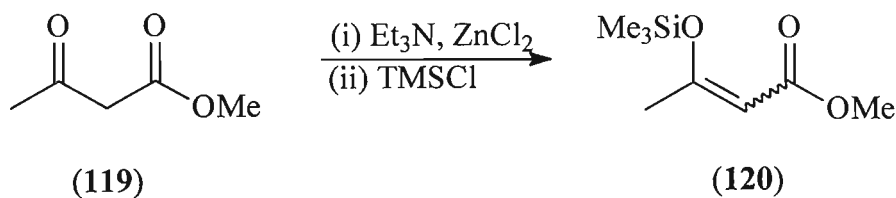
2.1.3. Attempted Reaction of Methyl 2,4-dibromo-3-oxobutanoate (116) and 1-Benzyl-2-methylenepyrrolidine (117)

It was our intention to carry out the Noyori annulation reaction using the dibromo ketoester (116) and enamine (117) to give us our desired spirocycle product (118) (Scheme 2.5). The dibromo ketoester (116) was chosen with the cephalotaxine synthesis in mind, the rationale being that the ester moiety could be eliminated by hydrolysis and decarboxylation in order to obtain the correct functionality on the cephalotaxine E ring. The enamine (117) was chosen as a model compound, the benzyl group acting *in lieu* of the cephalotaxine A and B rings.



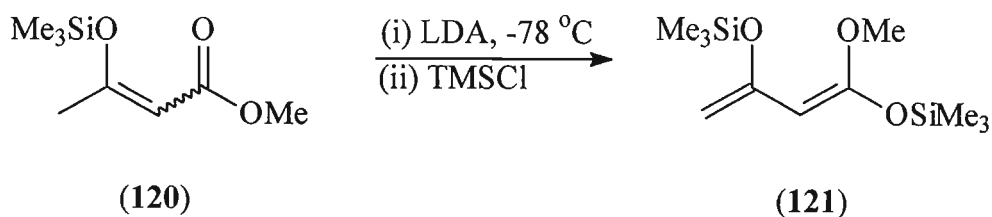
Scheme 2.5.

Once again both starting materials, the dibromo ketoester (116) and enamine (117), had to be synthesised as they are not commercially available. The synthesis of the dibromo ketoester (116) was not as simple as for 2,4-dibromo-3-pentanone (114) where the corresponding ketone was brominated in a one step reaction. Rather, following the method of Chan and Brownbridge,⁶³ dibromo ketoester (116) is synthesised in three consecutive steps from methyl acetoacetate, going *via* the corresponding bis-silyl enol ether (121). Thus for the first step, as suggested by Chan and Brownbridge,⁶⁴ the method of Danishefsky and Kitahara⁶⁵ was followed to convert methyl acetoacetate (119) into methyl 3-[(trimethylsilyl)oxy]-2-butenolate (120) (Scheme 2.6). Zinc chloride in triethylamine is used to promote enolate formation of methyl acetoacetate (119) with the enolate subsequently being trapped by TMSCl to form the desired silyl enol ether (120). Purification by distillation was carried out satisfactorily to afford a clear liquid in a 63 % yield, though problems with “bumping” were encountered. The product was characterised by GC-MS, IR and NMR spectroscopy with the ¹H NMR data showing a good correlation with the data obtained by Chan and Brownbridge.⁶⁴ Both *E* and *Z* isomers (3:1) are observed in both the GC-MS and NMR spectra as expected.



Scheme 2.6.

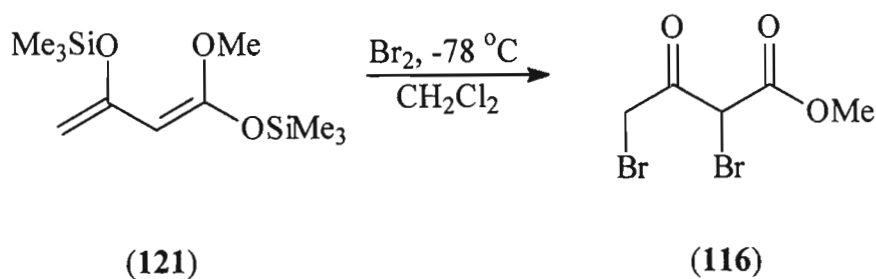
Converting the silyl enol ether (**120**) to (1*E*)-1,3-bis[(trimethylsilyl)oxy]-1,3-butadienyl methyl ether (**121**) (also known as Chan's diene) required the use of a stronger base for the enolate formation than in the synthesis of (**120**). Thus following the method of Chan and co-workers,⁶⁶ LDA formed from *n*-butyllithium and diisopropylamine, was used (Scheme 2.7). TMSCl was once again used as the silylating agent. Because of the use of the moisture-sensitive reagent LDA, great care was taken to ensure that both glassware and solvent (THF) were dry. The reaction was carried out at $-78\text{ }^\circ\text{C}$ as the research of Chan and co-workers showed that if the temperature of the reaction increased above $-42\text{ }^\circ\text{C}$ formation of the desired product was hindered. The crude bis-silyl enol ether (**121**) proved difficult to purify as the silyl enol ether functional groups are highly labile on silica gel and distillation is precluded as the compound decomposes at elevated temperatures. A ^1H NMR of the crude sample offered the necessary proof that the compound had been formed and it was decided that the compound could be used for the next step in the synthesis of methyl 2,4-dibromo-3-oxobutanoate (**116**) without further purification.



Scheme 2.7.

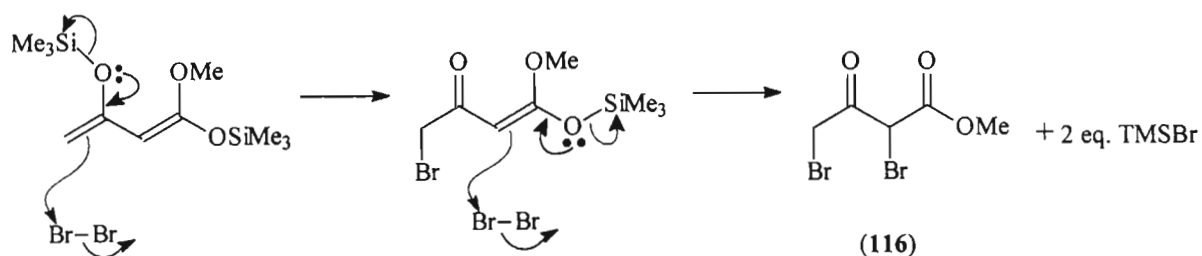
In a communication, Chan and Brownbridge had reported the formation of the dibromo ketoester (**116**) from bis-silyl enol ether (**121**) by addition of 2 molar equivalents of bromine.⁶³ No actual method for the synthesis, or spectral data, was provided in the communication and since no follow-up paper was published a method for the bromination reaction had to be developed.

Attempted personal communication with the author was equally unhelpful. Various unsuccessful attempts were made to form the dibromo ketoester (**116**) by adding bromine in chloroform to (**121**) dropwise and leaving the mixture to stir for lengthy periods. Only complex mixtures of products were obtained with no evidence of the desired product being seen. A method which proved reasonably successful involved adding the bromine solution to bis-silyl enol ether (**121**) at 0 °C in one portion, leaving the mixture for one minute and then quenching the reaction with saturated aqueous NaHCO₃. Unfortunately this method was not reproducible and further attempts at altering the conditions of the reaction were made. The method which finally proved successful and reproducible is shown in Scheme 2.8 and involved adding bromine at -78 °C using dichloromethane as solvent rather than chloroform (which is a solid at -78 °C).



Scheme 2.8.

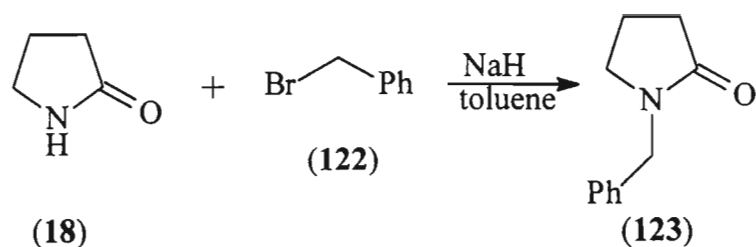
Various reaction times were investigated (5 minutes, 30 minutes, 1 hour, and 3 hours) and it was found that the yields did not appear to differ significantly. However, the main factor in achieving an acceptable yield proved to be the quality of the starting material. Though it was reported that the bis-silyl enol ether (**121**) could keep in the freezer for up to two weeks without obvious degradation,⁶⁶ significantly better yields were obtained using freshly prepared (**121**). According to the work of Chan and co-workers,^{64,66} the bis-silyl enol ether (**121**) reacts with electrophiles preferentially at C-4, though there is also a second nucleophilic site at C-2. Scheme 2.9 shows the first attack on the bromine taking place from the more reactive C-4 position and then the second attack taking place from the less reactive C-2 position.



Scheme 2.9.

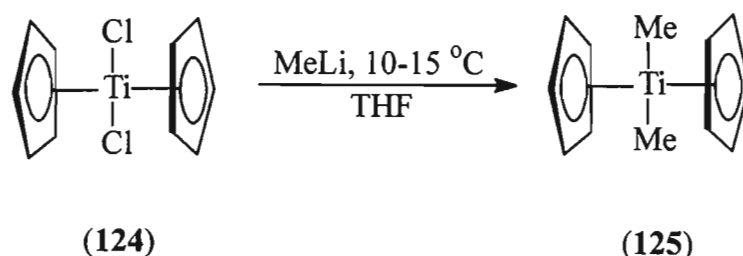
Purification of dibromoketo ester (**116**) proved problematic in that chromatographic methods only resulted in its decomposition. The product also tends to decompose at high temperatures which prevented the use of distillation. Thus the highest level of purification that was achieved was by removing lower boiling impurities using Kugelrohr distillation under vacuum. Unfortunately the purity of the dibromo ketoester (**116**) was not as high as desired. Like the bis-silyl enol ether (**121**), the dibromo ketoester (**116**) also appeared to degrade with time even if stored in the freezer under N_2 . A full range of NMR spectra were obtained for dibromo ketoester (**116**) as no data has been published on the compound. In the 1H spectrum the methyl group appeared as a singlet at 3.86 ppm, the diastereotopic CH_2 protons as two doublets at 4.25 and 4.38 ppm, and the CH as a singlet at 5.20 ppm. Unfortunately a high resolution mass spectrum (HRMS) was not obtained as the sample had decomposed on arrival at the laboratory which carried out the analysis. Finding a method for the synthesis of the dibromo ketoester was extremely time consuming, but finally with a reliable method in hand the synthesis of the enamine (**117**) could be started.

The synthesis of the enamine (**117**) is documented by Petasis and Lu in their work on the methylenations of heteroatom-substituted carbonyls.⁵⁸ They achieved the formation of the enamine (**117**) by reaction of *N*-benzyl-2-pyrrolidinone (**123**) with dimethyltitanocene (Cp_2TiMe_2). As neither of these are commercially available both needed to be synthesised. The *N*-benzyl-2-pyrrolidinone (**123**) was easily synthesised from 2-pyrrolidinone (**18**) and benzyl bromide (**122**) with NaH acting as a base (Scheme 2.10) using the method of Bielawski *et al.*⁶⁷ Purification was carried out by column chromatography, rather than by distillation as Bielawski *et al.* suggested, and the product was obtained in a 84 % yield and characterised by GC-MS, IR and NMR spectroscopy.



Scheme 2.10.

The synthesis of Cp_2TiMe_2 (**125**) was carried out using the method of Clauss and Bestian.⁶⁸ This involved adding methyllithium (MeLi) to a THF solution of titanocene dichloride (**124**) (Cp_2TiCl_2) at 10–15 °C (Scheme 2.11). It was found that the speed at which the MeLi was added affected the yield with better yields being achieved when the MeLi was added dropwise rather than in one portion. The product, Cp_2TiMe_2 (**125**), was obtained as an orange solid which was recrystallised from pentane by cooling to give needle-like crystals in a yield of 73 %. As the compound decomposes at high temperatures⁶⁸ it was not possible to confirm the successful synthesis of Cp_2TiCl_2 by GC-MS. However, NMR and IR spectra clearly proved the presence of the desired compound. The ^1H NMR spectrum contained only two singlets, one integrating for the 10 cyclopentadienyl protons at 6.06 ppm and a second peak situated at -0.15 ppm integrating for the six methyl protons. This latter methyl peak is shifted further upfield than expected due to the shielding effect of the cyclopentadienyl rings.



Scheme 2.11.

The IR spectrum for Cp_2TiMe_2 (**125**) as a KBr disc is shown in shown in Figure 2.2 and the assignments are made as follows:⁶⁹ in the region 3150–2800 cm^{-1} C-H stretchings are seen while at 1442 cm^{-1} C-C bond stretching occurs. At 1014 cm^{-1} in-plane C-H bending occurs with the peak at 814 cm^{-1} being characteristic of a C-H out-of-plane bending. Finally at 462 cm^{-1} the Ti- C_p stretching appears. The peak at 3428 cm^{-1} is caused by water in the KBr.

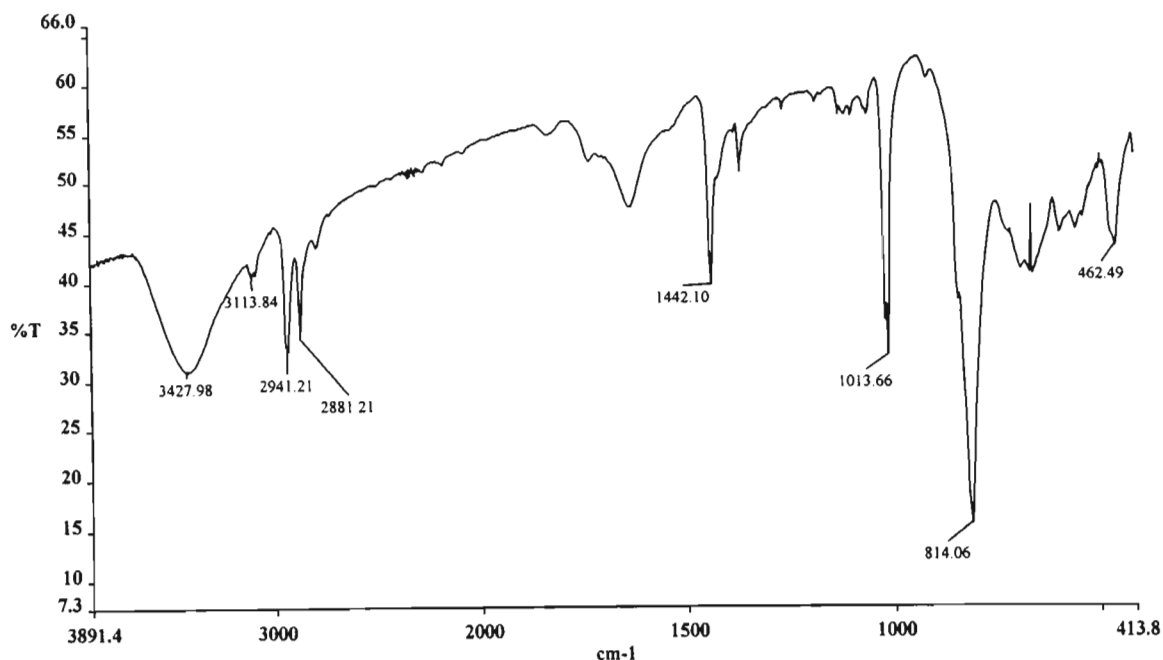
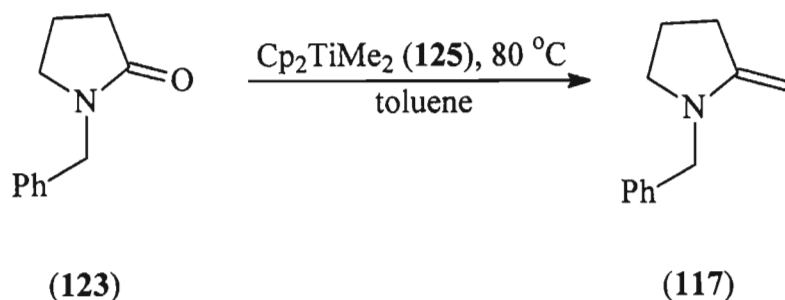


Figure 2.2. IR spectrum of Cp_2TiMe_2 (**125**).

With the desired starting materials prepared the reaction to prepare the enamine (**117**) was carried out using the method of Petasis and co-workers.^{58,70} This involved heating a toluene solution of *N*-benzyl-2-pyrrolidinone (**123**) and Cp_2TiMe_2 (**125**) in the dark overnight (Scheme 2.12).



Scheme 2.12.

Petasis and Lu stated in their work that the purification of this compound was difficult and that it should rather be used in further reactions without isolation.⁵⁸ As we were already in a situation where one of our reactants for the intended Noyori annulation reaction, the dibromo ketoester (**116**), was not as pure as desired, it was decided that an attempt should be made to purify the enamine (**117**) but it was indeed found to be difficult. Detection of the enamine (**117**) was also problematic as it appeared to decompose on being subjected to GC-MS analysis. Tentative proof

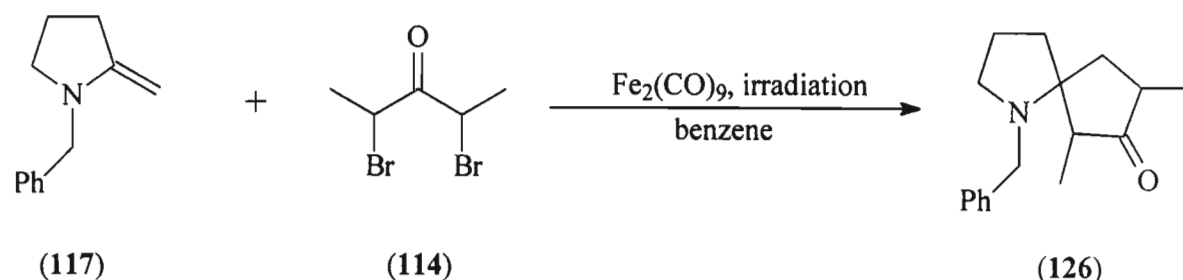
of the product having been formed was the apparent presence of the two vinyl protons in the ^1H NMR spectrum situated at approximately 3.6 ppm. According to the GHSQC spectrum these vinyl peaks showed a correspondence to a methylene signal in the ^{13}C NMR spectrum (identified as such from the DEPT spectrum). Work by Tehrani and De Kimpe who had used Cp_2TiMe_2 (**125**) in the methylenation of lactams also spoke of the difficulties of purification of products similar to ours.⁷¹ For their products, distillation resulted in severe degradation, but they were able to achieve some degree of purification by suspending the evacuated reaction mixture in pentane and then filtering the solution through Celite Filter Cel to remove the insoluble titanium salts formed during the reaction. This procedure was carried out on our product until there was no further precipitation of the titanium salts. Thus this was the partial purification procedure which we adopted for the enamine (**117**) and as Petasis and Lu⁵⁸ had shown the enamine (**117**) could be used successfully in a reaction without purification we decided to persevere with the Noyori annulation reaction of the enamine (**117**) and dibromo ketoester (**116**) as shown earlier in Scheme 2.5.

The Noyori annulation of the enamine (**117**) and dibromo ketoester (**116**) was carried out under the same conditions as the successful “test” reaction which formed the cyclopentenone (**115**). Thus benzene solutions of the enamine (**117**) and dibromo ketoester (**116**) were added to a flask containing $\text{Fe}_2(\text{CO})_9$. The mixture was heated to 60 °C for 10 minutes with irradiation, and then left to stir overnight at room temperature with further irradiation. After the dilution of the reaction mixture with ethyl acetate, and washing with NaHCO_3 and brine, the reaction mixture was subjected to column chromatography in order to separate the reaction products. From the fractions collected there were no spirocycle-type products seen when GC-MS or NMR analysis was carried out. The only compound clearly isolated and positively identified was unreacted *N*-benzyl-2-pyrrolidinone (**123**) from the reaction to form the enamine (**117**)! Overall there were a number of reaction products which gave complicated NMR spectra and any functional groups present were difficult to identify. Even though Noyori and co-workers had stated that the annulation reaction afforded good yields in benzene,⁵⁴ toluene was also tried as a solvent for the reaction. The change of solvent, however, did not appear to alter the situation at all, a complex mixture of compounds still being observed in the reaction mixture. On reflection, it was realised that considering this was a novel reaction that was being attempted, using two only partially purified reactants was not at all sensible. A second and more important realisation was that the

dibromo ketoester chosen for the reaction was not ideal when looking at the mechanism of the Noyori reaction. As was discussed in Section 2.1.1, Noyori and co-workers had stated that a dibromo ketone with carbocation-stabilising substituents was required. An ester, if anything, would have a destabilising effect on the carbocation intermediate. The ester functionality would not stabilise the enolate (**105**) or oxyallyl-Fe(II) (**106**) intermediates seen in the mechanism (Scheme 2.1). Thus, in retrospect, it is not altogether surprising that this reaction failed to give a spirocycle. It was obvious then that a different dibromo ketone would have to be used in the reaction. We decided to continue using enamine (**117**). Though it could not be purified, literature precedent had shown the enamine (**117**) could be a useful reactant even in an impure form.⁵⁸ As the dimethyl substituted α,α' -dibromo ketone (**114**) had been used for the “test” Noyori reaction and could be synthesised and purified with relative ease, it was chosen as a replacement for the dibromo ketoester (**116**).

2.1.4. Reaction of 2,4-Dibromo-3-pentanone (**114**) and 1-Benzyl-2-methylenepyrrolidine (**117**)

Scheme 2.13 shows the intended reaction between dibromo ketone (**114**) and enamine (**117**) to give the expected product, spirocycle (**126**).



Scheme 2.13.

The reaction was carried out under the same conditions as the “test” reaction and the reaction of the enamine (**117**) and dibromo ketoester (**116**). After column chromatography one product which was isolated appeared from its NMR spectra to have most of the desired features of the molecule except notably there was no evidence of a carbonyl carbon atom in the ^{13}C NMR spectrum. The yield of this particular compound was extremely low, being only 8 % based on the dibromo ketone (**114**). Even though a signal characteristic of a carbonyl carbon was absent from the NMR spectra of the compound, the spectra were analysed further as no other fractions

collected from the chromatography exhibited promising NMR spectra.

Shown in Figure 2.3 is the ^1H NMR spectrum of the compound and in Figure 2.4 the ^{13}C spectrum. Also shown in the two figures is the azaspirocyclic structure (**127**) which was the structure proposed based on the NMR data and a HRMS spectrum of the compound, which confirmed the lack of oxygen in the molecule. The HRMS result corresponded to the molecular formula $\text{C}_{17}\text{H}_{21}\text{N}$. The ^1H and ^{13}C NMR spectra were assigned with the aid of DEPT, COSY, GHSQC, and GHMQC spectra and the proposed assignments will now be discussed.

In the ^1H NMR spectrum the two methyl protons are seen as singlets at 1.29 and 1.30 ppm, their separation being only 0.01 ppm. As these peaks were singlets it immediately indicated that the originally anticipated compound (**126**) had not been obtained as both methyl groups would have been doublets due to adjacent CH's. From 1.5 ppm to 3.0 ppm the diastereotopic CH_2 protons on the pyrrolidine ring are seen and these were assigned using the COSY spectrum. Thus the multiplet from 1.68 to 1.81 ppm is one of the C-4 protons, while the multiplet from 1.80 to 1.89 ppm is both C-3 protons. From 1.97 to 2.05 ppm, the second C-4 proton resonates, and finally the two C-2 protons are each seen as separated multiplets at around 2.5 and 2.9 ppm. Two clear doublets are seen at 3.22 and 3.60 ppm, both having the same coupling constant of 13.3 Hz and are thus assigned as the diastereotopic benzyl methylene protons. In the region between 1 and 4 ppm that has been discussed to far, some impurities can be seen, notably the fairly large singlet at around 3 ppm. Other smaller peaks have very similar shifts and appearances to the assigned peaks, seeming to indicate a very similar compound was present in the solution. Up to this point the assignments have been made with confidence though in the region from 6 to 7 ppm the assignment of the cyclopentadiene protons ring are tentative. For our proposed structure only two peaks are required for the C-9 and C-7 protons, but a number of peaks are seen in this region which we attributed to impurities. However, as the C-9 and C-7 protons should be singlets we assign the only two singlets seen in this region, at 6.21 and 6.41 ppm to the C-9 and C-7 methine protons respectively. Finally, the phenyl protons are easily assigned as the multiplet in the region 7.18 to 7.31 ppm.

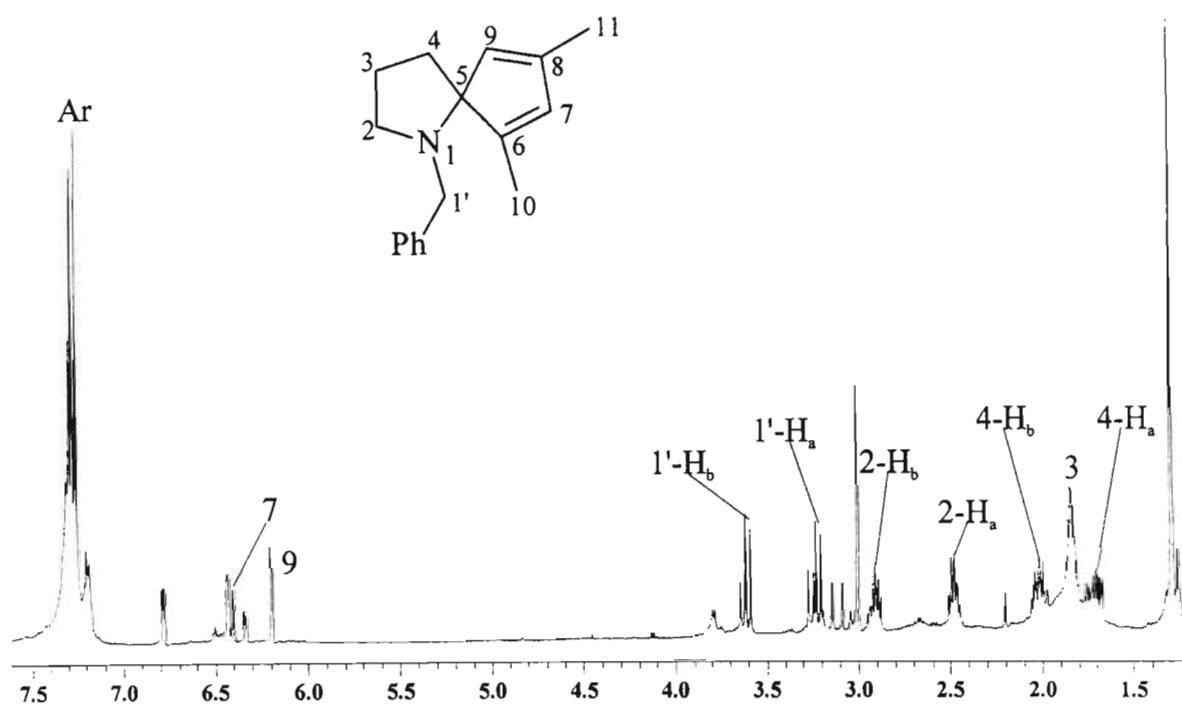


Figure 2.3. ¹H NMR spectrum of the product resulting from the reaction of 2,4-dibromo-3-pentanone (114) and 1-benzyl-2-methylenepyrrolidine (117). The proposed structure of the product, azaspirocycle (127), is shown.

Figure 2.4 shows the ¹³C NMR spectrum for the reaction product and the following assignments are made. The only two methyl groups present according to the DEPT spectrum are at 17.06 and 17.67 ppm, however C-10 and C-11 could not be distinguished. According to the DEPT spectrum the methylene groups are seen between 20 and 60 ppm. The C-3 carbon resonates at 21.56 ppm, the C-4 carbon at 39.07 ppm and the C-2 carbon at 49.87 ppm. The benzyl methylene carbon appears at 53.23 ppm. Most notably at 63.22 ppm a quaternary carbon is observed, presumably the spiro carbon. This is one of the most convincing pieces of evidence for the formation of some kind of spirocycle. As for the methine peaks in the ¹H NMR spectrum it becomes difficult to assign the carbon methine signals as there are more than required for the proposed structure. However, using the peaks assigned in the ¹H NMR spectrum in conjunction with the 2D GHSQC spectrum the C-9 and C-7 carbons are assigned to the peaks at 126.39 ppm and 131.65 ppm respectively. The aromatic carbon atoms are assigned to the signals at 128.01, 128.13 and 128.34 ppm.

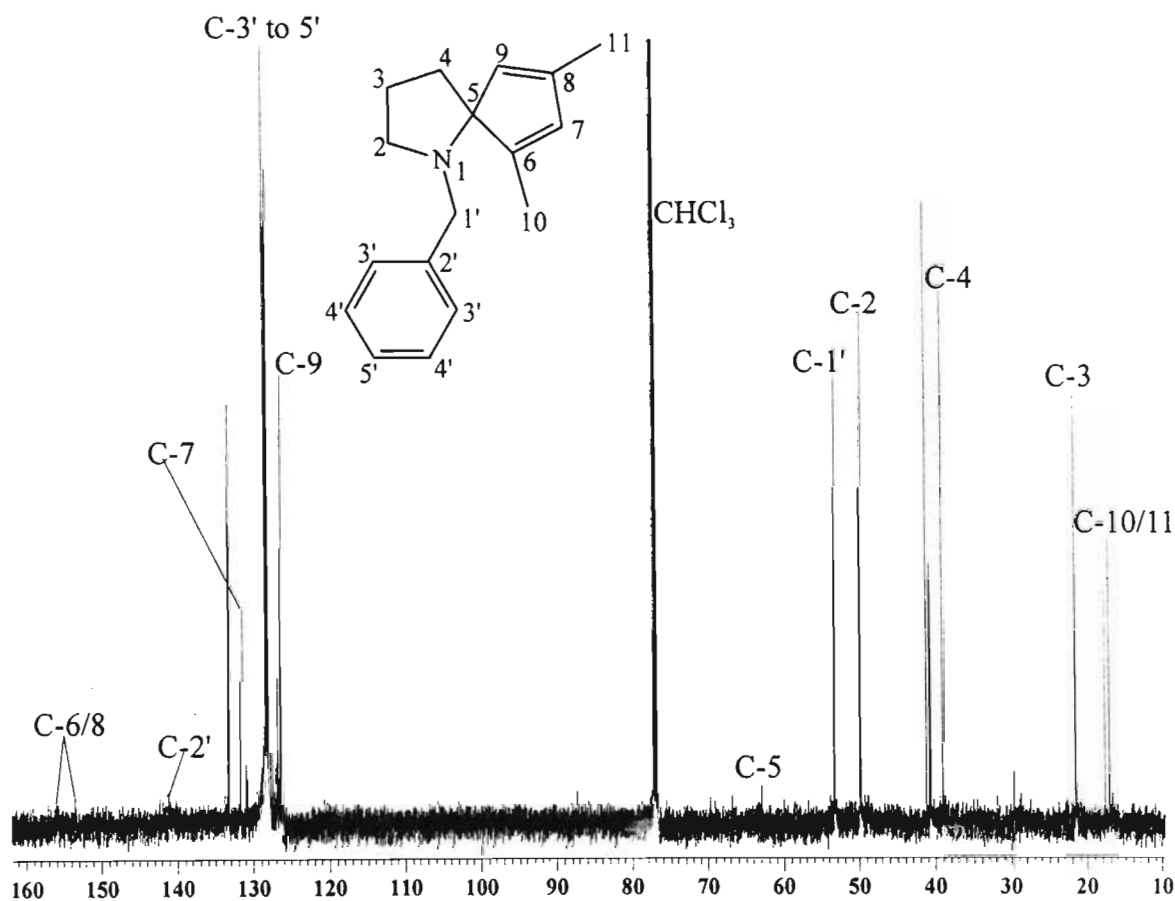


Figure 2.4. ^{13}C NMR spectrum of the product resulting from the reaction of 2,4-dibromo-3-pentanone (**114**) and 1-benzyl-2-methylenepyrrolidine (**117**). The proposed structure of the product, azaspirocycle (**127**), is shown.

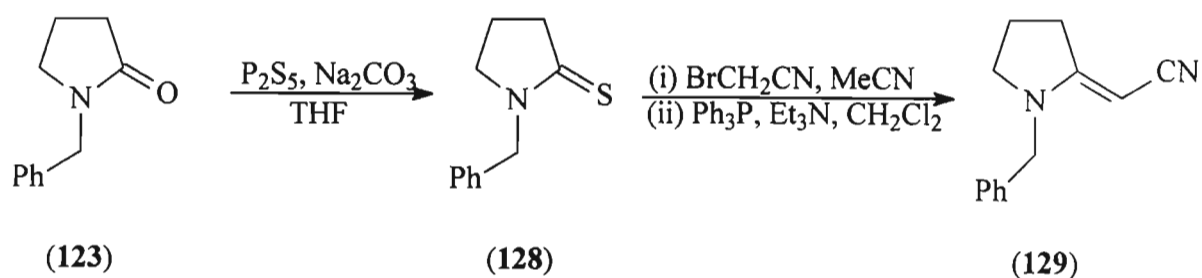
The remaining quaternary carbons were assigned with the aid of the GHMQC spectrum. The phenyl quaternary carbon atom appears at 141.09 ppm and the C-6 and C-8 quaternary carbons, which could not be distinguished, at 153.48 and 155.92 ppm. In the ^{13}C NMR spectrum a similar situation to that observed in the ^1H NMR spectrum was seen. A number of the peaks were doubled up, again indicating the presence of a slightly smaller amount of a very similar compound. For the proposed structure (**127**), two sets of peaks would not be expected as though there should be two enantiomers of the compound these would not be distinguishable by NMR. Thus the two possibilities are (a) there is a structurally similar impurity present or (b) our proposed structure is incorrect and the actual product is diastereomeric and two of these diastereomers are present in the NMR sample. To solve the problem it is obvious that a pure sample was required but with the low yield of the reaction it was extremely difficult to separate

the desired compound in a large enough quantity to obtain an NMR spectrum. Though the reaction was repeated with different reaction conditions the yield was not increased and we failed to obtain a purer sample.

The aim of the project was to use the Noyori annulation reaction to form the cephalotaxine spirocycle. Even though the reaction of 2,4-dibromo-3-pentanone (**114**) and 1-benzyl-2-methylenepyrrolidine (**117**) had appeared to form an azaspirocycle based on the NMR data, it was felt that this reaction had not achieved the desired aim. The anticipated product (**126**) had not been formed from the reaction and the putative spirocycle (**127**) had been achieved in extremely small quantities and was very difficult to purify. Thus, it was decided that pursuing this reaction would be fruitless considering the principal aim of the project.

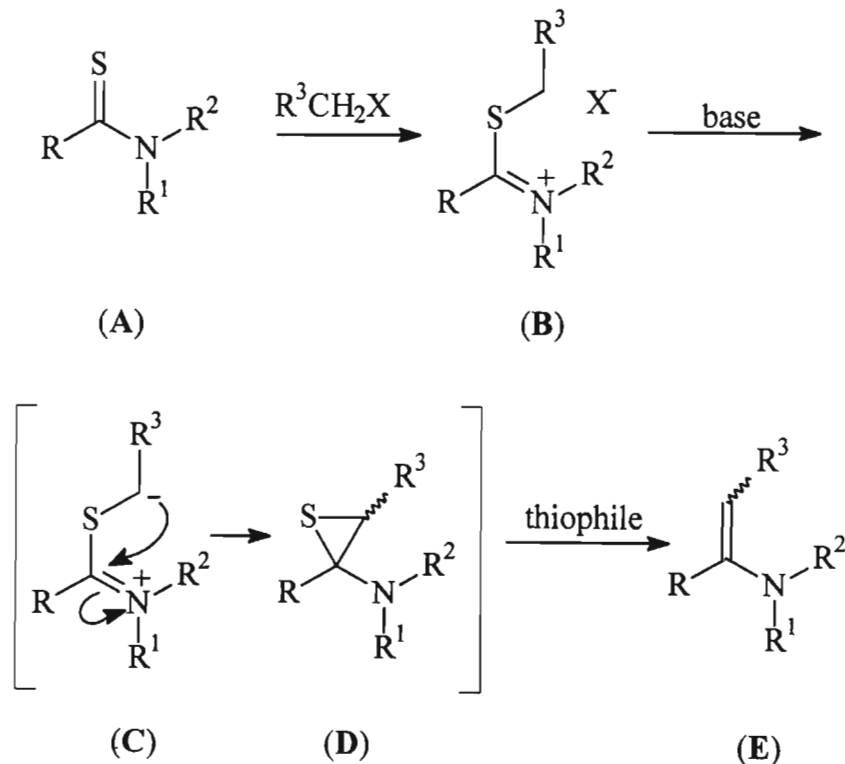
2.1.5. Synthesis of 1-Benzyl-7,9-dimethyl-8-oxo-1-azaspiro[4.4]nonane-6-carbonitrile (**130**)

Thus learning from our experience gained from the previous spirocycle reactions the starting materials for the Noyori annulation reaction were reexamined. The dibromo ketone (**114**) had been successfully used in the original “test” reaction and was not considered to be problematic and thus it was only the enamine that needed to be modified. From experience in our laboratory it was known that a nitrile group placed at the terminal end of the enamine (**117**) would stabilise this functionality. It was hoped that this electron-withdrawing moiety would also promote the formation of the Noyori annulation reaction product. Before the Noyori annulation reaction using these intended reactants could be carried out the vinylogous cyanamide (**129**) first had to be synthesised in a two step process from *N*-benzyl-2-pyrrolidinone (**123**). Scheme 2.14 shows the two reactions carried out.



Scheme 2.14.

The first step involved the conversion of *N*-benzyl-2-pyrrolidinone (**123**) to the corresponding thiolactam (**128**) which was achieved using the method of Brillon.⁷² Using this method P_2S_5 and Na_2CO_3 were reacted in a 1:1 ratio for 30 minutes to allow the formation of the THF soluble $(P_4S_{10}O)^{2-}Na_2^{2+}$ complex. Once this thionating agent was formed the *N*-benzyl-2-pyrrolidinone (**123**) was added and the resulting mixture left to stir for a further 3 hours. The product was purified by flash column chromatography and its formation confirmed by NMR spectroscopy, our NMR data agreeing with those of Brillon who had prepared the same compound.⁷² The ^{13}C NMR spectrum of the thiolactam (**128**) showed clearly the appearance of the thiocarbonyl quaternary peak at 201.73 ppm while the carbonyl quaternary signal of the lactam precursor (**123**) had disappeared from its position at 174.97 ppm. The synthesis of the vinylogous cyanamide (**129**) was then achieved using an Eschenmoser coupling reaction. In general this reaction involves the alkylation of a secondary or tertiary thioamide followed by a sulfide contraction, resulting in the elimination of the sulfur atom. The method of forming a carbon-carbon bond by this procedure was first noted by Knott in 1955.⁷³ However it took a further 16 years for the potential of the reaction to be realised by Eschenmoser and co-workers who demonstrated its general synthetic use.⁷⁴ The mechanism of this reaction is shown in Scheme 2.15.⁷⁵



Scheme 2.15. Mechanism of the Eschenmoser coupling reaction.

In the first step of the mechanism an α -thioiminium salt (**B**) is formed by the alkylation of the thioamide (**A**) with an electrophile. In the second step the addition of a base results in the abstraction of an α -proton in the side chain of the salt (**B**) to form the carbanion (**C**). The carbanion reacts with the iminium species to form the episulfide (**D**). The sulfur atom is extruded by a thiophile and the double bond is formed resulting in the desired enamine (**E**). Depending on the substrates used in the Eschenmoser coupling reaction, the product obtained can be either an (*E*)- or (*Z*)-isomer or a mixture of both. In our situation only one isomer was observed and is assigned to be the (*E*)-isomer as in the case of tertiary thiolactams the (*E*)-isomer is found to form exclusively.⁷⁵ No evidence of the vinylogous cyanamide (**129**) was found in the literature but its formation was confirmed by GC-MS, IR and NMR spectroscopy. The ¹³C NMR spectrum of the vinylogous cyanamide (**129**) shown in Figure 2.5 was particularly useful for its characterisation. Though the spectrum is very similar to that of the thiolactam precursor (**128**), two new peaks appear, these being the methine C-2' carbon at 54.46 ppm and the nitrile carbon at 114.53 ppm as a small, obviously quaternary peak. In the GHMQC spectrum of the compound, which shows correlations between a carbon atom and the protons of the neighboring carbon atom, the quaternary peak at 114.53 ppm showed a correlation to the vinylic proton, confirming that the peak is due to the nitrile carbon. This also confirmed that the peak at 122.66 ppm, which is slightly larger, is not the nitrile carbon but simply an impurity.

The ¹H NMR spectrum of the novel vinylogous cyanamide (**129**) is shown in Figure 2.6 with the most notable peak being the vinyl proton at 3.58 ppm which once again confirms the formation of the desired product. As for the ¹³C NMR spectrum the ¹H NMR spectrum is very similar to that of the thiolactam precursor (**128**). The C-4 protons appear at 2.01 ppm in the form of five lines, the C-3 and C-5 protons both appear as triplets at 2.94 and 3.42 ppm respectively, the benzyl methylene protons resonate as a singlet at 4.28 ppm, and the phenyl protons are found as a multiplet at *ca.* 7.3 ppm. The peaks at 3.80 and 5.30 ppm are impurities.

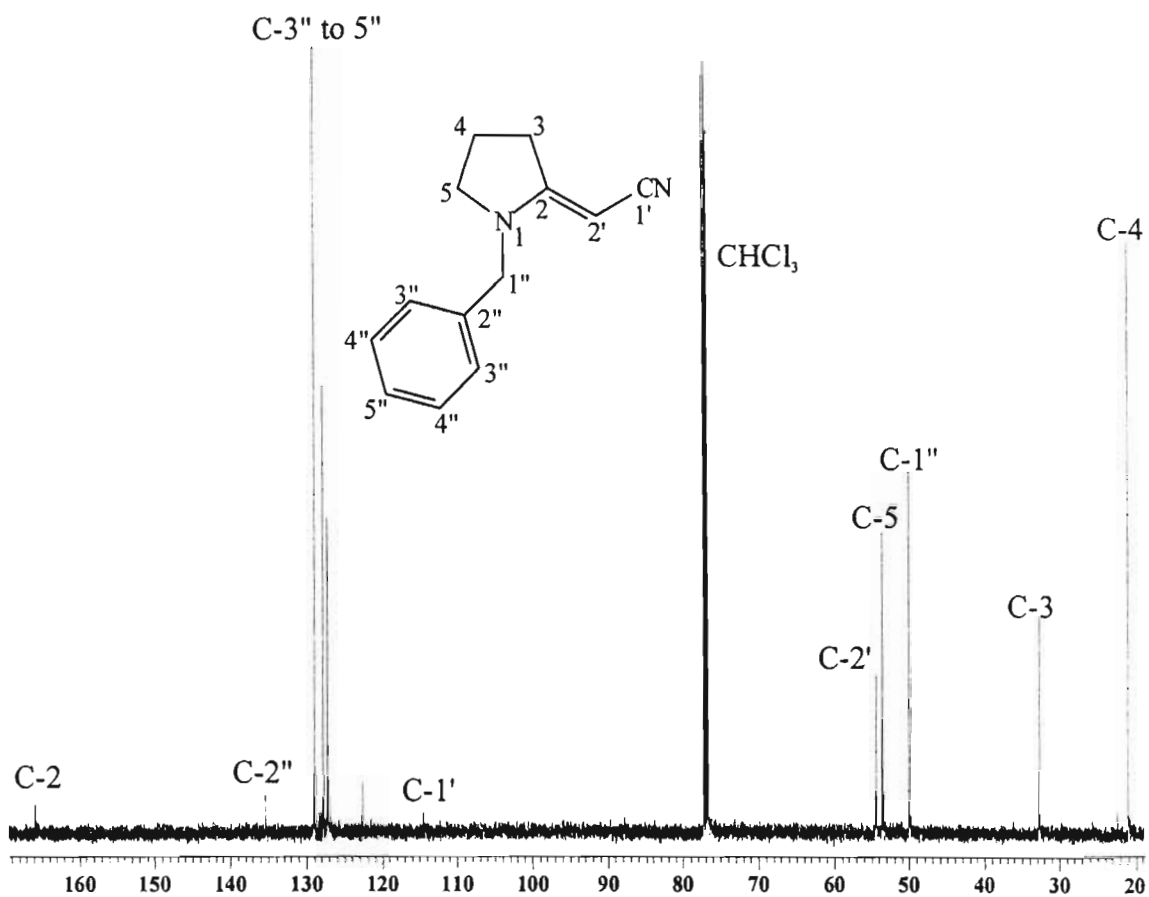


Figure 2.5. ^{13}C NMR spectrum of vinyllogous cyanamide (129).

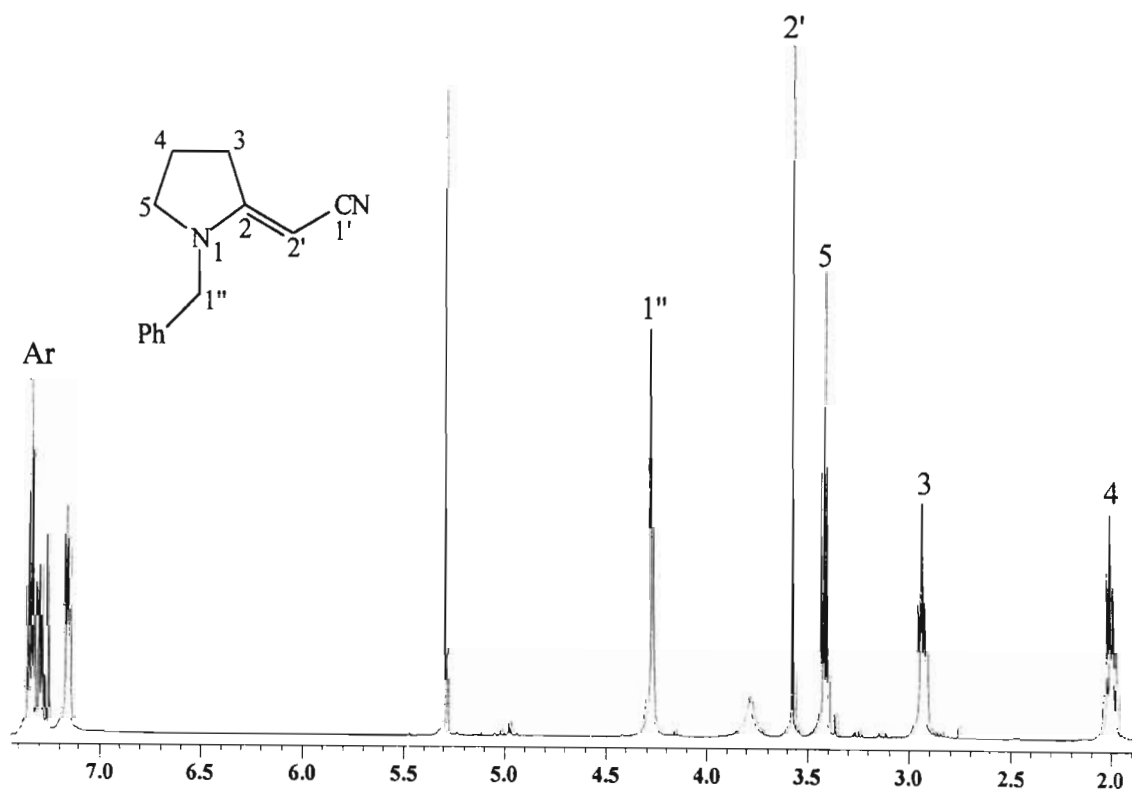


Figure 2.6. ^1H NMR spectrum of vinyllogous cyanamide (129).

diastereomer, but these were not pure and covered in red oil, and so an attempt was made to recrystallise these. NMR spectra were collected for the large, colourless crystals and indeed a single diastereomer had crystallised out as clean spectra were obtained and the peaks in both the ^1H and ^{13}C spectra could be unambiguously assigned with the help of DEPT, COSY, GHSQC and GHMQC spectra. The ^1H NMR spectrum obtained from the crystals of this novel compound is shown in Figure 2.7 and the assignments are made as follows. The two methyl groups adjacent to the carbonyl group both appear as doublets as expected with the C-10 methyl group appearing at 1.14 ppm while the C-11 methyl group is at 1.27 ppm. All the methylene protons on the pyrrolidine ring are diastereotopic. Thus at around 1.8 ppm one C-3 proton resonates while the other appears as part of the multiplet between 1.99 and 2.11 ppm. One C-4 proton appears at around 1.9 ppm with the other also being part of the multiplet between 1.99 and 2.11 ppm. The last pyrrolidine methylene group at C-2 has one diastereotopic proton appearing at around 2.8 ppm and the other at approximately 3.0 ppm. The two methine protons on C-9 and C-7 appear as a multiplet between 2.36 and 2.46 ppm, while the methine proton which is α to the nitrile group is clearly seen as a doublet at 2.75 ppm. The benzyl methylene protons are again diastereotopic, each appearing as a doublet at 3.81 and 3.84 ppm, and finally the aryl protons appear as a multiplet around 7.3 ppm. The peak at approximately 1.6 ppm is a minor impurity.

The ^{13}C NMR spectrum for the spirocycle (**130**) is shown in Figure 2.8. Probably the most important peak in the ^{13}C NMR spectrum is the quaternary carbon at the spirofused centre which appears clearly at 71.08 ppm. The other important features of the molecule are all evident such as the two methyl groups at 8.70 and 14.06 ppm, the nitrile quaternary carbon at 119.69 ppm, the aryl methine carbon atoms at *ca.* 128 ppm, and the carbonyl carbon atom signal is the furthest downfield at 213.71 ppm.

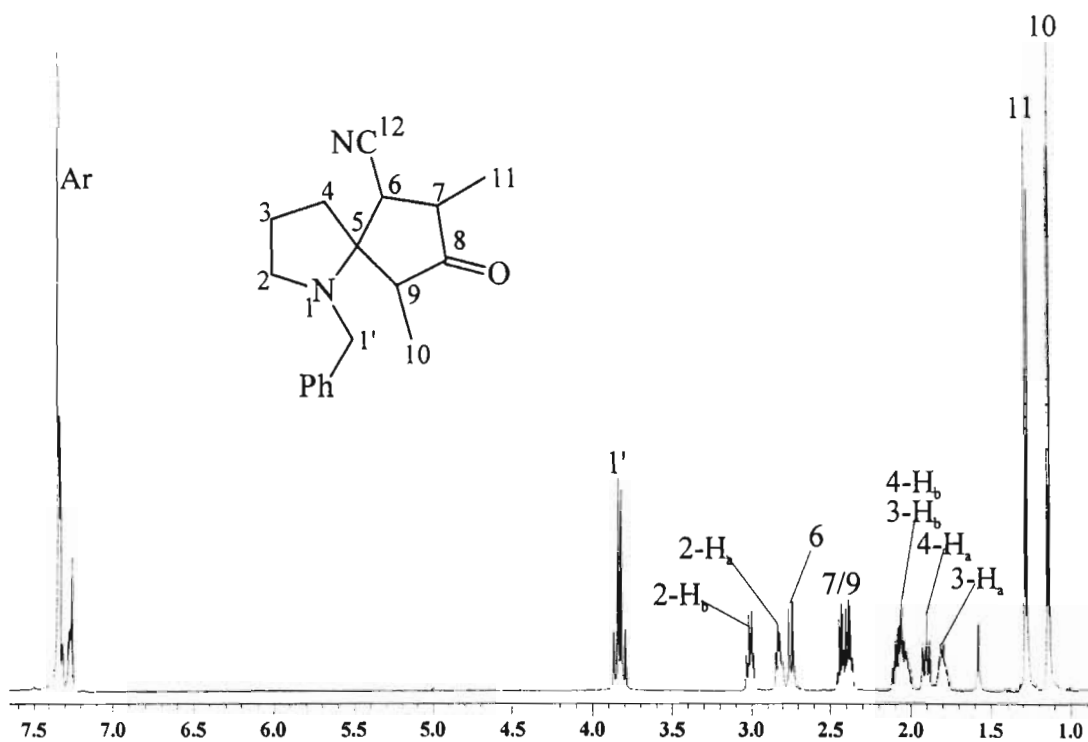


Figure 2.7. ^1H NMR spectrum of spirocycle (130).

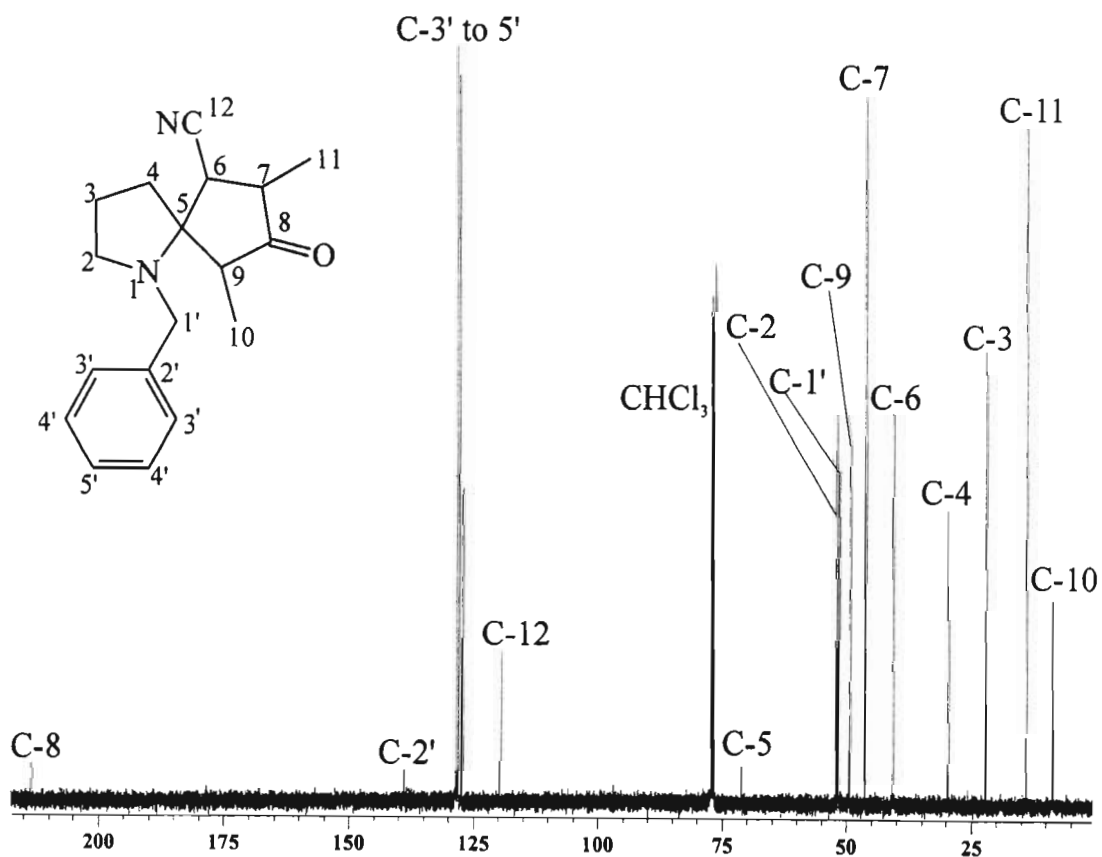


Figure 2.8. ^{13}C NMR spectrum of spirocycle (130).

Further NOESY experiments were carried on the crystalline diastereomer in an attempt to assign the relative stereochemistry at the four stereogenic centres. Irradiation of the C-10 methyl group showed a through space correlation to the methine proton at C-7 (Figure 2.9) apparently indicating a *trans* relationship between the two methyl groups. Though the C-7 and C-9 protons appear in the same multiplet, the COSY spectrum clearly indicated that the C-7 proton resonates further downfield, thus the two protons could be distinguished in the proton spectrum even though they were not perfectly resolved. The *trans* relationship of the methyl groups was further confirmed by irradiation of the C-11 methyl group, as this showed a correlation to the C-9 proton (Figure 2.10). Irradiation of this C-11 methyl group also showed a correlation to the C-6 proton α to the nitrile group, thus again indicating a *trans* relationship between the C-11 methyl group and the nitrile moiety. Finally irradiation of the benzyl methylene protons showed a correlation to both the C-9 and C-6 protons (Figure 2.11). The C-9 and C-6 protons both appeared to be *cis* to one another from the observations described above and thus if the benzyl group was showing a correlation to both protons it appeared that the ring nitrogen would also be *cis* to them.

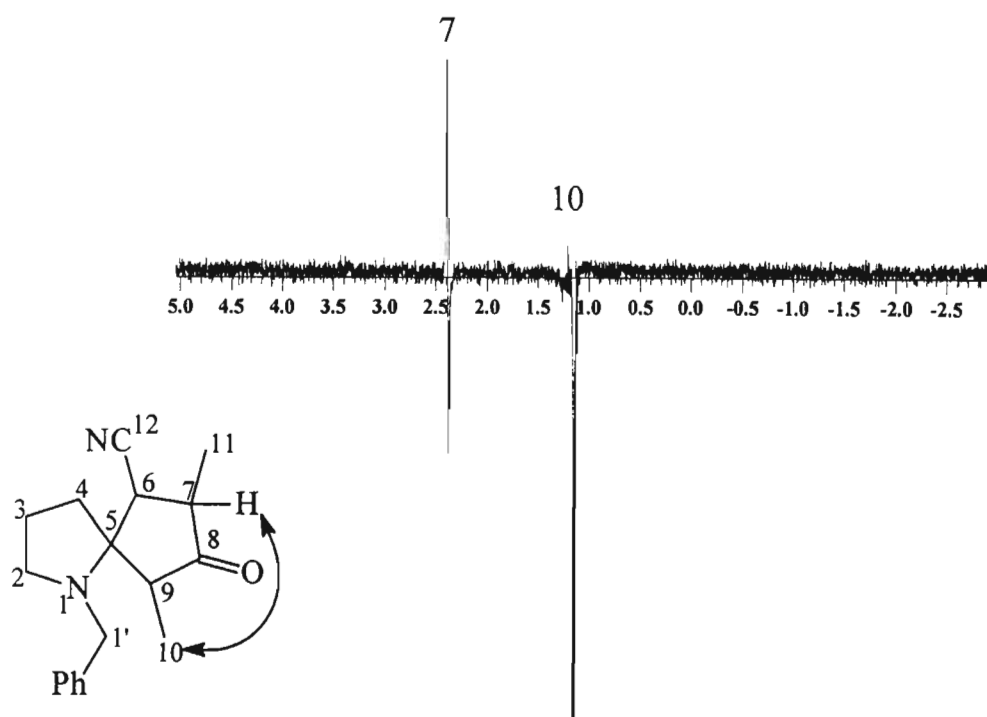


Figure 2.9. NOESY spectrum showing irradiation of the spirocycle (**130**) C-10 methyl group and the response exhibited by the C-7 methine proton.

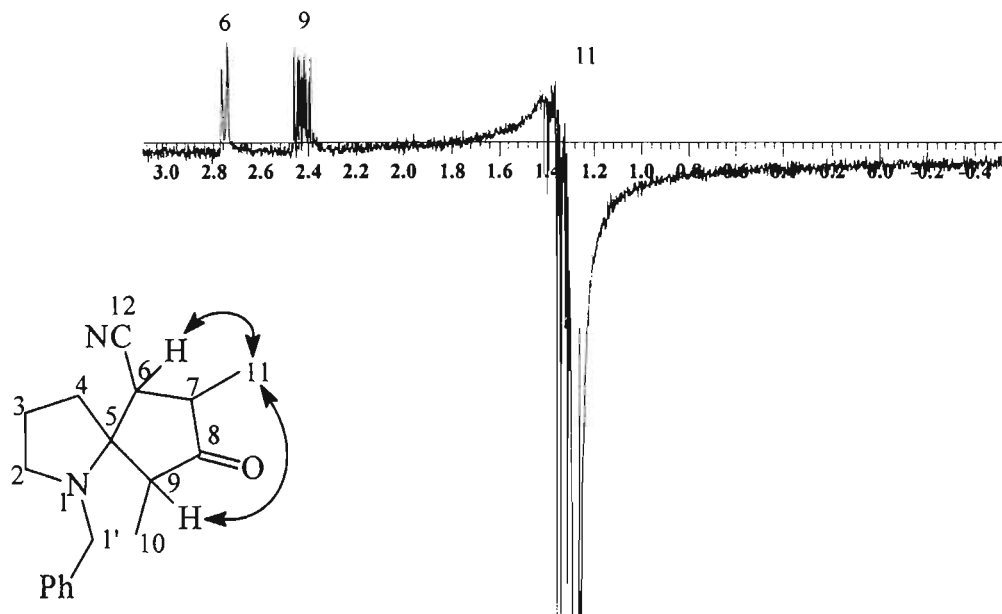


Figure 2.10. NOESY spectrum showing irradiation of the spirocycle (130) C-11 methyl group and the response exhibited by the C-6 and C-9 methine protons.

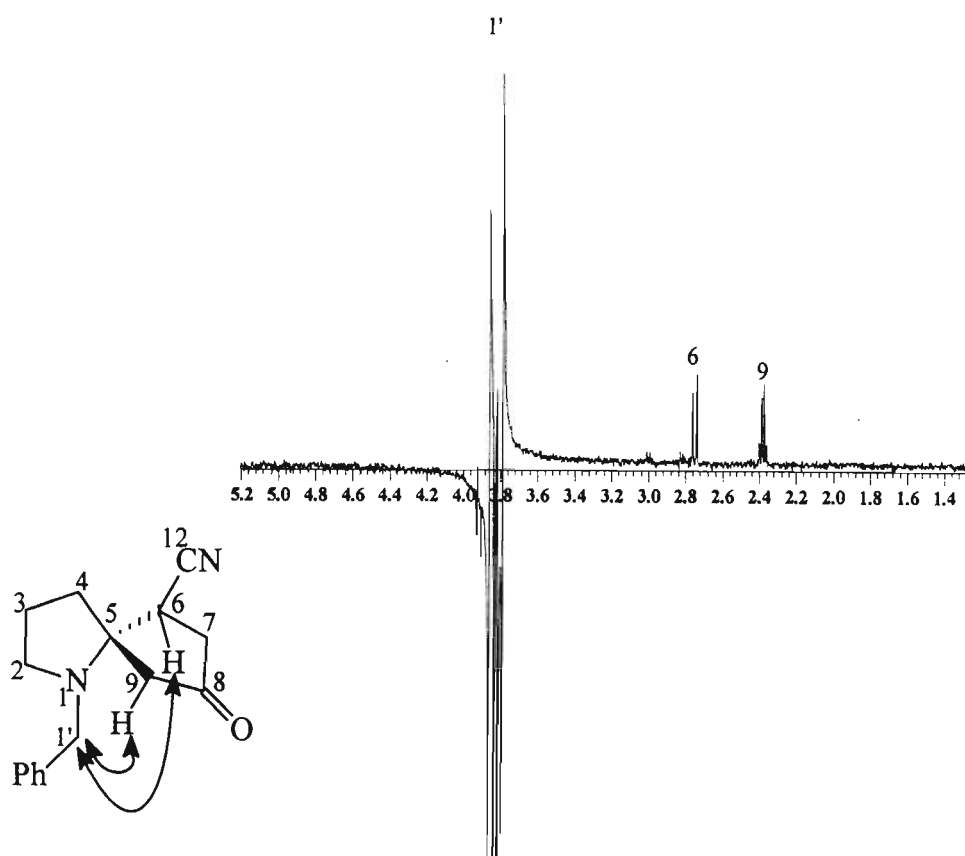


Figure 2.11. NOESY spectrum showing irradiation of the spirocycle (130) benzyl methylene protons and the response exhibited by the C-6 and C-9 methine protons (methyl groups omitted for clarity).

Based on the above NOESY experimental data the relative stereochemistry of azaspirocycle (**130**) was predicted to be $5S^*$, $6S^*$, $7S^*$, $9S^*$ as shown in Figure 2.12. The methyl groups are *trans* to one another, the nitrile and C-10 methyl are *cis*, and the ring nitrogen *trans* to these latter groups and *cis* to the C-11 methyl group.

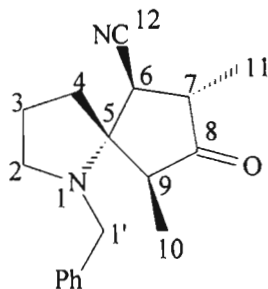


Figure 2.12. Relative stereochemistry predicted from NOESY results for the crystalline diastereomer of azaspirocycle (**130**).

As the diastereomer under investigation was crystalline and the crystals obtained were of excellent quality it seemed obvious that an attempt should be made to obtain a crystal structure, especially since the compound was novel and interesting from a stereochemical point of view. The X-ray structure would confirm whether our prediction of the relative stereochemistry based on the NOESY data was correct. The crystal structure was indeed obtained and is shown in Figure 2.13.

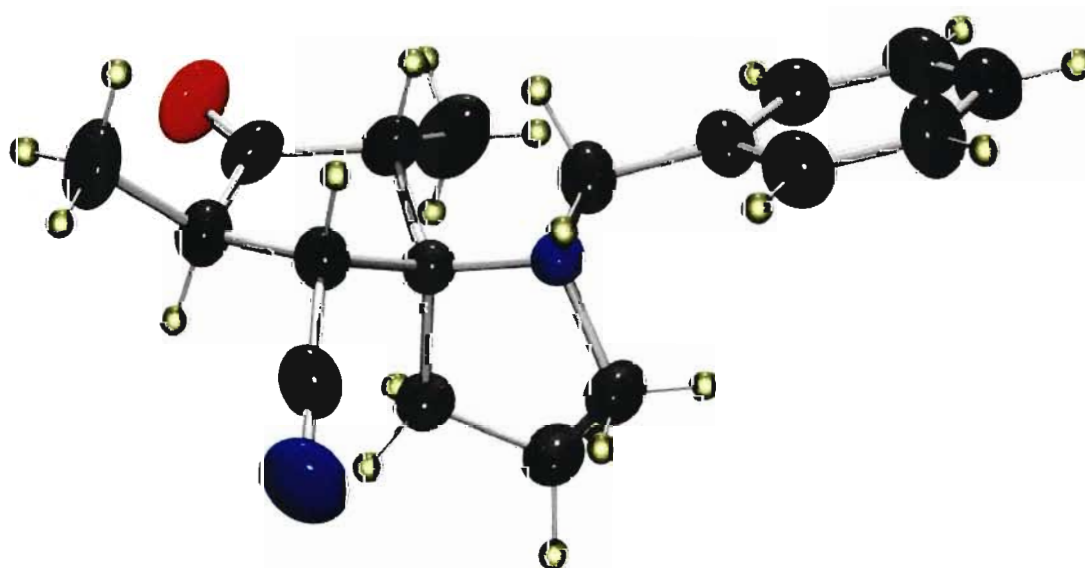


Figure 2.13. X-ray crystal structure of spiropcycle (**130**).

From the X-ray crystal structure it was found that the crystal system was triclinic and the space group P_1 . The total number of molecules per unit cell (Z) was four, with two molecules per asymmetric unit. The two molecules in the asymmetric unit showed no fundamental differences from one another and so only one molecule from the asymmetric unit of the crystal structure is shown in Figure 2.13. Further crystal structure data for the spirocycle (**130**) is shown in Appendix A. The X-ray crystal structure confirmed that the relative stereochemistry for the crystalline diastereomer of azaspirocycle (**130**) was indeed $5S^*$, $6S^*$, $7S^*$, $9S^*$ as was predicted in Figure 2.12 from the NOESY results.

Figure 2.14. shows the lattice packing diagram for the crystal structure. As can be seen the molecules are close packed and arranged in an orderly fashion. Bond distances of atoms in adjacent molecules were measured in order to assess whether any intermolecular interactions were taking place, but this was not found to be the case.

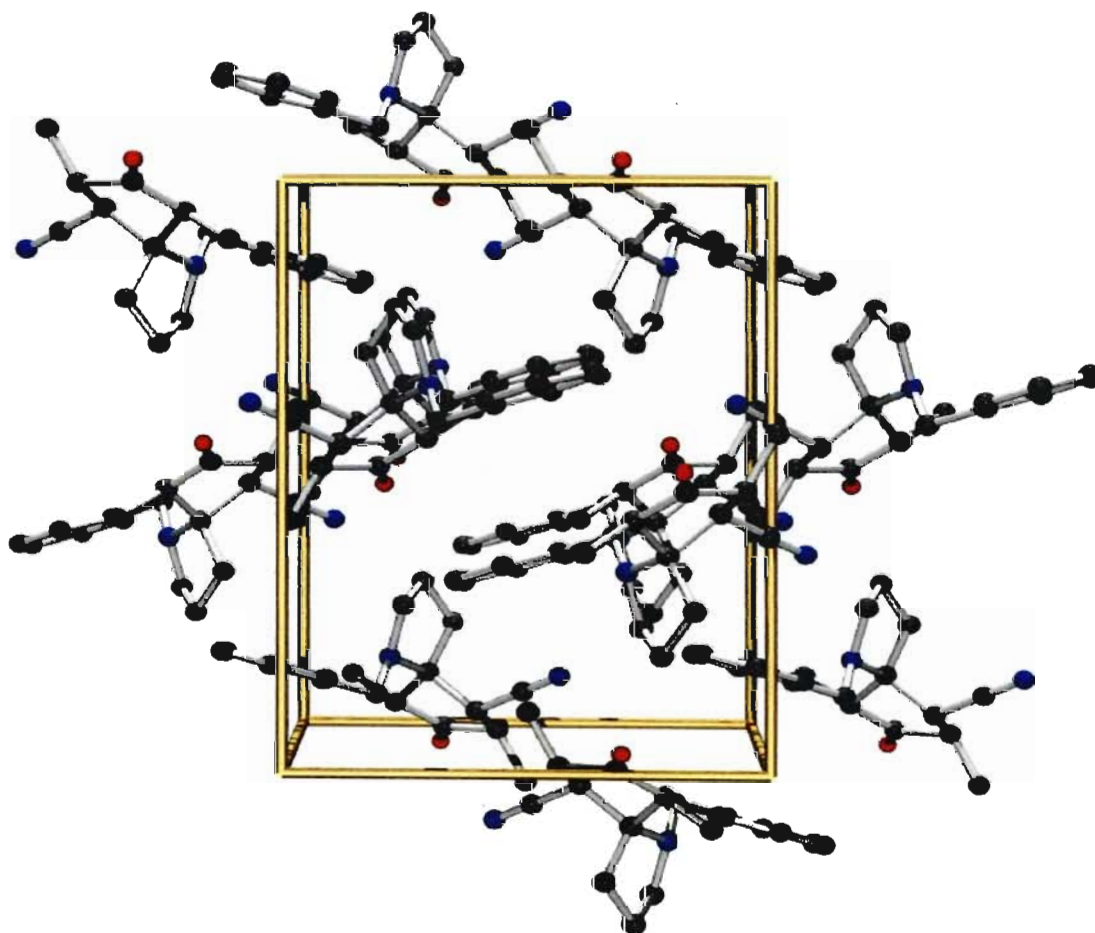


Figure 2.14. Crystal packing diagram for spirocycle (**130**) as viewed down the a -axis.

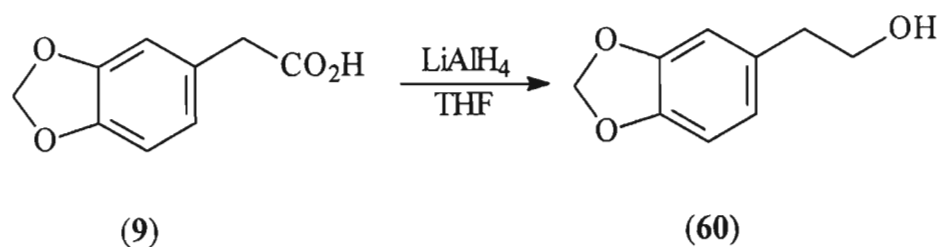
With one of the diastereomers of the spirocycle (**130**) successfully isolated and characterised the focus was turned to the other remaining diastereomers. As was mentioned earlier, it was observed that other crystals had formed in the fractions obtained after the chromatography and as these were covered in a red oil so an attempt was made to purify them by recrystallisation. However, it was found that on evaporation of the recrystallisation solvent nothing but the red oil remained and no crystals had formed. At the same time it was noted that the crystals from which the X-ray structure had been obtained were also forming a red oil-like substance on the surface of the solid. It was realised that the spirocycle is obviously not as stable as was initially assumed after the formation of the large, colourless crystals. An NMR was run on some of the red oil-like substance, and though it appeared as though a small amount of the spirocycle (**130**) remained, at least one decomposition product, if not more, had indeed formed. Unfortunately because the compound decomposed before the diastereomers were properly separated their individual yields could not be determined. The diastereomer which crystallised out was at least 12 % of the total diastereomeric mixture, though there was in all likelihood more of this diastereomer mixed in fractions with other diastereomers. Because of time constraints and the fact that no more work could be carried out on the spirocycle (**130**) diastereomers due to the decomposition of these products, the investigation into the Noyori annulation reaction to form the cephalotaxine spirocycle was concluded. The aim to synthesise the cephalotaxine spirocycle had been successfully achieved in a reasonably efficient manner with a novel compound being synthesised, one of its diastereomers fully characterised, and its crystal structure obtained. This work could without doubt be continued as it shows much potential, but it was not possible to exploit the possibilities in the framework of this masters project. The future of this work has been discussed in Section 2.3.

2.2. PROGRESS TOWARDS THE CEPHALOTAXINE PENTACYCLIC SKELETON

Unfortunately the Noyori annulation studies carried out were not applied to the synthesis of the cephalotaxine pentacyclic skeleton due to time constraints. However, preliminary work on the cephalotaxine structure was carried out and was in its own right successful. The initial steps of the proposed route to the cephalotaxine skeleton outlined in Chapter 1 that were successfully carried out are now described.

2.2.1 Synthesis of 2-(1,3-Benzodioxol-5-yl)-1-ethanol (60)

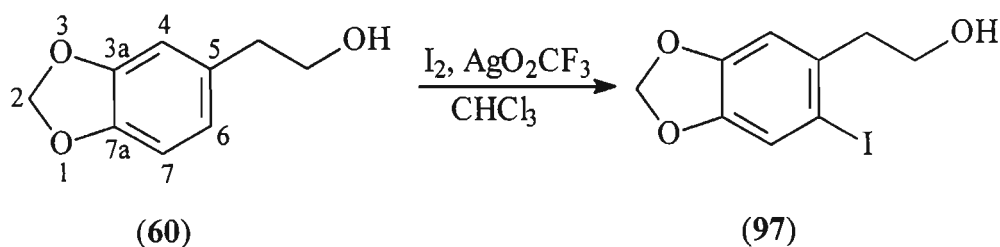
Using the method of Semmelhack *et al.*,^{29,30} the alcohol (60) was synthesised from the commercially available 3,4-methylenedioxyphenylacetic acid (9) (Scheme 2.17) using LiAlH_4 as a reductant. The only modification of the literature procedure was the use of THF as a solvent in place of diethyl ether. The reaction proceeded in a yield of 96 % with no purification being carried out as the product was analytically pure.



Scheme 2.17.

2.2.2. Synthesis of 2-(6-Iodo-1,3-benzodioxol-5-yl)-1-ethanol (97)

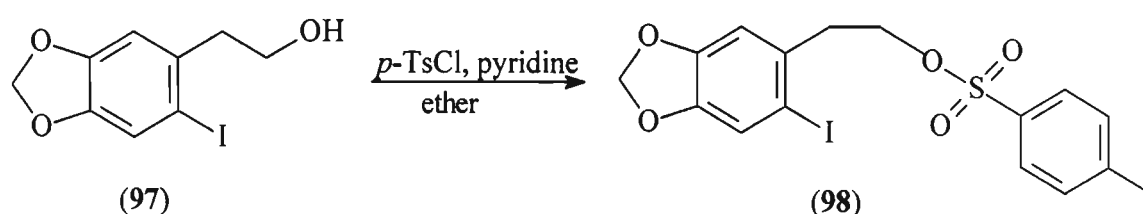
The procedure of Semmelhack *et al.*,^{29,30} with some modifications taken from the procedure of Tietze *et al.*,⁷⁶ was used to iodinate the alcohol (60) to form 2-(6-iodo-1,3-benzodioxol-5-yl)-1-ethanol (97) (Scheme 2.18). This was carried out using molecular iodine and silver trifluoroacetate. As iodine is the least reactive of the halogens in aromatic substitution reactions silver trifluoroacetate is used to generate iodine trifluoroacetate. This causes the electrophilic nature of the iodine to be enhanced and improves its reactivity in the electrophilic aromatic substitution reaction.⁷⁷ According to the method followed the product can be purified by crystallisation, but it was found to be quicker to purify the reaction mixture by radial chromatography rather than wait for crystals to grow, and then use the resulting pure oil of the iodinated product (97) in the next reaction. The product was obtained in a 52 % yield, which compared favourably with Semmelhack's 55 % yield.^{29,30} Tietze however reports a yield of 97 %, ⁷⁶ and though the procedure was repeated numerous times, the 52 % yield could not be improved upon. The iodination is extremely regioselective with the electrophilic substitution only taking place at C-6 (Scheme 2.18). This is evident from the ¹H NMR spectrum which only shows two singlets in the aromatic region corresponding to the C-4 and C-7 protons. Only on one occasion was a small quantity of the regioisomer with the iodine substituted at C-4 observed.



Scheme 2.18.

2.2.3. Synthesis of 2-(6-Iodo-1,3-benzodioxol-5-yl)ethyl 4-methylbenzenesulfonate (98) and 2-(6-Iodo-1,3-benzodioxol-5-yl)ethyl 4-nitrobenzenesulfonate (15a)

With the A and B cephalotaxine rings intact it was our intention to add the D ring in the form of 2-pyrrolidinone. However, as in the work of Semmelhack *et al.*,^{29,30} a better leaving group first needed to replace the alcohol functionality to facilitate the addition of 2-pyrrolidinone. Semmelhack *et al.*,^{29,30} synthesised 2-(6-iodo-1,3-benzodioxol-5-yl)ethyl 4-nitrobenzenesulfonate (15a) from the iodo alcohol (97) with the 4-nitrobenzenesulfonate, or nosylate, moiety acting as a good leaving group. As was mentioned in the project aims the reagent required for this reaction was 4-nitrobenzenesulfonyl chloride (4-NsCl) which we did not have available at the time and thus it was decided that the 4-methylbenzenesulfonate, or tosylate, analogue would be synthesised. Thus using the procedure of Semmelhack *et al.* the iodo alcohol (97) was reacted with *p*-toluenesulfonyl chloride (*p*-TsCl) in the presence of freshly distilled pyridine to give the desired tosylate (98) (Scheme 2.19.) which was purified using radial chromatography.



Scheme 2.19.

Initial yields were extremely poor but were improved upon, however only to the extent that a 39 % yield was the highest obtained. It was found that the yield was reduced significantly if undistilled pyridine was used. On being left to stand, the oil obtained after purification crystallised out to give colourless, X-ray quality crystals. After a search of the Cambridge

Crystallographic Database showed no crystal structure existed for this compound, further database searches (Beilstein and Science Citation Index) were carried out and it was found that the tosylate (**98**) was in fact novel. The X-ray structure of the tosylate was subsequently obtained and was found to be conformationally complex and warranted further study. The conformational analysis of the tosylate (**98**) which was carried out has been fully detailed in Chapter 3 of this dissertation. The ^1H and ^{13}C NMR spectra for the tosylate (**98**) are shown in Figures 2.15 and 2.16 respectively. The spectra are very similar to those collected for the iodo alcohol (**97**) except for the loss of the hydroxyl proton in the ^1H NMR spectrum and the appearance in both the proton and carbon NMR spectra of the peaks due to the tosylate functionality. In the ^1H NMR spectrum (Figure 2.15) the new signals due to the tosylate are the methyl group at 2.44 ppm and the tosyl ring protons which appear as doublets in the aromatic region. The H-3 and H-5 protons nearest the methyl group give rise to the doublet at 7.29 ppm while the H-2 and H-6 protons nearest the sulfone group give rise to the doublet at 7.71 ppm.

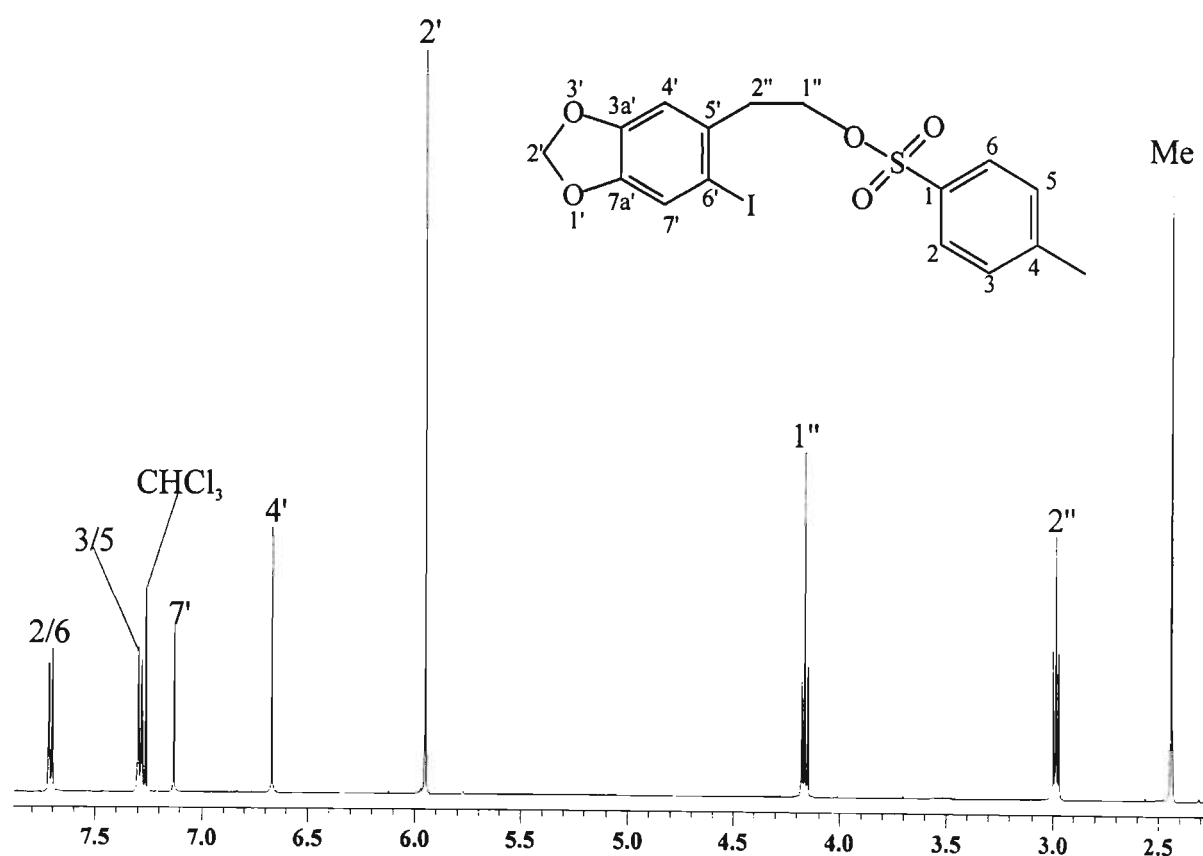


Figure 2.15. ^1H NMR spectrum of tosylate (**98**).

In the ^{13}C NMR spectrum the tosylate methyl carbon is found at 21.61 ppm, the C-2 and C-6 methine carbons at 127.87 ppm and the C-3 and C-5 methine carbons at 129.74 ppm. Finally the quaternary carbons on the aromatic tosyl ring, C-4 and C-1, resonate at 132.86 and 133.68 ppm respectively.

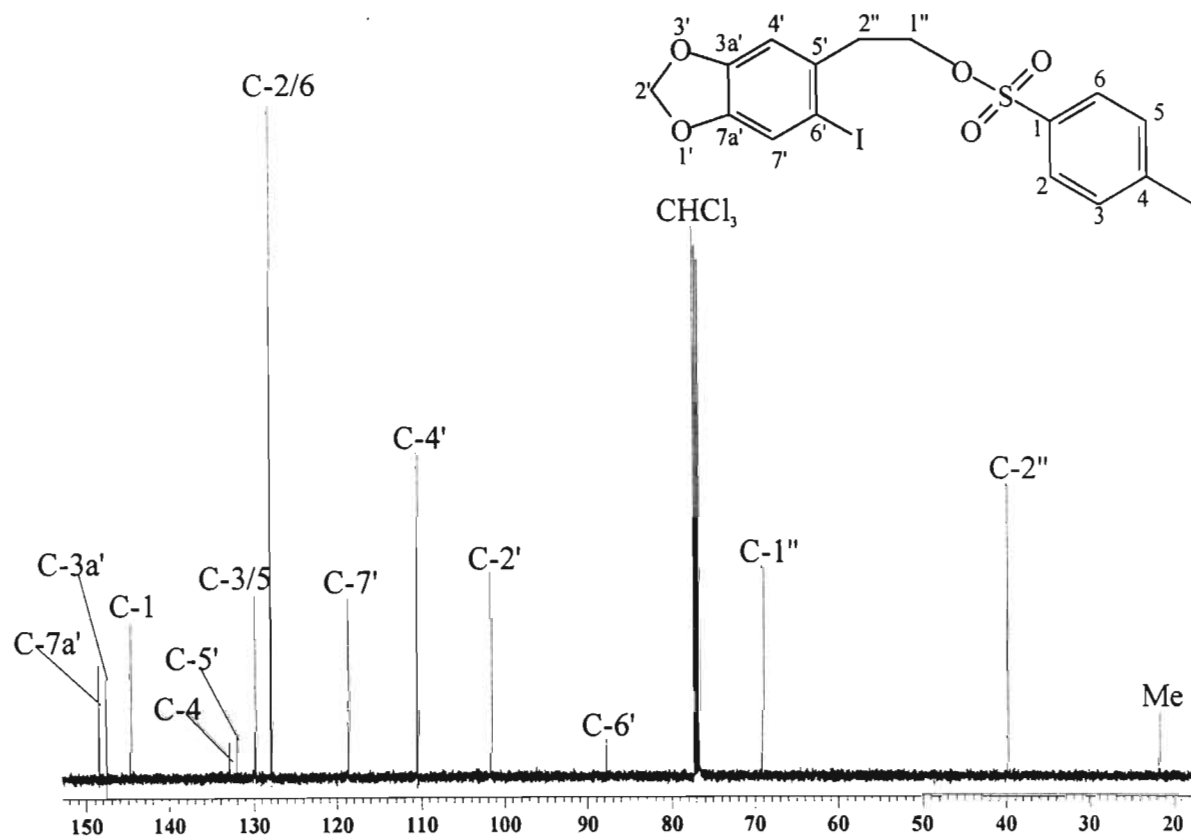
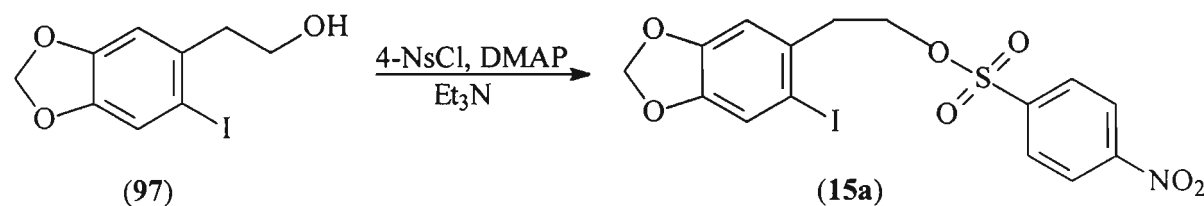


Figure 2.16. ^{13}C NMR spectrum of tosylate (**98**).

In order to confirm a hypothesis made during the conformational analysis study it was necessary to synthesise the nosylate (**15a**) of Semmelhack *et al.*^{29,30} The intention was to obtain the crystal structure of this compound which is not present in the Cambridge Crystallographic Database, though the compound itself is not novel. Thus the required reagent, 4-nitrobenzenesulfonyl chloride, was purchased and the synthesis of the nosylate (**15a**) carried out using the method of Tietze.⁷⁶ This method differed from the tosylate synthesis as triethylamine and DMAP were used in the place of pyridine (Scheme 2.20). The synthesis was also notably quicker taking only four hours as opposed to two days. The nosylate (**15a**) was successfully synthesised but unfortunately the yield obtained was very low being only 25 %. This was attributed to the 4-nitrobenzenesulfonyl chloride which was used. This particular reagent was 90 % technical grade

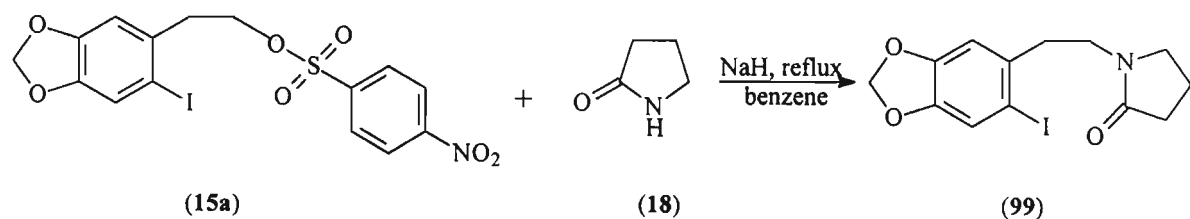
and it was found to be extremely difficult to remove the impurities resulting from the starting material which resulted in a reduction of the yield. Despite this the nosylate (**15a**) was successfully isolated and crystallised allowing the X-ray structure to be obtained (see Chapter 3).



Scheme 2.20.

2.2.4. Synthesis of 1-[2-(6-Iodo-1,3-benzodioxol-5-yl)ethyl]-2-pyrrolidinone (**99**)

With the nosylate (**15a**) synthesised it was used in the next reaction of the proposed synthetic sequence to add on the cephalotaxine D ring (Scheme 2.21). Though the original intention had been to use the method of Semmelhack *et al.*,^{29,30} the method of Nagasaka *et al.*⁴⁰ was preferred as it specifically involved the addition of a lactam as in our work. Thus the nosylate (**15a**) was reacted with 2-pyrrolidinone (**18**) in the presence of NaH to form the tertiary lactam (**99**). The product was synthesised in a 47 % yield and was characterised by GC-MS, IR, and NMR spectroscopy. This compound is novel and crystalline and an attempt was made to grow X-ray quality crystals to complete the characterisation. Unfortunately, crystals of sufficient quality were never obtained.



Scheme 2.21.

The ^1H NMR spectrum of the tertiary lactam (**99**) is shown below in Figure 2.17 and was assigned with the aid of the DEPT, COSY, and GHSQC, spectra and also by comparison with the other benzodioxol and 2-pyrrolidinone derivatives that were synthesised during the course of the project. The multiplet centred around 1.94 ppm is due to the C-4 protons, which are coupled to the two CH_2 groups on either side. Four triplets are seen moving further downfield

at 2.32, 2.82, 3.30, and 3.37 ppm which correspond to the C-3, C-2'', C-5, and C-1'' methylene groups respectively. The methylenedioxy protons resonate as a singlet at 5.89 ppm and finally the C-4' and C-7' aromatic protons are observed at 6.74 and 7.15 ppm respectively.

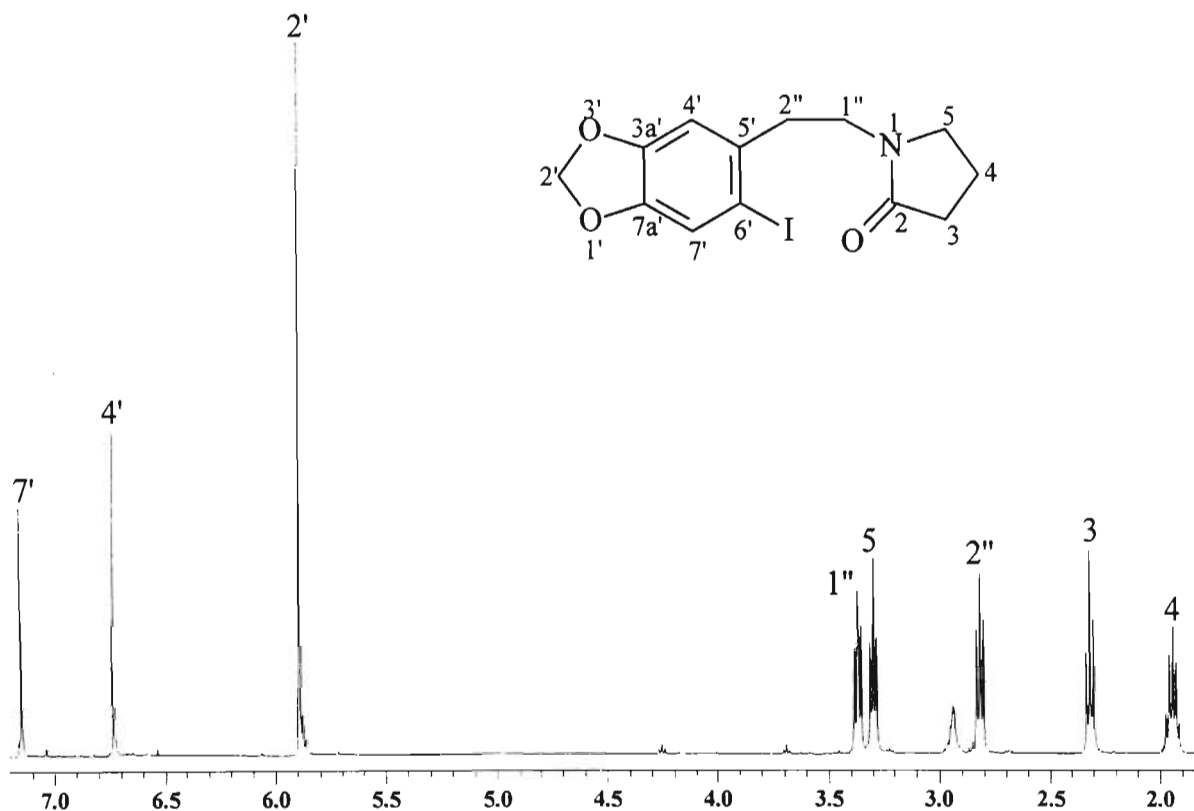


Figure 2.17. ^1H NMR spectrum of tertiary lactam (**99**).

The ^{13}C NMR spectrum of tertiary lactam (**99**) is shown in Figure 2.18. All the methylene carbons resonate between 15 and 50 ppm bar the methylene dioxy methylene group which appears further downfield at 101.51 ppm due to the deshielding effect of the oxygen atoms which flank it. The aromatic methine carbon atoms, C-7' and C-4', appear at 109.51 and 118.42 ppm respectively. Finally the quaternary carbons are all seen above 130 ppm except for the C-6' carbon which appears quite far upfield for a quaternary carbon at 87.48 ppm. This is, however, characteristic for a sp^2 -hybridised carbon atom attached to an iodine atom. The quintet which appears at 49 ppm is due to a small amount of CD_3OD which was added to the CDCl_3 solution of the tertiary lactam (**99**) to improve its solubility.

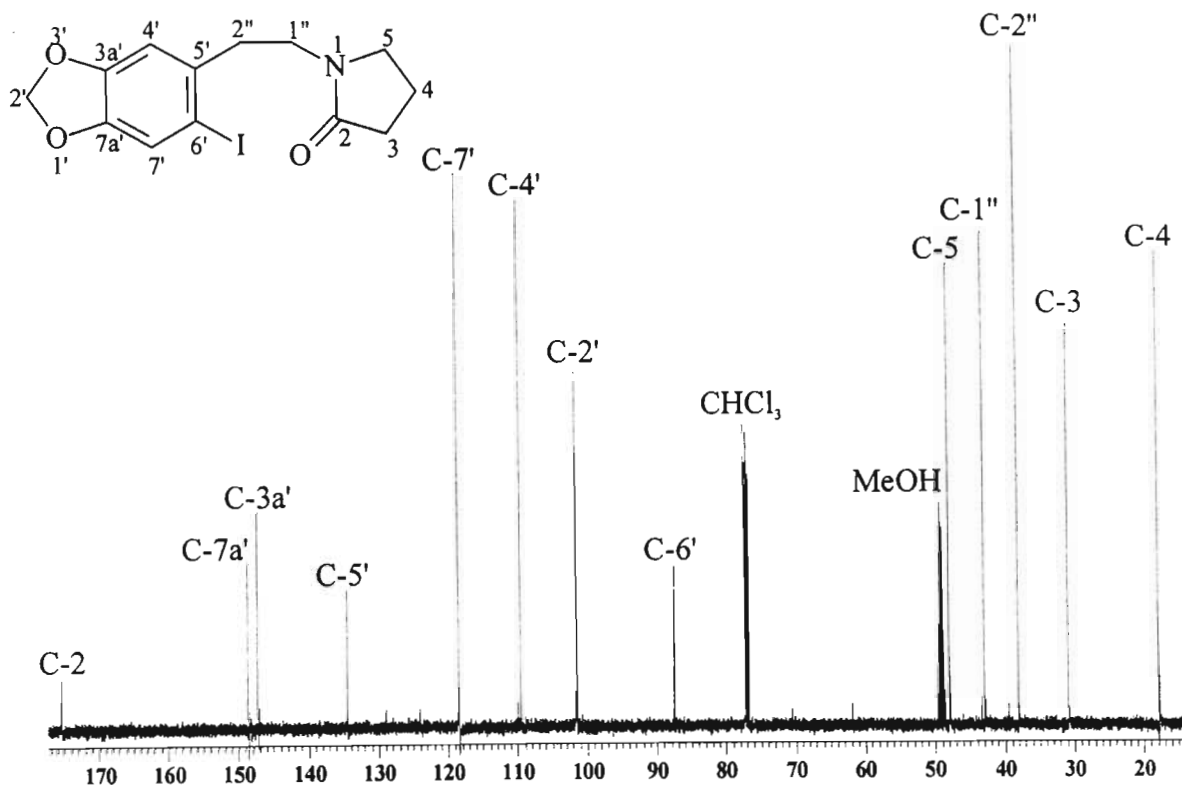


Figure 2.18. ^{13}C NMR spectrum of tertiary lactam (**99**).

Due to time constraints, no further work was carried out on the proposed route towards the cephalotaxine pentacyclic structure. Thus unfortunately the work carried out on the spirocycle synthesis using the Noyori annulation reaction could not be applied with the rest of the cephalotaxine structure intact. However this has left much interesting work to be carried out in the future which is discussed further in Section 2.3.

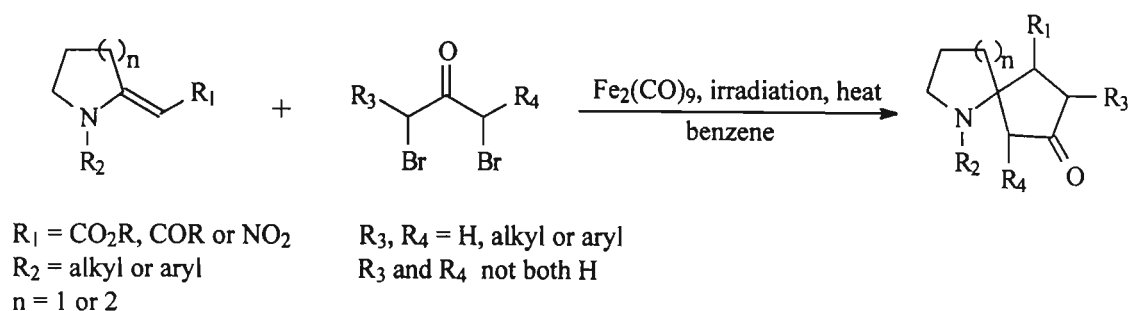
2.3. CONCLUSIONS AND FUTURE WORK

The first aim of the project, to use the Noyori annulation reaction to synthesise the cephalotaxine spirocycle, was successful. Much was learnt during this process about the reactants and ultimately the result was pleasing, a novel compound being produced, spirocycle (**130**), and a crystal structure obtained to conclusively prove the success of the reaction. The reaction itself which formed the spirocycle (**130**) was challenging with four stereogenic centres being created in one step. There is much potential to exploit this reaction and there are still a number of aspects of the reaction which deserve to be investigated. As a start the reaction conditions for the spirocycle formation need to be altered to optimise the yield of the reaction. In Noyori's annulation reactions involving enamines not all of the reactions were carried out under the same

conditions but varied slightly.⁵⁴ Conditions which were altered were temperature, length of reaction, and use of irradiation, in a number of cases no irradiation was used at all. Change of solvent from benzene was found to hinder the progress of the reaction. By altering our reaction conditions the overall diastereomeric yield should be increased from the current mediocre 24 % to yields comparable with those of Noyori's in the 60 to 100 % range.

A second aspect of the reaction which requires further investigation is the relative stereochemistry of the other diastereomers. In our work only one diastereomer was successfully isolated and characterised though from NMR analysis at least another four diastereomers had been formed in the reaction. In future studies these need to be isolated and characterised fully and for this to be achieved the decomposition of the compound needs to be addressed. Care should be taken with the techniques used for separation and the products should be stored preferably in solution, or if isolated, under nitrogen and at low temperatures.

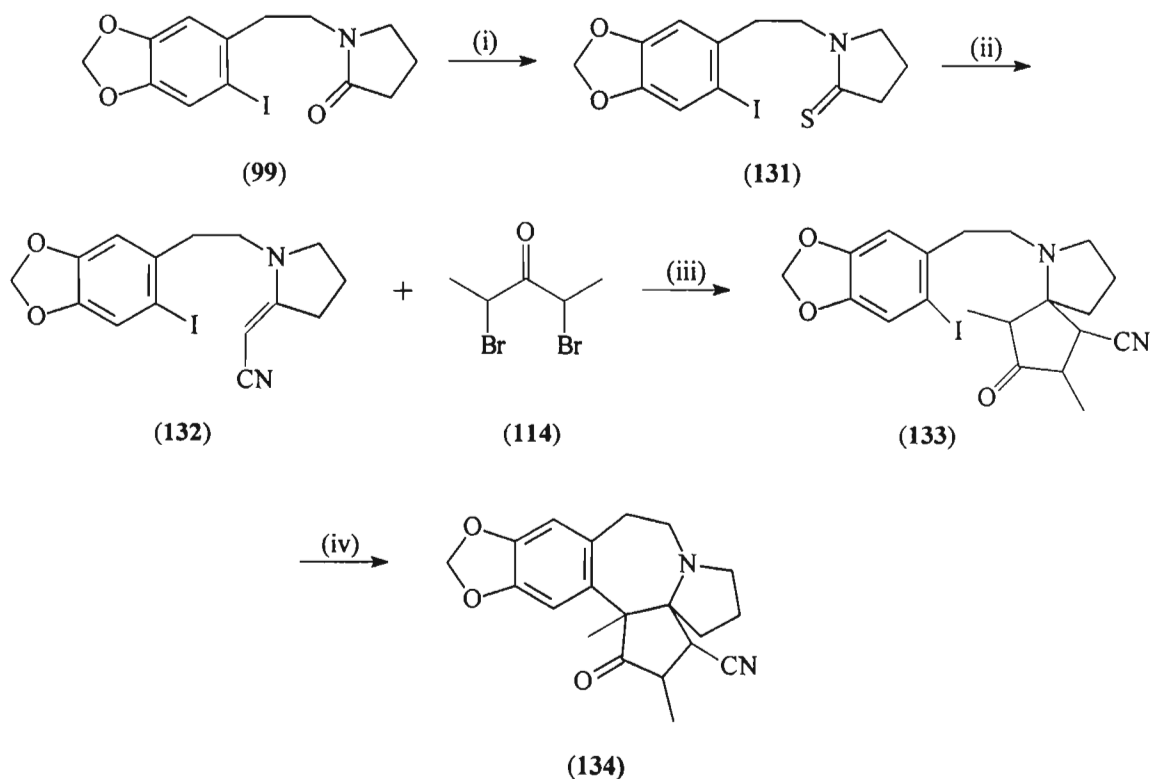
In terms of exploiting this reaction further there are a number of interesting possibilities to be pursued. By altering the various substituents on the enamine and α,α' -dibromo ketone reactants it will be interesting to see what functional groups can be tolerated by the reaction and whether the yield of the reaction can be improved. Substituents on the enamine used in the reaction to form the azaspirocyclic (**130**) that could be altered are the nitrile group and benzyl moiety. The pyrrolidine ring of the enamine could even be replaced with a six membered piperidine ring. The methyl groups of the α,α' -dibromo ketone could also be easily replaced with other functionalities. Scheme 2.22 shows some possible functional groups which could be used in the Noyori annulation to assess the generality of this reaction and to investigate the relative stereochemistry of the products and see whether different functional groups affect it.



Scheme 2.22.

The suggested functional group studies should not only create an interesting range of compounds but also provide an insight into how this type of reaction could be used in the synthesis of compounds other than cephalotaxine which contain azaspirocyclic systems. As noted by other workers,⁷⁸ there is a need for general methods which prepare suitably functionalised azaspirocyclic systems, as often these systems are the structural core of various alkaloids which are of synthetic and biological interest.

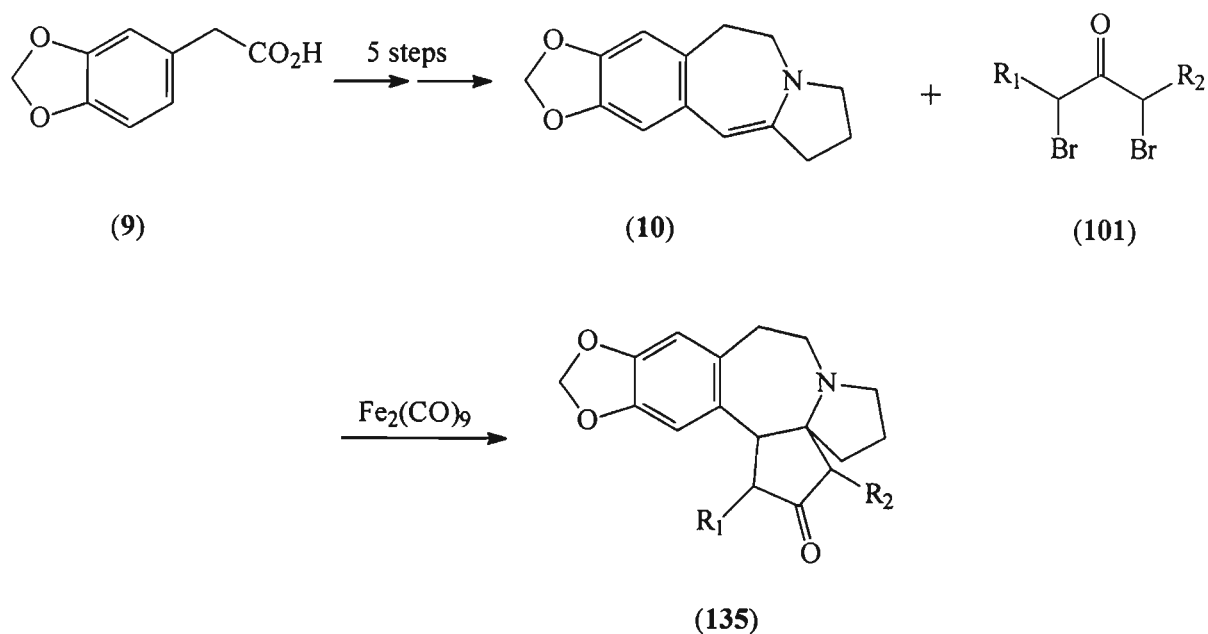
The second aim of the project, to pursue a novel route to the basic pentacyclic cephalotaxine structure based on the spirocycle synthesis, was not fully achieved though the initial stages of the synthetic route that had been proposed in the introduction were carried out. These initial reactions that were completed were successful, with two novel compounds, the tosylate (**98**) and tertiary lactam (**99**), being synthesised and fully characterised during the work. The crystal structure of the tosylate (**98**) also provided the basis for the conformational analysis study described in Chapter 3. For future studies, the proposed synthetic route to the basic pentacyclic cephalotaxine structure should be altered based on what was learnt during the work carried out on the spirocycle synthesis.



Scheme 2.23. (i) P_2S_5 , Na_2CO_3 ; (ii) (a) $BrCH_2CN$, (b) Ph_3P , Et_3N ; (iii) $Fe_2(CO)_9$; (iv) potassium *t*-butoxide, NH_3 , *h\nu*.

Thus, as shown in Scheme 2.23, from the tertiary lactam (**99**) the corresponding thiolactam (**131**) should be formed and then an Eschenmoser coupling reaction with bromoacetonitrile carried out on this product to form the vinylogous cyanamide (**132**). Based on our observations this vinylogous cyanamide (**132**) should be stable and will undergo the annulation reaction to form the azaspirocycle thereby forming the tetracyclic compound (**133**). The suggested final step to form the cephalotaxine pentacyclic structure is the same as in the initial proposed route in Chapter 1 (Scheme 1.17).

Besides the above proposed route to the cephalotaxine pentacyclic structure, a second route can also be suggested that can utilise the Noyori annulation reaction investigated during our work. In the work of Auerbach and Weinreb,^{27,28} the enamine intermediate (**10**) was synthesised in five steps from 3,4-methylenedioxyphenylacetic acid (**9**) (Scheme 2.24). It is possible that this enamine (**10**) could be subjected to the Noyori annulation reaction with an appropriate α,α' -dibromo ketone (**101**) to form the pentacyclic skeleton (**135**). This would be an extremely expeditious access to the basic pentacyclic cephalotaxine structure with only six steps required, the first five of which are established literature procedures.



Scheme 2.24.

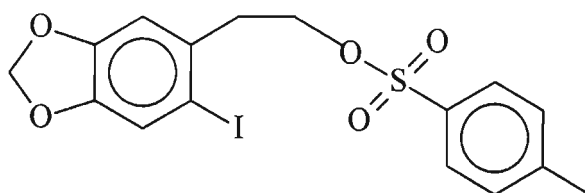
In conclusion, the work carried out during this project has achieved much of what was originally intended and has resulted in the synthesis of a number of novel compounds and in addition the methodology which was investigated can now be exploited further. Firstly, it should be possible to synthesise a range of azaspirocycles based on the studies carried out thus far and secondly, accessing the cephalotaxine pentacyclic structure is a feasible goal, with two efficient routes given as possibilities.

Chapter 3

Conformational Analysis

3.1. INTRODUCTION

When an X-ray quality crystal of the tosylate (**98**) was grown, it was already known that the compound was novel, thus it was obvious that no crystal structure previously existed. Since no other similar systems were documented in the Cambridge Crystallographic database it was decided that it would be interesting to attempt to obtain a X-ray crystal structure. This was carried out knowing that in general the crystal structures of small organic molecules are straightforward and unsurprising, even though it would be pleasing to obtain a definitive characterisation of the compound. When the X-ray structure was completed it was found that in fact it was not simple or straightforward at all, with multiple conformations of the tosylate molecule being present in the solid state. The excellent opportunity to analyse fully this surprisingly complex conformational system could not be ignored and thus this chapter on conformational analysis has been included in an otherwise purely synthetic organic chemistry dissertation.



(98)

Conformational analysis is a powerful tool which elegantly combines experimental techniques such as NMR spectroscopy and X-ray crystallography with a variety of computational methods. The actual conformations a molecule may take, the energetics of the conformations, and the implications of their shape and form can be analysed and assessed using the various methods. As conformational analysis research has grown dramatically in recent years a full literature review would only find place in a dissertation purely dedicated to this field of work. However, it is useful to gain some background knowledge by briefly looking at the general uses of

conformational analysis and the tools employed in carrying out the actual analysis, before discussing the conformational analysis which was carried out during our work.

The tools of conformational analysis vary widely. The most obvious is X-ray crystallography in which a molecule's conformation may be clearly observed in the solid state with little ambiguity. Whether this conformation is still present in solution or is merely an artefact of crystal packing may vary from system to system, though undoubtedly an X-ray structure is a good starting point for any conformational analysis study. The conformations of a molecule that are present in solution is of great interest as this is more relevant in biological systems and for synthetic reactions which are carried out in solution. The most popular technique used for solution analysis is NMR spectroscopy, particularly variable temperature ^1H NMR spectroscopy. When two conformations are present in solution and are in the slow exchange limit, two sets of ^1H NMR signals are seen (if the temperature is feasible for attainment in an NMR spectroscopy experiment). As the temperature is raised and the fast exchange limit is reached the signals coalesce until finally only a single set of sharp peaks is seen. Even if two distinct sets of signals cannot be observed because the slow exchange limit occurs at too low a temperature, some line broadening is often seen when more than one conformation is present in solution. The line shapes of the peaks in spectra such as these allow much kinetic information to be gained from the results. This includes the rate constants for the interconversion between conformations, the Arrhenius activation energy, E_a , and also the enthalpy and entropy of activation which naturally lead to the free energy of activation being determined as well.⁷⁹ This type of dynamic NMR spectroscopy is extremely well documented and is a commonly used technique. The Nuclear Overhauser Effect (NOE) is also vital in trying to identify a particular conformation and again is a popular tool in conformational analysis. NOE is a through-space phenomenon and so is ideally suited for analysis of how atoms are arranged in space.⁸⁰ In conformational analysis, NOE finds its best use in determining basic conformations of large molecules. It can be used for analysis of smaller molecules but the ability of NOE to help conclusively assign a local conformation is often limited.⁸⁰ NOE is more useful if only one conformation is present in solution but has varied success when multiple conformations are present. If two conformations are present in solution but are in the slow exchange limit and so cause two sets of ^1H NMR signals, then NOE can assist in distinguishing between the conformations and identifying the more dominant conformation. However, if conformations are in the fast exchange limit a

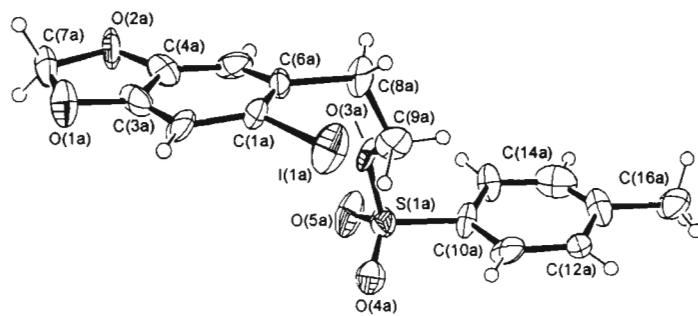
restricted amount of information can be gathered from the NOE data in general. It is for these reasons NOE is generally better for assessing the overall conformation of a macromolecule as in solution these larger molecules tend not to have bulk conformation changes, only local ones.⁸⁰ ¹³C NMR spectroscopy can also be used for conformational analysis though it is not as widely used because often most aims can be achieved by using ¹H NMR spectroscopy and NOE experiments alone. Low temperature carbon NMR spectroscopy, however, has found use and it has been shown that variable temperature ¹³C NMR spectroscopy can be used for calculating energy differences of conformations. Surprisingly only two papers have been published on this particular topic, one by Schneider and Freitag⁸¹ and the other more recently by Abraham and Ribeiro.⁸² The limited research on this topic is possibly due to the general assumption that a ¹H NMR spectrum is more easily obtained and provides all the necessary information in a one dimensional conformational NMR spectroscopy study. However, as Schneider and Freitag point out, carbon shifts can in some cases be determined more accurately than proton shifts when the proton spectrum is very complicated, for instance when many aliphatic signals are present. Though NMR spectroscopy is the most commonly used experimental tool in conformational analysis, others methods have also found use. UV-visible spectroscopy, IR spectroscopy and circular dichroism are all implemented periodically in conformational analysis. Raman spectroscopy and the Kerr effect can also be used. Timosheva and co-workers even demonstrated how the Cotton Mouton effect could be implemented in the conformational analysis of pyridiniummethanes and their derivatives.⁸³ Here NMR spectroscopy had not been able to conclusively provide conformations for these types of molecules and the Cotton Mouton effect was used to further investigate the systems.

Computational methods have now become increasingly important in conformational analysis. For example, Monte Carlo conformational searches are used to try and identify possible low energy conformations. Molecular mechanics (MM), molecular dynamics (MD), and quantum mechanics are all used to varying degrees to calculate geometry optimized conformations, energies and used in the general analysis of a conformationally interesting system. There are currently numerous commercial software packages available to carry out calculations for conformation analysis studies. In our work we have mainly used the HyperChem[®] Pro 6 program.

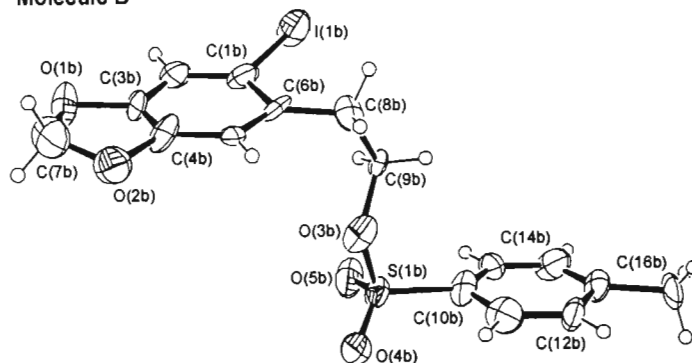
Conformational analysis finds use in a variety of fields, with a large area of interest being molecules with biological activity. These studies are used to assess the importance of a molecule's conformation in a biological system as the shape of a molecule is a leading factor in how well it will interact with a receptor site. As a result, conformational analysis is routinely employed in drug design. Conformational analysis on biological systems also extends to the investigation of amino acids, proteins and peptides so as to provide further insight into their behaviour. Obviously computational techniques are some of the more important tools in the analysis of biological molecules and potentially biologically active compounds. Drug companies use computational methods in attempts to find molecules with conformations which will not hinder but rather assist in the binding of the molecule to a targeted receptor site, so the conformational analysis is done even before a drug is made to try to predict its efficacy. With anti-AIDS agents being one of the largest current research topics in the drug development industry it is interesting that conformational analysis is being used in this research to assess the effect of conformation on a drug's efficacy. In a recent study on disubstituted 3',4'-di-*O*-(*S*)-camphanoyl-(+)-*cis*-khellactone analogues, which show varying degrees of anti-HIV activity, computational methods, X-ray crystallography and UV-vis spectroscopy were used to carry out a conformational analysis on these compounds.⁸⁴ The results were able to identify the possible reasons for some of the analogues being potent while others had no efficacy at all. This kind of information gained from conformational studies will obviously assist in the design of other anti-HIV drugs. Studies other than those concerned with biological molecules are carried out for various purposes. Often it is just to add to the body of knowledge in understanding how conformationally flexible molecules behave, at other times it is to elucidate the behaviour of a particular molecule in a reaction so that a reaction mechanism may be proposed.

In our work we have tried to combine several of the techniques mentioned above to carry out a thorough conformational analysis of the tosylate system (**98**). As has been mentioned previously, it was the unique X-ray structure of the tosylate which initiated this conformational analysis study and so it is an appropriate place to begin the discussion of the work that was carried out.

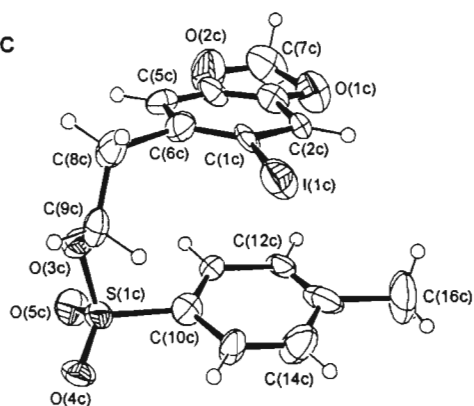
Molecule A



Molecule B



Molecule C



Molecule D

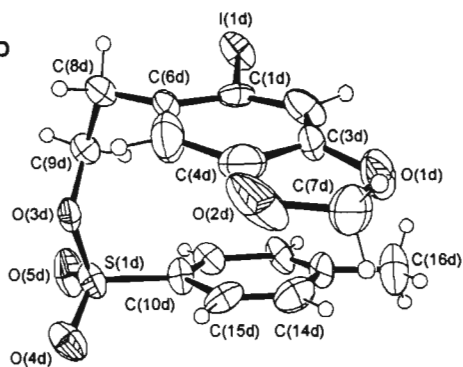


Figure 3.1. The four conformations of the tosylate (**98**) found in the X-ray structure.

3.2. X-RAY STRUCTURE OF TOSYLATE (98)

The structure of tosylate (**98**) was solved in the triclinic space group P_1 and the dimensions of the unit cell were found to be $a = 7.816(2) \text{ \AA}$, $b = 9.8178(18) \text{ \AA}$, $c = 23.165 \text{ \AA}$, $\alpha = 82.667(14)^\circ$, $\beta = 85.473(19)^\circ$, $\gamma = 73.273(19)^\circ$ ($V = 1686.7(6) \text{ \AA}^3$). Further crystal structure data for the tosylate is contained in Appendix B. The most interesting feature of the crystal structure is that there are four independent molecules in the asymmetric unit, each molecule having a unique conformation. The four conformations have been labeled molecules A to D and are shown in Figure 3.1. Though superficially it may appear that molecules A and B are the same and molecules C and D are the same, this is not the case. The similarity of molecules A and B is that they have both assumed a conformation in which the two phenyl ring systems are essentially coplanar and arranged in a step-like fashion.

Table 3.1. Selected values extracted from the tosylate crystal structure.

Molecule	Dihedral angle between ring planes ($^\circ$)	Mean absolute deviation from planarity of the fused bicycle moiety (\AA)	Atom in fused bicycle moiety with the largest displacement [displacement (\AA)]
A	6.7	0.04	O(1) [0.09]
B	10.3	0.04	C(7) [0.09]
C	14.6	0.03	O(1) [0.08]
D	15.5	0.02	C(2) [0.06]

Table 3.1 shows values for various features of molecules A to D: the dihedral angle between the two ring planes, the mean absolute deviation from planarity of the fused 1,3-benzodioxole ring system, and finally the atom in the fused ring moiety with the largest displacement. From Table 3.1 we see that the values for molecules A and B differ slightly but the most important difference between the two molecules can be discovered on closer inspection of the two conformations. Specifically, they are near mirror images with rotations having taken place in the chain linking the ring systems. For molecule A the torsion angle C(10)-S(1)-O(3)-C(9) has the value 68.0° , S(1)-O(3)-C(9)-C(8) is -170.5° , and O(3)-C(9)-C(8)-C(6) is -65.1° , while in molecule B the same three torsion angles have the values -75.2 , 172.0 , and 64.0° , respectively. As can be seen the torsion angles are essentially reversed moving from molecule A to molecule B. The same

“mirror image” phenomenon also applies for molecules C and D though their “shape” is distinctly different from molecules A and B with C and D adopting a hairpin conformation. The torsion angles C(10)-S(1)-O(3)-C(9), S(1)-O(3)-C(9)-C(8), and O(3)-C(9)-C(8)-C(6) are -62.1 , 146.8 , and -68.2 ° for molecule C and 68.4 , -148.0 , and 68.1 ° for molecule D, respectively. More interestingly, the distance between the phenyl rings in both molecules C and D is sufficiently small to suggest that intramolecular π -stacking is taking place. In both molecules the mean interatomic spacing between the atoms of the two phenyl rings is $3.60(17)$ Å which is within the limits for a possible π -donor/ π -acceptor interaction.

The packing of the molecules in the crystal lattice is elegant (Figure 3.2) with a basic four row pattern being evident. Row one consists of stepped molecules A, row two consists of hairpin molecules D with row three containing hairpin molecules C. The hairpin shape of the row two D molecules faces in the opposite direction from that of the row three C molecules. The final row contains stepped molecules B. An important feature of the lattice is the intermolecular π -stacking present in the rows of stepped molecules A and B. The π -stacking interactions take place between the 1,3-benzodioxole ring of one molecule with the tosyl ring of its neighbour. For the row comprising molecules A, the average interatomic distance of the interaction is $3.73(5)$ Å, which is within π -stacking limits.

The presence of four distinct conformations in a crystal structure is of course an unusual phenomenon, so as a result of the revelations of the tosylate crystal structure it was felt further investigation of the system was required. This was to involve various computational techniques such as MM which would be used to carry out geometry optimisations and dihedral angle searches of conformational space to investigate the energetics of the system, for instance to see if the solid state conformations of the tosylate are true minima on the potential energy surface of the molecule. The possible significance of the inter- and intramolecular π -stacking was also an area to be investigated using extended Hückel calculations. If used correctly MM is an especially powerful tool in computational chemistry and some introduction to this method has been given. Finally as was mentioned earlier, NMR spectroscopy is also an excellent tool for solution conformational analysis so it was hoped that more than one tosylate conformation would be identified using ^1H NMR spectroscopy so as to provide further understanding of the conformationally flexible system in solution.

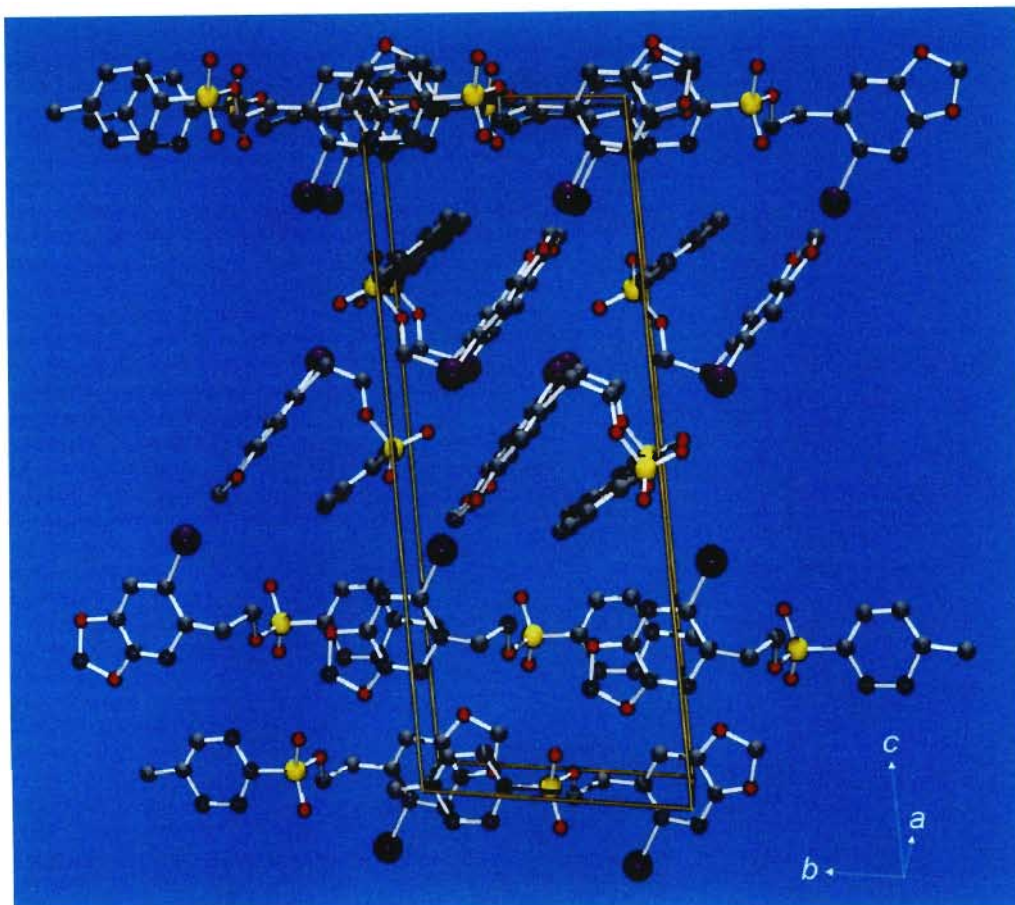


Figure 3.2. Unit cell crystal packing diagram for the tosylate (**98**).

3.3. INTRODUCTION TO MM CALCULATIONS

MM is one of the more commonly used methods in computational chemistry. It is generally fast and when correctly used can give results which agree very well with experiment. MM uses classical mechanics (as opposed to quantum mechanics) to calculate the potential energy surface of a molecule. Because MM does not treat electrons explicitly it is not used in the computational modeling of situations where electron participation is important, e.g. bond breaking and bond formation. MM is also known as force field methods⁸⁵ because so called “force fields” are used to describe how a collection of atoms that make up a molecule behave in relation to each other. A number of different force fields have been developed to cope with different types of molecules.

In general a force field designed for small molecules cannot be used for calculations on proteins for instance, and vice versa. When dealing with force fields there are three important aspects to consider: atom types, functional form and parameter sets. In a force field method each atom in a molecule is classed as an atom type according to its type of bonding and possibly the atoms it is bonded to as MM works on the basis that all similar structural units will behave in the same fashion. For example, in the AMBER force field parameter set⁸⁶ there are four defined oxygen atom types: (i) O, carbonyl oxygens; (ii) O2, carboxyl and phosphate nonbonded oxygens; (iii) OS, ether and ester oxygens; and (iv) OH, alcohol oxygens. Each atom type has a set of parameters associated with it which are the values used in the equations which calculate the potential energy surface of a molecule.

The software package which we used to carry out our computational studies, Hyperchem[®] Pro 6, has four different force fields available for use. These are AMBER, OPLS, BIO+ and MM+. AMBER stands for Assisted Model Building and Energy Refinement. It is primarily for calculations on proteins and nucleic acids and was initially a united atom force field.⁸⁶ United atom force fields include all atoms explicitly except for hydrogens bonded to carbon, whereas an all atom force field even includes carbon bonded hydrogens explicitly. United atom force fields are used to try to improve computational efficiency and its advantage can be seen for large molecules like proteins. An all atom version of AMBER has also been developed.⁸⁷ The united atom version of AMBER only has a limited number of atom types with an additional 5 being defined in the all atom version.^{86,87} As a result, if calculations are carried out on molecules other than proteins or nucleic acids using AMBER it is possible that the force field parameters required for the calculations will not be available. OPLS (Optimized Potentials for Liquid Simulations) is a force field which was initially developed for computer simulations of proteins in their natural environment, *i.e.* in solution or crystalline states.⁸⁸ A lot of the AMBER force field was incorporated into OPLS which is a united atom force field.⁸⁸ OPLS has also been extended to include parameters for nucleotide bases.⁸⁹ BIO+ is a Hyperchem[®] force field based on the CHARMM (Chemistry at HARvard Macromolecular Mechanics) force field.^{90,91} It is mainly for large molecules such as proteins. Many parameters used in CHARMM are unpublished and only available commercially.⁹² Finally MM+ is the Hyperchem[®] force field based on the MM2 force field of Allinger.⁹³ MM2 was primarily designed for use with a wide range of small organic molecules, *i.e.* not on the macromolecular scale, though it was extended to include calculations

on peptides.⁹⁴ MM+ uses the MM2(1991) parameter set provided by Allinger⁹² and has a method which determines default parameters for calculations if the required values are not present in the MM2(1991) parameter set. It is important to be aware of the possibility that MM+ may use default parameters as these can cause spurious results. Even a brief glance at the descriptions of the force fields available with Hyperchem[®] is enough to see that MM+ was the most appropriate force field for calculations on the tosylate molecule under investigation. It is a small organic molecule and is certainly not on the macromolecular scale.

After initial calculations on the tosylate using MM+ it was discovered that certain parameters for the molecule were not available in the MM2(1991) parameter set, for instance the parameters required to calculate E_{stretch} values were not available for the aromatic carbon-iodine bond as well as two other bonds. Moreover, a number of torsional parameters and angle bending parameters were unavailable. Using the MM+ default parameters for calculations on the tosylate did not provide satisfactory results and so it was essential to develop the relevant force field parameters before continuing with the intended calculations. In order to have an understanding of the force field parameters required, the manner in which MM+ calculates the potential surface of a molecule will be described.⁹² This description should also hopefully clarify the earlier qualitative description of how molecular mechanics calculations are carried out. It is important to emphasise that the description below only applies for MM+ as each force field uses its own set of functions to calculate the potential energy surface of a molecule, though there may be similarities between force fields.

To calculate the potential energy of a system the difference energies for various distortions of the molecule are added together:

$$E_{\text{Tot}} = E_{\text{bond}} + E_{\text{dipole}} + E_{\text{bond angle}} + E_{\text{stretch-bend}} + E_{\text{torsion}} + E_{\text{vdW}} \quad (1)$$

where E_{Tot} is the total energy

E_{bond} is the energy required to stretch a bond between two atoms

E_{dipole} is the energy arising from dipole-dipole interactions

$E_{\text{bond angle}}$ is the energy required to bend a bond angle

$E_{\text{stretch-bend}}$ is the energy due to the coupling between bond stretching and angle bending

E_{torsion} is the energy required for rotation about a torsion angle

E_{vdW} is the energy of non-bonded van der Waals interactions

Bond stretching energy

For small displacements from equilibrium the compression and stretching of a bond is assumed to mimic an harmonic oscillator and so E_{bond} can be calculated from Hooke's law:

$$E_{\text{bond}} = \sum_{\text{bonds}} K_r (r - r_0)^2 \quad (2)$$

where K_r is the force constant

r is the distance between two atoms in a bond

r_0 is the equilibrium bond length

However, to more accurately describe the stretching behaviour of a bond higher terms may be used or even a Morse function. In the case of MM+ a cubic stretch term is used and includes a switching function to account for situations where bond lengths are much longer than their r_0 values:

$$E_{\text{bond}} = 143.88 \sum_{\text{bonds}} \frac{1}{2} K_r (r - r_0)^2 [1 + \text{switch}(r - r_0, -1/3 CS, -4/3 CS) CS (r - r_0)] \quad (3)$$

CS is a constant set to an arbitrary value (default in MM+ is -2.0). Hyperchem® often uses switching functions to allow for smooth transitions on the potential energy surface. These functions work as follows:

$\text{switch}(x, a, b) = 1$ if $x \leq a$

$\text{switch}(x, a, b) = 0$ if $x \geq b$

$\text{switch}(x, a, b) = [(b - x)^2 (b + 2x - 3a)] / (b - a)^3$ if $a < x < b$

The factor of 143.88 in the E_{bond} term is simply to account for the fact that MM+ uses units of millidynes per Ångstrom for its force constants (as does MM2) and in order for energies to be

given in kcal/mol the conversion factor is required. Conversion factors are also seen in other calculations below.

From equation (3) we can see that K_r and r_0 as a pair should be unique for each pair of atoms. These values are the force field parameters, so for each pair of atom types present in the MM+ force field there is a K_r and r_0 value which are used in the calculation of E_{bond} for a particular molecule. In fact in the MM+ parameter set two values, r_0^A and r_0^B , are given for each r_0 for an atom pair. The parameter r_0^A is used for bonds where the two atoms each have less than two hydrogens attached while r_0^B is used when the two atoms have two or more directly attached hydrogens.

Dipole interaction energy

To account for the electrostatic contribution to the potential energy MM+ defines a set of bond dipole moments that are associated with polar bonds and the dipole interaction energy takes the following form:

$$E_{\text{dipole}} = 14.39418\varepsilon \sum_{ij \text{ polar bonds}} \mu_i \mu_j \left[\frac{\cos \chi - \cos \alpha_i \cos \alpha_j}{R_{ij}^3} \right] \quad (4)$$

where μ_i and μ_j are the two dipoles

ε is the dielectric constant

χ is the angle between the two dipole vectors

R_{ij} is the distance between the centres of the two dipoles

α_i and α_j are the angles the dipole vectors make with the \mathbf{R}_{ij} vector

μ_i and μ_j are the force field parameters in this situation, with χ , R_{ij} , α_i and α_j are found from the geometry of the dipoles in the molecule under investigation. 14.39418 is a conversion factor.

Angle bending energy

As for the stretching of a bond, the bending of an angles formed by three consecutively joined

atoms can be modeled with a harmonic function for small displacements of the angle from equilibrium. However, this function, as for bond stretching, does not always hold for large displacements and so MM+ includes a higher order term to give the energy for the bending of an angle as follows:

$$E_{bond\ angle} = 0.043828 \sum_{angles} \frac{1}{2} K_{\theta} (\theta - \theta_0)^2 [1 + SF(\theta - \theta_0)^4] \quad (5)$$

where K_{θ} is the force constant

θ is the angle formed by the three consecutively joined atoms

θ_0 is the equilibrium angle

SF is called a scale factor and again is set to an arbitrary value, the default in MM+ being 7.0×10^{-8} . Again there is a conversion factor (0.043828) to convert millidyne-Å per radian² to kcal/mol per degree².

For the calculation of the angle bending energy, K_{θ} and θ_0 are the force field parameters though in MM+ three θ_0 values (θ^A , θ^B , and θ^C) are stipulated in the parameter set for each bond angle. Often only θ^A is assigned in the parameter set but if θ^B is defined it is used when the central atom has one hydrogen attached, while θ^C is used when the central atom has two hydrogen atoms attached.

Stretch-bend energy

To account for the coupling between bond stretching and angle bending a stretch-bend cross term is incorporated in MM+. Three consecutively joined atoms are labeled i, j, and k, where k is the central atom and the coupling energy is calculated as follows:

$$E_{stretch-bend} = 2.51118 \sum_{angles} K_{sb} (\theta - \theta_0)_{ijk} [(r - r_0)_{ik} + (r - r_0)_{jk}] \quad (6)$$

Here K_{sb} is a force field parameter with θ_0 and r_0 already having been parameterized for the calculation of $E_{stretch}$ and E_{bend} . 2.51119 is again a conversion factor to give the energy in kcal/mol.

Torsion angle energy

Torsion angles are widely recognised to have a significant effect upon the energy of a molecule, a classic example being butane, which changes energy with rotation about the C(2)-C(3) bond as it moves from a cis to a gauche to a trans conformation. In MM+ the dihedral angle energy or torsional interaction energy takes the form of a truncated Fourier series:

$$E_{torsion} = \sum_{torsions} \frac{V_1}{2}(1 + \cos\phi) + \frac{V_2}{2}(1 - \cos 2\phi) + \frac{V_3}{2}(1 + \cos 3\phi) \quad (7)$$

where V_n is the dihedral force constant, n being the periodicity of the Fourier term

ϕ is the torsion angle

The phase angle is not explicitly included in the above equation as it is taken to be zero. V_1 , V_2 , and V_3 are the force field parameters and being in kcal/mol no conversion factor is required for the $E_{torsion}$ calculation.

Van der Waals energy

The van der Waals energy results from the repulsive or attractive forces experienced by two non-bonded atoms. Often the Lennard-Jones potential is used to calculate the van der Waals energy though it is not always considered to model the repulsive forces precisely. As a result MM+ uses an exponential term to describe the repulsive forces more accurately while using a $1/R^6$ term for the attractive forces (similar to the term found in the Lennard-Jones equation). Thus the van der Waals energy is calculated using what is known as a ‘‘Buckingham’’ or ‘‘Hill’’ type potential:

$$E_{vdW} = \sum_{ij \in vdW} \epsilon_{ij} (2.9 \times 10^5 e^{-12.5\rho_{ij}} - 2.25\rho_{ij}^{-6}) \quad (8)$$

where $\epsilon_{ij} = (\epsilon_i \epsilon_j)^{1/2}$, ϵ_i and ϵ_j being hardness parameters for atoms i and j respectively which determine the attractive well depth

$\rho_{ij} = R_{ij}/r_{ij}^*$, R_{ij} being the non-bonded distance between atoms i and j and r_{ij}^* being the sum of the van der Waals radii of atoms i and j , *i.e.* $r_{ij}^* = r_i^* + r_j^*$

Equation 8 does not work very well at short interatomic distances so when r_{ij}^* is less than 3.311 Å, the van der Waals energy is calculated as follows:

$$E_{vdW} = 336.176 \sum_{ij \in vdW} \epsilon_{ij} \rho_{ij}^{-2} \quad (9)$$

In general, hydrogen bonds must be treated in a special manner and so in MM+ any XH bond lengths are reduced by 0.915 Å for calculations of van der Waals interactions with H atoms. CH interactions are also assigned specific ϵ and r^* values.

3.4. DEVELOPMENT OF FORCE FIELD PARAMETERS AND GEOMETRY OPTIMISATION

The first calculations to be carried out on molecules A-D were gas phase geometry optimizations. These were executed with the MM+ force field on HyperChem[®] Pro 6 using the Polak-Ribiere conjugate gradient algorithm with a root mean square gradient termination cut-off of 0.005 kcal Å⁻¹ mol⁻¹ and a dielectric constant of 1.5 D. The atomic coordinates of the X-ray structure for molecules A-D were used as the input. The results appeared to deviate more seriously than expected from the experimental X-ray data and it was discovered after using a facility provided by HyperChem[®] to log the progress of the calculation that certain parameters required for the tosylate were unavailable in the MM+ force field and default parameters had been used instead. As a result the relevant force field parameters for 3 bond lengths, 5 bond angles, and 9 torsional angles had to be developed. For the missing bond lengths the parameters required were the stretching force constant, K_r , the equilibrium bond length, r_0 , and the dipole μ . For the missing bond angles the bending constant, K_θ , and equilibrium bond angle, θ^A (θ^B and θ^C can be neglected) were required. Finally for the missing torsion angles the three dihedral force constants V_1 , V_2 , and V_3 had to be entered in the force field. Initial r_0 and θ^A values were taken from the crystal structure data by averaging the values of the relevant bond lengths and angles for the

molecules A-D. K_r values were calculated using a method suggested by Allinger *et. al.*⁹⁵ while K_θ , V_1 , V_2 , and V_3 were initially chosen by using existing MM+ parameters for atom sequences that were acceptably similar to those required. These parameters were then used for the geometry optimization that had been attempted originally and the differences between the newly calculated structure and X-ray structure were noted. The parameters were then adjusted slightly, the optimization performed again and the calculated and X-ray structures again compared to see if an improvement had been made. The process was repeated several times until it was felt that there was satisfactory agreement between the calculated geometry optimized structures and the observed structures. The new force field parameters that were developed are shown in Tables 3.2, 3.3, and 3.4. Once the force field parameters were satisfactory it was possible to continue with the geometry optimizations.

Table 3.2. Bond stretching parameters developed.

Atom	Atom	K_r (mdyn/Å)	r_0 (Å)	μ
C(sp ²)	I	2.620	2.090	1.400
O(sp ³)	S(sp ³)	4.620	1.580	0.000
C(sp ²)	S(sp ³)	3.260	1.750	0.000

Table 3.3. Angle bending parameters developed.

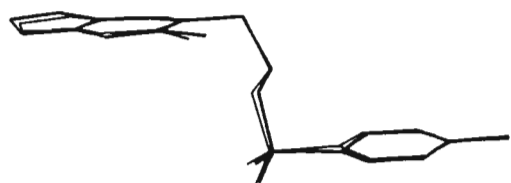
Atom	Atom	Atom	K_θ (mdynÅ/rad ²)	θ^A (°)
C(sp ³)	O(sp ³)	S(sp ³)	0.770	110.000
C(sp ²)	C(sp ²)	S(sp ³)	0.550	121.400
O(sp ³)	S(sp ³)	C(sp ²)	0.700	103.600
O(sp ³)	S(sp ³)	O(sp ²)	0.560	106.200
C(sp ²)	S(sp ³)	O(sp ²)	0.650	109.600

Table 3.4. Torsional parameters developed.

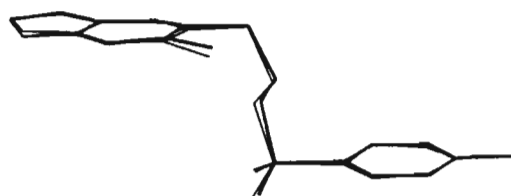
Atom	Atom	Atom	Atom	V ₁ (kcal/mol)	V ₂ (kcal/mol)	V ₃ (kcal/mol)
C(sp ³)	C(sp ³)	O(sp ³)	S(sp ³)	0.400	0.520	0.467
H	C(sp ³)	O(sp ³)	S(sp ³)	0.000	0.000	0.530
C(sp ³)	O(sp ³)	S(sp ³)	C(sp ²)	0.000	0.000	0.403
C(sp ³)	O(sp ³)	S(sp ³)	O(sp ²)	0.000	0.000	0.530
C(sp ²)	C(sp ²)	C(sp ²)	S(sp ³)	-0.270	9.000	0.000
C(sp ²)	O(sp ³)	C(sp ³)	O(sp ³)	0.000	5.000	0.000
C(sp ²)	C(sp ²)	S(sp ³)	O(sp ³)	0.000	0.000	0.000
C(sp ²)	C(sp ²)	S(sp ³)	O(sp ²)	1.243	1.445	-1.243
H	C(sp ²)	C(sp ²)	S(sp ³)	0.000	9.000	0.000

For each molecule A–D a gas phase geometry optimized structure was obtained as well as a calculated structure where the relevant molecule was optimized in its lattice environment. Figure 3.3 shows a least squares fit of the calculated gas phase structures and the experimentally observed structures for the four molecules as well as a fit for the lattice optimized structures and the observed structures. It is clear when observing these overlaid structures qualitatively that the agreement between the calculated and observed structures is very good. For each fit the root mean square deviation is given, but it should be noted that the average root mean square deviation improves from 0.36(1) Å for the gas phase structures to 0.26(4) Å for the lattice structures. The fact that the agreement between the calculated structures and observed structures improves with inclusion of the neighbouring interactions shows that these non-bonded interactions do affect the crystallographically observed conformations that the molecule assumes. From Figure 3.3 it is clearly seen that the improvement of the fits for the lattice optimized structures is caused by the closer agreement in the relative orientation of the two aromatic rings. Thus by including the neighbouring interactions in the lattice for the geometry optimisation calculations the intermolecular π - π interactions mentioned in the earlier discussion of the crystal packing diagram (Figure 3.2) are coming into play as a result. Finally it is noteworthy that the gas phase geometry optimised structures, being so close to the observed X-ray structures, indicate that the conformations observed in the crystal lattice appear to be genuine minima on the potential energy surface of the molecule and are not merely artifacts of crystal packing.

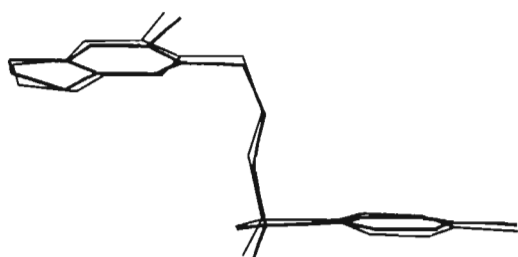
(a) (i) 0.367



(a) (ii) 0.253



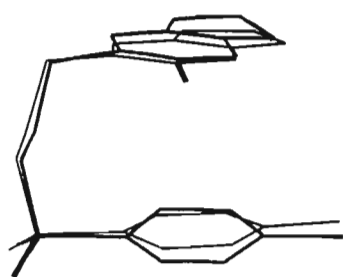
(b) (i) 0.365



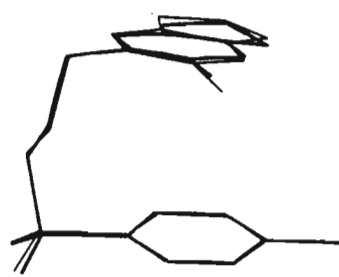
(b) (ii) 0.252



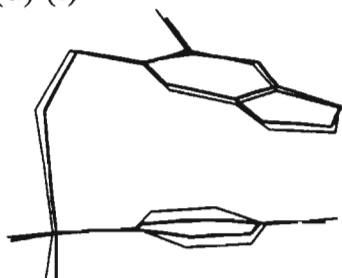
(c) (i) 0.365



(c) (ii) 0.220



(d) (i) 0.345



(d) (ii) 0.309



Figure 3.3. Least square fits of calculated gas phase optimized structures (thin lines) with observed X-ray structures (thick lines) (a(i)-d(i)), and also the calculated lattice optimized structures (thin lines) with observed X-ray structures (thick lines) (a(ii)-d(ii)). RMS fit errors are shown.

Table 3.5. Calculated energies of the gas phase and lattice optimised structures.

Molecule	Energy of gas phase optimised structure (kcal/mol)	Energy of lattice optimised structure (kcal/mol)
A	4.91	5.36
B	4.91	5.37
C	1.22	2.19
D	1.20	2.19

Table 3.5 shows the energies of the gas phase and lattice optimised structures as calculated by HyperChem[®]. These values may not be taken to have any intrinsic physical meaning in themselves as calculated energies will vary from force field to force field, but they may be compared in relation to each other.⁹² The solid state structures are slightly higher in energy than the gas phase structures indicating a slight increase in strain for the conformations in the lattice. However this energy difference is small (< 1 kcal/mol) which shows the adjustments to the conformations caused by neighbouring interactions in the lattice are fairly minor. We see from the table that the two stepped conformations, A and B, are of similar energies as are the two hairpin conformations, C and D. However the hairpin conformations are noticeably lower in energy being more stable by 3.7 kcal/mol for the gas phase optimised structures and 3.2 kcal/mol for the lattice optimised structures. It is quite feasible that the stabilisation of the hairpin conformations is caused by intramolecular π -stacking. The stepped and hairpin conformations are seen in both the crystal structure and the gas phase optimised structures so it appears that they are indeed minima on the potential energy surface of the molecule. As a result it was questioned whether it would be possible to detect these conformations in solution by NMR spectroscopy.

3.5. ¹H NMR SPECTROSCOPIC STUDIES

If the free energy of activation between two conformations is of the order of 5–24 kcal/mol, it is generally possible to identify the presence of the two conformations in solution using variable temperature NMR spectroscopy.⁹⁶ With the energy barrier in this range the conformations will be in slow exchange on the NMR timescale and as long as at least one proton is in a different magnetic environment in the two conformations it will be possible to see this in a ¹H NMR spectrum. For the tosylate no problems should be encountered in seeing the difference between the basic hairpin and stepped conformation forms should they be present in solution. It is

obvious that in the hairpin conformation the folding over of the molecule could cause the magnetic environments of the protons on the tosyl and benzodioxole rings to differ from their environments in the stepped conformation. The change in the magnetic environments should result in different shifts for particular peaks in the ^1H NMR spectrum of each conformation. Also the NOE correlations for the two conformations should be different, for instance, a correlation might be seen between the protons on the two phenyl rings when the molecule is in the hairpin conformation which would not be observed in the stepped form. If more than one conformation is present in solution, each placing the protons in different magnetic environments, either some line broadening should be seen or even two sets of distinct signals. A standard set of NMR spectra were obtained for the tosylate (**98**) in CDCl_3 at room temperature as part of its full characterisation. In Chapter 2 the ^1H NMR spectrum and ^{13}C NMR spectrum were shown in Figures 2.15 and 2.16 respectively.

The ^1H NMR of the tosylate showed only a single set of sharp peaks indicating that either (i) only one conformation is present at this temperature in solution or (ii) that the different conformations of the molecule are in the fast exchange limit at room temperature so that the average spectrum is observed with characteristically sharp peaks. The latter option is obviously the most reasonable as it is unlikely that this conformationally flexible molecule will stay in one conformation when surrounded by, and interacting with, solvent molecules. It was assumed that on cooling the exchange between the conformations would be slower and a change in the spectrum would be seen. However, lowering the temperature to $-60\text{ }^\circ\text{C}$ (with CDCl_3 as the solvent) and re-recording the ^1H NMR spectrum showed no significant change. The shift values of the peaks were essentially identical to those found in the spectrum recorded at $24\text{ }^\circ\text{C}$. This result is consistent with the magnetic environments of all the protons in the molecule being the same at $24\text{ }^\circ\text{C}$ and $-60\text{ }^\circ\text{C}$. Dissolving the tosylate in acetone- d_6 and lowering the temperature further to $-95\text{ }^\circ\text{C}$ still caused no apparent change in the spectrum. Since the X-ray structure showed that for molecules C and D the methylene carbon atom on the benzodioxole ring is within 4.5 \AA of the nearest carbon atom on the tosyl ring, it should be possible to see a correlation between the protons on the benzodioxole methylene group and those on the tosyl ring if the tosylate in solution was in the hairpin conformation. A 1D NOESY experiment was carried out at $-95\text{ }^\circ\text{C}$ in acetone- d_6 with irradiation of the O- CH_2 -O protons but no enhancements were seen from any of the tosyl ring protons. As a NOESY experiment can result in a positive or negative

response, it is possible under the correct conditions for no response to be seen in a NOESY spectrum even though there is a through space correlation between two protons. In order to ensure this was not the case here a further 1D ROESY experiment was carried out. This is a spin-lock experiment very similar to the NOESY experiment but which only shows a positive response, and so if there is indeed a through space correlation between two protons it will be seen. Generally the ROESY experiment is more time consuming to carry out which is why a NOESY experiment is usually used. The 1D ROESY experiment, however, also failed to show any correlations with the O-CH₂-O protons. These results show that the free energy of activation for conversion between the conformations is <5 kcal/mol and thus unobservable by NMR spectroscopy. It is quite possible that multiple conformations, not just the X-ray hairpin and stepped conformations, are constantly interconverting in solution and even at -95 °C they are in the fast exchange limit and so we see a time averaged signal.

3.6. TORSION ANGLE ANALYSIS

The geometry optimisation results give an indication that both the hairpin and stepped conformations were potential energy minima of the tosylate molecule. However, whether any one of the conformations of molecules A–D was the global minimum for the tosylate was as yet undetermined. To investigate the potential energy surface of the molecule further a dihedral angle search of conformational space was carried out using the three torsion angles found along the chain linking the two phenyl rings. These torsion angles are defined as follows: ψ_1 is the C(10)-S(1)-O(3)-C(9) torsion angle, ψ_2 is the S(1)-O(3)-C(9)-C(8) torsion angle, and ψ_3 is the O(3)-C(9)-C(8)-C(6) torsion angle. These three torsion angles were chosen as they are the angles about which rotation is most likely to occur to convert from the stepped to hairpin conformations, and possibly other conformations as well. The torsion angle analysis was carried out using a standard dihedral angle driving algorithm which, starting from the X-ray structure, rotated a chosen pair of torsion angles in 5° increments from 0° to 360° with geometry optimisation of the conformation at each grid point. The three conformation energy plots generated show the change in steric energy (ΔU_T) as a function of the relevant torsion angles. Figure 3.4 shows the surface and contour plots for the combinations of torsion angles ψ_1 and ψ_2 , Figure 3.5 shows the plots for ψ_2 and ψ_3 , and Figure 3.6 for ψ_1 and ψ_3 . On each of these plots an energy minimum can be identified and Table 3.6 gives these values for each graph. By averaging the value for each torsion angle we are able to find the conformation which these calculations indicate is the global

minimum for the tosylate. These average values are 75° , 215° , and 60° for ψ_1 , ψ_2 , and ψ_3 , respectively, which are in excellent agreement with the torsion angles of the gas phase geometry optimised structure of the hairpin molecule ($\psi_1 = 71^\circ$, $\psi_2 = 209^\circ$, $\psi_3 = 60^\circ$).

Table 3.6. Coordinates of the lowest energy conformations from each torsion angle analysis.

Torsion angles analysed	ψ_1 ($^\circ$)	ψ_2 ($^\circ$)	ψ_3 ($^\circ$)
ψ_1 and ψ_2	70	210	-
ψ_2 and ψ_3	-	220	60
ψ_1 and ψ_3	80	-	60

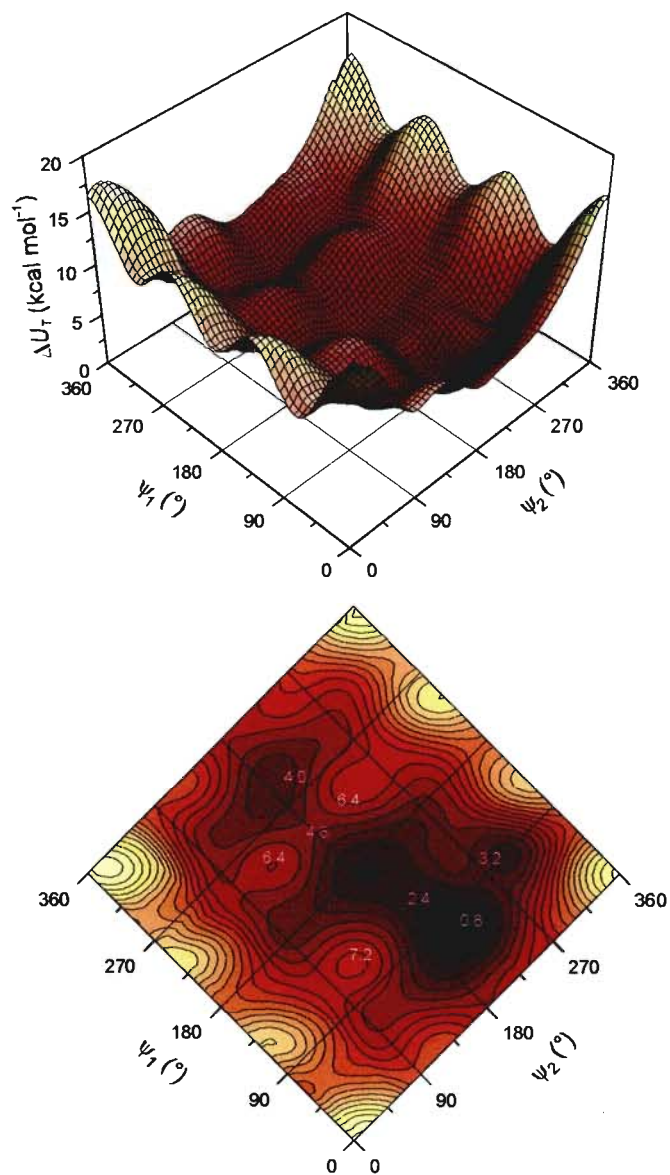


Figure 3.4. Surface and contour plots showing the change in total steric energy as a function of the torsion angles ψ_1 and ψ_2 for the tosylate (**98**).

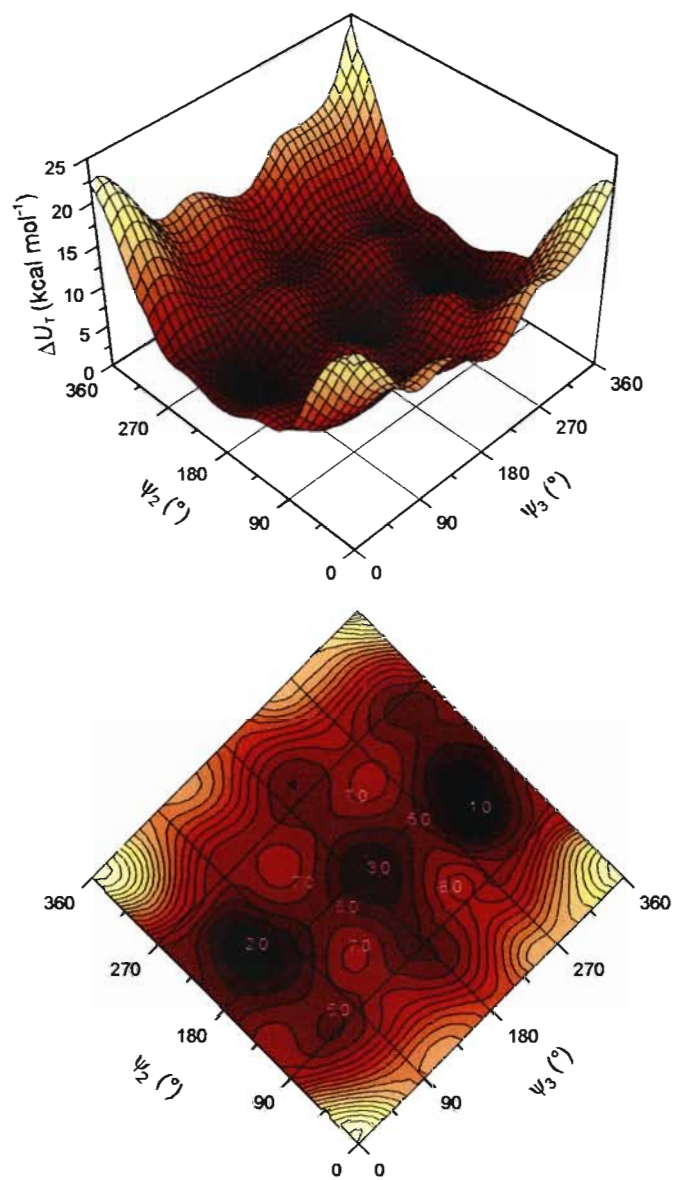


Figure 3.5. Surface and contour plots showing the change in total steric energy as a function of the torsion angles ψ_2 and ψ_3 for the tosylate (**98**).

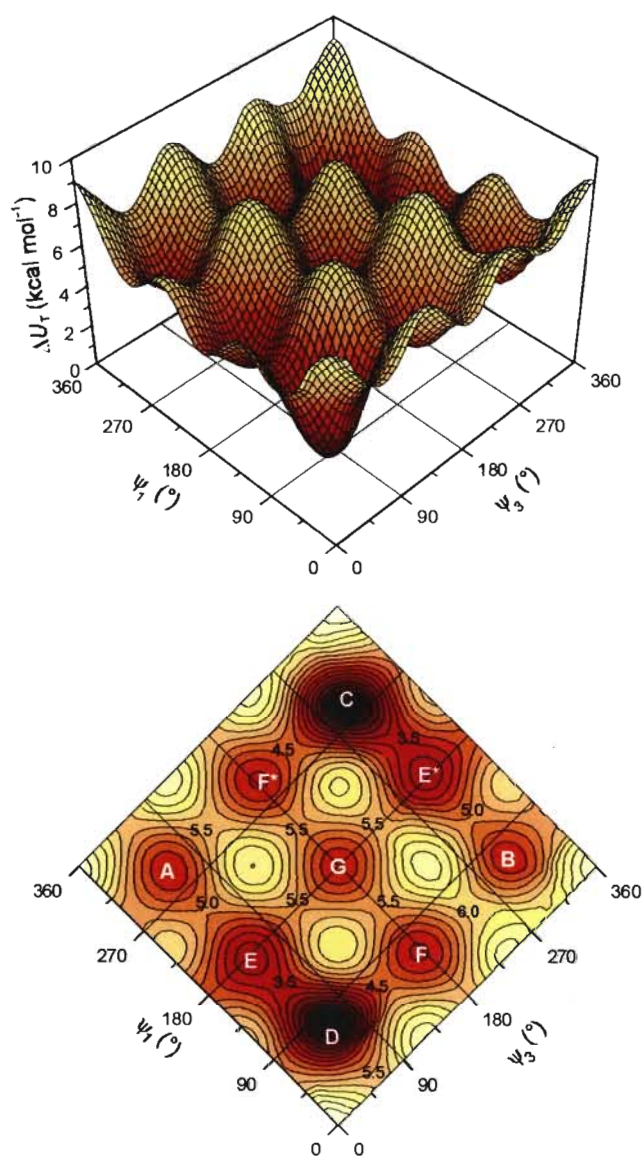
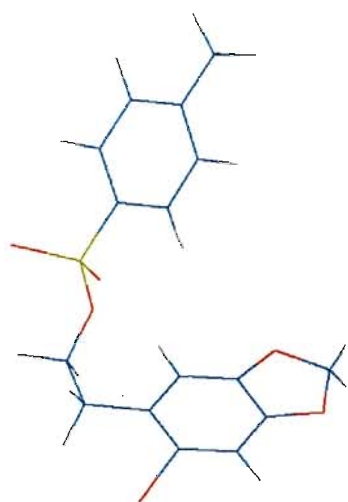
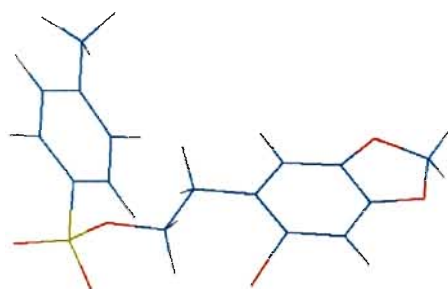


Figure 3.6. Surface and contour plots showing the change in total steric energy as a function of the torsion angles ψ_1 and ψ_3 for the tosylate (98).

From Figures 3.4 and 3.5 we see that the rotations about ψ_2 involve much larger energy changes than the rotations about ψ_1 and ψ_3 (Figure 3.6). It thus appears that rotations about ψ_1 and ψ_3 are inherently responsible for the conformational flexibility of the molecule. This is supported by Figure 3.6 where the four molecules A-D seen in the crystal structure can be clearly identified as energy minima on the conformational energy surface. An interesting feature of the plots in Figure 3.6 is the presence of a centre of inversion at the coordinates $\psi_1 = 180^\circ$ and $\psi_3 = 180^\circ$. The crystal structure of the tosylate showed that molecules A and B are mirror images, as are molecules C and D, and this is clearly reflected by the contour plot in Figure 3.6 where these four conformations have been identified. The plot indicates that rotations about ψ_1 and ψ_3 are the cause of the mirror imaging phenomenon of the stepped and hairpin conformations in the X-ray structure. Conformation D ($\Delta U_T = 0$ kcal/mol) is the lowest energy conformation along with its mirror image C. Conformation A ($\Delta U_T = 3.7$ kcal/mol) and its mirror image B are also energy minima but lie higher in energy relative to other conformations found on the surface such as conformation E (Figure 3.6). E has coordinates $\psi_1 = 178^\circ$, $\psi_3 = 57^\circ$ and $\Delta U_T = 2.8$ kcal/mol with its mirror image denoted E*. E is found half-way along the ψ_1 pathway from A to D and as a result has a half-opened hairpin shape which has been shown in Figure 3.7. Other low energy conformations identified on the contour map of Figure 3.6 are F ($\psi_1 = 62^\circ$, $\psi_3 = 179^\circ$, $\Delta U_T = 3.6$ kcal/mol) and its mirror image F* which are also opened hairpin conformations; conformation G is situated on the centre of symmetry ($\psi_1 = 180^\circ$, $\psi_3 = 180^\circ$, $\Delta U_T = 3.6$ kcal/mol). G is an extended stepped conformation having a staggered geometry. Conformations F and G are also shown in Figure 3.7. In total there are five unique energy minima on the contour map of Figure 3.6 (A, D, E, F, G) four of which have mirror images (A mirrored by B, C by D, E by E*, F by F*). With the hairpin conformation D being the potential energy global minimum of the tosylate it is obvious why it, along with its mirror image C, should appear in the crystal structure of (98). It is interesting then that conformations A and B, although not global minima, are also packed in the crystal structure to further stabilise the system.



Conformation E



Conformation F



Conformation G

Figure 3.7. Diagram showing conformations E, F, and G which are seen on the contour map generated from the torsion angle analysis of ψ_1 and ψ_3 .

3.7. π -STACKING AND X-RAY STRUCTURE OF NOSYLATE (15a)

The presence of intramolecular π -stacking in the hairpin molecules C and D, and intermolecular π -stacking in rows of A and B molecules in the crystal lattice has already been mentioned in the discussion of the X-ray structure. Looking at the tosylate molecule it is evident that the phenyl ring of the benzodioxole group is comparatively more electron rich than the tosyl ring as the former has the two oxygens of the methylenedioxy ring donating electron density. The tosyl ring is more electron poor mainly because of the electron-withdrawing sulfonyl group. Thus it appears the tosyl ring is the π -acceptor, the other phenyl ring being the π -donor. An extended Hückel single point calculation was carried out with HyperChem to assess this postulate. The Extended Hückel Theory (EHT) or Extended Hückel Method (EHM) is attributed mainly to Hoffmann.⁹⁷ It is a simple and fast semi-empirical quantum mechanics method which provides the approximate shape and energy ordering of molecular orbitals. It uses a single set of parameters which represent the binding energies of the electrons in each atomic orbital. These are the energies for the attraction between the nucleus of an atom and an electron in an atomic orbital of that atom. In the method only valence electrons are considered and there is no explicit treatment of electron-electron interactions, though some of their effects are included by parameterisation. Drawbacks of the method are that since electron-electron interactions are neglected atomic orbital binding energies are fixed and not dependent on charge density. Most notably in HyperChem[®], geometry optimisations and molecular dynamics calculations cannot be carried out with the method.⁹² However, an advantage of the method is that it is often the only computational model that can be used for large systems which contain transition metals. This is because the theory only needs atomic ionisation potentials so it is easily parameterised to the whole periodic table.⁸⁵ The most important point to note about the EHM is that its strength lies in providing qualitative information concerning the shape and ordering of molecular orbitals and it should not be used as a quantitative method. Thus from a single point calculation using the EHM, the molecular orbitals for the tosylate were calculated and could be qualitatively assessed.

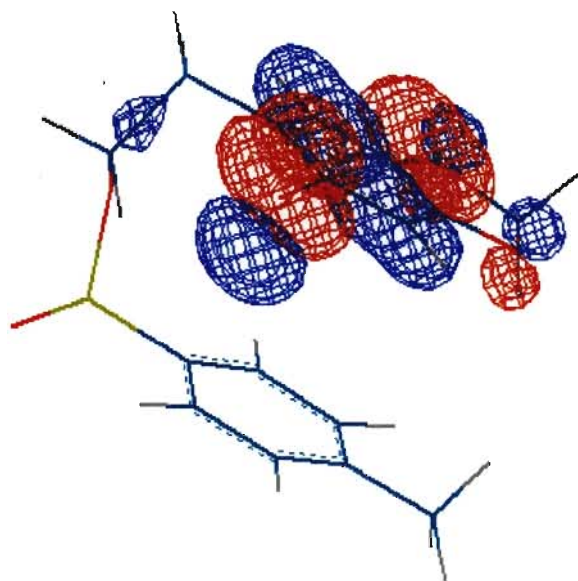


Figure 3.8. Plot of the HOMO calculated for the tosylate molecule using a single point extended Hückel calculation.

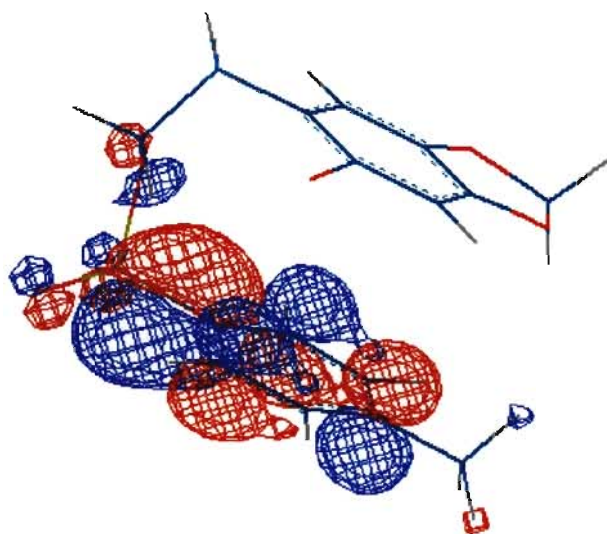
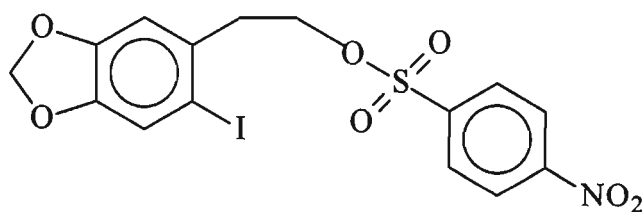


Figure 3.9. Plot of the LUMO calculated for the tosylate molecule using a single point extended Hückel calculation.

Figure 3.8 gives a plot of the highest occupied molecular orbital (HOMO) calculated for the tosylate and Figure 3.9 shows a plot of the calculated lowest unoccupied molecular orbital (LUMO). The HOMO is clearly centered on the phenyl ring fused to the methylenedioxy ring making this ring the π -donor, while the LUMO is found on the tosyl ring (the π -acceptor). The intramolecular π -stacking of the tosylate does not appear to be very strong because of the presence of the stepped molecules in the X-ray structure. If the intramolecular π -stacking were stronger it would stabilise the molecule to such an extent that the hairpin conformation would presumably be the exclusive conformation both in the solid state and in solution. As the formation of the tosylate was not synthetically complex it was decided it would be relatively simple to make an analogue of the tosylate such that the intramolecular π -stacking of the analogue would be strengthened to see if the hairpin conformation could be exclusively crystallised out. This would involve making the tosyl ring even more electron deficient or the other phenyl ring more electron rich. From a synthetic point of view making the tosyl ring more electron deficient is the simplest option as there are a number of *para*-substituted sulfonyl chloride derivatives commercially available which can be used for the synthesis, so the methyl group on the tosyl ring could be easily substituted by a highly electron withdrawing substituent. The substituent chosen was a nitro group, which is highly electron withdrawing and would presumably, in conjunction with the sulfonyl group, make the phenyl ring to which it is bonded extremely electron poor. The structure of this nosylate derivative (**15a**) is shown below.



(**15a**)

Though no X-ray crystal structure of the nosylate (**15a**) has been published it is a known compound and was synthesised with little difficulty following the method of Semmelhack *et al.*²⁹.³⁰ After a bulk crystallisation from CCl₄, X-ray quality crystals were grown by slow evaporation from THF. The X-ray crystal structure was obtained under the same conditions as the tosylate and is shown in Figure 3.10. Crystal structure data for the nosylate (**15a**) is contained in

Appendix C. It is pleasing to see that our intention to “tune” the molecule and force it into the hairpin conformation exclusively was successful. Only a single hairpin conformation is present with no mirror image being evident. The space group of the molecule is P_1 .

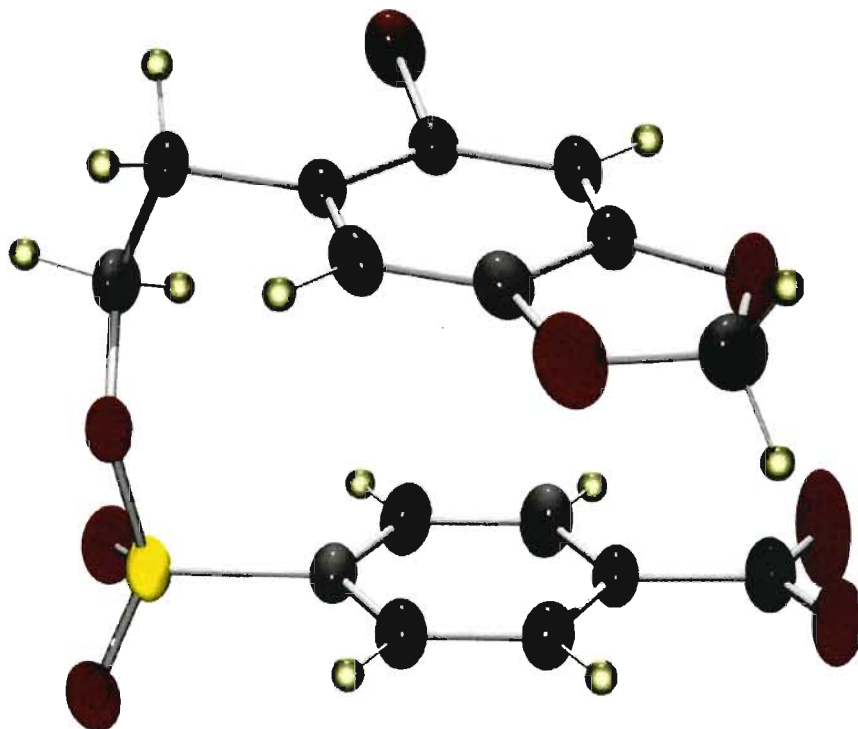


Figure 3.10. X-ray crystal structure diagram for the nosylate (**15a**).

3.8. CONCLUSION

The discovery from its X-ray structure that the apparently simple tosylate molecule is conformationally complex has led to an exciting conformational analysis study that has combined experimental and computational techniques to answer various questions about the system. The findings showed that of the conformations found in the tosylate (**98**) crystal structure, the two hairpin molecules, C and D, were in fact the global minima with their energies appearing to be stabilised by intermolecular π -stacking. This π -stacking effect was proved by synthesis of the nosylate (**15a**) and the acquisition of its X-ray structure. Changing the methyl group of the tosylate (**98**) for the electron withdrawing NO_2 group had increased the π -stacking effect as anticipated and the X-ray structure indicated that the nosylate had crystallised out exclusively

into the hairpin conformation. The nosylate was a suitable conclusion to the study as it showed how information gained from a conformational analysis could be used to “tune” a molecule’s conformation. Though the tosylate and nosylate molecules in themselves may not have wide applicability, the study itself is of academic interest. This work may be extended by manipulating the basic tosylate structure further by trying to make both rings electron rich to destroy the π -stacking effect and see if a situation arises where an analogue crystallises out exclusively in the stepped conformation, or perhaps even one of the other conformations seen in the preceding torsion angle analysis. Further analysis could even be carried out on the tosylate itself, with molecular dynamics calculations being used to model the behaviour of the tosylate in solution to try understand the NMR spectroscopy results that were obtained. Further NMR spectroscopy studies can also be carried out on the nosylate to see if the hairpin conformation may be seen in solution as here the increased strength of the π - π interactions may force the molecule into the hairpin conformation even in the presence of solvent molecules.

Chapter 4

Experimental

4.1. INSTRUMENTATION AND CHEMICALS

4.1.1. Solvents, Reagents and Reaction Conditions

Reagents were used as received from the supplier unless indicated otherwise. Solvents used in reactions were purified by standard techniques.⁹⁸ The BuLi solution in hexane was titrated with diphenylacetic acid and calculated to have a concentration of 1.0 M. The MeLi solution in ether was used from a newly-opened bottle and did not require titration. Et₃N and diisopropylamine were distilled from CaH₂ before use. Pyridine was dried and purified by stirring over KOH and then being distilled.

Reactions were carried out in flame-dried glassware under N₂ unless stated otherwise. Temperatures of -78 °C were obtained using a dry ice/acetone mixture. Where reactions have been irradiated a 400 W high pressure Hg lamp was used with a 10 % aqueous CuSO₄ solution functioning as a filter thereby blocking wavelengths of less than 350 nm. When solvents have been removed *in vacuo* this implies their evaporation under reduced pressure using a rotary evaporator.

4.1.2. Chromatography

For thin layer chromatography silica gel 60 F₂₅₄ aluminium backed plates were used. Silica gel 60, 230–400 mesh; and neutral aluminum oxide 90 (activity I), 70–230 mesh, were utilised for column and flash chromatography and silica gel 60 PF₂₅₄ for radial and preparative thin layer chromatography.

4.1.3. Spectroscopy and Physical Data

IR spectra were recorded with a Perkin Elmer Spectrum One spectrometer (resolution 1 cm⁻¹) as KBr discs or neat liquids between NaCl plates. In general, all values given are stretches (ν) unless otherwise specified where ν_a is an asymmetric stretch, ν_s a symmetric stretch, δ an in-plane bending or deformation, and π an out of plane bending. ¹H and ¹³C NMR spectra were recorded at 500 MHz and 125 MHz respectively with a 500 MHz Varian Unity Inova spectrometer equipped with an Oxford magnet (11.744 T) and switchable 5 mm probe. Standard ¹H and ¹³C

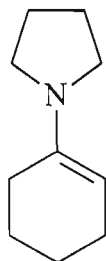
NMR pulse sequences were used for 1D and 2D spectra with all spectra being recorded in CDCl₃ unless specified otherwise. Spectra were referenced by taking the chloroform peak to be at 7.26 ppm in proton NMR spectra and 77.0 ppm in carbon NMR spectra. All shift values are reported in ppm and coupling constants, *J*, are given in Hz. High resolution mass spectra were obtained by the Mass Spectrometry Unit of the Cape Technikon on a double-focusing Kratos MS 80RF mass spectrometer. Low resolution mass spectra were recorded on a Hewlett-Packard gas chromatographic mass spectrometer (HP5988A). Melting points are uncorrected.

4.1.4. X-ray Structure Collection

The collections for all three crystal structures were carried out on an Enraf-Nonius CAD4 diffractometer using Mo K α radiation. The unit cell for each crystal was determined from 25 reflections ($\theta = 12^\circ$). For all data collections the ω - 2θ scan method was used with $\theta = 2-25^\circ$ and a scan angle of 1.35° (60 kV, 35 mA) for spirocycle (**130**), $\theta = 2-23^\circ$ and a scan angle of 1.10° (55 kV, 20 mA) for tosylate (**98**), and $\theta = 2-25^\circ$ and a scan angle of 1.00° (55 kV, 25 mA) for nosylate (**15a**). The crystal structure data was analysed and solved by Dr O.Q. Munro of this department. The data were reduced with the program XCAD (Oscail V8⁹⁹) using Lorentz and polarization correction factors. For the tosylate (**98**) a numerical absorption correction (DIFABS¹⁰⁰) was applied to the data. The structure was solved with the direct methods program SHELXS-97,¹⁰¹ as implemented by the crystallographic program Oscail.⁹⁹ The E-map led to the location of all non-hydrogen atoms; these were refined anisotropically with the program SHELXL-97.¹⁰¹ All hydrogens were included as idealized contributors in the least-squares process with standard SHELXL-97 idealization parameters. The final model was plotted using the program ORTEP.¹⁰² The complete crystallographic details, fractional atomic coordinates for all non-hydrogen atoms, fixed hydrogen atom coordinates, bond lengths, and bond angles, are given in Appendices A, B and C for the spirocycle (**130**), tosylate (**98**) and nosylate (**15a**) respectively.

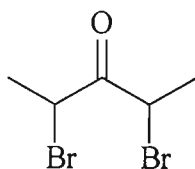
4.2. PREPARATIONS

1-(1-Cyclohexen-1-yl)pyrrolidine (112)



Cyclohexanone (5.00 ml, 48.1 mmol), pyrrolidine (4.00 ml, 47.9 mmol) and a catalytic quantity of toluene-4-sulfonic acid (0.1 g) were added to toluene (40 ml) in a round-bottomed flask (flame-dried glassware and a nitrogen atmosphere were not required). With a Dean and Stark water separator attached, the mixture was heated so that the toluene refluxed vigorously and water collected in the trap of the Dean and Stark apparatus. After approximately 1 hour the mixture was allowed to cool and the solvent and remaining pyrrolidine were removed *in vacuo*. Low boiling impurities (b.p. ≤ 100 °C at 15 mm Hg) were separated from the desired product by Kugelrohr distillation. The purified product was afforded as an orange coloured liquid (4.08 g, 56 %). ν_{\max} (film) / cm^{-1} 3051 (alkene CH), 3022–2827 (CH), 1717, 1642 (C=C); δ_{H} (500 MHz; CDCl_3) 1.49–1.58 (2H, m, CHCH_2CH_2), 1.63–1.71 (2H, m, CCH_2CH_2), 1.76–1.88 (4H, m, 2 NCH_2CH_2), 2.04–2.12 (2H, m, CHCH_2), 2.13–2.22 (2H, m, CCH_2), 2.94–3.03 (4H, m, 2 \times NCH_2), 4.23–4.32 (1H, m, CH); δ_{C} (125 MHz; CDCl_3) 22.97 (CHCH_2CH_2), 23.32 (CCH_2CH_2), 24.46, 24.48 (CHCH_2 , NCH_2CH_2), 27.49 (CCH_2), 47.39 (NCH_2), 93.49 (CH), 143.39 (NC); m/z (EI) 151 (M^+ , 100 %), 136 (85), 123 (75), 122(64), 108 (43), 95 (52), 94 (40), 70 (49), 55 (30).

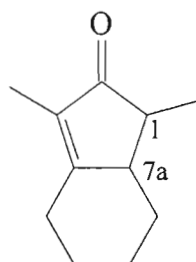
2,4-Dibromo-3-pentanone (114)



3-Pentanone (15.0 ml, 0.143 mol) was mixed with 48 % hydrobromic acid (14.3 ml) and chilled

with ice water (flame-dried glassware or a N₂ atmosphere were not required). Bromine (14.7 ml, 0.286 mol) was then added dropwise over 30 to 45 minutes. After the addition of the bromine was completed water (57 ml) was added and the organic layer separated and washed with an aq. sat. solution of sodium bicarbonate (50 ml) followed by an aq. sat. sodium bisulfite solution (50 ml). The organic layer was dried with MgSO₄ and then distilled under vacuum (b.p. 79–81 °C/15 mm Hg; lit.⁶¹ 75–76 °C/13 mmHg) to give a clear oil (12.416 g, 36 %) which was an inseparable mixture of diastereomers. ν_{\max} (film) /cm⁻¹ 3000–2800 (CH), 1724 (C=O), 641 (CBr); δ_{H} (500 MHz; CDCl₃) 1.80 and 1.88 (6H, both d, *J* 6.9, 2 × CH₃), 4.98 and 4.77 (4H, both q, *J* 6.9, 2 × CH); δ_{C} (125 MHz; CDCl₃) 19.49 and 21.74 (CH₃), 43.82 and 44.00 (CH), 196.02 and 198.32 (C=O); *m/z* (EI) one diastereomer: 246 (M⁺, 9 %; ⁸¹Br, ⁸¹Br), 244 (M⁺, 17; ⁸¹Br, ⁷⁹Br), 242 (M⁺, 8; ⁷⁹Br, ⁷⁹Br), 137 (100; ⁸¹Br), 135 (95; ⁷⁹Br), 109 (95; ⁸¹Br), 107 (92; ⁷⁹Br), 56 (87), other diastereomer: 246 (M⁺, 9 %; ⁸¹Br, ⁸¹Br), 244 (M⁺, 19; ⁸¹Br, ⁷⁹Br), 242 (M⁺, 9; ⁷⁹Br, ⁷⁹Br), 137 (85; ⁸¹Br), 135 (83; ⁷⁹Br), 109 (100; ⁸¹Br), 107 (98; ⁷⁹Br), 56 (67).

1,3-Dimethyl-1,4,5,6,7,7a-hexahydro-2H-inden-2-one (115)



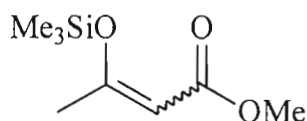
Fe₂(CO)₉ (1.09 g, 3.00 mmol) was added to a flame-dried flask under N₂. 1-(1-Cyclohexen-1-yl)pyrrolidine (112) (1.02 g, 6.74 mmol) in benzene (6 ml) and 2,4-dibromo-3-pentanone (114) (0.51 g, 2.09 mmol, passed through a basic alumina column before use) in benzene (6 ml) were both added to the reaction flask which was then stirred at 60 °C for 10 minutes with irradiation. The heating was then stopped and the solution left to stir overnight with further irradiation. The solution was diluted with ethyl acetate (20 ml) and then washed with saturated aqueous NaHCO₃ (25 ml) followed by a brine solution (25 ml). The organic layer was separated and dried with MgSO₄, filtered and the solvent removed *in vacuo*. The residual oil was passed through a short basic alumina column (Activity I) with ethyl acetate. After removal of the solvent the resulting product was purified by radial chromatography (5 % ethyl acetate/hexane) giving a pale yellow oil containing two diastereomers (0.12 g, 35 %) which were separated by preparative TLC (5 %

ethyl acetate/hexane). ν_{\max} (film) / cm^{-1} 3000–2800 (CH), 1700 (C=O), 1653 (C=C).

(1*R*^{*}, 7*aS*^{*})-diastereomer: R_f 0.24 (10 % ethyl acetate/hexane); δ_H (500 MHz; CDCl_3) 1.09 (3H, d, J 7.8, CHCH_3), 1.72 (3H, d, J 1.4, CCH_3), 1.0–3.0 (m, $4 \times \text{CH}_2$ and $2 \times \text{CH}$); δ_C (125 MHz; CDCl_3) 7.75 (CH_3C), 9.97 (CH_3CH), 20.95 (CCH_2), 25.56 (CCH_2CH_2), 26.93 (CHCH_2CH_2), 31.79 (CHCH_2), 46.12 (CHCH_3), 49.60 (CH_2CHCH), 135.24 (CCH_3), 168.58 (C=C CH_3), 208.23 (C=O); m/z (EI) 164 (M^+ , 75 %), 149 (100), 136 (70), 107 (52), 79 (60).

(1*R*^{*}, 7*aR*^{*})-diastereomer: R_f 0.31 (10 % ethyl acetate/hexane); δ_H (500 MHz; CDCl_3) or 1.14 (3H, d, J 7.8, CHCH_3), 1.67 (3H, d, J 1.4, CCH_3), 1.0–3.0 (m, $4 \times \text{CH}_2$ and $2 \times \text{CH}$); δ_C (125 MHz; CDCl_3) 7.64 (CH_3C), 14.95 (CH_3CH), 25.50 (CCH_2), 26.39 (CHCH_2CH_2), 28.27 (CCH_2CH_2), 33.75 (CHCH_2), 46.84 (CHCH_3), 49.25 (CH_2CHCH), 131.69 (CCH_3), 173.40 (C=C CH_3), 211.36 (C=O); m/z (EI) 164 (M^+ , 78 %), 149 (100), 136 (73), 107 (56), 79 (49).

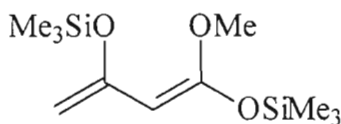
Methyl 3-[(trimethylsilyloxy)-2-butenolate (120)



A mixture of anhydrous powdered zinc chloride (1.0 g, 7.3 mmol) and triethylamine (freshly distilled from CaH_2 , 20.3 ml, 146 mmol) was stirred for one hour at room temperature to suspend the salt in the amine. Methyl acetoacetate (7.2 ml, 67 mmol) in toluene (*ca.* 30 ml) was added followed by TMSCl (17.8 ml, 133 mmol). The resulting mixture was stirred for 30 minutes before increasing the temperature to 40 °C and then left to stir overnight. The solution was allowed to cool to room temperature, added to diethyl ether (*ca.* 150 ml) and filtered through a sintered glass filter containing Celite Filter Cel. The filtrate and ether washings were combined and the solvent removed *in vacuo*. The remaining brown oil was distilled using short path distillation apparatus to afford the product as an inseparable mixture of *E* and *Z* isomers in the form of a clear, colourless liquid (7.92 g, 63 %); b.p 73–75 °C/12 mm Hg (lit.,⁶⁵ 54–55 °C/5 mm Hg); ν_{\max} (film) / cm^{-1} 3000–2840 (CH), 1718 (C=O), 1630 (C=C), 1387 (SiC), 1141 (ν_a C-C(=O)-O), 1039 (ν_a O-C-C), 849 (Si-O); δ_H (500 MHz; CDCl_3) 0.26 and 0.27 (*E/Z*, 9H, each s, SiMe_3), 1.89 (*Z*) and 2.26 (*E*) (3H, each s, $\text{CH}_3\text{C}=\text{C}$), 3.64 (*Z*) and 3.65 (*E*) (3H, each s, CO_2CH_3), 5.09 (*Z*) and 5.13 (*E*) (1H, each s, $-\text{CH}=\text{}$); δ_C (125 MHz; CDCl_3) 0.15 and 0.53 [*E/Z* (CH_3)₃], 20.67 (*E*) and 24.37 (*Z*) (CH_3C), 50.45 (*Z*) and 50.66 (*E*) (OCH_3), 99.22 (*E*) and 99.95 (*Z*) (CH),

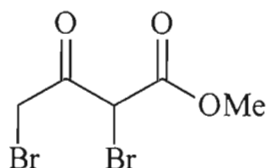
164.88 (*Z*) and 169.92 (*E*) (COSiMe_3), 165.96 (*Z*) and 168.34 (*E*) (COMe); m/z (EI) one structural isomer: 188 (M^+ , 6%), 173 (100), 157 (33), 89 (61), 73 (44), other structural isomer: 188 (M^+ , 1%), 173 (100), 89 (54), 73 (33).

(1*E*)-1,3-Bis[(trimethylsilyl)oxy]-1,3-butadienyl methyl ether (121)



Diisopropylamine (freshly distilled from CaH_2 , 2.0 ml, 14 mmol) was added to THF (50 ml) and after cooling the solution to 0 °C, *n*-BuLi (15 ml of 1.0 M solution in hexane, 15 mmol) was added. The reaction mixture was further cooled to -78 °C and methyl 3-[(trimethylsilyl)oxy]-2-butenate (**120**) (2.0 g, 11 mmol) was added. The solution was left to stir for 2 minutes before being quenched with TMSCl (2.5 ml, 19 mmol). After 10 minutes the solvent was removed *in vacuo* and the residue triturated with anhydrous hexane cooled to 0 °C. The precipitated salts were filtered off and the solvent removed *in vacuo* to afford the crude product (3.37 g). This compound was used without further purification. ν_{max} (film) $/\text{cm}^{-1}$ 3000–2870 (CH), 1652 (C=C), 1251, (SiC), 844 (SiO); δ_{H} (500 MHz; CDCl_3) 0.21 [9H, s, $(\text{CH}_3)_3\text{Si}$], 0.25 [9H, s, $(\text{CH}_3)_3\text{Si}$], 3.55 (3H, s, OCH_3), 3.95 (1H, d, J 1.1, H-CH=C), 4.15 (1H, d, J 1.1, H-CH=C), 4.47 (1H, s, C-CH=C); δ_{C} (125 MHz; CDCl_3) 0.22 [$(\text{CH}_3)_3\text{Si}$], 0.45 [$(\text{CH}_3)_3\text{Si}$], 54.95 (OCH_3), 77.56 (CH_2), 89.20 (CH), 153.36 ($\text{CH}_2=\text{C}$), 158.59 (COMe).

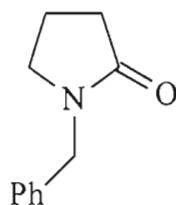
Methyl 2,4-dibromo-3-oxobutanoate (116)



Dichloromethane (35 ml) was added to freshly prepared crude (1*E*)-1,3-bis[(trimethylsilyl)oxy]-1,3-butadienyl methyl ether (**121**) (3.37 g, 12.9 mmol) and the solution cooled to -78 °C while being stirred. Bromine (1.35 ml, 26.3 mmol) was added and the mixture left to stir for half an hour before quenching with saturated aq. NaHCO_3 (15 ml). The product was extracted with

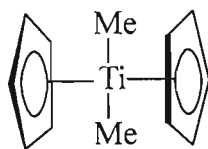
hexane (3 × 30 ml) and the solution dried with MgSO₄ before the solvent was removed *in vacuo*. Low-boiling impurities (b.p. ≤ 90 °C at 6 mm Hg) were separated from the desired product by Kugelrohr distillation. The residue was used without further purification. δ_{H} (500 MHz; CDCl₃) 3.86 (3H, s, CH₃), 4.25 (1H, d, *J* 13.3, CH_aH_b), 4.38 (1H, d, *J* 13.3, CH_aH_b) 5.20 (1H, s, CH); δ_{C} (125 MHz; CDCl₃) 31.04 (CH₂), 45.63 (CH), 54.34 (CH₃), 165.27 (CO₂Me), 190.60 (CO); *m/z* (EI) 276 (M⁺, 2%; ⁸¹Br, ⁸¹Br), 274 (M⁺, 4%; ⁸¹Br, ⁷⁹Br), 272 (M⁺, 2%; ⁷⁹Br, ⁷⁹Br), 154 (95; ⁸¹Br), 152 (100; ⁷⁹Br), 123 (51; ⁸¹Br), 121 (49; ⁷⁹Br), 69 (20).

1-Benzyl-2-pyrrolidinone (123)



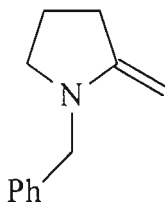
2-Pyrrolidinone (8.9 ml, 0.12 mol) and NaH (80% suspension in oil, 3.5 g, 0.12 mol) were added to toluene (*ca.* 175 ml) and left to stir at room temperature for 30 minutes. Benzyl bromide (14 ml, 0.12 mol) was added and the solution left to stir for a further 2 hours at 90 °C. The mixture was cooled and filtered and the product then purified by column chromatography using ethyl acetate to give a pale yellow oil (17.7 g, 84%). *R_f* 0.53 (ethyl acetate); ν_{max} (film) /cm⁻¹ 3100–2900 (CH), 1685 (C=O), 1083 (C-N); δ_{H} (500 MHz; CDCl₃) 1.99 (2H, 5 lines, *J* 7.6, CH₂CH₂CH₂), 2.44 (2H, t, *J* 8.1, CH₂C=O), 3.26 (2H, t, *J* 7.1, NCH₂CH₂), 4.45 (2H, s, CH₂Ar), 7.23–7.35 (5H, m, ArH's); δ_{C} (125 MHz; CDCl₃) 17.74 (CH₂CH₂CH₂), 30.95 (CH₂C=O), 46.61 (CH₂Ar), 46.62 (NCH₂CH₂), 127.55 (ArCH), 128.13 (ArCH), 128.68 (ArCH), 136.57 (NCH₂C), 174.97 (C=O); *m/z* (EI) 175 (M⁺, 100%), 146 (43), 104 (30), 91 (75, CH₂Ar), 84 (23, M⁺ - CH₂Ar).

Dimethyltitanocene (125)



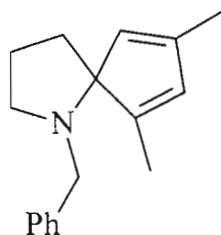
Titanocene dichloride (4.00 g, 16.1 mmol) was dissolved in dry THF (80 ml). While stirring at 10–15 °C in the dark (tin foil wrapped around the flask), MeLi (21.7 ml of 1.6 M in ether, 34.7 mmol) was added slowly to the solution. After stirring for approximately 5 minutes at room temperature the reaction was quenched with ice leaving an orange solution which was dried over anhydrous MgSO₄. The solution was filtered and the solvent removed under vacuum leaving an orange residue which was recrystallised from pentane by cooling to -78 °C to give orange, needle-like crystals (2.45 g, 73 %). ν_{\max} (KBr disc) /cm⁻¹ 3150–2800 (CH), 1442 (CC), 1014 (δ CH), 814 (π CH), 462 (Ti-C_p); δ_{H} (500 MHz; CDCl₃) -0.15 [6H, s, (CH₃)₂], 6.06 (10H, s, Cp₂); δ_{C} (125 MHz; CDCl₃) 45.45 [(CH₃)₂], 113.07 (Cp₂).

1-Benzyl-2-methylenepyrrolidine (117)



In a flask, toluene (10 ml) was added to dimethyl titanocene (**125**) (1.03 g, 4.95 mmol) followed by 1-benzyl-2-pyrrolidinone (**123**) (289 mg, 1.65 mmol) and the resulting mixture was heated to 80 °C and stirred overnight. On cooling to room temperature, pentane (20 ml) was added to the reaction flask to precipitate out the titanium salts which were then filtered off through Celite Filter Cel and the remaining solution concentrated *in vacuo*. The enamine was used without any further purification.

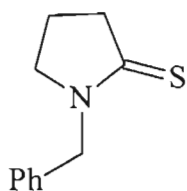
2.1.4. Reaction of 2,4-Dibromo-3-pentanone (114) and 1-Benzyl-2-methylenepyrrolidine (117)



Proposed product (127)

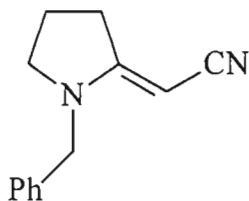
$\text{Fe}_2(\text{CO})_9$ (235 mg, 0.647 mmol) was added to a flame-dried flask under N_2 . 1-Benzyl-2-methylenepyrrolidine (117) (0.29 g, 1.7 mmol) in benzene (2ml) and 2,4-dibromo-3-pentanone (114) (134 mg, 0.549 mmol, passed through a basic alumina column before use) also in benzene (2 ml) were both added to the reaction flask which was then stirred at 60 °C for 10 minutes with irradiation. The heating was then stopped and the solution left to stir overnight with further irradiation. The solution was diluted with ethyl acetate (15 ml) and then washed with saturated aqueous NaHCO_3 (15 ml) followed by a brine solution (15 ml). The organic layer was separated and dried with MgSO_4 , filtered and the solvent removed under vacuum. The product was then purified on a neutral alumina column. Firstly, a solution of 1 % ethyl acetate/hexane was passed through the column to elute the more non-polar components and this was followed by pure ethyl acetate. The product was obtained as a yellow oil from the ethyl acetate fractions (11 mg, 8 %). R_f 0.66 (50 % ethyl acetate/hexane); ν_{max} (film) $/\text{cm}^{-1}$ 3100–2800 (CH), 1082 (C-N); δ_{H} (500 MHz; CDCl_3) 1.29 (3H, s, CH_3), 1.30 (3H, s, CH_3), 1.68–1.73 (1H, m, NCCH_aH_b), 1.80–1.89 (2H, m, $\text{CH}_2\text{CH}_2\text{CH}_2$), 1.97–2.05 (1H, m, NCCH_aH_b), 2.45–2.51 (1H, m, $\text{NCH}_a\text{H}_b\text{CH}_2$), 2.88–2.95 (1H, m, $\text{NCH}_a\text{H}_b\text{CH}_2$), 3.22 (1H, d, J 13.3, ArCH_aH_b), 3.60 (1H, d, J 13.3, ArCH_aH_b), 6.21 (1H, s, NCCH), 6.41 (1H, s, $\text{CH}_3\text{CCHCCH}_3$), 7.18–7.31 (5H, m, $\text{ArCH}'\text{s}$); δ_{C} (125 MHz; CDCl_3) 17.06 (CH_3), 17.67 (CH_3), 21.56 ($\text{CH}_2\text{CH}_2\text{CH}_2$), 39.07 (NCCH_2), 49.87 (NCH_2CH_2), 53.23 (ArCH_2), 62.97 (NC), 126.39 (NCCH), 128.01 (ArCH), 128.13 (ArCH), 128.34 (ArCH), 131.65 ($\text{CH}_3\text{CCHCCH}_3$), 141.09 (NCH_2C), 153.48 (CCH_3), 155.92 (CCH_3); m/z (EI) 239 (M^+ , 12 %), 224 (100), 174 (11), 120 (12), 91 (91, CH_2Ar) (Found: M^+ , 239.1669 $\text{C}_1\text{H}_{21}\text{N}$ requires 239.1674).

1-Benzyl-2-pyrrolidinethione (128)



To a flask containing THF (70 ml), phosphorus pentasulfide (5.64 g, 12.7 mmol) was added followed by sodium carbonate (1.35 g, 12.7 mmol). After the mixture was stirred for 30 minutes to ensure homogeneity, 1-benzyl-2-pyrrolidinone (**123**) (1.86 g, 10.6 mmol) was added and the mixture left to stir for a further 3 hours at room temperature. The reaction was then quenched with 10 % aqueous trisodium phosphate (50 ml) and the aqueous phase extracted with ethyl acetate (3 × 50 ml). The combined organic portions were dried with MgSO₄ and concentrated *in vacuo*. The remaining liquid was purified by flash chromatography (50 % ethyl acetate/hexane) to afford the product as a yellow oil (1.10 g, 54 %). *R*_f 0.36 (20 % ethyl acetate/hexane); ν_{\max} (film) /cm⁻¹ 3100–2875 (CH), 1507 (C=S), 1116 (C-N); δ_{H} (500 MHz; CDCl₃) 2.10 (2H, 5 lines, *J* 7.6, CH₂CH₂CH₂), 3.10 (2H, t, *J* 7.9, CH₂C=S), 3.58 (2H, t, *J* 7.3, NCH₂CH₂), 4.99 (2H, s, CH₂Ar), 7.29–7.36 (5H, m, ArH's); δ_{C} (125 MHz; CDCl₃) 19.39 (CH₂CH₂CH₂), 44.86 (CH₂C=S), 51.56 (CH₂Ar), 53.93 (NCH₂CH₂), 128.01 (ArCH), 128.26 (ArCH), 128.81 (ArCH), 135.07 (NCH₂C), 201.73 (C=S); *m/z* (EI) 191 (M⁺, 100 %), 149 (27), 148 (39), 106 (20), 103 (22), 91 (61, CH₂Ar).

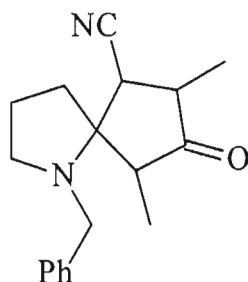
2-(1-Benzyl-2-pyrrolidinylidene)acetonitrile (129)



1-Benzyl-2-pyrrolidinethione (**128**) (1.10 g, 5.75 mmol) and bromoacetonitrile (0.60 ml, 8.67 mmol) were added to acetonitrile (5 ml) and the resulting mixture left to stir overnight at room temperature. Triphenylphosphine (2.26 g, 8.63 mmol) and triethylamine (freshly distilled from CaH₂, 1.20 ml, 8.63 mmol) were mixed in dichloromethane (5 ml) and this solution was then

added to the reaction mixture and left to stir. After 2 hours the reaction was quenched with saturated aqueous NaHCO_3 (10 ml) and the aqueous layer extracted with ethyl acetate (3×15 ml). The combined organic portions were dried with MgSO_4 , filtered and the solvent removed *in vacuo*. The remaining oil was dissolved in a 50 % CH_2Cl_2 /hexane mixture (50 ml) and cooled to cause the precipitation of the triphenylphosphine oxide by-product which was filtered off. The solids were washed with the cold CH_2Cl_2 /hexane mixture. This was repeated and then the remaining solution was reduced *in vacuo* and purified by radial chromatography (50 % CH_2Cl_2 /hexane) to afford a yellow oil (853 mg, 75 %). R_f 0.36 (100 % CH_2Cl_2); ν_{max} (film)/ cm^{-1} 3100–2860 (CH), 2248 ($\text{C}\equiv\text{N}$), 1617 ($\text{C}=\text{C}$), 1082 ($\text{C}-\text{N}$); δ_{H} (500 MHz; CDCl_3) 2.01 (2H, 5 lines, J 7.3, $\text{CH}_2\text{CH}_2\text{CH}_2$), 2.94 (2H, t, J 7.7, NCCCH_2), 3.42 (2H, t, J 6.9, NCH_2CH_2), 3.58 (1H, s, $\text{NC}=\text{CH}$), 4.28 (2H, s, CH_2Ar), 7.16–7.36 (5H, m, ArH's); δ_{C} (125 MHz; CDCl_3) 20.81 ($\text{CH}_2\text{CH}_2\text{CH}_2$), 32.75 (NCCCH_2), 50.08 (CH_2Ar), 53.62 (NCH_2CH_2), 54.46 ($\text{C}=\text{CHCN}$), 114.53 ($\text{C}\equiv\text{N}$), 127.17 (ArCH), 127.77 (ArCH), 128.86 (ArCH), 135.33 (NCH_2C), 165.82 ($\text{NC}=\text{C}$); m/z (EI) 198 (M^+ , 24%), 92 (9), 91 (100, CH_2Ar), 65 (13).

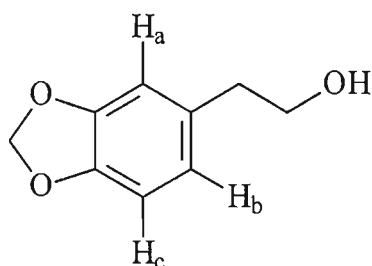
1-Benzyl-7,9-dimethyl-8-oxo-1-azaspiro[4.4]nonane-6-carbonitrile (130)



$\text{Fe}_2(\text{CO})_9$ (1.49 g, 4.10 mmol) was added to a flame-dried flask under N_2 . 2-(1-Benzyl-2-pyrrolidinylidene)acetonitrile (**129**) (0.85 g, 4.3 mmol) dissolved in benzene (10–15 ml) and 2,4-dibromo-3-pentanone (**114**) (1.57 g, 6.44 mmol, passed through a basic alumina column before use) also dissolved in benzene (10–15 ml) were both added to the reaction flask which was then stirred overnight under N_2 at 50 °C with irradiation. The solution was diluted with ethyl acetate (30 ml) and then washed with saturated aqueous NaHCO_3 (40 ml) followed by a brine solution (40 ml). The organic layer was separated and dried with MgSO_4 , filtered and the solvent removed under vacuum. The resulting product was purified by radial chromatography (10 % ethyl acetate/hexane) to give a mixture of diastereomers (292 mg, 24 %) with R_f values ranging from 0.36 to 0.65 (20 % ethyl acetate/hexane). The ($5S^*$, $6S^*$, $7S^*$, $9S^*$) diastereomer was

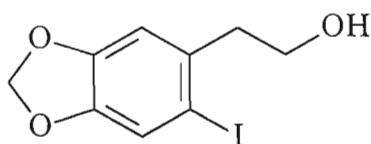
selectively crystallised out from an ethyl acetate/hexane solution to give large, colourless crystals. R_f 0.49 (20 % ethyl acetate/hexane), m.p. 108.5–110.5 °C; ν_{\max} (KBr disc) / cm^{-1} 3100–2800 (CH), 2237 (C \equiv N), 1747 (C=O), 1076 (C-N); δ_{H} (500 MHz; CDCl₃) 1.14 (3H, d, J 6.9, CCHCH₃), 1.27 (3H, d, J 7.3, CHCHCH₃), 1.75–1.85 (1H, m, CH₂CH_aH_bCH₂), 1.88–1.93 (1H, m, NCCH_aH_b), 1.99–2.11 (2H, m, CH₂CH_aH_bCH₂ and NCCH_aH_b), 2.36–2.46 (2H, m, 2CH₃CH), 2.75 (1H, d, J 11.4, CHC \equiv N), 2.80–2.84 (1H, m, NCH_aH_bCH₂), 2.98–3.03 (1H, m, NCH_aH_bCH₂), 3.81 (1H, d, J 13.3, ArCH_aH_b), 3.84 (1H, d, J 13.3, ArCH_aH_b), 7.25–7.35 (5H, m, ArCH^s); δ_{C} (125 MHz; CDCl₃) 8.70 (CCHCH₃), 14.06 (CHCHCH₃), 22.16 (CH₂CH₂CH₂), 29.76 (NCCH₂), 40.88 (CHC \equiv N), 46.40 (CHCHCH₃), 49.44 (CCHCH₃), 51.72 (CH₂Ar), 52.17 (NCH₂CH₂), 71.08 (C-N), 119.69 (C \equiv N), 127.29 (ArCH), 127.99 (ArCH), 128.52 (ArCH), 138.94 (CCH₂N), 213.71 (C=O); m/z (EI) 282 (M⁺, 18 %), 200 (13), 188 (14), 187 (100), 186 (28), 91 (71, CH₂Ar) (Found: M⁺, 282.1734 C₁₈H₂₂N₂O requires 282.1732).

2-(1,3-Benzodioxol-5-yl)-1-ethanol (60)



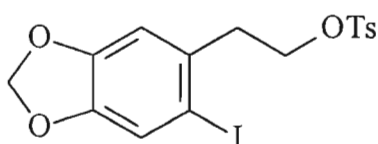
3,4-Methylenedioxyphenylacetic acid (0.50 g, 2.8 mmol) was added to a stirred solution of LiAlH₄ (0.2 g, 5.3 mmol) in THF (15 ml). The solution was stirred for 1.5 hours at 25 °C and then quenched with water (0.3 ml) followed by aq. NaOH (15 %, 0.3 ml) and finally additional water (1 ml). The resulting suspension was filtered and the unwanted solids washed thoroughly with chloroform. The combined filtrate and washings were dried with MgSO₄, filtered and concentrated *in vacuo* to give the desired product analytically pure as a colourless liquid (449 mg, 96 %). ν_{\max} (film) / cm^{-1} 3362 (OH), 3100–2800 (CH), 1247 and 1041 (C-O); δ_{H} (500 MHz; CDCl₃) 1.58 (1H, s, OH), 2.79 (2H, t, J 6.4, ArCH₂), 3.81 (2H, t, J 6.4, CH₂OH), 5.93 (2H, s, OCH₂O), 6.68 (1H, dd, J 7.9, 1.7, H_b), 6.72 (1H, d, J 1.8, H_a), 6.76 (1H, d, J 7.9, H_c); δ_{C} (125 MHz; CDCl₃) 38.87 (ArCH₂), 63.76 (CH₂OH), 100.89 (OCH₂O), 108.36 (CH_c), 109.34 (CH_a), 121.91 (CH_b), 132.18 (CCH₂), 146.20 (OCCHCH), 147.81 (OCCHC); m/z (EI) 166 (M⁺, 24 %), 136 (10), 135 (100, M⁺ - CH₂OH), 77 (19), 51 (10).

2-(6-Iodo-1,3-benzodioxol-5-yl)-1-ethanol (97)



To a stirred mixture of 2-(1,3-benzodioxol-5-yl)-1-ethanol (**60**) (1.14 g, 6.87 mmol) and silver trifluoroacetate (1.67 g, 7.56 mmol) in CH_2Cl_2 (40 ml) under N_2 , solid iodine (2.09 g, 8.24 mmol) was added. The mixture was then left to stir at 25 °C for 2 hours after which it was washed with saturated aqueous sodium thiosulfate (40 ml). The aqueous phase was extracted with CH_2Cl_2 (2 × 40 ml) and the combined organic layers were dried with MgSO_4 and concentrated *in vacuo* leaving a brown residue which was taken up in hot CCl_4 (30 ml) and treated with activated charcoal (*ca.* 1 g). The charcoal was filtered off, the solvent removed *in vacuo* and the remaining oil purified by radial chromatography (10 % ethyl acetate/hexane) to give the product (1.04 g, 52 %) which was recrystallised from CCl_4 giving colourless, needle-like crystals with m.p. 63.5–64.5 °C (lit.³⁰ 68–69.5 °C). R_f 0.17 (20 % ethyl acetate/hexane); ν_{max} (KBr disc)/ cm^{-1} 3313 (OH), 2950–2800 (CH), 1225 and 1037 (C-O), 532 (CI); δ_{H} (500 MHz; CDCl_3) 1.53 (1H, s, OH), 2.94 (2H, t, J 6.7, ArCH_2), 3.81 (2H, t, J 6.7, CH_2OH) 5.95 (2H, s, OCH_2O), 6.79 (1H, s, CHCCH_2), 7.25 (1H, s, CHCI); δ_{C} (125 MHz; CDCl_3) 43.50 (ArCH_2), 62.47 (CH_2OH), 88.07 (CI), 101.60 (OCH_2O), 110.13 (CHCCH_2), 118.76 (CHCI), 134.29 (CCH_2), 147.20 (CCHCCH_2), 148.49 (CCHCI); m/z (EI) 292 (M^+ , 49 %), 261 (100, $\text{M}^+ - \text{CH}_2\text{OH}$), 165 (14), 134 (13), 76 (13).

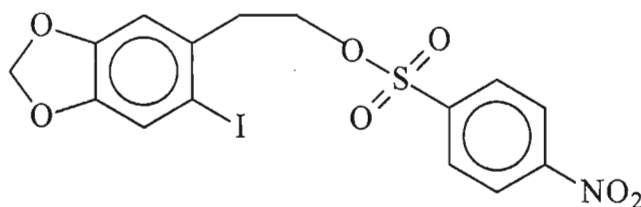
2-(6-Iodo-1,3-benzodioxol-5-yl)ethyl 4-methylbenzenesulfonate (98)



2-(6-Iodo-1,3-benzodioxol-5-yl)-1-ethanol (**97**) (512 mg, 1.75 mmol) and *p*-toluenesulfonyl chloride (0.50 g, 2.6 mmol) were dissolved separately in diethylether (5 ml each) and then combined. Pyridine (0.5 ml, dried over KOH and freshly distilled) was then added to the solution and the mixture left overnight (not under N_2) to allow formation of colorless and yellow crystals. The supernatant liquid was then removed and left to stand allowing more crystals to form. The combined crystals and remaining liquid were partitioned between CH_2Cl_2 (30 ml) and water (15

ml). The organic layer was separated, washed with ice-cold HCl (5 %, 30 ml), dried with MgSO₄, filtered and concentrated *in vacuo* leaving a yellow residue which was purified by radial chromatography (15 % ethyl acetate/hexane) giving an oil (315 mg, 39 %) which crystallised on standing. The colorless crystalline product had m.p. 50–54 °C; R_f 0.33 (20 % ethyl acetate/hexane); ν_{\max} (KBr disc)/cm⁻¹ 3100–2900 (CH), 1358 (ν_a S(=O)₂), 1248 and 1096 (C-O), 1176 (ν_s S(=O)₂), 554 (CI); δ_H (500 MHz; CDCl₃) 2.44 (3H, s, Me), 2.98 (2H, t, *J* 6.9, ArCH₂), 4.16 (2H, t, *J* 6.9, CH₂OTs), 5.95 (2H, s, OCH₂O), 6.67 (1H, s, CHCCH₂), 7.13 (1H, s, CHCI), 7.29 (2H, d, *J* 8.2, CHCMe), 7.71 (2H, d, *J* 8.2, CHCS); δ_C (125 MHz; CDCl₃) 21.61 (Me), 39.81 (ArCH₂), 69.10 (CH₂OTs), 87.78 (CI), 101.67 (OCH₂O), 110.42 (CHCCH₂), 118.64 (CHCI), 127.87 (CHCS), 129.74 (CHCMe), 131.97 (CCH₂), 132.86 (CMe), 144.68 (CS), 147.52 (CCHCCH₂), 148.45 (CCHCI); *m/z* (EI) 446 (M⁺, 19 %), 274 (100, M⁺ - HOTs), 261 (29, M⁺ - CH₂OTs) (Found: M⁺, 455.9682. C₁₆H₁₅IO₅S requires 455.9685).

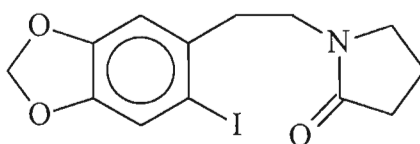
2-(6-Iodo-1,3-benzodioxol-5-yl)ethyl 4-nitrobenzenesulfonate (15a)



2-(6-Iodo-1,3-benzodioxol-5-yl)-1-ethanol (**97**) (1.04 g, 3.56 mmol) was added to CH₂Cl₂ 20 ml) and cooled to 0 °C. Et₃N (freshly distilled from CaH₂, 0.14 ml, 1.0 mmol) and DMAP (43 mg, 0.36 mmol) were added to the stirred solution followed by *p*-nitrobenzenesulfonyl chloride (90 % technical grade, 1.14 g, 4.63 mmol) in small portions. The mixture was allowed to warm to room temperature and then left to stir for a further four hours. After this time further CH₂Cl₂ was added (*ca.* 20 ml) and the mixture washed with aq. sat. sodium chloride (20 ml). The organic layer was dried with MgSO₄ and concentrated *in vacuo*. Repeated recrystallisation from 20 % CH₂Cl₂/ethyl acetate resulted finally in the collection of yellow crystals (432 mg, 25 %). X-ray quality crystals were grown by slow evaporation from THF. The strongly coloured yellow crystals had m.p. 114–116 °C (lit. 126.5–127 °C); ν_{\max} (KBr disc)/cm⁻¹ 3100–2900 (CH), 1529 [ν_a (N=O)₂], 1364 [ν_a S(=O)₂], 1350 [ν_s (N=O)₂], 1245 and 1095 (C-O), 1187 [ν_s S(=O)₂], 849

(CN), 569 (CI); δ_{H} (500 MHz; CDCl_3) 3.02 (2H, t, J 6.5, ArCH_2), 4.32 (2H, t, J 6.5, CH_2OSO_2), 5.94 (2H, s, OCH_2O), 6.60 (1H, s, CHCCH_2), 7.11 (1H, s, CHCl), 7.96 (2H, dd, J 7.0, 2.0, CHCS), 8.31 (2H, dd, J 7.0, 2.0, CHCN); δ_{C} (125 MHz; CDCl_3) 39.65 (ArCH_2), 70.58 (CH_2OSO_2), 87.78 (CI), 101.86 (OCH_2O), 110.41 (CHCCH_2), 118.73 (CHCl), 124.24 (CHCN), 129.10 (CHCS), 131.51 (CCH_2), 141.61 (CS), 147.69 (CCHCCH_2), 148.44 (CCHCl), 150.55 (CN).

1-[2-(6-iodo-1,3-benzodioxol-5-yl)ethyl]-2-pyrrolidinone (99)



2-(6-Iodo-1,3-benzodioxol-5-yl)ethyl 4-nitrobenzenesulfonate (**15a**) (155 mg, 0.325 mmol), NaH (80 % suspension in oil, 0.02 g), and 2-pyrrolidinone (50 μl , 650 μmol) were added to benzene (10 ml). The mixture was heated under reflux and the progress of the reaction monitored by TLC (50 % ethyl acetate/hexane). When it was observed that all the nosylate (**15a**) had reacted the mixture was passed through a silica gel plug column with ethyl acetate and then the solvent removed *in vacuo*. The product was purified by radial chromatography (25 % ethyl acetate/hexane) and was obtained as cream coloured crystals (55 mg, 47 %) on removal of the solvent *in vacuo*. The crystals had m.p. 96.5-99.5 $^{\circ}\text{C}$; R_f 0.23 (50 % ethyl acetate/hexane); ν_{max} (KBr disc) $/\text{cm}^{-1}$ 3070-2850 (CH), 1685 (C=O), 1231 and 1040 (C-O); δ_{H} (500 MHz; CDCl_3) 1.94 (2H, 5 lines, J 7.6, $\text{CH}_2\text{CH}_2\text{CH}_2$), 2.32 (2H, t, J 8.1, $\text{CH}_2\text{C}=\text{O}$), 2.82, (2H, t, J 7.5, ArCH_2), 3.30 (2H, t, J 7.1, $\text{CH}_2\text{CH}_2\text{CH}_2\text{N}$), 3.37 (2H, t, J 7.5, ArCH_2CH_2), 5.89 (2H, s, OCH_2O), 6.74 (1H, s, CHCCH_2), 7.15 (1H, s, CHCl); δ_{C} (125 MHz; CDCl_3) 17.79 ($\text{CH}_2\text{CH}_2\text{CH}_2$), 30.82 ($\text{CH}_2\text{C}=\text{O}$), 38.06 (ArCH_2), 42.88 (ArCH_2CH_2), 47.91 ($\text{CH}_2\text{CH}_2\text{CH}_2\text{N}$), 87.48 (CI), 101.51 (OCH_2O), 109.51 (CHCCH_2), 118.42 (CHCl), 134.40 (CHCCH_2), 147.11 (CCHCCH_2), 148.51 (CCHCl), 175.47 (C=O); m/z (EI) 359 (M^+ , 2 %), 274 (56), 232 (55), 98 (100), 70 (32).

Chapter 5

References

1. S.W. Pelletier (Ed.), *Alkaloids: Chemical and Biological Perspectives, Vol 1*, John Wiley and Sons, New York, 1983.
2. G.A. Cordell, *Introduction to Alkaloids: A Biogenetic Approach*, John Wiley and Sons, New York, 1981.
3. W.W. Paudler, G.I. Kerley, and J. McKay, *J. Org. Chem.*, 1963, **28**, 2194.
4. R.G. Powell, D. Weisleder, C.R. Smith, Jr., and I.A. Wolff, *Tetrahedron Lett.*, 1969, **46**, 4081.
5. D.J. Abraham, R.D. Rosenstein, and E.L. McGandy, *Tetrahedron Lett.*, 1969, **46**, 4085.
6. S.K. Arora, R.B. Bates, R.A. Gandy, and R.G. Powell, *J. Org. Chem.*, 1974, **39**, 1269.
7. R.G. Powell, D. Weisleder, C.R. Smith, Jr., and W.K. Rohwedder, *Tetrahedron Lett.*, 1970, **11**, 815.
8. K.L. Mikolajczak, R.G. Powell, and C.R. Smith, Jr., *Tetrahedron*, 1972, **28**, 1995.
9. C.R. Smith, Jr., R.G. Powell, and K.L. Mikolajczak, *Cancer Treat. Rep.*, 1976, **60**, 1157.
10. R.G. Powell, D. Weisleder, and C.R. Smith, Jr., *J. Pharm. Sci.*, 1972, **61**, 1227.
11. I. Takano, I. Yasuda, M. Nishijima, Y. Yanagi, K. Takeya, and H. Itokawa, *Phytochemistry*, 1997, **44**, 735.
12. M. Huang, *Mol. Pharmacol.*, 1975, **11**, 511.
13. M. Fresno, A. Jiménez, and D. Vázquez, *Eur. J. Biochem.*, 1977, **72**, 323.
14. T.H. Corbett, D.P. Griswold, Jr., B.J. Roberts, J.C. Peckham, and F.M. Schabel, Jr., *Cancer*, 1977, **40**, 2660.
15. W.R. Cobb, A.E. Bogden, S.D. Reich, T.W. Griffin, D.E. Kelton, and D.J. LePage, *Cancer Treat. Rep.*, 1983, **67**, 173.
16. R.P. Warrell, Jr., C.J. Coonley, and T.S. Gee, *J. Clin. Oncol.*, 1985, **3**, 617.
17. J.M. Whaun and N.D. Brown, *Annals of Tropical Medicine and Parasitology*, 1990, **84**, 229.
18. N. Savaraj, K. Lu, I. Dimery, L.G. Feun, M. Burgess, M. Keating, and T.L. Loo, *Cancer Treat. Rep.*, 1986, **70**, 1403.

19. J.A. Ajani, I. Dimery, S.P. Chawla, K. Pinnamaneni, R.S. Benjamin, S.S. Legha, and I.H. Krakoff, *Cancer Treat. Rep.*, 1986, **70**, 375.
20. J.A. Stewart, P.A. Cassileth, J.M. Bennett, and M.J. O'Connell, *Am. J. Clin. Oncol.*, 1988, **11**, 627.
21. R.S. Witte, S. Lipsitz, T.L. Goodman, R.F. Asbury, G. Wilding, C.M. Strnad, T.J. Smith and D.G. Haller, *Invest. New Drugs*, 1999, **17**, 173.
22. T. Ohnuma and J.F. Holland, *J. Clin. Oncol.*, 1985, **3**, 604.
23. C.T.C. Tan, E. Luks, D.M. Bacha, P. Steinherz, L. Steinherz, and A. Mondora, *Cancer Treat. Rep.*, 1987, **71**, 1245.
24. J.A. Neidhart, D.C. Young, E. Kraut, B. Howinstein, and E.N. Metz, *Cancer Res.*, 1986, **46**, 967.
25. I. Takano, I. Yasuda, M. Nishijima, Y. Hitotsuyanagi, K. Takeya, and H. Itokawa, *J. Org. Chem.*, 1997, **62**, 8251.
26. S.M. Weinreb and M.F. Semmelhack, *Acc. Chem. Res.*, 1975, **8**, 158.
27. J. Auerbach and S.M. Weinreb, *J. Am. Chem. Soc.*, 1972, **94**, 7172.
28. J. Auerbach and S.M. Weinreb, *J. Am. Chem. Soc.*, 1975, **97**, 2503.
29. M.F. Semmelhack, B.P. Chong, and L.D. Jones, *J. Am. Chem. Soc.*, 1972, **94**, 8629.
30. M.F. Semmelhack, B.P. Chong, R.D. Stauffer, T.D. Rogerson, A. Chong and L.D. Jones, *J. Am. Chem. Soc.*, 1975, **97**, 2507.
31. S. Yasuda, T. Yamada, and M. Hanaoka, *Tetrahedron Lett.*, 1986, **27**, 2023.
32. M.E. Kuehne, W.G. Bornmann, W.H. Parsons, T.D. Spitzer, J.F. Blount, and J. Zubieta, *J. Org. Chem.*, 1988, **53**, 3439.
33. T.P. Burkholder and P.L. Fuchs, *J. Am. Chem. Soc.*, 1988, **110**, 2341.
34. T.P. Burkholder and P.L. Fuchs, *J. Am. Chem. Soc.*, 1990, **112**, 9601.
35. H. Ishibashi, M. Okano, H. Tamaki, K. Maruyama, T. Yakura, and M. Ikeda, *J. Chem. Soc., Chem. Commun.*, 1990, 1436.
36. M. Ikeda, M. Okano, K. Kosaka, M. Kido, and H. Ishibashi, *Chem. Pharm. Bull.*, 1993, **41**, 276.
37. X. Lin, R.W. Kavash, and P.S. Mariano, *J. Am. Chem. Soc.*, 1994, **116**, 9791.
38. X. Lin, R.W. Kavash, and P.S. Mariano, *J. Org. Chem.*, 1996, **61**, 7335.
39. N. Isono and M. Mori, *J. Org. Chem.*, 1995, **60**, 115.
40. T. Nagasaka, H. Sato, and S. Saeki, *Tetrahedron: Asymmetry*, 1997, **8**, 191.

41. L.J. Dolby, S.J. Nelson, and D. Senkovich, *J. Org. Chem.*, 1972, **37**, 3691.
42. B. Weinstein and A.R. Craig, *J. Org. Chem.*, 1976, **41**, 875.
43. F.G. Fang, M.E. Maier, S.J. Danishefsky, and G. Schulte, 1990, **55**, 831.
44. I. Tse and V. Snieckus, *J. Chem. Soc., Chem. Commun.*, 1976, 505.
45. L.F. Tietze and H. Schirok, *J. Am. Chem. Soc.*, 1999, **121**, 10264.
46. M. Ikeda, S.A.A. El Bialy, K. Hirose, M. Kotake, T. Sato, S.M.M. Bayomi, I.A. Shehata, A.M. Abdelal, L.M. Gad, and T. Yakura, *Chem. Pharm. Bull.*, 1999, **47**, 983.
47. R.G. Powell and K.L. Mikolajczak, *Phytochemistry*, 1973, **12**, 2987.
48. R.G. Powell, *Phytochemistry*, 1972, **11**, 1467.
49. J.W. Ullrich, F. Chiu, T. Tiner-Harding, and P.S. Mariano, *J. Org. Chem.*, 1984, **49**, 220.
50. F. Chui, J.W. Ullrich, and P.S. Mariano, *J. Org. Chem.*, 1984, **49**, 228.
51. J.A. Gewert, J. Görlitzer, S. Götze, J. Looft, P. Menningen, T. Nöbel, H. Schirock, and C. Wulff, *Organic Synthesis Workbook*, Wiley-VCH, Weinheim, 2000, pp.143–160.
52. H. Takaya, S. Makino, Y. Hayakawa, and R. Noyori, *J. Am. Chem. Soc.*, 1978, **100**, 1765.
53. Y. Hayakawa, K. Yokoyama, and R. Noyori, *J. Am. Chem. Soc.*, 1978, **100**, 1791.
54. Y. Hayakawa, K. Yokoyama, and R. Noyori, *J. Am. Chem. Soc.*, 1978, **100**, 1799.
55. H. Takaya, Y. Hayakawa, S. Makino, and R. Noyori, *J. Am. Chem. Soc.*, 1978, **100**, 1778.
56. Y. Hayakawa, Y. Baba, S. Makino, and R. Noyori, *J. Am. Chem. Soc.*, 1978, **100**, 1786.
57. P.J. Stang, M. Hanack, and L.R. Subramanian, *Synthesis*, 1982, 85.
58. N.A. Petasis and S. Lu, *Tetrahedron Lett.*, 1995, **36**, 2393.
59. R. Noyori, Y. Hayakawa, H. Takaya, S. Murai, R. Kobayashi, and N. Sonoda, *J. Am. Chem. Soc.*, 1978, **100**, 1759.
60. L.M. Harwood and C.J. Moody, *Experimental Organic Chemistry: Principles and Practice*, Blackwell Scientific Publications, Oxford, 1989.
61. N. De Kimpe, L. D'Hondt, and L. Moens, *Tetrahedron*, 1992, **48**, 3183.
62. C.J. Rousset, S. Iyer, and E. Negishi, *Tetrahedron: Asymmetry*, 1997, **23**, 3921.
63. T. Chan and P. Brownbridge, *J. Chem. Soc., Chem. Commun.*, 1979, 578.
64. T. Chan and P. Brownbridge, *J. Am. Chem. Soc.*, 1980, **102**, 3534.
65. S. Danishefsky and T. Kitahara, *J. Am. Chem. Soc.*, 1974, **96**, 7807.
66. P. Brownbridge, T. Chan, M.A. Brook, and G.J. Kang, *Can. J. Chem.*, 1983, **61**, 688.

67. J. Bielawski, S. Brandänge, and B. Rodriguez, *Acta Chem. Scand. Ser. B*, 1987, **41**, 198.
68. K. Clauss and H. Bestian, *Justus Liebigs Ann. Chem.*, 1962, **654**, 8.
69. K. Nakamoto, *Infrared and Raman Spectra of Inorganic and Coordination Compounds*, 4th edition. John Wiley & Sons, New York, 1986.
70. N.A. Petasis and E.I. Bzowej, *J. Am. Chem. Soc.*, 1990, **112**, 6392.
71. K.A. Tehrani and N. De Kimpe, *Tetrahedron Lett.*, 2000, **41**, 1975.
72. D. Brillon, *Synth. Commun.*, 1990, **20**, 3085.
73. E.B. Knott, *J. Chem. Soc.*, 1955, 916.
74. M. Roth, P. Dubs, E. Götschi, and A. Eschenmoser, *Helv. Chim. Acta*, 1971, **54**, 710.
75. K. Shiosaki, *Comprehensive Organic Chemistry* (B.M. Trost, ed.), Vol 2, Pergamon Press, Oxford, 1991, pp. 865–892.
76. L.F. Tietze, H. Schirok, M. Wöhrmann, and K. Schrader, *Eur. J. Org. Chem.*, 2000, 2433.
77. D.G. Hey, G.D. Meakins, and M.W. Pemberton, *J. Chem. Soc. (C)*, 1966, 1331.
78. D.S. Middleton, N.S. Simpkins, and N.K. Terrett, *Tetrahedron Lett.*, 1989, **30**, 3865.
79. H. Günther, *NMR Spectroscopy*, John Wiley and Sons, Chichester, 1987.
80. D. Neuhaus and M.P. Williamson, *The Nuclear Overhauser Effect in Structural and Conformational Analysis*, 2nd ed, Wiley-VCH, New York, 2000.
81. H. Schneider and W. Freitag, *J. Am. Chem. Soc.*, 1976, **98**, 478.
82. R.J. Abraham and D.S. Ribeiro, *J. Chem. Soc., Perkin Trans. 2*, 2001, 302.
83. A.P. Timosheva, I.A. Kushnikovskii, S.G. Vul'fson, and A.N. Vereshchagin, *Bull. Acad. Sci. USSR, Div. Chem. Sci.*, 1991, **40**, 2405.
84. L. Xie, Y. Takeuchi, L.M. Cosentino, A.T. McPhail, and K. Lee, *J. Med. Chem.*, 2001, **44**, 664.
85. F. Jensen, *Introduction to Computational Chemistry*, John Wiley and Sons, Chichester, 1999.
86. S.J. Weiner, P.A. Kollman, D.A. Case, U.C. Singh, C. Ghio, G. Alagona, S. Profeta, Jr., and P. Weiner, *J. Am. Chem. Soc.*, 1984, **106**, 765.
87. S.J. Weiner, P.A. Kollman, D.T. Nguyen, and D.A. Case, *J. Comp. Chem.*, 1986, **7**, 230.
88. W.L. Jorgensen and J. Tirado-Rives, *J. Am. Chem. Soc.*, 1988, **110**, 1657.
89. J. Pranata, S.G. Wierschke, and W.L. Jorgensen, *J. Am. Chem. Soc.*, 1991, **113**, 2810.
90. J.C. Smith and M. Karplus, *J. Am. Chem. Soc.*, 1992, **114**, 801.

91. B.R. Brooks, R.E. Bruccoleri, B.D. Olafson, D.J. States, S. Swaminathan, and M. Karplus, *J. Comp. Chem.*, 1983, **4**, 187.
92. *Hyperchem[®] Computational Chemistry*, Hypercube, Inc., Canada, 1996.
93. N.L. Allinger, *J. Am. Chem. Soc.*, 1977, **99**, 8127.
94. J. Lii, S. Gallion, C. Bender, H. Wikström, N.L. Allinger, K.M. Flurchick, and M.M. Teeter, *J. Comp. Chem.*, 1989, **10**, 503.
95. N.L. Allinger, X. Zhou, and J. Bergsma, *J. Mol. Struct.*, 1994, **312**, 69.
96. R.K. Harris, *Nuclear Magnetic Resonance Spectroscopy*, Longman Scientific and Technical, Avon, 1986.
97. R. Hoffmann, *J. Chem. Phys.*, 1963, **39**, 1397.
98. D.D. Perrin, W.L.F. Armarego, and D.R. Perrin, *Purification of Laboratory Chemicals, 2nd edition*, Pergamon Press, Oxford, 1980.
99. P. McArdle, *Oscail Version 8*, Crystallography Center, Chemistry Department, NUI Galway, Ireland. (a) P. McArdle, *J. Appl. Cryst.*, 1995, **28**, 65–65.
100. N.P. Walker and D. Stuart, *Acta Crystallogr., Sect. A*, 1983, **A39**, 158–166.
101. G.M. Sheldrick, *SHELXL-97 and SHELXS-97*, University of Gottingen. (a) G. M. Sheldrick, *Acta Crystallogr., Sect. A*, 1990, **A46**, 467–473. (b) G. M. Sheldrick, *Acta Crystallogr., Sect. D*, 1993, **D49**, 18–23. (c) G. M. Sheldrick and T. R. Schneider, *Methods in Enzymology*, 1997, **277**, 319–343.
102. L.J. Farrugia, *ORTEP3 for Windows V1.01 beta*, Department of Chemistry, University of Glasgow, Glasgow, Scotland, 1998. (a) L.J. Farrugia, *J. Appl. Crystallogr.*, 1997, **30**, 565. (b) M.N. Burnett and C.K. Johnson, *ORTEP III, Oak Ridge National Laboratory report ORNL-6896*, 1996.

APPENDICES

Appendix A

Table A1. Crystal data and structure refinement for spirocycle (**130**).

Empirical formula	C ₁₈ H ₂₂ N ₂ O
Formula weight	282.38 g/mol
Temperature	293(2) K
Wavelength	0.70930 Å
Crystal system	Triclinic
Space group	P $\bar{1}$
Unit cell dimensions	a = 10.543(3) Å b = 10.614(4) Å c = 14.570(3) Å α = 90.04(3)° β = 93.68(2)° γ = 90.11(3)°
Volume	1627.2(8) Å ³
Z	4
Density (calculated)	1.153 Mg/ m ³
Absorption coefficient	0.072 mm ⁻¹
F(000)	608
Crystal size	0.8 x 0.6 x 0.5 mm
Theta range for data collection	2.31 to 24.92°
Index ranges	-3 ≤ h ≤ 12 -12 ≤ k ≤ 12 -17 ≤ l ≤ 17
Reflections collected	6866
Independent reflections	5716 ($R_{\text{int}} = 0.0180$)
Completeness to theta = 24.92°	99.7 %
Absorption correction	None
Refinement method	Full-matrix least-squares on F^2
Data / restraints / parameters	5716 / 0 / 399
Goodness-of-fit (based on F^2)	1.107
Final R indices [$I > 2\sigma(I)$]	$R_1 = 0.0719$, $wR_2 = 0.2259$
R indices (all data)	$R_1 = 0.0835$, $wR_2 = 0.2384$
Largest diff. peak and hole	0.568 and -0.305 e.Å ⁻³

Table A2. Atomic coordinates ($\times 10^4$) and equivalent isotropic displacement parameters ($\text{\AA}^2 \times 10^3$) for spirocycle (**130**).^a

Atom	x	y	z	$U(\text{eq})$
C(1A)	2166(2)	7829(2)	3844(1)	50(1)
C(2A)	2703(2)	8376(2)	2968(2)	61(1)
C(3A)	1981(3)	7730(3)	2175(2)	83(1)
C(4A)	766(3)	7334(3)	2544(2)	87(1)
C(5A)	1819(2)	8896(2)	4523(2)	57(1)
C(6A)	3106(2)	9339(3)	4958(2)	68(1)
C(7A)	3883(3)	8150(3)	4979(2)	72(1)
C(8A)	3165(3)	7121(2)	4468(2)	67(1)
C(9A)	1045(3)	9897(2)	4103(2)	72(1)
C(10A)	3062(4)	9982(4)	5887(2)	101(1)
C(11A)	3974(4)	6141(4)	4004(3)	115(1)
C(13A)	-727(3)	5675(2)	3743(2)	68(1)
C(14A)	-2074(3)	5801(3)	3621(2)	85(1)
C(15A)	-2815(3)	4795(3)	3330(2)	84(1)
C(16A)	-2249(3)	3697(3)	3137(2)	84(1)
C(17A)	-987(4)	3545(3)	3230(2)	88(1)
C(18A)	-262(3)	4523(3)	3531(2)	77(1)
N(1A)	1118(2)	7024(2)	3495(1)	53(1)
N(2A)	436(3)	10685(3)	3773(3)	107(1)
O(1A)	4945(2)	8060(3)	5344(2)	107(1)
C(12A)	49(3)	6799(3)	4062(2)	66(1)
C(19A)	956(15)	5988(13)	4089(10)	74(5)
C(1B)	2837(2)	2829(2)	1156(1)	50(1)
C(2B)	2295(2)	3379(2)	2035(2)	61(1)
C(3B)	3016(3)	2731(3)	2825(2)	84(1)
C(4B)	4231(3)	2333(3)	2458(2)	88(1)
C(5B)	3179(2)	3893(2)	479(2)	56(1)
C(6B)	1894(2)	4340(3)	42(2)	68(1)
C(7B)	1118(3)	3152(3)	22(2)	72(1)
C(8B)	1833(3)	2121(2)	532(2)	67(1)
C(9B)	3958(3)	4899(2)	900(2)	71(1)
C(10B)	1936(4)	4978(4)	-882(2)	100(1)
C(11B)	1022(4)	1148(4)	996(3)	116(1)
C(13B)	5727(3)	673(2)	1256(2)	68(1)
C(14B)	5259(3)	-475(3)	1469(2)	77(1)
C(15B)	5985(4)	-1454(3)	1767(2)	90(1)
C(16B)	7246(3)	-1299(3)	1862(2)	84(1)
C(17B)	7811(3)	-208(3)	1668(2)	84(1)
C(18B)	7074(3)	804(3)	1376(2)	85(1)
N(1B)	3881(2)	2025(2)	1504(1)	53(1)
N(2B)	4560(3)	5686(3)	1229(3)	108(1)

Table A2. Continued

O(1B)	57(2)	3062(3)	-344(2)	107(1)
C(12B)	4949(3)	1801(3)	939(2)	63(1)
C(19B)	4036(14)	973(13)	917(10)	86(5)

^a $U(\text{eq})$ is defined as one third of the trace of the orthogonalized U_{ij} tensor. The esd's of the least significant digits are given in parentheses.

Table A3. Bond lengths for spirocycle (130).^a

Bond	Length (Å)	Bond	Length (Å)
C(1A)–N(1A)	1.460(3)	C(1B)–N(1B)	1.459(3)
C(1A)–C(2A)	1.542(3)	C(1B)–C(8B)	1.545(3)
C(1A)–C(8A)	1.544(3)	C(1B)–C(2B)	1.550(3)
C(1A)–C(5A)	1.563(3)	C(1B)–C(5B)	1.557(3)
C(2A)–C(3A)	1.506(4)	C(2B)–C(3B)	1.506(4)
C(3A)–C(4A)	1.481(4)	C(3B)–C(4B)	1.481(4)
C(4A)–N(1A)	1.450(3)	C(4B)–N(1B)	1.452(3)
C(5A)–C(9A)	1.452(4)	C(5B)–C(9B)	1.456(4)
C(5A)–C(6A)	1.533(4)	C(5B)–C(6B)	1.536(4)
C(6A)–C(7A)	1.505(4)	C(6B)–C(7B)	1.502(4)
C(6A)–C(10A)	1.519(4)	C(6B)–C(10B)	1.511(4)
C(7A)–O(1A)	1.212(3)	C(7B)–O(1B)	1.212(3)
C(7A)–C(8A)	1.498(4)	C(7B)–C(8B)	1.499(4)
C(8A)–C(11A)	1.531(4)	C(8B)–C(11B)	1.526(4)
C(9A)–N(2A)	1.142(4)	C(9B)–N(2B)	1.135(4)
C(13A)–C(18A)	1.362(4)	C(13B)–C(14B)	1.357(4)
C(13A)–C(14A)	1.426(4)	C(13B)–C(18B)	1.426(4)
C(13A)–C(12A)	1.502(4)	C(13B)–C(12B)	1.509(4)
C(13A)–C(19A)	1.843(15)	C(13B)–C(19B)	1.848(14)
C(14A)–C(15A)	1.373(4)	C(14B)–C(15B)	1.347(5)
C(15A)–C(16A)	1.348(4)	C(15B)–C(16B)	1.338(5)
C(16A)–C(17A)	1.338(5)	C(16B)–C(17B)	1.340(4)
C(17A)–C(18A)	1.345(5)	C(17B)–C(18B)	1.378(4)
N(1A)–C(19A)	1.416(13)	N(1B)–C(19B)	1.422(12)
N(1A)–C(12A)	1.459(3)	N(1B)–C(12B)	1.457(3)

^a The esd's of the least significant digits are given in parentheses.

Table A4. Bond Angles for spirocycle (130).^a

Angle	Degree	Angle	Degree
N(1A)–C(1A)–C(2A)	104.01(17)	N(1B)–C(1B)–C(8B)	113.19(18)
N(1A)–C(1A)–C(8A)	113.09(18)	N(1B)–C(1B)–C(2B)	104.07(17)
C(2A)–C(1A)–C(8A)	113.52(19)	C(8B)–C(1B)–C(2B)	113.20(19)
N(1A)–C(1A)–C(5A)	116.14(17)	N(1B)–C(1B)–C(5B)	116.44(17)
C(2A)–C(1A)–C(5A)	111.34(18)	C(8B)–C(1B)–C(5B)	99.04(18)
C(8A)–C(1A)–C(5A)	99.15(18)	C(2B)–C(1B)–C(5B)	111.28(18)
C(3A)–C(2A)–C(1A)	105.7(2)	C(3B)–C(2B)–C(1B)	105.4(2)
C(4A)–C(3A)–C(2A)	104.8(2)	C(4B)–C(3B)–C(2B)	105.1(2)
N(1A)–C(4A)–C(3A)	103.7(2)	N(1B)–C(4B)–C(3B)	103.7(2)
C(9A)–C(5A)–C(6A)	114.2(2)	C(9B)–C(5B)–C(6B)	114.0(2)
C(9A)–C(5A)–C(1A)	114.4(2)	C(9B)–C(5B)–C(1B)	114.3(2)
C(6A)–C(5A)–C(1A)	104.25(18)	C(6B)–C(5B)–C(1B)	104.70(18)
C(7A)–C(6A)–C(10A)	114.0(3)	C(7B)–C(6B)–C(10B)	114.0(3)
C(7A)–C(6A)–C(5A)	102.6(2)	C(7B)–C(6B)–C(5B)	102.3(2)
C(10A)–C(6A)–C(5A)	115.4(2)	C(10B)–C(6B)–C(5B)	115.7(2)
O(1A)–C(7A)–C(8A)	125.6(3)	O(1B)–C(7B)–C(8B)	125.7(3)
O(1A)–C(7A)–C(6A)	124.3(3)	O(1B)–C(7B)–C(6B)	124.0(3)
C(8A)–C(7A)–C(6A)	110.1(2)	C(8B)–C(7B)–C(6B)	110.4(2)
C(7A)–C(8A)–C(11A)	115.9(3)	C(7B)–C(8B)–C(11B)	115.8(3)
C(7A)–C(8A)–C(1A)	104.0(2)	C(7B)–C(8B)–C(1B)	103.9(2)
C(11A)–C(8A)–C(1A)	116.7(2)	C(11B)–C(8B)–C(1B)	116.7(2)
N(2A)–C(9A)–C(5A)	180.0(4)	N(2B)–C(9B)–C(5B)	179.6(3)
C(18A)–C(13A)–C(14A)	115.4(3)	C(14B)–C(13B)–C(18B)	115.6(3)
C(18A)–C(13A)–C(12A)	125.8(3)	C(14B)–C(13B)–C(12B)	125.8(3)
C(14A)–C(13A)–C(12A)	118.8(3)	C(18B)–C(13B)–C(12B)	118.6(3)
C(18A)–C(13A)–C(19A)	82.4(5)	C(14B)–C(13B)–C(19B)	81.9(5)
C(14A)–C(13A)–C(19A)	161.9(6)	C(18B)–C(13B)–C(19B)	162.2(6)
C(12A)–C(13A)–C(19A)	43.8(5)	C(12B)–C(13B)–C(19B)	44.2(5)
C(15A)–C(14A)–C(13A)	120.4(3)	C(15B)–C(14B)–C(13B)	124.0(3)
C(16A)–C(15A)–C(14A)	119.0(3)	C(16B)–C(15B)–C(14B)	118.7(3)
C(17A)–C(16A)–C(15A)	122.4(3)	C(15B)–C(16B)–C(17B)	122.3(3)
C(16A)–C(17A)–C(18A)	118.6(3)	C(16B)–C(17B)–C(18B)	119.3(3)
C(17A)–C(18A)–C(13A)	124.1(3)	C(17B)–C(18B)–C(13B)	120.1(3)
C(19A)–N(1A)–C(4A)	136.7(6)	C(19B)–N(1B)–C(4B)	136.0(6)
C(19A)–N(1A)–C(12A)	53.1(7)	C(19B)–N(1B)–C(12B)	53.7(7)
C(4A)–N(1A)–C(12A)	114.8(2)	C(4B)–N(1B)–C(12B)	114.8(2)
C(19A)–N(1A)–C(1A)	111.0(6)	C(19B)–N(1B)–C(1B)	111.4(6)
C(4A)–N(1A)–C(1A)	109.91(19)	C(4B)–N(1B)–C(1B)	109.96(18)
C(12A)–N(1A)–C(1A)	119.54(19)	C(12B)–N(1B)–C(1B)	119.56(19)
N(1A)–C(12A)–C(13A)	112.3(2)	N(1B)–C(12B)–C(13B)	112.5(2)
N(1A)–C(19A)–C(13A)	97.1(8)	N(1B)–C(19B)–C(13B)	97.0(8)

^a The esd's of the least significant digits are given in parentheses.

Table A5. Anisotropic displacement parameters ($\text{\AA}^2 \times 10^3$) for spirocycle (130).^a

Atom	U_{11}	U_{22}	U_{33}	U_{23}	U_{13}	U_{12}
C(1A)	51(1)	51(1)	48(1)	-2(1)	6(1)	8(1)
C(2A)	55(1)	72(1)	56(1)	2(1)	14(1)	5(1)
C(3A)	103(2)	98(2)	50(1)	6(1)	11(1)	-22(2)
C(4A)	96(2)	104(2)	60(2)	6(2)	-9(2)	-20(2)
C(5A)	55(1)	56(1)	60(1)	-7(1)	12(1)	5(1)
C(6A)	67(2)	73(2)	63(1)	-13(1)	6(1)	-7(1)
C(7A)	63(2)	97(2)	55(1)	0(1)	-2(1)	10(1)
C(8A)	72(2)	68(1)	60(1)	-1(1)	-4(1)	21(1)
C(9A)	67(2)	62(1)	89(2)	-9(1)	17(1)	10(1)
C(10A)	113(3)	108(2)	82(2)	-42(2)	5(2)	-11(2)
C(11A)	123(3)	111(3)	109(3)	-22(2)	-19(2)	74(2)
C(13A)	78(2)	67(1)	62(1)	-5(1)	23(1)	-14(1)
C(14A)	89(2)	69(2)	97(2)	-3(2)	16(2)	12(2)
C(15A)	60(2)	87(2)	106(2)	-5(2)	8(2)	-7(1)
C(16A)	91(2)	82(2)	82(2)	3(2)	23(2)	-10(2)
C(17A)	115(3)	68(2)	83(2)	3(1)	27(2)	12(2)
C(18A)	78(2)	84(2)	72(2)	2(1)	16(1)	14(1)
N(1A)	55(1)	58(1)	45(1)	1(1)	8(1)	1(1)
N(2A)	97(2)	81(2)	145(3)	12(2)	20(2)	37(2)
O(1A)	76(1)	144(2)	97(2)	-8(1)	-27(1)	12(1)
C(12A)	61(2)	72(2)	67(2)	-16(2)	20(1)	-7(2)
C(19A)	81(10)	69(8)	71(8)	14(6)	-6(7)	-19(7)
C(1B)	50(1)	53(1)	47(1)	-7(1)	7(1)	-5(1)
C(2B)	56(1)	73(1)	55(1)	-10(1)	14(1)	-2(1)
C(3B)	106(2)	97(2)	49(1)	-14(1)	10(1)	23(2)
C(4B)	95(2)	106(2)	61(2)	-14(2)	-9(2)	25(2)
C(5B)	54(1)	57(1)	59(1)	-2(1)	13(1)	-1(1)
C(6B)	68(2)	74(2)	63(1)	6(1)	6(1)	10(1)
C(7B)	63(2)	97(2)	55(1)	-8(1)	-1(1)	-7(1)
C(8B)	72(2)	69(1)	58(1)	-8(1)	-4(1)	-17(1)
C(9B)	64(2)	62(1)	89(2)	2(1)	18(1)	-7(1)
C(10B)	110(3)	107(2)	84(2)	34(2)	5(2)	16(2)
C(11B)	126(3)	112(3)	107(3)	13(2)	-22(2)	-72(2)
C(13B)	78(2)	68(2)	61(1)	-2(1)	21(1)	18(1)
C(14B)	79(2)	85(2)	70(2)	-9(1)	17(1)	-11(2)
C(15B)	120(3)	69(2)	82(2)	-12(1)	29(2)	-11(2)
C(16B)	89(2)	82(2)	83(2)	-10(2)	24(2)	13(2)
C(17B)	60(2)	87(2)	107(2)	-2(2)	7(2)	11(1)
C(18B)	90(2)	69(2)	98(2)	-6(2)	19(2)	-8(2)
N(1B)	55(1)	59(1)	45(1)	-8(1)	8(1)	2(1)
N(2B)	98(2)	81(2)	146(3)	-20(2)	20(2)	-34(2)

Table A5. Continued

O(1B)	77(1)	144(2)	98(2)	-2(1)	-27(1)	-8(1)
C(12B)	57(2)	70(2)	65(2)	10(1)	21(1)	10(2)
C(19B)	88(10)	79(9)	88(9)	-27(7)	-5(7)	29(7)

^a The esd's of the least significant digits are given in parentheses. The anisotropic displacement factor exponent takes the form: $-2 \pi [h^2 a^{*2} U_{11} + \dots + 2 h k a^* b^* U_{12}]$.

Table A6. Hydrogen atom coordinates ($\times 10^4$) and equivalent isotropic displacement parameters ($\text{\AA}^2 \times 10^3$) for spirocycle (130).^a

Atom	x	y	z	$U(\text{eq})$
H(2A1)	2574	9280	2938	73
H(2A2)	3605	8205	2960	73
H(3A1)	1831	8304	1662	100
H(3A2)	2447	7006	1970	100
H(4A1)	150	8013	2502	105
H(4A2)	412	6607	2214	105
H(5A)	1344	8514	5008	68
H(6A)	3477	9930	4533	81
H(8A)	2695	6665	4923	80
H(10A)	2550	10728	5823	151
H(10B)	3908	10208	6111	151
H(10C)	2700	9418	6314	151
H(11A)	3429	5520	3704	173
H(11B)	4535	5740	4459	173
H(11C)	4465	6549	3557	173
H(14A)	-2453	6570	3740	102
H(15A)	-3696	4869	3268	101
H(16A)	-2753	3021	2932	101
H(17A)	-620	2779	3088	106
H(18A)	613	4404	3600	93
H(12A)	-491	7538	4047	79
H(12B)	368	6667	4694	79
H(19A)	1083	6220	4732	89
H(19B)	1501	5285	3956	89
H(2B1)	2427	4283	2067	73
H(2B2)	1392	3206	2043	73
H(3B1)	3169	3304	3339	101
H(3B2)	2547	2007	3029	101
H(4B1)	4851	3010	2503	106
H(4B2)	4579	1604	2787	106
H(5B)	3654	3512	-7	68
H(6B)	1525	4932	467	81
H(8B)	2298	1664	76	80
H(10D)	2438	5732	-818	150
H(10E)	1088	5189	-1110	150
H(10F)	2309	4418	-1307	150
H(11D)	1564	529	1299	174
H(11E)	461	743	542	174
H(11F)	531	1559	1441	174
H(14B)	4384	-594	1404	93
H(15B)	5617	-2222	1905	107
H(16B)	7749	-1972	2071	101
H(17B)	8692	-134	1729	101

Table A6. Continued

H(18B)	7455	1573	1258	103
H(12C)	5491	2542	957	76
H(12D)	4631	1671	306	76
H(19C)	3901	1191	271	103
H(19D)	3493	271	1060	103

^a $U(\text{eq})$ is defined as one third of the trace of the orthogonalized \mathbf{U}_{ij} tensor.

Appendix B

Table B1. Crystal data and structure refinement for tosylate (**98**).

Empirical formula	C ₁₆ H ₁₅ IO ₅ S
Formula weight	446.24 g/mol
Temperature	293(2) K
Wavelength	0.71073 Å
Crystal system	Triclinic
Space group	P ₁
Unit cell dimensions	a = 7.816(2) Å b = 9.8178(18) Å c = 23.165(4) Å α = 82.667(14)° β = 85.473(19)° γ = 73.273(19)°
Volume	1686.7(6) Å ³
Z	4
Density (calculated)	1.757 Mg/m ³
Absorption coefficient	2.044 mm ⁻¹
F(000)	880
Crystal size	0.85 x 0.60 x 0.60 mm
Theta range for data collection	2.18 to 22.98°
Index ranges	-2 ≤ h ≤ 8 -10 ≤ k ≤ 10 -25 ≤ l ≤ 25
Reflections collected	6672
Independent reflections	6672 (R _{int} = 0.0000) ^a
Reflections observed (>2σ)	6204
Max. and min. transmission	0.3735 and 0.2755
Refinement method	Full-matrix least-squares on F ²
Data / restraints / parameters	6672 / 555 / 829
Goodness-of-fit (based on F ²)	1.183
Final R indices [I>2σ(I)]	R ₁ = 0.0394, wR ₂ = 0.1304
R indices (all data)	R ₁ = 0.0474, wR ₂ = 0.1673
Absolute structure parameter	0.26(4)
Largest diff. peak and hole	0.891 and -1.190 e.Å ⁻³

^a DIFABS absorption correction applied. R_{int} before correction = 0.0075.

Table B2. Atomic coordinates ($\times 10^4$) and equivalent isotropic displacement parameters ($\text{\AA}^2 \times 10^3$) for tosylate (**98**).^a

Atom	x	y	z	$U(\text{eq})$
I(1A)	1069(2)	2492(1)	8569(1)	74(1)
S(1A)	-5116(6)	5391(4)	9944(2)	50(1)
O(1A)	-200(20)	-2171(13)	9895(7)	72(4)
O(2A)	-600(20)	-1229(12)	10748(6)	64(4)
O(3A)	-3128(13)	4539(9)	10086(5)	38(2)
O(4A)	-5470(20)	5129(13)	9385(7)	68(4)
O(5A)	-6150(20)	5032(14)	10467(7)	78(4)
C(1A)	340(20)	1357(16)	9355(8)	46(4)
C(2A)	330(30)	-61(15)	9279(8)	60(5)
C(3A)	10(20)	-829(19)	9775(8)	55(5)
C(4A)	-390(20)	-225(18)	10314(7)	48(4)
C(5A)	-460(30)	1180(19)	10338(8)	60(5)
C(6A)	40(20)	1941(14)	9842(7)	40(3)
C(7A)	-410(20)	-2534(16)	10494(8)	54(4)
C(8A)	10(20)	3537(15)	9861(8)	50(4)
C(9A)	-1750(30)	4650(18)	9670(6)	53(5)
C(10A)	-5183(18)	7183(14)	9900(7)	39(4)
C(11A)	-4930(30)	7843(17)	9376(9)	69(6)
C(12A)	-4870(20)	9324(18)	9341(9)	59(5)
C(13A)	-5010(30)	9978(19)	9851(10)	55(5)
C(14A)	-5190(30)	9240(30)	10310(9)	72(6)
C(15A)	-5240(20)	7814(14)	10387(7)	44(4)
C(16A)	-4790(30)	11484(18)	9741(8)	69(5)
I(1B)	389(2)	8462(1)	3472(1)	73(1)
S(1B)	6602(7)	5604(4)	2088(2)	54(1)
O(1B)	1510(20)	13146(13)	2161(7)	71(4)
O(2B)	2240(20)	12092(16)	1273(6)	69(4)
O(3B)	4674(19)	6496(12)	1889(4)	56(3)
O(4B)	7668(19)	5920(14)	1629(7)	69(4)
O(5B)	6880(20)	5940(14)	2641(8)	71(4)
C(1B)	1160(20)	9520(19)	2735(8)	52(4)
C(2B)	1150(20)	10926(19)	2735(9)	60(5)
C(3B)	1540(20)	11686(14)	2217(8)	53(5)
C(4B)	1810(20)	11146(16)	1709(7)	53(5)
C(5B)	1787(16)	9795(14)	1663(6)	32(3)
C(6B)	1520(20)	8882(16)	2187(8)	44(4)
C(7B)	1800(30)	13370(20)	1545(10)	82(7)
C(8B)	1540(20)	7422(18)	2113(8)	52(4)
C(9B)	3160(20)	6355(13)	2347(7)	48(4)
C(10B)	6500(20)	3804(16)	2148(8)	53(4)
C(11B)	6600(30)	3160(20)	1630(9)	68(6)

Table B2. Continued

Atom	x	y	z	<i>U</i> (eq)
C(12B)	6550(20)	1761(16)	1658(9)	50(4)
C(13B)	6440(30)	987(18)	2242(9)	48(5)
C(14B)	6440(30)	1660(20)	2734(9)	72(6)
C(15B)	6460(20)	2989(16)	2669(7)	48(4)
C(16B)	6480(30)	-567(17)	2194(12)	95(8)
I(1C)	389(2)	3446(1)	6042(1)	63(1)
S(1C)	-2590(6)	505(4)	4786(2)	43(1)
O(1C)	-2830(20)	7106(16)	4239(7)	77(4)
O(2C)	-5543(19)	6633(17)	4346(8)	93(5)
O(3C)	-3648(16)	1404(13)	5302(6)	51(3)
O(4C)	-1589(16)	-856(11)	5040(5)	48(3)
O(5C)	-3901(19)	635(16)	4391(7)	67(4)
C(1C)	-1650(20)	4454(17)	5514(9)	57(5)
C(2C)	-1370(20)	5494(16)	5060(8)	52(5)
C(3C)	-2980(20)	6195(17)	4705(7)	43(4)
C(4C)	-4340(20)	5807(17)	4794(9)	46(4)
C(5C)	-4686(19)	4852(18)	5187(7)	44(4)
C(6C)	-3240(30)	4182(19)	5543(7)	50(4)
C(7C)	-4720(40)	7530(30)	4060(11)	84(7)
C(8C)	-3510(30)	2855(19)	6024(8)	62(5)
C(9C)	-2780(20)	1497(18)	5803(7)	49(4)
C(10C)	-1150(20)	1511(19)	4491(7)	49(4)
C(11C)	-1810(20)	2749(16)	4146(7)	41(3)
C(12C)	-580(30)	3520(15)	3917(8)	50(5)
C(13C)	1080(30)	3118(18)	4013(10)	72(6)
C(14C)	1770(30)	1780(20)	4423(10)	84(7)
C(15C)	660(20)	1081(19)	4629(9)	62(6)
C(16C)	2500(40)	3980(30)	3771(16)	128(12)
I(1D)	1057(2)	7502(1)	5997(1)	64(1)
S(1D)	4051(6)	10420(5)	7246(2)	50(1)
O(1D)	4240(30)	3703(16)	7812(7)	82(5)
O(2D)	6920(30)	4340(17)	7703(8)	116(7)
O(3D)	5182(16)	9530(13)	6770(5)	50(3)
O(4D)	3060(20)	11766(15)	6977(8)	80(5)
O(5D)	5331(17)	10361(15)	7670(7)	62(4)
C(1D)	3250(20)	6442(16)	6561(6)	42(4)
C(2D)	2960(30)	5355(18)	6956(8)	60(5)
C(3D)	4060(30)	4789(18)	7314(7)	51(4)
C(4D)	5930(40)	5030(30)	7314(10)	73(5)
C(5D)	6100(30)	6160(20)	6836(11)	80(7)
C(6D)	4840(20)	6868(15)	6457(7)	38(4)
C(7D)	5850(40)	3460(20)	8027(10)	85(7)
C(8D)	5120(30)	7959(18)	6060(8)	55(4)
C(9D)	4150(30)	9495(18)	6255(8)	52(4)
C(10D)	2600(20)	9451(14)	7529(7)	39(4)

Table B2. Continued

Atom	x	y	z	<i>U</i>(eq)
C(11D)	870(30)	9920(20)	7406(8)	54(4)
C(12D)	-260(20)	9020(20)	7652(9)	55(5)
C(13D)	300(20)	7850(20)	7991(8)	54(4)
C(14D)	2200(30)	7380(20)	8146(8)	65(5)
C(15D)	3230(30)	8190(20)	7921(7)	55(5)
C(16D)	-840(30)	7000(20)	8251(12)	85(7)

^a *U*(eq) is defined as one third of the trace of the orthogonalized U_{ij} tensor. The esd's of the least significant digits are given in parentheses.

Table B3. Bond lengths for tosylate (**98**).^a

Bond	Length (Å)	Bond	Length (Å)
I(1A)-C(1A)	2.136(17)	S(1A)-O(4A)	1.416(16)
S(1A)-O(5A)	1.467(14)	S(1A)-O(3A)	1.576(11)
S(1A)-C(10A)	1.734(14)	O(1A)-C(3A)	1.37(2)
O(1A)-C(7A)	1.40(2)	O(2A)-C(4A)	1.35(2)
O(2A)-C(7A)	1.443(18)	O(3A)-C(9A)	1.41(2)
C(1A)-C(6A)	1.31(2)	C(1A)-C(2A)	1.43(2)
C(2A)-C(3A)	1.34(3)	C(3A)-C(4A)	1.42(2)
C(4A)-C(5A)	1.37(2)	C(5A)-C(6A)	1.38(3)
C(6A)-C(8A)	1.57(2)	C(8A)-C(9A)	1.55(2)
C(10A)-C(11A)	1.33(2)	C(10A)-C(15A)	1.35(2)
C(11A)-C(12A)	1.46(2)	C(12A)-C(13A)	1.40(3)
C(13A)-C(14A)	1.23(3)	C(13A)-C(16A)	1.52(3)
C(14A)-C(15A)	1.40(3)	I(1B)-C(1B)	2.03(2)
S(1B)-O(4B)	1.358(15)	S(1B)-O(5B)	1.412(17)
S(1B)-O(3B)	1.580(14)	S(1B)-C(10B)	1.780(16)
O(1B)-C(7B)	1.43(3)	O(1B)-C(3B)	1.416(18)
O(2B)-C(4B)	1.37(2)	O(2B)-C(7B)	1.42(3)
O(3B)-C(9B)	1.55(2)	C(1B)-C(2B)	1.38(3)
C(1B)-C(6B)	1.46(2)	C(2B)-C(3B)	1.39(3)
C(3B)-C(4B)	1.33(2)	C(4B)-C(5B)	1.35(2)
C(5B)-C(6B)	1.45(2)	C(6B)-C(8B)	1.46(2)
C(8B)-C(9B)	1.48(2)	C(10B)-C(15B)	1.36(2)
C(10B)-C(11B)	1.41(3)	C(11B)-C(12B)	1.38(3)
C(12B)-C(13B)	1.47(3)	C(13B)-C(14B)	1.39(3)
C(13B)-C(16B)	1.54(2)	C(14B)-C(15B)	1.30(3)
I(1C)-C(1C)	2.025(19)	S(1C)-O(5C)	1.395(15)
S(1C)-O(4C)	1.419(12)	S(1C)-O(3C)	1.606(13)
S(1C)-C(10C)	1.747(18)	O(1C)-C(3C)	1.33(2)
O(1C)-C(7C)	1.49(3)	O(2C)-C(7C)	1.32(3)
O(2C)-C(4C)	1.46(2)	O(3C)-C(9C)	1.42(2)
C(1C)-C(6C)	1.34(3)	C(1C)-C(2C)	1.42(3)
C(2C)-C(3C)	1.50(3)	C(3C)-C(4C)	1.22(3)
C(4C)-C(5C)	1.29(3)	C(5C)-C(6C)	1.40(2)
C(6C)-C(8C)	1.65(2)	C(8C)-C(9C)	1.43(3)
C(10C)-C(11C)	1.36(2)	C(10C)-C(15C)	1.41(2)
C(11C)-C(12C)	1.42(2)	C(12C)-C(13C)	1.27(3)
C(13C)-C(14C)	1.51(3)	C(13C)-C(16C)	1.61(3)
C(14C)-C(15C)	1.28(3)	I(1D)-C(1D)	2.173(15)
S(1D)-O(4D)	1.418(15)	S(1D)-O(5D)	1.441(15)
S(1D)-O(3D)	1.552(12)	S(1D)-C(10D)	1.722(16)
O(1D)-C(7D)	1.33(3)	O(1D)-C(3D)	1.45(2)
O(2D)-C(4D)	1.23(3)	O(2D)-C(7D)	1.47(3)
O(3D)-C(9D)	1.50(2)	C(1D)-C(6D)	1.41(2)
C(1D)-C(2D)	1.37(3)	C(2D)-C(3D)	1.21(3)
C(3D)-C(4D)	1.55(3)	C(4D)-C(5D)	1.49(3)

Table B3. Continued

Bond	Length (Å)	Bond	Length (Å)
C(5D)-C(6D)	1.35(3)	C(6D)-C(8D)	1.38(2)
C(8D)-C(9D)	1.59(2)	C(10D)-C(11D)	1.34(2)
C(10D)-C(15D)	1.42(2)	C(11D)-C(12D)	1.46(2)
C(12D)-C(13D)	1.29(3)	C(13D)-C(16D)	1.44(3)
C(13D)-C(14D)	1.48(3)	C(14D)-C(15D)	1.32(3)

^a The esd's of the least significant digits are given in parentheses.

Table B4. Bond Angles for tosylate (**98**).^a

Angle	Degree	Angle	Degree
O(4A)-S(1A)-O(5A)	121.6(11)	O(4A)-S(1A)-O(3A)	109.1(8)
O(5A)-S(1A)-O(3A)	103.7(8)	O(4A)-S(1A)-C(10A)	107.1(8)
O(5A)-S(1A)-C(10A)	109.0(7)	O(3A)-S(1A)-C(10A)	105.2(7)
C(3A)-O(1A)-C(7A)	111.3(13)	C(4A)-O(2A)-C(7A)	107.7(14)
C(9A)-O(3A)-S(1A)	119.0(10)	C(6A)-C(1A)-C(2A)	126.6(16)
C(6A)-C(1A)-I(1A)	120.6(12)	C(2A)-C(1A)-I(1A)	112.7(13)
C(3A)-C(2A)-C(1A)	113.7(16)	C(2A)-C(3A)-O(1A)	132.8(15)
C(2A)-C(3A)-C(4A)	121.9(15)	O(1A)-C(3A)-C(4A)	105.0(17)
O(2A)-C(4A)-C(5A)	129.5(16)	O(2A)-C(4A)-C(3A)	110.2(15)
C(5A)-C(4A)-C(3A)	120.3(16)	C(4A)-C(5A)-C(6A)	118.3(15)
C(1A)-C(6A)-C(5A)	118.7(14)	C(1A)-C(6A)-C(8A)	121.5(13)
C(5A)-C(6A)-C(8A)	119.4(14)	O(1A)-C(7A)-O(2A)	104.9(13)
C(6A)-C(8A)-C(9A)	114.6(15)	O(3A)-C(9A)-C(8A)	109.3(13)
C(11A)-C(10A)-C(15A)	121.3(14)	C(11A)-C(10A)-S(1A)	117.6(12)
C(15A)-C(10A)-S(1A)	120.5(12)	C(10A)-C(11A)-C(12A)	117.8(16)
C(13A)-C(12A)-C(11A)	119.8(18)	C(14A)-C(13A)-C(12A)	116.1(18)
C(14A)-C(13A)-C(16A)	131(2)	C(12A)-C(13A)-C(16A)	113.1(18)
C(13A)-C(14A)-C(15A)	128.2(18)	C(10A)-C(15A)-C(14A)	116.6(15)
O(4B)-S(1B)-O(5B)	118.3(11)	O(4B)-S(1B)-O(3B)	102.4(8)
O(5B)-S(1B)-O(3B)	109.8(8)	O(4B)-S(1B)-C(10B)	112.7(9)
O(5B)-S(1B)-C(10B)	109.2(9)	O(3B)-S(1B)-C(10B)	103.1(7)
C(7B)-O(1B)-C(3B)	99.3(15)	C(4B)-O(2B)-C(7B)	102.0(14)
C(9B)-O(3B)-S(1B)	113.5(9)	C(2B)-C(1B)-C(6B)	119.0(18)
C(2B)-C(1B)-I(1B)	119.4(13)	C(6B)-C(1B)-I(1B)	121.2(14)
C(1B)-C(2B)-C(3B)	119.3(17)	C(4B)-C(3B)-C(2B)	122.7(15)
C(4B)-C(3B)-O(1B)	112.9(16)	C(2B)-C(3B)-O(1B)	124.1(17)
C(3B)-C(4B)-C(5B)	122.2(16)	C(3B)-C(4B)-O(2B)	110.9(15)
C(5B)-C(4B)-O(2B)	126.7(16)	C(4B)-C(5B)-C(6B)	119.2(14)
C(5B)-C(6B)-C(8B)	116.8(14)	C(5B)-C(6B)-C(1B)	117.5(14)
C(8B)-C(6B)-C(1B)	125.6(18)	O(1B)-C(7B)-O(2B)	113.1(15)
C(6B)-C(8B)-C(9B)	111.9(14)	C(8B)-C(9B)-O(3B)	104.3(12)
C(15B)-C(10B)-C(11B)	118.6(15)	C(15B)-C(10B)-S(1B)	123.0(13)
C(11B)-C(10B)-S(1B)	118.2(14)	C(12B)-C(11B)-C(10B)	120.0(18)
C(11B)-C(12B)-C(13B)	117.2(17)	C(14B)-C(13B)-C(12B)	120.1(16)
C(14B)-C(13B)-C(16B)	129(2)	C(12B)-C(13B)-C(16B)	110.4(17)
C(15B)-C(14B)-C(13B)	118.7(19)	C(14B)-C(15B)-C(10B)	125.2(18)
O(5C)-S(1C)-O(4C)	121.2(8)	O(5C)-S(1C)-O(3C)	104.1(8)
O(4C)-S(1C)-O(3C)	108.1(7)	O(5C)-S(1C)-C(10C)	109.3(10)
O(4C)-S(1C)-C(10C)	110.1(8)	O(3C)-S(1C)-C(10C)	102.3(7)
C(3C)-O(1C)-C(7C)	99.0(17)	C(7C)-O(2C)-C(4C)	105.5(16)
C(9C)-O(3C)-S(1C)	121.5(11)	C(6C)-C(1C)-C(2C)	116.3(17)
C(6C)-C(1C)-I(1C)	125.2(15)	C(2C)-C(1C)-I(1C)	118.5(12)
C(1C)-C(2C)-C(3C)	114.1(15)	C(4C)-C(3C)-O(1C)	119.4(18)
C(4C)-C(3C)-C(2C)	120.6(16)	O(1C)-C(3C)-C(2C)	119.3(17)

Table B4. Continued

Angle	Degree	Angle	Degree
C(3C)-C(4C)-C(5C)	129.3(17)	C(3C)-C(4C)-O(2C)	105.6(17)
C(5C)-C(4C)-O(2C)	125.1(16)	C(4C)-C(5C)-C(6C)	112.5(16)
C(1C)-C(6C)-C(5C)	127.1(18)	C(1C)-C(6C)-C(8C)	117.1(17)
C(5C)-C(6C)-C(8C)	115.7(16)	O(2C)-C(7C)-O(1C)	108.8(17)
C(9C)-C(8C)-C(6C)	111.4(14)	O(3C)-C(9C)-C(8C)	111.7(16)
C(11C)-C(10C)-C(15C)	120.0(16)	C(11C)-C(10C)-S(1C)	119.3(13)
C(15C)-C(10C)-S(1C)	120.7(14)	C(10C)-C(11C)-C(12C)	116.8(16)
C(13C)-C(12C)-C(11C)	124.2(17)	C(12C)-C(13C)-C(14C)	118(2)
C(12C)-C(13C)-C(16C)	125(2)	C(14C)-C(13C)-C(16C)	116(2)
C(15C)-C(14C)-C(13C)	118(2)	C(14C)-C(15C)-C(10C)	122.9(18)
O(4D)-S(1D)-O(5D)	119.7(9)	O(4D)-S(1D)-O(3D)	109.0(9)
O(5D)-S(1D)-O(3D)	103.8(7)	O(4D)-S(1D)-C(10D)	109.1(9)
O(5D)-S(1D)-C(10D)	110.0(9)	O(3D)-S(1D)-C(10D)	104.0(7)
C(7D)-O(1D)-C(3D)	109.1(17)	C(4D)-O(2D)-C(7D)	103(2)
C(9D)-O(3D)-S(1D)	114.2(11)	C(6D)-C(1D)-C(2D)	127.8(15)
C(6D)-C(1D)-I(1D)	117.3(11)	C(2D)-C(1D)-I(1D)	114.7(13)
C(3D)-C(2D)-C(1D)	118.6(18)	C(2D)-C(3D)-O(1D)	136.8(19)
C(2D)-C(3D)-C(4D)	125.1(19)	O(1D)-C(3D)-C(4D)	97.9(17)
O(2D)-C(4D)-C(5D)	133(3)	O(2D)-C(4D)-C(3D)	117(2)
C(5D)-C(4D)-C(3D)	110(2)	C(6D)-C(5D)-C(4D)	126(2)
C(5D)-C(6D)-C(1D)	112.4(16)	C(5D)-C(6D)-C(8D)	120.1(18)
C(1D)-C(6D)-C(8D)	127.3(16)	O(1D)-C(7D)-O(2D)	112.8(16)
C(6D)-C(8D)-C(9D)	112.7(15)	O(3D)-C(9D)-C(8D)	102.5(15)
C(11D)-C(10D)-C(15D)	119.9(17)	C(11D)-C(10D)-S(1D)	120.2(13)
C(15D)-C(10D)-S(1D)	119.7(14)	C(10D)-C(11D)-C(12D)	117.0(17)
C(13D)-C(12D)-C(11D)	123.5(16)	C(12D)-C(13D)-C(16D)	123.2(17)
C(12D)-C(13D)-C(14D)	118.9(15)	C(16D)-C(13D)-C(14D)	117.8(19)
C(15D)-C(14D)-C(13D)	117.5(18)	C(14D)-C(15D)-C(10D)	123(2)

^a The esd's of the least significant digits are given in parentheses.

Table B5. Anisotropic displacement parameters ($\text{\AA}^2 \times 10^3$) for tosylate (**98**).^a

Atom	U_{11}	U_{22}	U_{33}	U_{23}	U_{13}	U_{12}
I(1A)	93(1)	51(1)	65(1)	-3(1)	17(1)	-6(1)
S(1A)	37(2)	30(2)	80(3)	-7(2)	-8(2)	-5(2)
O(1A)	92(11)	36(6)	91(10)	-19(6)	11(8)	-19(6)
O(2A)	100(10)	24(5)	76(8)	-2(5)	-9(7)	-29(6)
O(3A)	30(5)	16(4)	55(6)	9(4)	11(4)	4(4)
O(4A)	77(10)	35(6)	90(9)	-10(6)	-26(8)	-5(6)
O(5A)	77(9)	49(6)	92(9)	19(6)	32(8)	-14(6)
C(1A)	46(9)	22(7)	67(10)	4(7)	-14(8)	-3(7)
C(2A)	74(12)	22(7)	72(10)	-7(6)	-31(8)	13(7)
C(3A)	47(10)	46(9)	76(12)	-41(8)	-10(8)	-4(8)
C(4A)	30(8)	60(10)	58(10)	-11(8)	10(7)	-24(7)
C(5A)	72(12)	55(10)	47(9)	-22(7)	-31(8)	8(8)
C(6A)	31(7)	22(6)	68(9)	3(6)	-3(6)	-11(6)
C(7A)	51(9)	27(7)	87(12)	-19(7)	16(8)	-14(6)
C(8A)	46(9)	22(6)	72(8)	-18(6)	22(7)	7(6)
C(9A)	76(12)	61(9)	21(7)	-16(6)	-3(7)	-11(9)
C(10A)	24(7)	21(6)	61(9)	0(6)	24(6)	1(5)
C(11A)	88(13)	27(7)	81(12)	-20(8)	-50(10)	18(8)
C(12A)	51(10)	37(8)	93(12)	16(8)	-41(9)	-17(7)
C(13A)	38(9)	37(8)	94(14)	-19(8)	16(9)	-13(7)
C(14A)	62(13)	89(15)	62(10)	-35(10)	-1(9)	-7(11)
C(15A)	55(9)	26(7)	52(8)	-25(6)	23(7)	-9(7)
C(16A)	79(13)	38(8)	81(9)	-4(6)	-31(9)	3(8)
I(1B)	92(1)	51(1)	64(1)	-4(1)	16(1)	-7(1)
S(1B)	60(3)	25(2)	68(3)	0(2)	11(2)	-5(2)
O(1B)	95(10)	35(6)	87(10)	-4(6)	-24(8)	-21(6)
O(2B)	68(8)	66(8)	65(8)	5(6)	4(7)	-14(6)
O(3B)	79(8)	48(6)	30(4)	-1(4)	-5(5)	1(6)
O(4B)	51(8)	46(7)	104(10)	-3(6)	6(7)	-10(6)
O(5B)	75(10)	45(6)	96(10)	-13(6)	-25(8)	-14(6)
C(1B)	39(9)	49(9)	61(11)	-21(8)	10(8)	0(8)
C(2B)	49(10)	55(10)	78(12)	-36(9)	22(8)	-14(8)
C(3B)	44(9)	15(6)	90(13)	11(7)	-5(9)	1(6)
C(4B)	59(10)	31(8)	58(10)	-4(7)	-29(8)	14(7)
C(5B)	17(6)	30(7)	44(7)	0(5)	2(5)	-3(5)
C(6B)	31(7)	37(7)	53(10)	-24(7)	-6(7)	16(6)
C(7B)	70(14)	68(12)	98(15)	31(11)	-22(11)	-16(10)
C(8B)	48(9)	47(8)	66(10)	5(7)	-30(8)	-19(7)
C(9B)	42(9)	9(5)	82(10)	6(5)	8(8)	3(6)
C(10B)	40(9)	30(7)	84(11)	-3(7)	-39(8)	6(6)
C(11B)	58(12)	59(11)	75(12)	16(9)	-12(10)	-5(9)
C(12B)	52(9)	27(7)	71(11)	-14(7)	-8(8)	-5(7)
C(13B)	41(9)	28(8)	71(11)	-2(7)	-22(8)	1(7)
C(14B)	81(14)	45(10)	68(12)	13(8)	27(10)	0(9)

Table B5. Continued

Atom	U_{11}	U_{22}	U_{33}	U_{23}	U_{13}	U_{12}
C(15B)	45(8)	36(8)	59(9)	6(6)	8(7)	-13(7)
C(16B)	50(9)	21(7)	220(20)	-17(10)	2(12)	-14(7)
I(1C)	62(1)	48(1)	84(1)	-6(1)	-20(1)	-22(1)
S(1C)	37(2)	39(2)	55(3)	-10(2)	-5(2)	-13(2)
O(1C)	86(10)	71(8)	79(9)	3(7)	-14(7)	-33(7)
O(2C)	51(7)	81(10)	134(13)	26(9)	-16(7)	-12(7)
O(3C)	35(6)	54(7)	62(8)	-15(6)	3(6)	-8(5)
O(4C)	50(7)	32(5)	66(6)	-20(4)	-3(5)	-8(5)
O(5C)	50(8)	73(9)	88(10)	-16(7)	-23(7)	-23(7)
C(1C)	40(9)	32(7)	112(13)	-29(8)	-2(9)	-22(7)
C(2C)	47(9)	30(7)	86(11)	-21(7)	25(8)	-23(7)
C(3C)	55(9)	40(7)	34(8)	-5(6)	-12(6)	-12(7)
C(4C)	41(8)	27(7)	72(11)	-5(7)	-24(7)	-6(6)
C(5C)	22(7)	54(10)	57(9)	-30(8)	-9(7)	-2(7)
C(6C)	47(10)	57(9)	48(7)	-18(6)	11(7)	-18(8)
C(7C)	90(14)	67(12)	99(15)	-10(10)	-45(12)	-14(10)
C(8C)	52(9)	51(9)	70(10)	15(7)	19(8)	-9(7)
C(9C)	46(9)	60(10)	43(9)	7(7)	8(7)	-25(8)
C(10C)	49(10)	61(10)	44(8)	-18(7)	-6(7)	-20(9)
C(11C)	28(7)	38(7)	55(9)	-7(6)	1(7)	-8(6)
C(12C)	67(12)	19(6)	57(10)	1(6)	18(9)	-8(7)
C(13C)	103(18)	29(8)	79(13)	-11(8)	11(12)	-11(10)
C(14C)	60(12)	74(13)	96(14)	25(10)	25(11)	-5(10)
C(15C)	21(9)	47(9)	103(15)	27(9)	-8(9)	-2(7)
C(16C)	110(20)	140(20)	160(30)	-30(19)	53(19)	-94(18)
I(1D)	67(1)	46(1)	86(1)	-5(1)	-24(1)	-19(1)
S(1D)	39(2)	41(2)	75(3)	-11(2)	-3(2)	-17(2)
O(1D)	124(14)	56(7)	77(9)	28(6)	-36(9)	-51(8)
O(2D)	165(16)	75(9)	128(14)	26(9)	-114(12)	-53(10)
O(3D)	47(7)	54(7)	60(6)	-12(5)	12(5)	-33(6)
O(4D)	66(9)	55(8)	118(13)	25(7)	-20(9)	-28(7)
O(5D)	42(7)	52(7)	97(9)	-37(7)	-1(7)	-8(6)
C(1D)	55(10)	44(8)	24(6)	-8(5)	-13(6)	-4(7)
C(2D)	63(11)	47(9)	73(11)	-2(8)	-44(9)	-13(8)
C(3D)	65(11)	41(8)	57(9)	-8(7)	10(8)	-30(8)
C(4D)	84(14)	80(12)	58(9)	-21(8)	-1(9)	-23(11)
C(5D)	86(16)	57(12)	102(17)	-7(11)	22(14)	-37(12)
C(6D)	47(9)	25(6)	45(8)	-10(6)	3(7)	-16(6)
C(7D)	130(20)	52(11)	70(12)	14(9)	-6(13)	-33(12)
C(8D)	63(11)	58(10)	58(9)	-25(8)	8(8)	-33(8)
C(9D)	64(11)	44(9)	54(10)	-11(7)	3(8)	-25(8)
C(10D)	24(8)	22(6)	65(10)	2(6)	0(7)	1(6)
C(11D)	49(10)	50(9)	66(11)	-13(8)	-4(8)	-14(8)
C(12D)	20(7)	59(10)	94(13)	-19(9)	-1(8)	-19(7)
C(13D)	29(8)	78(12)	65(10)	-17(9)	21(7)	-34(8)

Table B5. Continued

Atom	U_{11}	U_{22}	U_{33}	U_{23}	U_{13}	U_{12}
C(14D)	72(13)	67(11)	44(9)	3(8)	-6(9)	-5(10)
C(15D)	61(11)	61(11)	30(8)	2(7)	-2(8)	-3(9)
C(16D)	73(13)	49(9)	129(18)	-5(10)	37(13)	-22(9)

^a The esd's of the least significant digits are given in parentheses. The anisotropic displacement factor exponent takes the form: $-2 \pi [h^2 a^{*2} U_{11} + \dots + 2 h k a^* b^* U_{12}]$.

Table B6. Hydrogen atom coordinates ($\times 10^4$) and equivalent isotropic displacement parameters ($\text{\AA}^2 \times 10^3$) for tosylate (**98**).^a

Atom	x	y	z	$U(\text{eq})$
H(2A)	519	-417	8919	71
H(5A)	-837	1609	10679	72
H(7A1)	627	-3278	10637	65
H(7A2)	-1464	-2867	10583	65
H(8A1)	992	3728	9610	60
H(8A2)	228	3662	10255	60
H(9A1)	-1601	5606	9637	64
H(9A2)	-2046	4479	9293	64
H(11A)	-4787	7376	9043	82
H(12A)	-4750	9832	8980	71
H(14A)	-5306	9685	10648	86
H(15A)	-5307	7327	10756	53
H(16A)	-4678	11747	9329	103
H(16B)	-3740	11510	9922	103
H(16C)	-5821	12144	9902	103
H(2B)	893	11362	3077	72
H(5B)	1938	9453	1301	39
H(7B1)	2760	13822	1460	98
H(7B2)	725	14029	1380	98
H(8B1)	1494	7341	1702	62
H(8B2)	489	7218	2311	62
H(9B1)	3022	5397	2387	58
H(9B2)	3413	6567	2724	58
H(11B)	6690	3682	1271	81
H(12B)	6592	1322	1323	60
H(14B)	6425	1162	3104	86
H(15B)	6454	3419	3005	58
H(16D)	6380	-1051	2577	143
H(16E)	7584	-1046	2003	143
H(16F)	5496	-576	1972	143
H(2C)	-294	5720	4989	62
H(5C)	-5774	4634	5228	52
H(7C1)	-5312	8499	4148	101
H(7C2)	-4743	7505	3644	101
H(8C1)	-2932	2860	6378	74
H(8C2)	-4779	2997	6120	74
H(9C1)	-1515	1357	5706	59
H(9C2)	-2901	740	6103	59
H(11C)	-3018	3077	4062	49
H(12C)	-1012	4375	3682	60
H(14C)	2957	1469	4522	101
H(15C)	1077	252	4882	74
H(16G)	3645	3483	3923	192

Table B6. Continued

Atom	x	y	z	<i>U</i>(eq)
H(16H)	2108	4924	3891	192
H(16I)	2585	4043	3353	192
H(2D)	1927	5063	6948	72
H(5D)	7175	6397	6797	96
H(7D1)	6489	2456	8018	102
H(7D2)	5696	3653	8431	102
H(8D1)	4689	7888	5687	66
H(8D2)	6398	7848	6009	66
H(9D1)	4242	10246	5948	62
H(9D2)	2905	9594	6365	62
H(11D)	413	10775	7175	65
H(12D)	-1461	9307	7559	66
H(14D)	2653	6552	8393	78
H(15D)	4415	7929	8023	66
H(16J)	-136	6153	8470	128
H(16K)	-1414	6728	7950	128
H(16L)	-1728	7546	8505	128

^a *U*(eq) is defined as one third of the trace of the orthogonalized U_{ij} tensor.

Appendix C

Table C1. Crystal data and structure refinement for nosylate (**15a**).

Empirical formula	C ₁₅ H ₁₂ INO ₇ S
Formula weight	477.22 g/mol
Temperature	293(2) K
Wavelength	0.70930 Å
Crystal system	Triclinic
Space group	P $\bar{1}$
Unit cell dimensions	a = 7.363(2) Å b = 9.482(2) Å c = 13.300(8) Å α = 76.89(3)° β = 73.99(4)° γ = 78.14(2)°
Volume	859.2(6) Å ³
Z	2
Density (calculated)	1.845 Mg/m ³
Absorption coefficient	2.023 mm ⁻¹
F(000)	468
Crystal size	0.60 x 0.40 x 0.20 mm
Theta range for data collection	2.23 to 24.93°
Index ranges	-1 ≤ h ≤ 8 -11 ≤ k ≤ 11 -15 ≤ l ≤ 15
Reflections collected	3845
Independent reflections	3018 ($R_{\text{int}} = 0.0101$)
Reflections observed (>2 σ)	2891
Max. and min. transmission	0.6878 and 0.3766
Refinement method	Full-matrix least-squares on F^2
Data / restraints / parameters	3018 / 0 / 226
Goodness-of-fit (based on F^2)	1.117
Final R indices [$I > 2\sigma(I)$]	$R_1 = 0.0408$, $wR_2 = 0.1002$
R indices (all data)	$R_1 = 0.0422$, $wR_2 = 0.1010$
Largest diff. peak and hole	1.148 and -1.181 e.Å ⁻³

Table C2. Atomic coordinates ($\times 10^4$) and equivalent isotropic displacement parameters ($\text{\AA}^2 \times 10^3$) for nosylate (**15a**).^a

Atom	x	y	z	$U(\text{eq})$
I	2254(1)	3646(1)	8217(1)	72(1)
S	7491(2)	6693(1)	5327(1)	55(1)
O(1)	1458(5)	8650(4)	9744(3)	76(1)
O(2)	4676(6)	8709(5)	9497(4)	85(1)
O(3)	8007(4)	5683(4)	6341(3)	59(1)
O(4)	8944(5)	7598(4)	4937(3)	71(1)
O(5)	7150(6)	5859(4)	4656(3)	75(1)
O(6)	300(5)	11260(4)	7611(3)	77(1)
O(7)	-1278(6)	10022(6)	7128(5)	122(2)
N	214(6)	10299(5)	7180(4)	65(1)
C(1)	3289(6)	5300(5)	8625(3)	45(1)
C(2)	1895(6)	6384(5)	9059(3)	50(1)
C(3)	2532(6)	7460(5)	9324(3)	50(1)
C(4)	4449(7)	7490(5)	9174(3)	53(1)
C(5)	5819(6)	6437(5)	8752(3)	53(1)
C(6)	5233(6)	5299(5)	8464(3)	46(1)
C(7)	2794(9)	9428(6)	9888(5)	76(2)
C(8)	6736(7)	4129(5)	7979(4)	57(1)
C(9)	7118(7)	4356(5)	6785(4)	63(1)
C(10)	5312(6)	7776(5)	5846(3)	47(1)
C(11)	5385(6)	8929(5)	6306(4)	52(1)
C(12)	3706(6)	9762(5)	6735(4)	52(1)
C(13)	2004(6)	9415(5)	6693(3)	49(1)
C(14)	1910(7)	8287(6)	6230(4)	63(1)
C(15)	3602(7)	7449(5)	5799(4)	60(1)

^a $U(\text{eq})$ is defined as one third of the trace of the orthogonalized U_{ij} tensor. The esd's of the least significant digits are given in parentheses.

Table C3. Bond lengths for nosylate (**15a**).^a

Bond	Length (Å)	Bond	Length (Å)
I-C(1)	2.108(4)	S-O(5)	1.418(4)
S-O(4)	1.421(4)	S-O(3)	1.558(3)
S-C(10)	1.772(4)	O(1)-C(3)	1.373(5)
O(1)-C(7)	1.419(7)	O(2)-C(4)	1.375(6)
O(2)-C(7)	1.425(7)	O(3)-C(9)	1.467(6)
O(6)-N	1.201(6)	O(7)-N	1.205(6)
N-C(13)	1.477(6)	C(1)-C(6)	1.387(6)
C(1)-C(2)	1.397(6)	C(2)-C(3)	1.355(6)
C(3)-C(4)	1.375(6)	C(4)-C(5)	1.363(6)
C(5)-C(6)	1.403(7)	C(6)-C(8)	1.515(6)
C(8)-C(9)	1.507(7)	C(10)-C(15)	1.377(7)
C(10)-C(11)	1.385(6)	C(11)-C(12)	1.376(6)
C(12)-C(13)	1.378(6)	C(13)-C(14)	1.371(7)
C(14)-C(15)	1.385(7)		

^a The esd's of the least significant digits are given in parentheses.

Table C4. Bond Angles for nosylate (**15a**).^a

Angle	Degree	Angle	Degree
O(5)-S-O(4)	120.1(2)	O(5)-S-O(3)	110.9(2)
O(4)-S-O(3)	104.1(2)	O(5)-S-C(10)	108.6(2)
O(4)-S-C(10)	108.6(2)	O(3)-S-C(10)	103.12(18)
C(3)-O(1)-C(7)	105.5(4)	C(4)-O(2)-C(7)	105.9(4)
C(9)-O(3)-S	118.4(3)	O(6)-N-O(7)	122.7(4)
O(6)-N-C(13)	119.1(4)	O(7)-N-C(13)	118.2(4)
C(6)-C(1)-C(2)	122.9(4)	C(6)-C(1)-I	121.4(3)
C(2)-C(1)-I	115.6(3)	C(3)-C(2)-C(1)	116.5(4)
C(2)-C(3)-O(1)	127.6(4)	C(2)-C(3)-C(4)	122.0(4)
O(1)-C(3)-C(4)	110.4(4)	C(5)-C(4)-O(2)	128.7(4)
C(5)-C(4)-C(3)	121.9(4)	O(2)-C(4)-C(3)	109.4(4)
C(4)-C(5)-C(6)	118.3(4)	C(1)-C(6)-C(5)	118.4(4)
C(1)-C(6)-C(8)	122.6(4)	C(5)-C(6)-C(8)	119.1(4)
O(1)-C(7)-O(2)	108.7(4)	C(9)-C(8)-C(6)	113.6(4)
O(3)-C(9)-C(8)	107.9(4)	C(15)-C(10)-C(11)	121.7(4)
C(15)-C(10)-S	120.0(3)	C(11)-C(10)-S	118.2(3)
C(12)-C(11)-C(10)	119.1(4)	C(11)-C(12)-C(13)	118.6(4)
C(14)-C(13)-C(12)	122.9(4)	C(14)-C(13)-N	119.3(4)
C(12)-C(13)-N	117.8(4)	C(13)-C(14)-C(15)	118.4(4)
C(10)-C(15)-C(14)	119.2(4)		

^a The esd's of the least significant digits are given in parentheses.

Table C5. Anisotropic displacement parameters ($\text{\AA}^2 \times 10^3$) for nosylate (**15a**).^a

Atom	U_{11}	U_{22}	U_{33}	U_{23}	U_{13}	U_{12}
I	65(1)	73(1)	81(1)	-36(1)	-2(1)	-17(1)
S	50(1)	58(1)	44(1)	-15(1)	1(1)	8(1)
O(1)	62(2)	62(2)	101(3)	-43(2)	2(2)	2(2)
O(2)	76(3)	89(3)	102(3)	-50(2)	-1(2)	-27(2)
O(3)	43(2)	63(2)	57(2)	-11(2)	-3(1)	7(1)
O(4)	55(2)	74(2)	63(2)	-9(2)	7(2)	-1(2)
O(5)	83(3)	79(2)	57(2)	-34(2)	-7(2)	10(2)
O(6)	68(2)	74(2)	85(3)	-43(2)	-6(2)	10(2)
O(7)	43(2)	145(5)	196(6)	-105(4)	-7(3)	-3(2)
N	48(2)	67(3)	74(3)	-26(2)	-6(2)	3(2)
C(1)	43(2)	50(2)	40(2)	-12(2)	-5(2)	-4(2)
C(2)	37(2)	59(3)	52(2)	-17(2)	-2(2)	-2(2)
C(3)	46(2)	50(2)	46(2)	-15(2)	-1(2)	1(2)
C(4)	54(3)	59(3)	46(2)	-16(2)	-6(2)	-11(2)
C(5)	35(2)	73(3)	48(2)	-12(2)	-7(2)	-4(2)
C(6)	41(2)	53(2)	35(2)	-6(2)	-5(2)	4(2)
C(7)	88(4)	56(3)	78(4)	-26(3)	2(3)	-13(3)
C(8)	45(2)	59(3)	53(2)	-8(2)	-4(2)	15(2)
C(9)	61(3)	50(3)	58(3)	-16(2)	6(2)	11(2)
C(10)	44(2)	47(2)	44(2)	-12(2)	-9(2)	4(2)
C(11)	41(2)	59(3)	58(3)	-20(2)	-13(2)	0(2)
C(12)	50(2)	51(2)	57(3)	-22(2)	-12(2)	-1(2)
C(13)	42(2)	49(2)	52(2)	-15(2)	-7(2)	4(2)
C(14)	47(3)	63(3)	86(4)	-28(3)	-17(2)	-4(2)
C(15)	55(3)	54(3)	75(3)	-30(2)	-16(2)	2(2)

^a The esd's of the least significant digits are given in parentheses. The anisotropic displacement factor exponent takes the form: $-2 \pi [h^2 a^{*2} U_{11} + \dots + 2 h k a^* b^* U_{12}]$.

Table C6. Hydrogen atom coordinates ($\times 10^4$) and equivalent isotropic displacement parameters ($\text{\AA}^2 \times 10^3$) for nosylate (**15a**).^a

Atom	x	y	z	<i>U</i> (eq)
H(2)	598	6368	9161	60
H(5)	7109	6472	8658	64
H(7A)	2587	9453	10636	91
H(7B)	2631	10429	9505	91
H(8A)	7919	4113	8173	69
H(8B)	6324	3182	8281	69
H(9A)	7965	3518	6526	75
H(9B)	5930	4466	6572	75
H(11)	6555	9136	6324	62
H(12)	3720	10544	7046	62
H(14)	738	8089	6206	76
H(15)	3584	6674	5483	72

^a *U*(eq) is defined as one third of the trace of the orthogonalized U_{ij} tensor.